AUBURN

SAMUEL GINN
COLLEGE OF ENGINEERING

Research Report for ALDOT Project 930-799

SELF-CONSOLIDATING CONCRETE FOR PRESTRESSED APPLICATIONS—PHASE II: BRIDGE CONSTRUCTION AND IN-PLACE PERFORMANCE

Submitted to

The Alabama Department of Transportation

Prepared by

Samuel D. Keske, Robert W. Barnes, Anton K. Schindler,
Brandon R. Johnson, Morgan A. Ellis, D. Eric Miller, and Tyler L. Neal

APRIL 2015

Highway Research Center
Harbert Engineering Center
Auburn, Alabama 36849

www.eng.auburn.edu/research/centers/hrc.html

1. Report No. FHWA/ALDOT 930-799	**2. Government Accession No.**	**3. Recipient Catalog No.**
4 Title and Subtitle Self-Consolidating Concrete for Prestressed Applications—Phase II: Bridge Construction and In-Place Performance		**5 Report Date** April 2015 **6 Performing Organization Code**
7. Author(s) Samuel D. Keske, Robert W. Barnes, Anton K. Schindler, Brandon R. Johnson, Morgan A. Ellis, D. Eric Miller, and Tyler L. Neal		**8 Performing** FHWA/ALDOT 930-799
9 Performing Organization Name and Address Highway Research Center 238 Harbert Engineering Center Auburn, AL 36849		**10 Work Unit No. (TRAIS)** **11 Contract or Grant No.**
12 Sponsoring Agency Name and Address Alabama Department of Transportation 1409 Coliseum Boulevard Montgomery, AL 36130-3050		**13 Type of Report and Period Covered** Technical Report **14 Sponsoring Agency Code**

15 Supplementary Notes
Project performed in cooperation with the Alabama Department of Transportation

16 Abstract

Prior to statewide acceptance of self-consolidating concrete (SCC) in precast, prestressed bridge member production, the Alabama Department of Transportation sponsored an investigation of the material to be performed by the Auburn University Highway Research Center. Two parts of that research are presented in this report: an extension of an earlier laboratory investigation of fresh stability test methods to quantify the unique fresh behavior of SCC, and a field investigation of as-built material and long-term structural behavior in the first full-scale SCC girders produced and placed in an in-service bridge in Alabama.

During the laboratory investigation, the Visual Stability Index, Sieve Stability, and Surface Settlement tests correlated most strongly to multiple measures of hardened concrete uniformity; a testing protocol utilizing these test methods is recommended. In the field investigation, the utilized SCC exhibited slightly increased time-dependent creep and shrinkage, at least in representative cylinders. Long-term SCC-girder prestress maintenance was found to be practically identical and at least as conservatively predictable as in companion, geometrically identical vibrated-concrete (VC) girders. Full-scale elastic responses to the weight of the cast-in-place deck and to service-level live loads were also practically identical in the SCC and VC girders, and SCC performed more conservatively than expected of VC of the same elastic stiffness. Use of cylinder-measured mechanical and time-dependent property results led to conservative predictions of full-scale behavior, and use of design properties led to highly conservative predictions. Based on these results, SCC is an acceptable alternative to VC for precast, prestressed girders when using current design and production procedures.

17 Key Words SCC, stability test methods, uniformity, creep, shrinkage, effective prestress, camber, live-load response, deflection		**18 Distribution Statement** No restrictions. This document is available to the public through the National Technical Information Service, Springfield, Virginia 22161	
19 Security Classification (of this report) Unclassified	**20 Security Classification (of this page)** Unclassified	**21 No. of pages** 271	**22 Price**

Form DOT F 1700.7 (8-72)

Research Report

ALDOT Research Project 930-799

SELF-CONSOLIDATING CONCRETE FOR PRESTRESSED APPLICATIONS—PHASE I: BRIDGE CONSTRUCTION AND IN-PLACE PERFORMANCE

Prepared by

Samuel D. Keske

Robert W. Barnes

Anton K. Schindler

Brandon R. Johnson

Morgan A. Ellis

D. Eric Miller

Tyler L. Neal

Highway Research Center
and
Department of Civil Engineering
at
Auburn University

APRIL 2015

DISCLAIMERS

The contents of this report reflect the views of the authors, who are responsible for the facts and the accuracy of the data presented herein. The contents do not necessarily reflect the official views or policies of Auburn University or the Federal Highway Administration. This report does not constitute a standard, specification, or regulation.

NOT INTENDED FOR CONSTRUCTION, BIDDING, OR PERMIT PURPOSES

Robert W. Barnes, Ph.D., P.E.
Anton K. Schindler, Ph.D., P.E.
Research Supervisors

ACKNOWLEDGEMENTS

Material contained herein was obtained in connection with a research project "Implementation of Self-Consolidating Concrete for prestressed applications—Phase II: Bridge construction and in-place performance," ALDOT Project 930-799, conducted by the Auburn University Highway Research Center. Funding for the project was provided by the Alabama Department of Transportation. The cooperation and assistance of the ALDOT Materials and Tests Bureau, Bridge Bureau, and Maintenance Bureau, Hanson: Pelham Prestress, BASF Construction Chemicals, and Racon General Contractors are gratefully acknowledged. The contributions of Wes Bullock and Levent Isbiliroglu to this work are appreciated. The authors particularly acknowledge the contributions of the following individuals:

Buddy Black	ALDOT, State Bridge Engineer
Buddy Cox	ALDOT, State Materials and Tests Engineer
Lyndi Blackburn	ALDOT, Assistant Bureau Chief – Materials and Tests Bureau
Sergio Rodriguez	ALDOT, Special Projects Engineer, Montgomery
Craig Philips	ALDOT, Hillabee Creek Bridge Project Manager
Daniel Jones	ALDOT, Maintenance Bureau
Nathan Emmerich	Hanson: Pelham Prestress, Quality Control Manager
Dwain Hamby	Hanson: Pelham Prestress, Engineering Manager
Frankie Smith	Hanson: Pelham Prestress, Plant Manager
Rickey Swancey	BASF, Senior Sales Representative

ABSTRACT

Self-consolidating concrete (SCC) is a high-performance concrete in the fresh state—because of its highly fluid fresh behavior, it requires no mechanical consolidation during placement. Prior to statewide acceptance of SCC in precast, prestressed bridge member production, the Alabama Department of Transportation (ALDOT) sponsored an investigation of the material performed by the Auburn University Highway Research Center. Multiple aspects of that investigation are synthesized in this Phase II report, including material stability behavior evaluated in a laboratory setting and material and structural behavior evaluated in full-scale girders that were placed in an in-service bridge. In both settings, SCC was evaluated relative to vibrated concrete (VC) and considering existing design standards and construction practices.

An extension of the Phase I project, the laboratory investigation focused on quantification of SCC stability, a unique property of the material that is important to assess during construction. Five fresh concrete stability tests were conducted on twenty SCC mixtures each placed in walls of heights equaling 54, 72, and 94 inches. Fresh test results were then compared to the results of hardened uniformity testing conducted on the concrete walls. Analyses indicate that acceptable mechanical properties can be achieved in a range of mixtures and that some SCC fresh stability tests correlate well with hardened concrete uniformity. Suitable fresh SCC tests and acceptance criteria are recommended, as is a testing protocol for use during implementation of SCC in the production of precast, prestressed elements.

The full-scale implementation of precast, prestressed SCC girders consisted of seven BT-54 bulb-tees and seven BT-72 bulb-tees placed in a bridge in rural Alabama. Many long-term material and structural properties were assessed during the bridge construction and for up to 650 days after, until when the girders were approximately 1,000 days old and had been in service for one year. At all ages through three years, SCC exhibited greater time-dependent deformability (approximately 5–10% greater creep and 30% greater shrinkage) than VC in representative cylinders. However, time-dependent prestress maintenance and elastic deformation responses to construction and service loads were practically identical in the SCC and VC girders.

Full-scale SCC structural behavior was no less predictable than that of VC according to simplified and refined *AASHTO LRFD* design methods. All measured behaviors were accurately or conservatively predicted, and the use of design material properties in place of measured values led to distinct under-prediction of structural performance. Future time-dependent changes in full-scale behavior (other than transient thermal effects) are expected to be minimal during the remaining service life of these girders. Based on these laboratory and full-scale results, it is concluded that SCC is an acceptable alternative to vibrated concrete in the construction of precast, prestressed bridge girders using current design and production procedures.

TABLE OF CONTENTS

LIST OF FIGURES

LIST OF TABLES

LIST OF ABBREVIATIONS AND SYMBOLS

A	Adjustment factor applied to the existing *AASHTO LRFD* time-dependent deformation provisions to account for differences in measured material behavior of SCC
A_{AL}	Adjustment factor applied to referenced time-dependent deformation provisions to account for properties of Alabama concrete (used specifically in this work)
$A_{subscript}$	Area, described by "subscript", except concerning A_{AL} as noted above (areas are always noted with a subscript to differentiate from adjustment factors noted above)
AASHTO	American Association of State Highway and Transportation Officials
AEA	Air-entraining admixture
ALDOT	Alabama Department of Transportation
AMS	Average maximum strain, used to quantify transfer length
AUHRC	Auburn University Highway Research Center
BT-54	Bulb-tee girder 54 inches in height
BT-72	Bulb-tee girder 72 inches in height
cgp	Center of gravity of bottom-bulb prestress
CI	Confidence interval, a statistical measure of reliability of a measurement
CTE	Coefficient of thermal expansion
d_b	Nominal bar diameter, as of (where appropriate) the diameter of non-prestressed steel or prestressing strand reinforcement
DEMEC	Demountable mechanical strain gauge
DIA	Digital image analysis
DOT	Department of Transportation
e	Eccentricity of prestress force, as in relation to the centroid of the transformed area, e_{tr}, or gross area, e_{pg}
E	Modulus of elasticity, as of concrete, E_c, concrete specifically at transfer, E_{ci}, prestressed reinforcement, E_p, or deformed steel reinforcement, E_s
ERSG	Electrical-resistance strain gauge
f_c	Measured compressive strength (or f_{ci} specifically for measured compressive strength at the time of prestress transfer)
f'_c	Specified compressive strength (or f'_{ci} specifically for specified compressive strength at the time of prestress transfer)

f_{cgp}	Concrete stress at the center of gravity of prestressing
f_{ct}	Splitting tensile strength
f_{pe}	Effective prestress in prestressing strands after all losses
f_{pj}	Jacking stress in prestressing strand
f_{pt}	Stress in the prestressing strand immediately after release
f_{pbt}	Stress in the prestressing strand immediately prior to release
HRWRA	High-range water-reducing admixture
HVSI	Hardened visual stability index
I	Moment of inertia, as of the gross section, I_g, or transformed section, I_{tr}
$J(t,t_i)$	Compliance at a time, t, due to a load applied since an earlier time, t_i (also known as J)
k	Correction factor for nonstandard concrete composition or conditions, used by the *AASHTO LRFD* provisions to model time-dependent deformation
K_1	Aggregate modification factor used in calculation of E_c
$K_{subscript}$	Transformed-section coefficient to account for time-dependent interaction between concrete and steel, as with respect to behavior prior to composite-deck action, K_{id}, or after, K_{df}
L	Length, (where appropriate) of ultrasonic pulse path or girder length
l_t	Transfer length
M	Bending moment at a given cross section due to an applied load
MC	Model Code, specifically the European CEB-FIB Model Code 2010
n	Modular ratio, used in transformed-section analysis to transform areas of different materials based on relative E
NMSA	Nominal maximum size aggregate (also known as nominal aggregate size)
pcy	Pounds per cubic yard, used for concrete batch proportions
R^2	Regression coefficient of determination, used (as noted) to describe linear or non-linear strength of fit
RGB	Red/green/blue color model
s/agg	Sand-to-total-aggregate ratio by mass
SCC	Self-consolidating concrete
SCM	Supplementary cementitious material

SSD	Saturated surface-dry
t	Time, used in various predictions of time-dependent material and structural behavior
T_{50}	Time for SCC slump flow to reach a diameter of 50 cm (20 in.)
UPV	Ultrasonic pulse velocity
VC	Vibrated concrete (also known as conventionally vibrated concrete)
VMA	Viscosity-modifying admixture
V/S	Volume-to-surface-area ratio
VSI	Visual stability index
v_t	Time-correction factor as determined in Equation 3-2
v_u	Ultimate creep coefficient as determined in Equation 3-1
VWSG	Vibrating-wire strain gauge
w/cm	Water-to-cementitious material ratio, by mass
w_c	Weight of concrete, unreinforced
WRA	Water-reducing admixture
X	Independent variable, used in various equations related to the measurement or prediction of time-dependent deformation
y	Vertical distance from the centroid to the location at which strain or stress is determined, as with respect to the transformed section, y_{tr}
Y	Dependent variable, used in various equations related to the measurement or prediction of time-dependent deformation
β_c	Coefficient to account for development of creep over time after loading, used by the European Model Code provisions
γ	Correction factor for nonstandard concrete composition or exposure conditions, used in Equation 3-1 or Equation 3-6
Δ	Change, as in change in temperature, ΔT, stress, Δf, or strain, $\Delta \varepsilon$
ε	Strain, used or calculated in various applications related to time-dependent or elastic deformation (or microstrain $\mu\varepsilon$, equal to $\varepsilon(10)^{-6}$)
$\varphi(t,t_o)$	Creep coefficient at a time t due to a load maintained since an earlier time t_o, used by the European Model Code provisions
$\psi(t,t_i)$	Creep coefficient at a time t due to a load maintained since an earlier time t_i, used by the *AASHTO LRFD* provisions
ω_{BP}	Bazant-Panula coefficient of variation, a statistical indicator of strength of curve fitment (always positive; results approaching 0 indicate better fit)

CHAPTER 1: INTRODUCTION

1.1 BACKGROUND ON SCC FOR PRECAST, PRESTRESSED GIRDERS

ACI 237 (2007) defines self-consolidating concrete (SCC) as a highly fluid, non-segregating concrete that can spread through reinforcement and completely fill formwork without the use of mechanical consolidation. Because of its fluid nature, SCC can efficiently fill congested or irregularly shaped members more easily than vibrated concrete (VC) while providing an improved surface finish. Its use also eliminates the need for vibratory consolidation efforts and associated construction labor and hazards and reduces wear and tear on formwork and equipment. Therefore, one of the most advantageous uses of SCC is in the production of precast, prestressed bridge girders, where reinforcement congestion and member shape can make filling and consolidation of VC difficult.

SCC achieves its unique fresh characteristics through the use of different constituent materials, proportions, or both. However, research concerning the effects of these mixture changes on the material has produced some mixed results, both with regard to fresh behavior and hardened-material and structural behavior. Understanding these effects is critical in the especially demanding environment associated with the production of precast, prestressed girders. Consequently, prior to statewide acceptance of SCC in precast, prestressed bridge member production, the Alabama Department of Transportation (ALDOT) sponsored a comprehensive investigation of SCC to be performed by the Auburn University Highway Research Center (AUHRC).

Past AUHRC laboratory-based research projects associated with this investigation have included formulation of SCC mixture proportions (Schindler et al. 2007), studies of the structural behavior when prestressed (Boehm et al. 2010; Levy et al. 2010), and evaluation of time-dependent properties (Kavanaugh 2008). The final phase of the investigation was to produce Alabama's first in-service bridge with precast, prestressed SCC girders, a task which took place from September, 2010 to November, 2011. AUHRC personnel monitored the entire process from the plant production through the addition of a cast-in-place concrete deck over the girders. The completed bridge is shown in Figure 1.1.

Figure 1.1: Erection of precast, prestressed girders over Hillabee Creek

1.2 STATEMENT OF OBJECTIVES

The primary objective of this research was to determine the acceptability of SCC for use in ALDOT precast, prestressed applications, particularly concerning long-term performance. Performance characteristics reported include evaluation of the

- Applicability and improvement of SCC fresh stability assessment,
- Differences in long-term material behavior in response to changes in the mixture proportions, as well as their predictability and significance, and
- Differences in long-term time-dependent and elastic structural performance due to changes in material behavior, as well as their significance relative to current design and construction practices.

1.3 REPORT METHODOLOGY AND OUTLINE

Like the related report on early-age SCC behavior by Keske et al. (2015), the work documented in this report was conducted in two parts. The first involved an extension of the evaluation of fresh concrete stability test methods conducted by Keske et al. (2015) during the production of many different SCC mixtures, and the second involved the evaluation of a variety of behaviors in a one-to-one comparison of the SCC and VC girders placed in the Hillabee Creek Bridge with

minimal researcher interference or direct involvement. Thus, different investigative approaches were associated with each part.

The laboratory investigation, which is presented in Chapter 2, focused on quantification of SCC fresh stability and the relationship between fresh stability and hardened concrete uniformity. In the investigation, five fresh concrete stability tests were conducted on a variety of SCC mixtures each placed in walls of heights equaling 54, 72, and 94 inches. Walls were also constructed with control VC mixtures of similar proportions and materials, and the in-place concrete uniformity of each group of walls was evaluated nondestructively and destructively. Fresh SCC test results were then compared to the results of the hardened concrete uniformity testing to evaluate the correlations between these tests.

The evaluation of the full-scale project production took a different approach—researcher involvement in the design of the bridge, selection of mixtures, and production of the girders was minimized specifically so that the as-produced results of the process would be assessed. Furthermore, only one SCC and one VC mixture were used throughout production. The plant personnel used the implemented VC mixture regularly and were familiar with its expected behavior, so the producer chose to create an SCC using the same aggregate source (but a different gradation), cementitious materials, and water-to cementitious material ratio (*w/cm*) as in the VC for convenience. Thus, this research involved the assessment of a variety of hardened-material and structural behaviors of comparable SCC and VC on a one-to-one basis. Topics relevant to bridge construction and in-place performance that are assessed include

- Time-dependent deformation of concrete materials, including thermal, creep, and shrinkage effects,
- Elastic responses of precast, prestressed girders to construction and service loads, and
- Time-dependent structural behavior of precast, prestressed girders, particularly regarding long-term maintenance of prestress.

The laboratory analysis involved the intentional varying of fresh concrete properties and proportions (frequently to intentionally yield concretes of a poor stability), so results from it should be considered separately from the results of the evaluation of full-scale trial production that are presented in Chapters 3–5. Conversely, while conclusions regarding the acceptability of SCC for full-scale implementation are derived from the latter part of this investigation, the results should not be considered to be universal to all SCC. Self-consolidating behavior can be achieved in mixtures of infinitely varying constituents and proportions, so the presented results are most directly applicable to concretes made using comparable mixture constituents, proportions, and construction practices as employed in this project. Equally important are conclusions regarding whether the differences between SCC and VC are *expectable* or *predictable* in response to differences in their mixture properties, as these conclusions are more widely applicable.

CHAPTER 2: ASSESSMENT OF FRESH STABILITY

2.1 INTRODUCTION

SCC differs from VC primarily in the fresh state, and it can be proportioned to achieve practically any behavior in the hardened state (Bartos 2005). The unique, self-consolidating nature of SCC is practically described by three fresh properties: filling ability, passing ability, and stability. ACI 237 (2007) defines these properties:

- Filling ability (or unconfined flowability) refers to SCC's ability to fill formwork under its own weight,
- Passing ability (or confined flowability) refers to SCC's ability to pass through constricted spaces and around obstacles without blockage, and
- Stability (or segregation resistance) refers to SCC's ability to maintain a uniform distribution of its constituents during flow and setting.

Much research has been conducted to show that properly proportioned and prepared SCC can behave acceptably similarly to VC in the hardened state. Many researchers (Cussigh 1999; Daczko 2003; Khayat et al. 1997; and Soylev and Francois 2003) have determined that SCC exhibits acceptably similar hardened properties to those of their vibrated counterparts in concretes for many different applications; however, investigations continue concerning SCC in some especially demanding applications such as the production of precast, prestressed girders, where many properties and aspects of structural behavior need additional consideration.

With regard to the effect of fresh properties on structural behavior, the primary concern must be the *hardened uniformity* of the final product. Hardened properties of concrete (strength, stiffness, etc.) are affected by mixture proportioning, but that concept is not unique to SCC. Instead, the unique fresh nature of SCC is inherently only capable of affecting hardened concrete uniformity. Considering the three fresh properties described above, the effect of filling and passing ability on hardened concrete uniformity can be assessed visually or using widely accepted, standardized test methods. Both fresh properties depend on the intended application (ACI 237 2007)—elements with minimal confinement, congestion, or filling restriction require relatively less filling and passing ability. Elements with heavy reinforcement congestion, irregularly shaped formwork, or long flow distances (such as precast, prestressed girders) require relatively high filling and passing ability.

Like filling and passing ability, the degree of stability required of SCC can depend on the application (ACI 237 2007). However, assessment of this property in the fresh state and determination of its effects on hardened concrete properties may not be intuitive or easily tested.

Furthermore, the relevance of fresh property testing and in-situ uniformity testing to global structural behavior of concrete is unclear. The testing of in-place hardened properties can be difficult to interpret or time- and labor-intensive and can only be performed after completion of the placement. Therefore, proper identification of stability in the fresh state, as well as understanding of the relationship between fresh stability results and hardened concrete uniformity, is paramount to the successful implementation of SCC.

In a previous phase of this research, the results of which were published by Keske et al. (2013b) and in the complimentary report on ALDOT Project 930-738, five fresh stability test methods and two hardened concrete uniformity test methods were conducted on eleven concrete mixtures. The second phase was conducted to both extend the AUHRC's investigation to a wider range of potentially viable SCC mixtures, as well as to strengthen conclusions concerning the relationships between fresh- and hardened-concrete properties and test methods. Primary objectives of the second phase were thus to

- Investigate the applicability of five previously identified fresh SCC stability test methods in an extended variety of SCC mixtures,
- Investigate the applicability of alternative testing times in those fresh concrete stability tests that appeared promising during the first phase of research but could benefit from abbreviation or extension of testing, and
- Affirm the recommended testing protocol that ALDOT should implement to assess SCC stability during the production of precast, prestressed elements.

2.2 LITERATURE REVIEW

The work documented in this chapter represents an extension of the research documented in Chapter 2 of the complimentary ALDOT 930-738 report (Keske et al. 2015), so, for brevity, only pertinent information from that publication is given here. Emphasis is given to portions of the existing literature that were not directly discussed in the previous report. Specifically, literature related to the assessment of hardened concrete uniformity via inspection of cores is of interest, as this testing was conducted during this research phase.

2.2.1 Fresh Concrete Stability Test Methods

The five fresh stability test methods that were evaluated during this research are described in this section. They include the visual stability index (VSI), column segregation test, rapid penetration test, sieve stability test, and surface settlement test.

2.2.1.1 Visual Stability Index

The visual stability index (VSI) is the most widely used test to assess the stability of SCC (Lange et al. 2008) and was included in the first SCC-specific test to be standardized by ASTM. The VSI involves assigning a rating to the level of segregation seen in a sample of SCC. This sample, the patty left after testing the slump flow according to ASTM C1611 (2005), is inspected for visible signs of segregation. A rating from 0–3 is then assigned based on appearance, with 0 showing no signs of segregation and 3 showing clear segregation with aggregate piling in the center and with a well-defined mortar halo (> 0.5 in.).

The VSI is qualitative in nature and is subject to each technician's assessment. Therefore, while it is useful for rapid quality assurance during production, the VSI should not be used to determine prequalification acceptance or rejection of a mixture (ACI 237 2007). Several summary reports (EPG 2005; Ozyildirim and Lane 2003) suggest that the VSI is sufficient for initial segregation inspection; Keske et al. (2013b) recommend its use for this purpose in SCC production in the state of Alabama. Other researchers (Bonen and Shah 2004; 2005; Lange et al. 2008) suggest that a low VSI (showing good segregation resistance) does not ensure adequate stability.

2.2.1.2 Column Segregation Test

The column segregation test (ASTM C1610 2006) was the second SCC stability test to be standardized by ASTM and is, therefore, often used to assess the static stability of SCC. In a comprehensive study, Assaad et al. (2004) evaluated SCC properties using the column segregation test, VSI test, rheological tests, and compressive strength. They found that the column segregation test is sensitive to sedimentation of aggregate, which was confirmed by Mouret et al. (2008). As both sources note, the column segregation test is more sensitive when total aggregate content is low (Assaad et al. 2004; Mouret et al. 2008). Higher coarse aggregate content must be complimented by lower mortar content. The increase in coarse aggregate limits the ability of any individual particles to settle, resulting in reduced column segregation values. Meanwhile, the decrease in binder content makes the mixture more sensitive to bleeding and segregation of binder (Assaad et al. 2004; Ng et al. 2006; Ye et al. 2005).

Because the column segregation test is affected by coarse aggregate content in this way, Assaad et al. (2004) and Khayat and Mitchell (2009) recommend using the column segregation test in conjunction with the surface settlement test described in Section 2.2.1.5, which is more sensitive to bleeding segregation. Similarly, Mouret et al. (2008) recommend using it in conjunction with the sieve stability test described in Section 2.2.1.4, as they found that the column segregation and sieve stability tests respond differently to segregation.

Many researchers (Bui et al. 2007; Koehler and Fowler 2010; Keske et al. 2013b) have found the column test to be too slow and laborious to implement for quality assurance due to the 15-minute testing period and difficulty of separating and wet-sieving the test sample. However, Assaad et al. (2004), Khayat and Mitchell (2009), and Mouret et al. (2008) recommend using it for quality assurance testing of SCC stability.

2.2.1.3 Rapid Penetration Test

The rapid penetration test (ASTM C1712 2009) was developed to be a quicker, technician-friendly alternative to the column segregation test (Bui et al. 2007). To that effect, the test is run on SCC already placed in the inverted slump cone for VSI and slump flow testing. After allowing the sample to settle for 80 seconds, a weighted hollow penetration cylinder is placed on the top surface and allowed to settle under its own weight. After 30 seconds, the penetration depth of the cylinder is read to the nearest millimeter, which may be related directly to the mortar layer depth at the top of the sample and indirectly correlated to segregation resistance.

ASTM C1712 (2009) was developed by establishing a relationship between its results and those of the column segregation test (Bui et al. 2007). A relationship between the column segregation test results and the mortar layer depth at the top of hardened cylinders was also determined after vertically cutting the cylinders and measuring the depth to the first coarse aggregate particle. Bui et al. (2007) found that mortar depth relates to segregation index and penetration depth, thereby allowing use of the penetration test in place of the column test. According to ASTM C1712 (2009) and Bui et al. (2007), the test is useful for both mixture prequalification and quality assurance, as it is faster than the column segregation test and is not subjective like the VSI.

ASTM C1712 (2009) recommends establishing a new correlation between the penetration and column segregation tests whenever dealing with new mixture proportions; penetration depth limits discussed earlier are only applicable to mixtures with less than 65% total aggregate volume. Koehler and Fowler (2010) have found the rapid penetration test to be poorly related to both the column segregation test and sieve stability test (described in the next section). The Self-Compacting Concrete European Project Group (EPG 2005) found the rapid penetration test to have greater scatter than the sieve stability test, and they recommend it as a secondary alternative to the sieve stability test. The test's use in peer-reviewed research has been limited, although similar tests (including those described in a previous report for ALDOT Project 930-738) have been used elsewhere.

2.2.1.4 Sieve Stability Test

The current form of the sieve stability test was standardized by the SCC European Project Group (EPG 2005) following a three-year study by the EPG representative organizations. The test, which is detailed in Appendix B.1 of Keske et al. (2015), requires an approximately fifty pound sample of SCC and approximately eighteen minutes of testing time. After sitting for fifteen minutes, the top portion of the sample is poured from a specified height (usually with the assistance of a pouring apparatus) onto a sieve and pan. It then rests on the sieve for two minutes to allow separation of mortar and aggregate. After those two minutes, the sieve and retained SCC are removed from above the pan, and the sieved fraction is calculated by dividing the weight of SCC passing onto the pan by the total weight of SCC tested.

The EPG Guidelines (2005) specify the use of a 5 mm sieve, but the PCI guidelines (2004) allow a No. 4 (0.25 in.) sieve to be used in place of a 5 mm sieve because the No. 4 sieve is more common in the U.S. The EPG Guidelines (2005) recommend a sieved fraction 5%–15%, as SCC with a sieved fraction less than 5% may begin to lack the flowability necessary to prevent bugholes and provide a good surface finish. More specifically, the guidelines classify sieve stability using the following classes (EPG 2005):

- S ≤ 20% for Class 1, which is applicable for slabs and applications with limited flow distances and clear spacing greater than 3 in.,
- S ≤ 15% for Class 2, which is applicable for vertical applications with limited flow distances and clear spacing greater than 3 in., and
- S ≤ 10% in demanding applications with greater flow distances and clear spacing less than 3 in., such as for precast, prestressed girders.

Because SCC is dropped from a height of 20 in. onto the sieve, El-Chabib and Nehdi (2006) and Koehler and Fowler (2010) question what form of segregation the sieve stability test identifies. Gravity causes an increase in kinetic energy as the SCC falls, resulting in forced segregation of mortar from aggregate. Also, mixtures with a high mortar fraction and low coarse aggregate fraction may be more susceptible to testing poorly, as more mortar is present to pass through the sieve (El-Chabib and Nehdi 2006; Schwartzentruber and Broutin 2005).
Ng et al. (2006) contradict this observation regarding mixture proportioning. They found that mixtures with a high coarse aggregate fraction are more susceptible to testing poorly. For the same reason that the column segregation test becomes less sensitive as coarse aggregate content increases (see Section 2.2.1.2), the sieve test becomes *more* sensitive if it is able to identify bleeding and separation of mortar from aggregate. Mouret et al. (2008) found that the sieve test identifies segregation that the column test does not and vice versa, while others (EPG 2005; Koehler and Fowler 2010) have found the two tests to be highly correlated.

During a comprehensive study of SCC behavior, the sieve stability test was the best indicator of segregation when compared with the column segregation test and the rapid penetration test (EPG 2005). Although the form of segregation it identifies is unclear, EPG (2005) and Koehler and Fowler (2010) found that the sieve test seems to relate well with in-situ segregation. Johnson et al. (2010), on the other hand, present mixed results when comparing sieve stability results to results of DIA. They found the two to relate well in some trials and not in others. A lack of correlation was more frequently observed in mixtures with ¾ in. aggregate (Johnson et al. 2010).

Because of its simple nature, EPG (2005) recommends the sieve stability test as the primary on-site quality assurance measure of stability for SCC projects in the European Union. PCI (2004) found the sieve test to be unsuitable for on-site use due to its prolonged test duration. Keske et al. (2013a) documented similar concerns from a precast, prestressed concrete producer. According to the producer they worked with, suspending placement for the 18 min. testing time is impractical and could detrimentally affect the placement of the tested SCC.

2.2.1.5 Surface Settlement Test

The surface settlement test was recommended by Khayat and Mitchell (2009) as the primary stability test for SCC in precast, prestressed bridge element production. The test has not been standardized by ASTM or by other European equivalents, but it has been used in SCC research for several years (Khayat 1998; Khayat et al. 1997; Khayat et al. 2003).

The principle of the test is simple: measure the settlement of a thin acrylic plate as it settles into a column of fresh SCC. The maximum settlement is recorded as a percentage of the height of the column of SCC, and the rate of settlement is calculated as a percentage of column height penetrated per hour. Either by settlement rate or maximum settlement, the test aims to study the presence of bleed water and paste at the top surface of the column and the settlement of the uppermost coarse aggregate particles. Khayat and Mitchell (2009) and Keske et al. (2013b) recommend assessment by rate in order to improve testing convenience.

Assaad et al. (2004) and Sonebi and Bartos (2002) have shown that the surface settlement test gives a good measurement of the development of bleeding, which they confirmed by comparison to other concrete stability tests and uniformity tests. Like the column segregation test and sieve test, though, surface settlement can be affected by the binder content and coarse aggregate content (Khayat 1999; Khayat et al. 2000; Sonebi and Bartos 2002). Increasing coarse aggregate content makes aggregate settlement more difficult, but at the expense of higher bleeding risk. Sonebi and Bartos (2002) also found that the test is sensitive to fine aggregate content, grading, and surface roughness, as these properties affect the bleeding potential of the mixture. Assaad et al. (2004) and Khayat and Mitchell (2009) therefore recommend that the

settlement test compliment the column segregation test, as the two tests can be used to identify different forms of segregation.

2.2.2 Hardened Concrete Uniformity Test Methods

Of the hardened properties of SCC most frequently affected by segregation, three were selected for identification of hardened concrete uniformity: ultrasonic pulse velocity (UPV), bond to reinforcement, and distribution of constituents in the hardened concrete. Distribution of constituents in hardened concrete can be qualitatively assessed by visual inspection (Lange et al. 2008) and quantifiably assessed using image-analysis software (Fang and Labi 2006). Assessment by UPV and pullout testing was used during the previous phase of this research, so literature from that report is briefly summarized in this report. The details of the core assessment methods, as well as past research in which they have been employed, are described in the following subsections.

2.2.2.1 Ultrasonic Pulse Velocity Test

Nondestructive ultrasonic pulse velocity testing (UPV) can directly measure changes in the overall quality of hardened concrete (Abo-Qudais 2005; Naik et al. 2004; Sahmaran et al. 2007), and it has been used previously during AUHRC research (Keske et al. 2013b). The test is conducted by placing two metal couplers on flat surfaces of the concrete specimen, initiating rapidly repeating ultrasonic pulses at one coupler, and measuring the average time required for the pulses to reach the other coupler. Once the travel length between couplers is determined, the average speed of pulses through that travel path is calculated. The speed of the ultrasonic pulse is affected by several factors:

- Density and porosity, in which speeds are higher in denser, less porous material (Lin et al. 2007; Lin et al. 2003; Sahmaran et al. 2007),
- Interface quality between mortar and coarse aggregate, in which a better interface results in better transmission of waves (Abo-Qudais 2005; Soshiroda et al. 2006),
- Aggregate size, in which presence of larger aggregate results in reduced speed (Abo-Qudais 2005),
- Moisture content and concrete saturation, in which the water-filled pores transmit faster pulses (Abo-Qudais 2005; Mindess et al. 2003), and
- Strength and elasticity, in which speeds are higher in material of a higher strength or higher stiffness (Abo-Qudais 2005; Lin et al. 2007; Soshiroda et al. 2006).

The factors that affect UPV results are all related to SCC uniformity: strength and elasticity relate to *w/cm*, density relates to distribution of constituents and mortar quality, and interface quality relates to presence of excess water (Mehta and Monteiro 2006). The ability to simultaneously account for these factors makes the UPV very useful for assessing the effects of possible segregation and for detecting changes in concrete quality at different locations within a concrete element.

For testing concrete, Gaydecki et al. (1992) recommend a frequency of 55–85 kHz and ASTM C597 (2002) recommends a frequency range of 40–80 kHz, both with a preference for higher frequencies when using shorter path lengths. There is no upper or lower limit to the path length, *L*, but Naik et al. (2004) recommend *L* be between 4 in. and 28 in. for 54 kHz transducers (the frequency used in this research). Cussigh (1999) used an *L* of 10 inches. At a frequency of 54 kHz, aggregate should have nominal dimensions no greater than 2.75 in., which is not a concern for precast, prestressed SCC. For reinforcement parallel to the direction of pulse transmission to not influence the signal, the bars must generally be laterally spaced at least 0.25*L* away from the test point, with a conservative estimate of 0.35*L* (Naik et al. 2004).

2.2.2.2 Pullout Testing

Bond between reinforcement and concrete is a material mechanical property of broad applicability to structural performance. Although many configurations have been used to test it, the principle is the same: apply tension to steel reinforcement cast into concrete specimens while recording the force applied. If the total bonded surface area is known, the bond stress is determined by dividing the pullout force by the surface area.

During this research, pullout testing was configured to cause pullout (concrete shear) failure. Pullout testing that results in pullout failure can give a measure of concrete quality and uniformity not affected by inadequate cover or steel quality (Khayat et al. 2003), which makes it useful for studying the potential effects of segregation in SCC.

It would seem most appropriate to study the bond capacity of SCC used in precast, prestressed applications by pulling out seven-wire prestressing strand instead of deformed steel reinforcement. Many researchers have studied the interaction between strand and concrete in large specimens with long bonded lengths. Khayat et al. (2003), Khayat and Mitchell (2009), and Stocker and Sozen (1970), on the other hand, tested bond to strand using a shortly bonded, pullout-failure-inducing configuration. However, in preliminary testing for this research, the researchers were unable to develop adequate bond between shortly bonded strand and the surrounding concrete, so pullout testing for this research was conducted using deformed steel reinforcement only.

2.2.2.3 Hardened Visual Stability Index

Visual inspection of cores can be conducted according to AASHTO PP-58 *Static Segregation of Hardened Self-Consolidating Concrete (SCC) Cylinders* (AASHTO 2012). The test and its result are typically referred to as the Hardened Visual Stability Index (HVSI). It is conceptually similar to the Visual Stability Index (VSI) fresh concrete stability test method—both involve assignment of an integer stability index value in the range of 0–3, with 0 indicating absolute uniformity and 3 indicating extreme segregation. Despite its potential subjectivity, Fang and Labi (2006), Johnson et al. (2010), and Lange et al. (2008) all found that the HVSI relates well with the quantifiable results of digital image analysis (DIA) when a standard procedure for determining the HVSI is used.

Lange et al. (2008) found that both HVSI and DIA results relate well with measured differential shrinkage stress, as well as finite element models of this stress. They found that increasing HVSI and decreasing DIA uniformity relate to increasing differential shrinkage stress in specimens, where larger shrinkage strain in paste-rich regions is restrained by aggregate-rich regions that shrink less.

HVSI inspection is conducted following the planar cutting of a specimen with a concrete saw. AASHTO PP-58 (2012) requires that the HVSI be assessed using a flat, rectangular surface that was revealed by cutting a specimen lengthwise. In that test method, an integer HVSI value ranging from 0–3 is assigned according to Table 2.1. Specimens representative of each HVSI value are illustrated in Figure 2.2–Figure 2.5. As alluded to in the table and shown in the figures, specimens are graded while oriented such that the “top” and “bottom” of the cut plane are oriented parallel to the direction of concrete placement. Wetting is required prior to evaluation in order to enhance the contrast between coarse aggregate and other constituents.

Table 2.1: Hardened Visual Stability Index Values from AASHTO PP-58 (2012)

HVSI Rating	Criteria
0, Stable	No mortar layer at the top of the cut plane; no variance in size/percent area of coarse aggregate distribution over ht.
1, Stable	No mortar layer at the top of the cut plane; slight variance in size/percent area of coarse aggregate distribution over ht.
2, Unstable	Mortar layer of less than 1 in. at the top of specimen; distinct variance in size/percent coarse agg. distribution over ht.
3, Unstable	Clearly segregated; mortar layer greater than 1 in. or considerable variance in size/percent area of coarse agg. distribution over height, or both

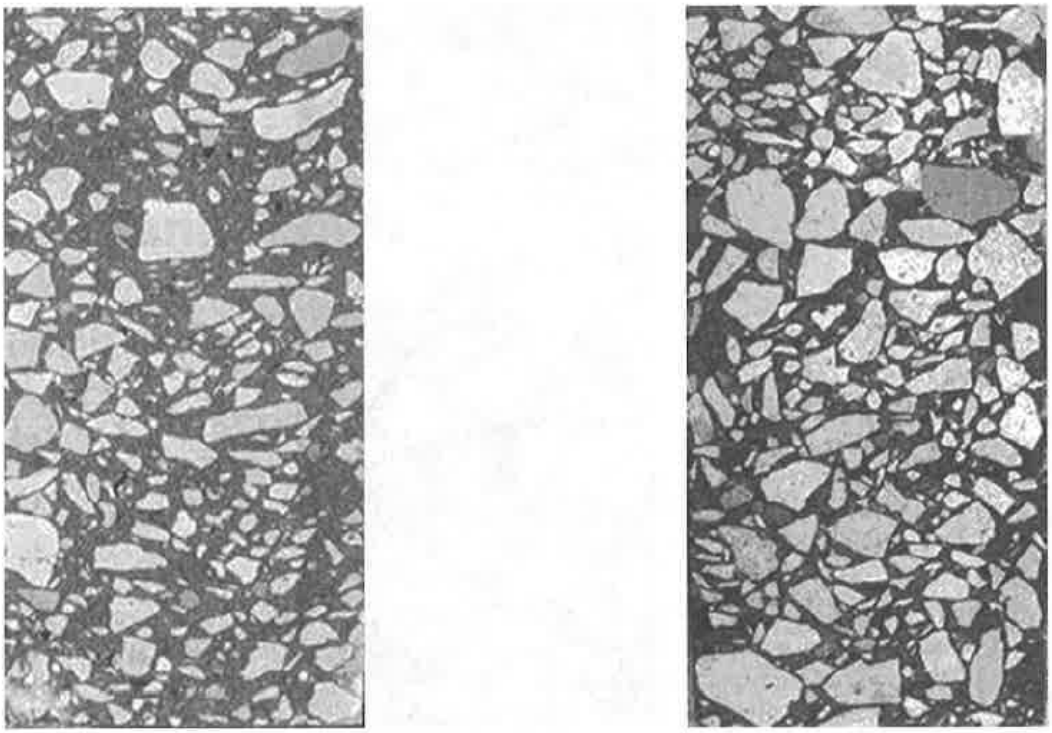

Figure 2.2: Cylinders exhibiting HVSI = 0, Stable (AASHTO PP-58 2012)

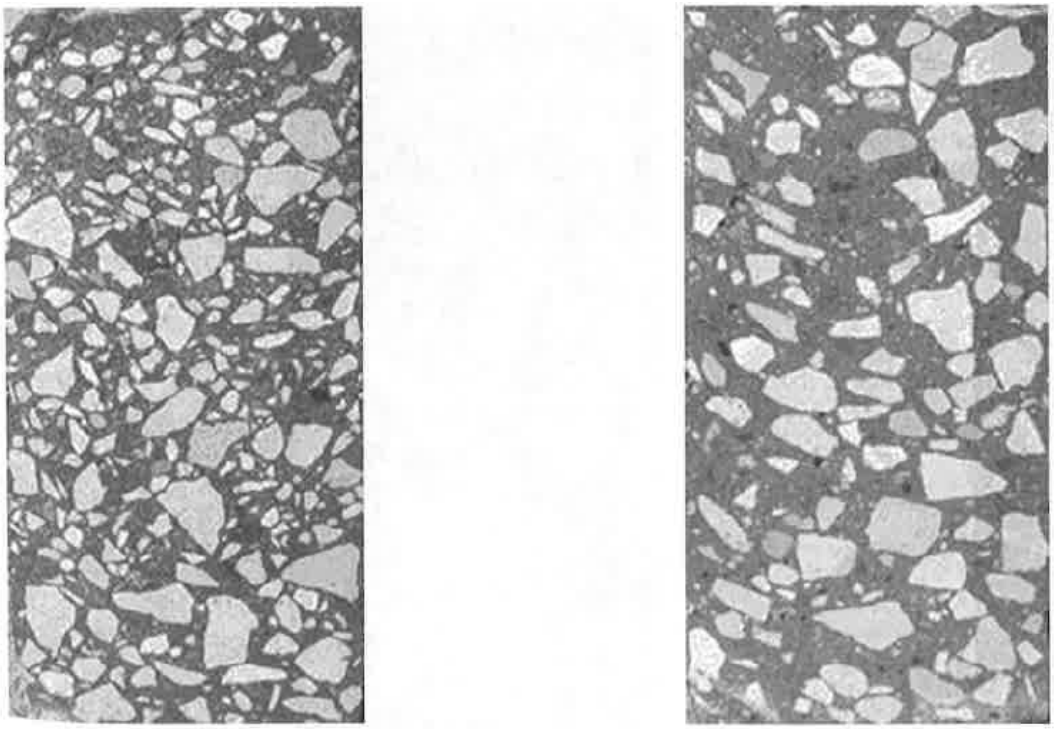

Figure 2.3: Cylinders exhibiting HVSI = 1, Stable (AASHTO PP-58 2012)

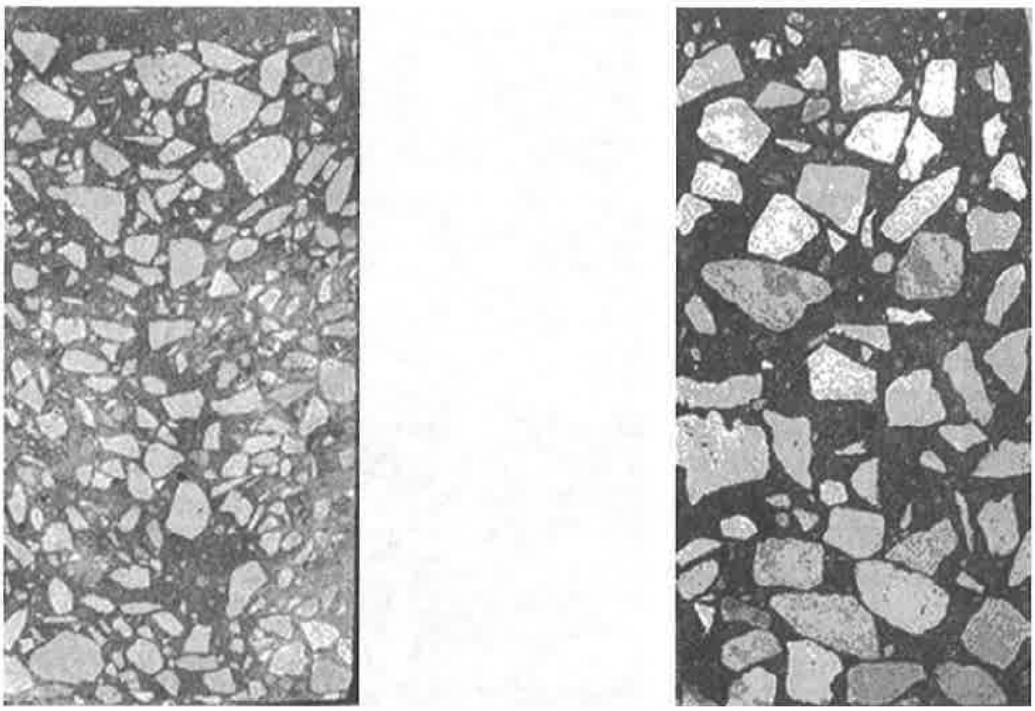

Figure 2.4: Cylinders exhibiting HVSI = 2, Unstable (AASHTO PP-58 2012)

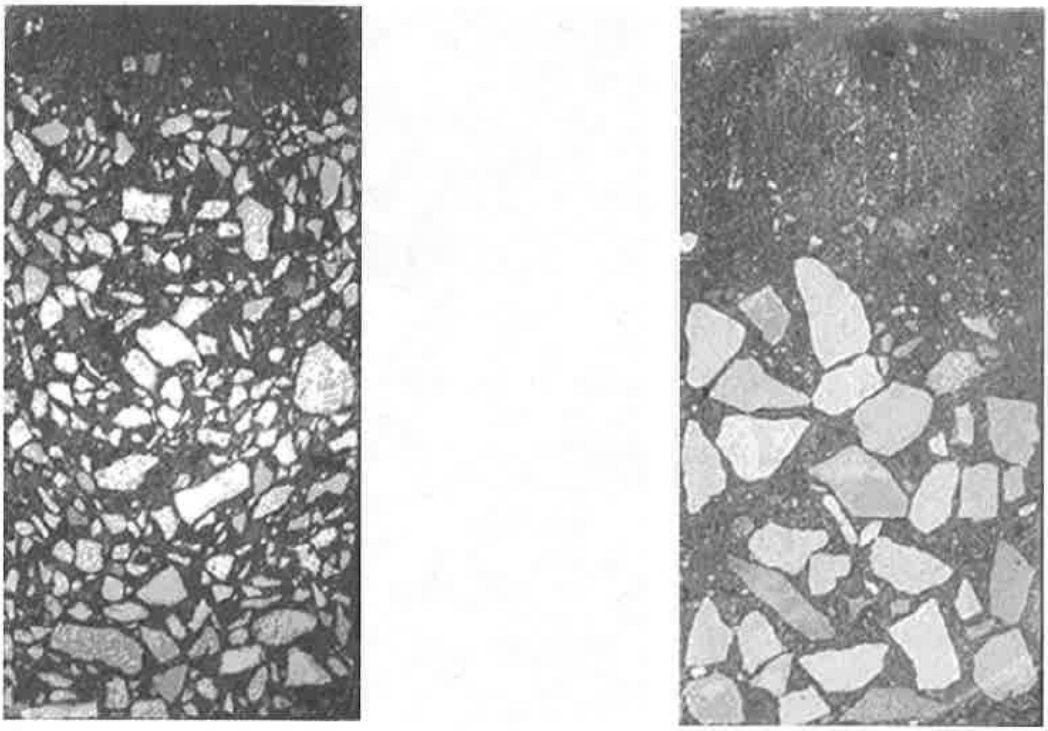

Figure 2.5: Cylinders exhibiting HVSI = 3, Unstable (AASHTO PP-58 2012)

2.2.2.4 Assessment of Digital Images

Flat surfaces, like those exposed for HVSI testing, are more easily scanned for DIA than three-dimensional surfaces, although researchers have frequently studied non-rectangular cross sections. Peterson et al. (2002) and Johnson et al. (2010) analyzed circular discs cut from cylindrical specimens. Khan and Kurtis (2010) analyzed planes of full-scale bulb-tee girders as shown in Figure 2.6.

Figure 2.6: Saw-cut cross section of a bulb-tee girder digitally analyzed for hardened concrete constituent distribution (Khan and Kurtis 2010)

Assessment of hardened concrete constituent uniformity by DIA involves calculation of exposed surface area of constituents, with an assumed relationship between surface area and implicit volume. This is deemed acceptable due to the random distribution of these three-dimensional constituents—while each plane may expose different constituents, the exposed area should be representative of the constituent volumes present due to the random distribution of constituents (Horta 2005; Shen 2007). DIA can focus on any of a wide range of concrete characteristics, including

- Air content and distribution, in which the analysis focuses on the small, circular voids present in the hardened sample (Peterson et al. 2002),
- Coarse aggregate size, volume, and distribution, in which the analysis focuses on large, discrete areas of aggregate that contrast with mortar (Lange et al. 2008; Horta 2005), or
- Aggregate lattice structure and “particle packing” arrangement, in which the analysis focuses on the macroscopic arrangement of constituents (Shen 2007).

Procedures developed for identification of these constituents have depended on the goals of the research. Researchers utilizing DIA to study hardened concrete have concluded that

- Contrast between the desired constituent and the surrounding material should be applied through the use of stains, paints or powders (Peterson et al. 2002),
- Phenolphthalein, a pH indicator for basic substances, can provide good contrast between cement and aggregate (Peterson et al. 2002),
- The quality of the DIA depends on the resolution and lighting of the digital image and is affected by polishing of the sample (Horta 2005; Johnson et al. 2010),
- Required resolution for DIA of coarse aggregate segregation need not exceed 1200 dpi, and a resolution as low as 300 dpi can be efficient and reasonably accurate (Johnson et al. 2010),
- Identification of aggregate cross-sectional area is more accurate than identification of gradation, as distinction between one large particle and multiple smaller particles is difficult (Fang and Labi 2006), and
- DIA is more difficult in concrete with varied aggregate coloration than in concrete with a uniform aggregate coloration (Johnson et al. 2010).

In all instances, researchers (Fang and Labi 2006; Johnson et al. 2010; Khan and Kurtis 2010; Peterson et al. 2002; Shen 2007) have utilized similar software algorithms for DIA. That process, which is illustrated in Figure 2.7, is typically as follows:

- Use color thresholds (RGB or similar) to delineate desired constituents from the surrounding material,
- Convert digital image to a binary format in which the desired constituent is one color and all other material is the other,
- Based on image resolution, use pixel counts to filter or delineate particles of distinct areas or average diameters, and
- Analyze filtered particles as necessary.

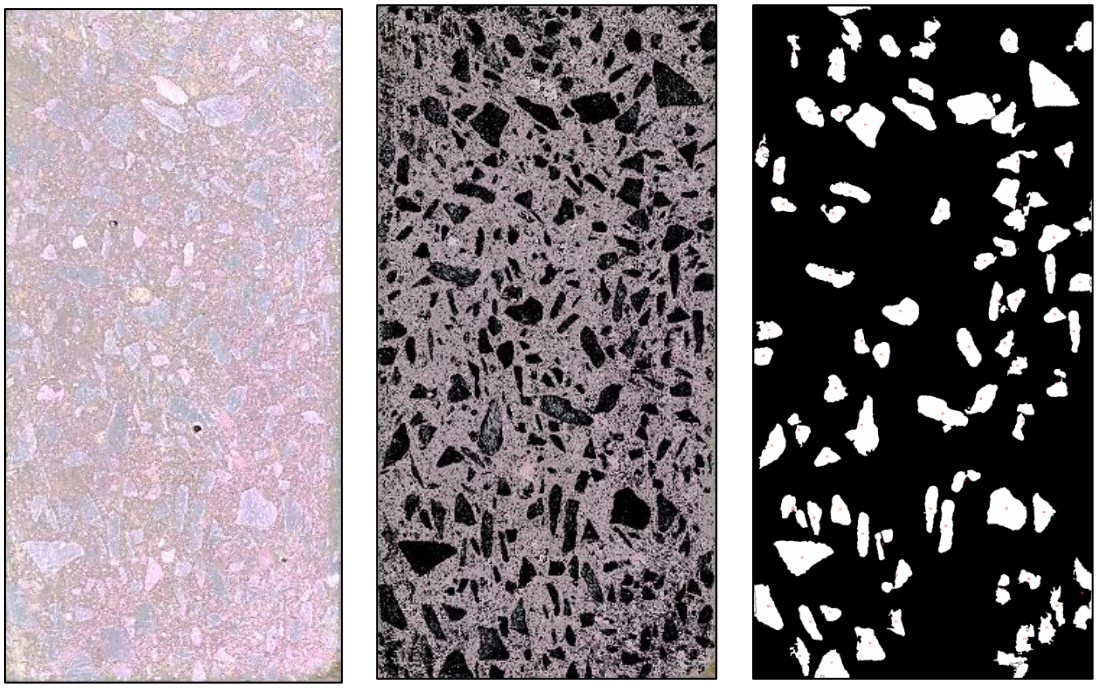

Figure 2.7: Digital imaging of a concrete specimen (*left*) as scanned, (*middle*) after color threshold and binary conversion, and (*right*), after identification of coarse aggregate

Fang and Labi (2006), Horta (2005), Johnson et al. (2010), Peterson et al. (2002), and Shen (2007) have independently attempted to automate the DIA process, but with limited success. Procedures (such as polishing and staining of specimens) and software algorithms (such as selection of a standard color threshold or pixel count) have varied widely. They determined that these variations are necessary because of the unique concrete material, scanning hardware, and computer software utilized in each situation.

2.2.3 Existing Acceptance Criteria

All of the fresh concrete stability tests described earlier have been used either to confirm the stability of tested SCC or to establish a level of segregation above which SCC should not be accepted. The measures of hardened concrete uniformity described in the previous subsection (from which many of these fresh test criteria were derived) can also be used to determine acceptable in-place uniformity. Test outputs at which tests indicate that problems with segregation may occur, as well as the origins and applicability of these outputs, are discussed in the following sections.

2.2.3.1 Fresh Property Test Criteria

Table 2.2 includes the outputs at which each fresh concrete stability test method indicates that problems associated with segregation may occur. Only results for tests that were chosen for evaluation during this research are included in the table; criteria established during the first phase of this AUHRC research are also presented.

Table 2.2: Acceptance limits for various stability test methods

Test Method	Acceptability Criteria		Recommended By
Visual Stability Index (ASTM C1611)	VSI ≤ 1		Khayat and Mitchell (2009)
	VSI ≤ 1.5		PCI (2004)
Column Segregation (ASTM C1610)	I_{seg} ≤ 15 %		Khayat and Mitchell (2009), Koehler and Fowler (2010)
	I_{seg} ≤ 10%		ACI 237 (2007)
Rapid Penetration (ASTM C1712)	Depth ≤ 0.4 in. = Seg. Resistant ≤ 1 in. = Moderately Resistant		Bui et al. (2007), ASTM C1712 (2009)
Sieve Stability	S ≤ 20% (Class 1) S ≤ 15% (Class 2) S ≤ 10% (demanding[1])		EPG (2005)
	5% ≤ S ≤ 15%		PCI (2004)
	S ≤ 10%		Keske et al. (2013b)
Surface Settlement	NMSA ≤ ½ in.	Set. rate ≤ 0.27 %/hr Set. max ≤ 0.5%	Khayat and Mitchell (2009)
	NMSA > ½ in.	Rate ≤ 0.12 %/hr Max ≤ 0.3%	
	Rate ≤ 0.15 %/hr		Keske et al. (2013b)

Note: [1] = when flow exceeds 15 ft or clear spacing is less than 3 in.

2.2.3.2 Ultrasonic Pulse Velocity and Pullout Uniformity

An acceptable level of concrete quality has been established using UPV results, but only for one known aggregate source (Solis-Carcano and Moreno 2008). To establish what UPV results

would be acceptable in cast members, Solis-Carcano and Moreno (2008) recorded velocities in cylinders prepared from 100 mixtures of varying compositions, and then they matched velocities to strengths in the mixtures. In subsequent tests of as-cast members, the pulse velocities measured in as-cast members were used to determine acceptable strength uniformity.

Cussigh (1999) did not directly determine a UPV variation that would be acceptable, but instead compared VC of varying degrees of consolidation and SCCs of varying stability. Whatever level of UPV variation was observed in conventionally accepted VC would serve as the benchmark for SCC UPV acceptability (Cussigh 1999). Meanwhile, during the first phase of this research, an acceptable level of UPV uniformity was established based on an observed correlation between UPV results and pullout results.

Although not unique to SCC (the top-bar effect can occur in all concretes), AASHTO (2013) and ACI 318 (2011) recognize the top-bar effect and account for it with a single factor, commonly known as the 'top-bar factor.' The top-bar factor is used in each code's equation for development length and applies to top-cast bars with greater than 12 in. of concrete cast below them. In these top-cast bars, the development length is multiplied by the top-bar factor in order to ensure the same bond capacity as in bottom-cast bars. The factor is defined as equaling

- 1.4 in *AASHTO LRFD* (2013) Section 5.11.2.1.2, and
- 1.3 in ACI 318 (2011) Section 12.2.4.

The top-bar factor was not created to limit the heterogeneity of SCC, but it does allow for a certain level of in-situ variability. If the top-bar effect present in an SCC is less than the code-accepted top-bar factor, then whatever heterogeneity is present must be acceptable for issues related to bond strength. Using this assumption, researchers have compared top-bar effects to the code-accepted top-bar factor to test the viability of SCC as a replacement for VC (Almeida Filho et al. 2008; Esfahani et al. 2008), or to determine acceptance criteria of fresh SCC stability test methods (Khayat and Mitchell 2009).

2.2.3.3 Distribution of Constituents in Hardened Concrete

Determination of acceptable concrete uniformity by inspection of hardened samples can focus on paste-layer depth, distribution of coarse aggregate within a sample, or changes in distribution of coarse aggregate between samples taken at multiple locations within large specimens. Shen et al. (2007) utilized the first of these measurements—paste-layer depth—to determine HVSI and wire-probe penetration acceptance criteria. Through the testing of small-scale samples and application of finite element models, they correlated paste layer depth to differential shrinkage stress (in which concrete with more stratified paste and aggregate layers shrinks differently than concrete with well-dispersed constituents). They found that a paste-layer depth exceeding

approximately ¼ in. and an HVSI exceeding 1 were observed in concrete that experienced unacceptable differential stresses, and thus, unacceptable hardened uniformity (Lange et al. 2008).

Khan and Kurtis (2010) determined the acceptability of hardened concrete constituent variation based on inference from ASTM C94, which governs the placement of ready-mixed concrete. According to that standard (ASTM C94-11a), the within-batch variation of coarse aggregate content, by percentage, is not to exceed 6%. The specification also includes limits on variation of f_c, air content, slump, unit weight of mortar, and unit weight of concrete. If the variation of more than one of these six measurements exceeds the proposed limit, then the concrete is considered non-uniform (ASTM C94 2011). Thus, if DIA of samples taken from various points within a specimen (within or between cross sections of BT-54 bulb-tees, in their research) exhibited greater than 6% coarse aggregate content coefficient of variation (COV), then the hardened concrete uniformity was deemed unacceptable. Notably, Khan and Kurtis (2010) utilized COV to determine acceptability, while ASTM C94 (2011) specifies a simple percentage difference for constituent variation calculation.

Johnson et al. (2010) also determined acceptability of coarse aggregate content and gradation variation using DIA, but with variation limits based on fresh test results (sieve stability S ≤ 20% and VSI ≤ 1.0). Their primary hardened concrete uniformity measure was a paste-area ratio, which they determined by sawing cylinders into discs and comparing the paste area at different heights within the cylinder. Based on correlation to the sieve stability test, they determined that the ratio of paste in the top of a cylinder to paste in the bottom of a cylinder should not exceed 1.15.

2.3 EXPERIMENTAL PROGRAM

2.3.1 Summary of Work

Five fresh concrete stability tests were selected for evaluation during this research:

- Visual stability index (ASTM C1611 2005),
- Column segregation test (ASTM C1610 2006),
- Rapid penetration test (ASTM C1712 2009),
- Sieve stability test (EPG 2005), and
- Surface settlement test (Khayat and Mitchell 2009).

To assess in-situ concrete uniformity, 3 yd^3 batches of concrete were delivered by ready-mixed concrete trucks to the Auburn University laboratory, and they were then placed in walls of three heights: 54 in., 72 in., and 94 in. The three specimen heights selected are approximately

incremental in height difference and correspond to the heights of typical precast bridge elements. This made it possible to study the potential correlation between section height and segregation.

The walls were tested using UPV testing, pullout testing, and HVSI and DIA testing in order to determine the in-situ effects of segregation. UPV testing is a nondestructive test method to evaluate the relative uniformity of hardened concrete specimens, and the pullout testing is a direct, destructive method for evaluation of the bond strength of concrete. To ensure that coring would not affect these two tests, HVSI and DIA testing was conducted last on cores taken from the top and bottom of the 72 in. walls.

Segregation can affect constituent dispersion and bond quality, and tests of these properties have been used to study the uniformity of SCC. During this research project, the test methods were used as complimentary, but independent, assessments of in-situ concrete uniformity. Therefore, each result was used to independently assess the ability of the fresh concrete stability test methods to identify hardened concrete uniformity.

The researchers desired to assess the fresh stability tests over the full range of segregation severity, so a total of twenty precast, prestressed-suitable SCC mixtures and four VC mixtures were placed that would provide varied fresh stability test results and degrees of in-situ uniformity. The SCC mixtures were divided into four approximately equal groups, each of which was tested over a range of segregation severity. The VC mixtures were intended to serve as control mixtures for the SCC groups. Full-scale testing was conducted on a seven- to eight-day cycle.

2.3.2 Mixture Preparation

To accommodate the fresh concrete stability testing and wall casting for this research, approximately 2.25 yd^3 of concrete were needed for each concrete batch. To account for waste and ensure sampling uniformity, 3 yd^3 were produced for each testing cycle. As it was impossible to mix such a large volume in a single batch at the Auburn University (AU) Structural Engineering Laboratory in the Harbert Engineering Center (“the laboratory”), the majority of batching and mixing took place at the Twin City Concrete plant (“the plant”) in Auburn, Alabama. Certain aspects of mixture preparation thus required the cooperation of Twin City Concrete, while other aspects of concrete production unique to the research project were conducted at the laboratory upon receipt of each batch.

2.3.2.1 Ready-Mixed Concrete Plant Mixing Procedures

Prior to batching, AU staff gathered samples of coarse and fine aggregate to determine their moisture content at the laboratory. Plant staff then batched all materials except HRWR

admixture, VMA, and a predetermined amount of additional water into a ready-mixed concrete truck for mixing and delivery. AU staff added hydration-stabilizing admixture directly into ready-mixed concrete truck before it departed for delivery to the laboratory. Additional mixing took place as the truck drove to the laboratory, a trip that took approximately fifteen minutes. Per AU staff requests, the ready-mixed concrete trucks used minimal mixer rotation during transport.

2.3.2.2 Laboratory Mixing Procedures

Upon arrival of the ready-mixed concrete truck at the laboratory, several activities were conducted before discharging the concrete for placement:

1) Add a predetermined amount of water (if desired to adjust stability and filling ability) using five-gallon buckets,
2) Add an initial dose of HRWRA (every mixture) and VMA (if desired to adjust stability),
3) Mix the concrete in the ready-mixed concrete truck for 30 drum revolutions at half of the truck's maximum rotational speed,
4) Wait two minutes to allow the dispersed chemical admixtures to take effect, and
5) Rotate the mixer to bring the concrete up to a visible level in the truck, and either add additional HRWRA (if visibly necessary to achieve required filling ability), add additional VMA (if visibly necessary to further adjust stability), or dispense a small sample for acceptance testing.

Once the mixture reached the apparent level of filling ability desired, the truck's chute was positioned above a waste container, and a five-gallon bucket of concrete was captured directly from the chute as concrete was discharged into the waste container. The mixer was not rotated during acceptance testing of the sample, which took approximately four minutes. The chute of the ready-mixed concrete truck was washed before any additional concrete was dispensed in order to remove deleterious material.

Acceptance of each batch of SCC was based on the filling ability and stability as determined by the slump flow test and VSI, and acceptance of each VC batch was based on the slump test. The goal for the various SCC mixtures was to create concretes that achieved high levels of filling ability (slumps exceeding 25 in.) while exhibiting VSI values ranging from 0.0–3.0. The goal for the four VC mixtures was to obtain the workability necessary for precast, prestressed applications with slumps of 3.5–7.0 inches.

In mixtures that did not achieve a minimum of 25 in. of slump flow, or that were more stable than desired for a particular testing cycle, HRWRA was added in 1–3 oz/cwt increments until the SCC exhibited the desired fresh properties. Similar to initial mixing, the adjusted mixture was mixed for thirty revolutions at a slow speed and allowed to rest for two minutes before

retesting. Partly because chemical admixture effectiveness would diminish over time, and partly because remixing added air content, no batch was accepted that required more than three dosages of chemical admixture (consisting of an initial dosage plus two additions).

2.3.2.3 Sampling for Required Tests

Once a desirable combination of slump flow and VSI was achieved, the batch was dispensed from the ready-mixed concrete truck into a 1.5 yd^3 placement bucket. During SCC placements, the following placement order was followed:

1) Fill a sampling container with enough concrete to perform all fresh concrete stability tests and start to fill strength cylinders.
2) Cast the 94-inch-tall wall in a single lift.
3) Refill the bucket from the ready-mixed concrete truck.
4) Cast the 72-inch-tall wall in a single lift.
5) Refill the bucket from the ready-mixed concrete truck.
6) Refill the sampling container to finish casting of all strength cylinders.
7) Cast the 54-inch-tall wall in a single lift.

During VC placements, the above order of placement was adjusted to accommodate consolidation efforts. Following the recommendations set forth by PCI (2004), lifts of approximately 18 in. were placed and then consolidated using a 1-inch-diameter internal vibrator. The same order of wall placement was followed as previously described for the placement of SCC.

2.3.3 Fresh Testing

The VSI was chosen for evaluation because it is the most frequently specified on-site quality assurance test method. The column segregation test was chosen because it is the only considered test that involves physically determining the aggregate distribution over the height of a sample, and it is an ASTM standardized test method for characterization of the static stability of SCC. The rapid penetration test was chosen because it the fastest test offering a completely objective result and is the most recently ASTM standardized test to assess SCC stability.

The sieve stability test was selected because it is recommended by a European consortium of concrete producers as the primary stability test in Europe (EPG 2005) and was found to characterize stability well by Keske et al. (2013b). The surface settlement test was selected because it is recommended in NCHRP Report 628 (Khayat and Mitchell 2009) as the primary stability test for precast, prestressed SCC and was also found to effectively characterize

stability by Keske et al. (2013b). All fresh concrete stability tests were conducted in accordance with the recommendations set forth in Section 2.2.1 or, where available, their respective ASTM standards. The test procedures given in Appendix B of Keske et al. (2015) were derived from the most current version of test instructions available to the researcher at the beginning of testing in November 2009.

Pairs of each of these five tests were used in conjunction with the casting of the three walls described in Section 2.3.4. A total of 10 ft^3 of concrete was needed to perform all fresh stability testing, so wheelbarrows and plastic-lined boxes with a volume exceeding 16 ft^3 were filled for sampling. The first tests begun were the tests for air content, unit weight, and temperature, all of which were conducted with a single sample. The tests for air content, unit weight, and temperature were conducted only once.

The two slump flow and VSI tests were run consecutively. The two iterations were conducted consecutively so that a single operator could conduct them (to eliminate between-user variation) while ensuring that the time spent evaluating the VSI of the first sample would not interfere with evaluation of the second sample. Also, rapid penetration testing was conducted on the same sample as the slump flow and VSI during the placement of SCC-1 and SCC-2 and was conducted separately during the placement of SCC-3 and SCC-4. This occurrence is further discussed in a later paragraph.

The order of filling and initiation of the other tests, in which pairs of samples were tested simultaneously, was as follows:

1) Rapid penetration test (when conducted separately),
2) Sieve stability test,
3) Column segregation test, and
4) Surface settlement test.

This order of preparation and initiation was used during every testing cycle. Although fresh properties may not have been identical at the beginning of each fresh test, all tests were initiated quickly enough (within ten minutes) that very little change was expected in fresh concrete behavior. Also, to reduce the risk of time-sensitive changes in the material during the initiation of all tests, hydration-stabilizing admixture was added to each batch in the ready-mixed concrete truck to delay setting until long after wall casting. Information on the hydration-stabilizing admixture, as well the other mixture constituents, is located in Section 2.3.4.4.

2.3.3.1 Slump Flow, Rapid Penetration Test, and Visual Stability Index

During SCC placements, the slump flow test was first performed prior to initiating wall placement (as part of acceptance testing). It was performed again to coincide with the other fresh concrete

stability tests, and only the result of that second test was used for analysis. During the placement of the first nine SCC mixtures (SCC-1 and SCC-2), the second slump flow (after beginning the casting of walls) was tested in conjunction with the rapid penetration test and the VSI. Performing all three of these tests simultaneously met the individual time requirements specified for each, so it was convenient to conduct all three tests on the same sample.

During the placement of the latter eleven SCC mixtures (SCC-3 and SCC-4), the slump flow and VSI were conducted on separate samples from those used for rapid penetration testing. This was done because 1) the additional rest period required for the rapid penetration test appeared to occasionally affect the outcome of the VSI test, and 2) additional rapid penetration testing of SCC-3 and SCC-4 was conducted after rest periods of five and ten minutes, which necessitated the simultaneous use of six rapid penetration samples. These additional pairs were conducted to determine if prolonging the rest period of the test would improve the test's accuracy. During the latter eleven tests, each pair of rapid penetration tests was conducted simultaneously.

2.3.3.2 Column Segregation Test

The column segregation test was conducted in accordance with ASTM C1610 (2006) using the apparatus shown in Figure 2.8. The two column segregation tests were started simultaneously using concrete collected from a single sampling container. Although the white column segregation mold shown has four segments, only the top and bottom portions of concrete were collected for comparison—four-part segmentation improved the ease of testing, but ASTM C1610 only requires comparison of aggregate volumes of the top and bottom quartiles.

Figure 2.8: Two column segregation molds used during simultaneous testing

2.3.3.3 Sieve Stability Test

The sieve stability test, which measures the percentage of SCC passing through a sieve as it falls from a predetermined height, was conducted according to the procedure outlined in Appendix B.1 of Keske et al. (2015). As suggested in the European Guidelines for SCC (EPG 2005) to ensure a consistent pouring height, the sieve stability test was operated with the use of the pouring apparatus. A waterproof, rubberized scale with a precision of 0.005 lb was used for the sieve stability test. The European Project Group (2005) recommended using a 5 mm (0.20 in.) sieve, but the American equivalent, a No. 4 (0.25 in.) sieve was used instead. This was deemed acceptable considering the literature reviewed in Section 2.2.1.4, as well as considering the practicality of using a US standard sieve more commonly available in the US than a metric sieve.

During the latter eleven SCC placements (SCC-3 and SCC-4), an additional three pairs of the sieve stability test were conducted as described in Appendix B.1 of Keske et al. (2015), except that their rest periods were varied. This was done to evaluate the efficiency and applicability of abbreviating the sieve stability test rest time. The three alternative rest times were eighty seconds, five minutes, and ten minutes. These times were chosen to equal the standard rest time for the rapid penetration test (eighty seconds) and provide incremental periods up to the standard sieve stability rest time (fifteen minutes).

2.3.3.4 Surface Settlement Test

The surface settlement test, which measures the settlement of an acrylic plate into a column of concrete, was conducted according to the procedure outlined in Appendix B.2 of Keske et al. (2015) and recommended by NCHRP 628 (Khayat and Mitchell 2009). A linear variable differential transformer (LVDT) was recommended by Khayat and Mitchell (2009) to continuously record the settlement of the acrylic plate. However, readings were only necessary every five minutes, and the Auburn University researchers desired to use a measurement instrument offering the least risk of either applying downward pressure or resisting settlement of the surface settlement plate. Therefore, a springless digital dial gauge and springless analog dial gauge were used. The gauges are shown in Figure 2.9.

Figure 2.9: Surface settlement test equipment with (*left*) analog dial gauge and (*right*) digital indicator

The gauges displayed displacements of up to 2 in. with a precision of 0.0001 in., which met the requirements of Khayat and Mitchell (2009). The gauges were supplied by Chicago Dial Instruments. Removal of the return spring meant the measurement rod was able to fall freely as the plate settled. The rod weighed one gram, which was accounted for in manufacturing an acrylic settlement plate of the required weight.

2.3.4 Hardened Concrete Testing

During each testing cycle, hardened concrete testing (UPV, pullout, and coring) was conducted on walls to establish the level of in-situ uniformity of each concrete mixture, and strength cylinders were cast to establish each concrete's strength profile. The construction and testing considerations for these activities are described in the following subsections.

2.3.4.1 Large-Scale Walls

Since section height can potentially affect the degree of segregation, specimens of three heights were cast, each matching the height of a typical precast component:

- 54 in. to match an AASHTO Type IV or AASHTO/PCI BT-54 bridge girder,
- 72 in. to match an AASHTO Type VI or AASHTO/PCI BT-72 bridge girder, and
- 94 in. to match an AASHTO-PCI-ASBI 2400-1 standard segment.

The wall heights selected changed in approximately even increments, making it possible to observe height-based trends in segregation. While some dynamic segregation could occur during the filling of the walls, height trends were primarily due to static segregation rather than variable dynamic effects of free-fall placement because a trunk was used to place concrete in the 94 in. and 72 in. walls. This trunk limited the free-fall drop height in those walls to less than 60 in., in accordance with the guidelines for free-fall placement of concrete set forth in *AASHTO Bridge Construction Specifications* (2010) Section 8.7.3.1.

A consistent width and thickness of 40 in. and 8 in., respectively, was utilized in all walls. These dimensions, as well as the location of form ties and hoist anchors permanently cast into the walls, were selected primarily in consideration of the hardened concrete testing configuration desired. The details of those configurations are described in Sections 2.3.4.2 and 2.3.4.3. As explained in those sections, a lateral distance of at least 4 in. was kept between each UPV reading location and the nearest pullout bar, form tie, or wall edge, and 8 in. was kept between pullout bars.

Selection of a wall width of 40 in. thus made it possible to test five vertical lines of UPV measurement locations and four vertical lines of pullout bars, alternating each vertical line with a lateral spacing of 4 in. on-center. A thickness of 8 in. was selected for all walls based on past studies and testing configurations identified in Sections 2.2.2.1 and 2.2.2.2 and on the calculation that unreinforced walls of that thickness would be structurally sound under flexural and tensile loads encountered during maneuvering and testing.

Threaded-rod form ties were used to control the outward deflection of forms under the pressure exerted by the fresh concrete. The 94 in. wall used eight ties, the 72 in. wall used six, and the 54 in. wall used four. These ties, and hoist anchors cast into the walls to assist in lifting and moving, were all placed to keep at least 4 in. clear spacing to any UPV measurement location and at least 3 in. clear spacing from the nearest pullout bar. The minimum clear spacing between parallel reinforcement required by ACI 318 (2011) to allow uninhibited placement was 1 in., which was exceeded in all cases.

As described in Section 2.2.2.1, UPV testing for the purpose of comparative uniformity testing is most effective at very early ages. A testing age of two days was selected as a compromise between early-age testing needs and strength needs to ensure that the walls would

be sufficiently strong during form removal and moving. Work crews began stripping the formwork from each wall while the next wall was being moved and anchored, which allowed for UPV testing of the walls to be conducted continuously at as close to an age of forty-eight hours as possible. Although the completion of form removal typically took two hours, all form ties and joints were loosened at 48 hours to allow exposure to laboratory humidity and temperature conditions.

After the forms were removed, wax construction pencils were used to mark a UPV measurement location grid onto each wall, and UPV testing was conducted as soon as possible thereafter. The walls were then left in this position until an age of at least six days, after which they were laid horizontally in order to conduct pullout testing at a concrete age of thirteen days. The walls were left in a vertical orientation for as long as possible in order to limit the risk of damage from loads that could occur either while being moved or while supported horizontally prior to testing.

To tip the walls from their as-cast vertical orientation to the horizontal orientation needed to conduct pullout testing, the walls were then lifted with an overhead crane, moved into place on concrete blocks, and tipped over to lie horizontally on the concrete blocks. Local stresses from lifting were only experienced near the points where hoist anchors were cast into the walls, which were always at least 8 in. from the nearest pullout specimen location. While on the blocks, the walls rested on rubber pads that were aligned near their corners. This support system was used to limit the flexural stresses experienced by the walls while in a horizontal orientation and to ensure adequate clearance for instrumentation during pullout testing.

2.3.4.2 Ultrasonic Pulse Velocity Testing

Ultrasonic pulse velocity (UPV) testing was conducted on each group of walls two days after casting. The testing equipment used was a Pundit Plus portable ultrasonic instrument from Germann Industries. Following the testing recommendations of Section 2.2.2.1, the Pundit Plus was configured for continuous 54 kHz testing. It displayed ten readings per second at a precision of ± 0.1 microseconds. An alcohol-based ultrasound jelly was used between each metal coupler and wall surface to create a continuous ultrasound path, and the couplers were pressed firmly against the wall surfaces until an unchanging reading was observed.

Rows of UPV and pullout testing were approximately uniform, with slight variations to avoid pullout bars and form ties. As mentioned in Section 2.2.2.1, UPV testing through concrete at 54 kHz requires a minimum of 2.8 in. of clear spacing to the nearest obstacle oriented parallel to the direction of wave transmission. Typical spacing between UPV measurement points was six to eight inches, and no point was located less than four inches from the nearest edge or obstacle. The configuration used during the testing of SCC-1 and SCC-2 is shown in Figure 2.10, and the configuration used during the testing of SCC-3 and SCC-4 is shown in Figure 2.11.

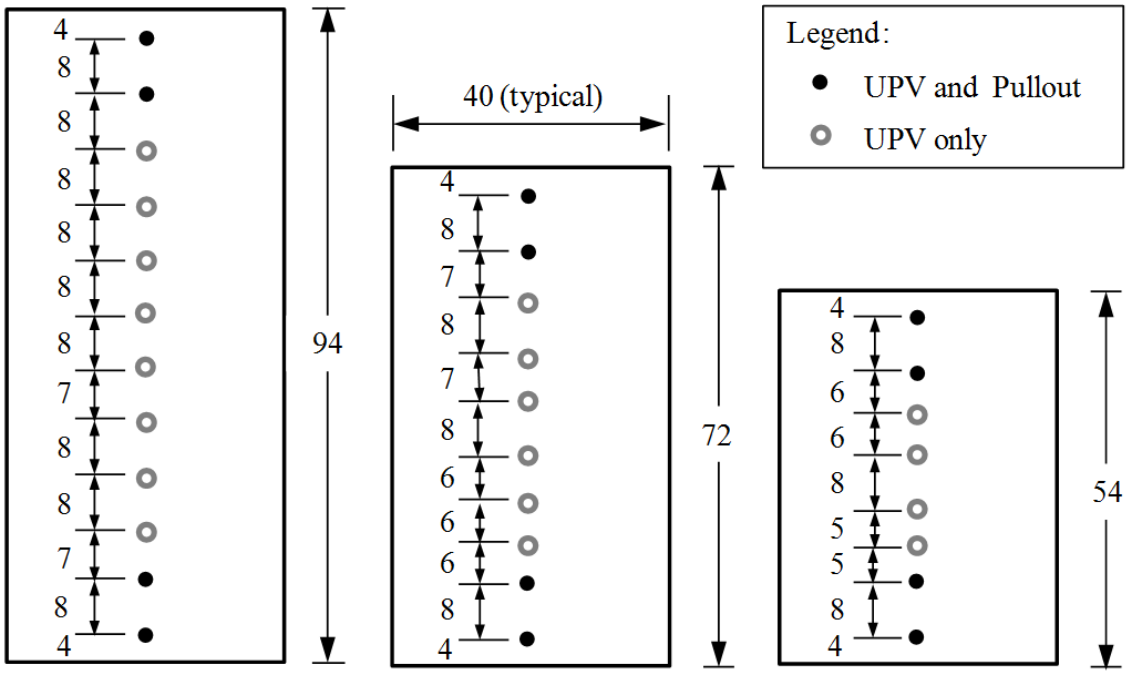

Figure 2.10: Location of UPV measurement and pullout testing locations on SCC-1 and SCC-2 walls (*Note: All measurements in inches*)

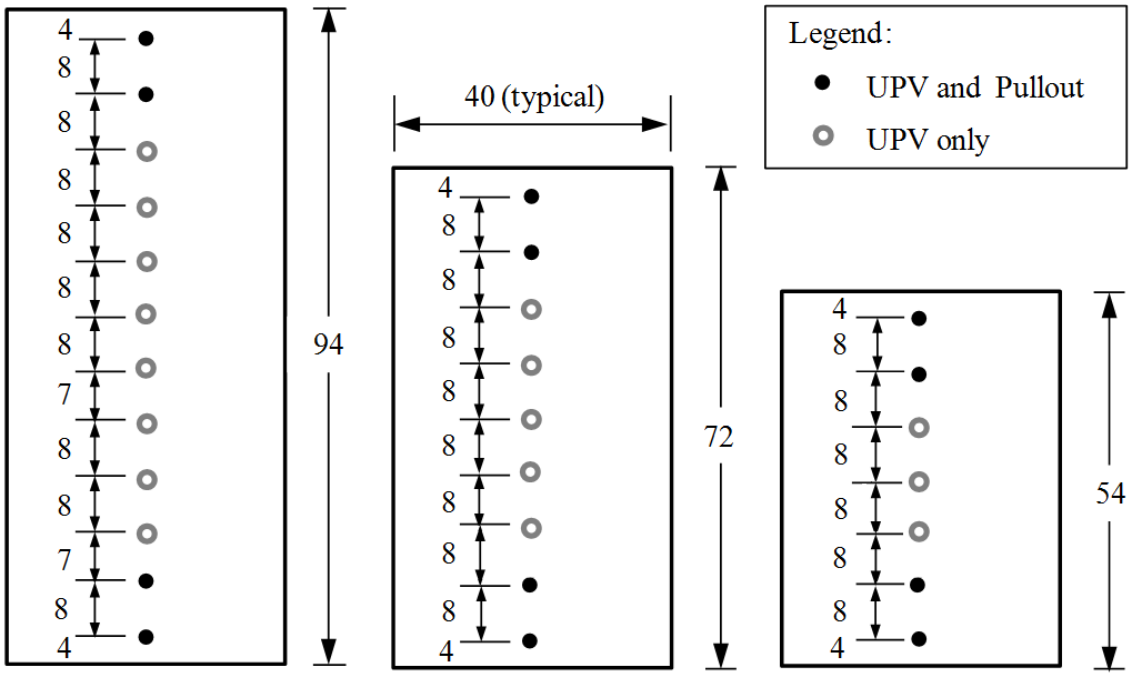

Figure 2.11: Location of UPV measurement and pullout testing locations on SCC-3 and SCC-4 walls (*Note: All measurements in inches*)

UPV measurement points were labeled to ensure proper location of wall thickness measurements necessary to calculate pulse velocities. The caliper used to measure wall thicknesses was constructed by welding parallel rectangular steel tubing 9 ± 0.01 in. apart. One leg of the caliper was laid flush with one side of the 8 in. thick wall, and a 1/100th in. gradation steel ruler was used to read the distance from the other side of the wall to the inner face of the second leg. Using this system, the wall thickness at each UPV test location was measured with a precision of ± 0.02 in., which falls well within the precision required by ASTM C597 (2002).

2.3.4.3 Pullout Testing

Pullout testing was conducted on the walls thirteen days after casting. The location of each four-bar row of pullout bar specimens is noted in Figure 2.10 and Figure 2.11. To ensure adequate cover as described in Section 2.2.2.2, the top and bottom rows of bars were located four inches from the top and bottom of each wall. A distance of eight inches was employed between each vertical line of bars so that

- An 8 in. wide reaction frame would be equally spaced between the bar being pulled out and the nearest adjacent bars,
- A 4 in. radius would be kept between the reaction frame and pullout bar in order to dissipate potential confining forces, and
- A 4 in. radius would be kept between the nearest UPV testing location and any pullout bar, as previously explained in Section 2.3.4.2.

2.3.4.3.1 Configuration of Bars

Pullout testing for this project was conducted using No. 4 reinforcing bars from two batches provided by Nucor Steel, Inc. of Birmingham, Alabama. The batches exhibited a yield stress of 68 ksi in tensile testing by Nucor, which was confirmed by the AU researchers through the tensile testing of randomly selected bars from the batch.

Based on the past research described in Section 2.2.2.2, a bonded length of 2.5 d_b, or 1.25 in., was selected in order to ensure a shearing pullout failure of the concrete, instead of splitting or conical failure. The short bonded length also limited the possibility of steel yielding due to the bond strength of this high-strength concrete. This preparation involved several steps:

1. Nonabsorbent paper was first cut into 1.25-inch-wide strips after being marked with a 1/100th in. gradation steel ruler.
2. After the bar was cleaned, the paper was taped to the desired location along the length of the pullout specimen,
3. At least one inch on either side of the paper was coated with Type I silicone,

4. After allowing the silicone to dry for at least one day, the paper was peeled away, leaving an exposed length of 2.5 d_b enclosed on both ends by permanent silicone.
5. Lastly, commercially available strand-debonding sheathing was placed on both sides of the exposed section (over the silicone) and securely taped into place using electrical tape.

Once it was encapsulated in concrete, the bonded region of steel began 4 in. away from the loaded face of the concrete wall, similar to the configurations used by Khayat (1998) and Sonebi and Bartos (1999). Unlike those configurations, the end of the bonded region was not flush with the unloaded face of the wall. It was decided that placing the bonded region close to the middle of the wall thickness would remove the risk of uncharacteristic pullout behavior from two sources: different collection of bleed water and aggregate at the face of the wall, and flexural stresses experienced by the wall under its own weight. The surface friction and the preferred orientation of aggregate at the face of the wall could lead to irregularity at this face, and flexure experienced by the wall in a horizontal, simply supported orientation could place the concrete near the top face in compression while reducing the compression at the bottom face of concrete.

To both accommodate sealing the other joints and avoid contaminating the pullout bars with form release agent, the pullout bars were placed in the erected formwork after the forms had been sealed and sprayed. Consequently, insertion of the bars was the last activity performed before placement of concrete, leaving at least twenty-four hours between when the bars were sealed with Type I silicone on the outer face of the formwork and when the concrete was cast.

2.3.4.3.2 Configuration of Pullout Testing Equipment

Both the 8 in. tall reaction chair and the center-hole hydraulic cylinder (jack) used in this research project, as well as the aluminum load cell and chuck placed above them, are illustrated in Figure 2.12. This configuration was based on the configuration used by Khayat and Mitchell (2009), which was discussed earlier. The load cell had a precision of ± 0.5 lb and was capable of resisting up to 40,000 pounds of compressive force. The jack, with a capacity of 120,000 pounds, was operated with an air-powered hydraulic pump.

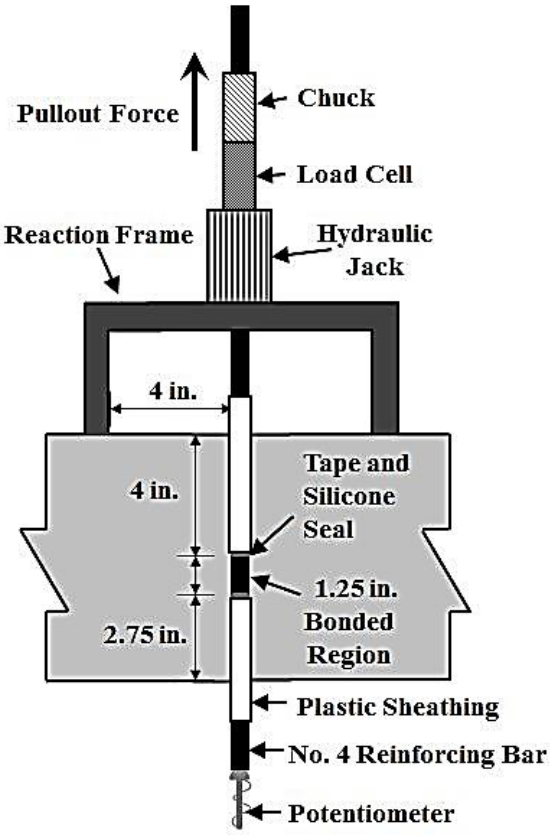

Figure 2.12: Pullout testing configuration

Loading was displacement-controlled by controlling the airflow into an air-powered hydraulic pump serving a 120,000-pound center-hole hydraulic cylinder (jack). Displacement of the unloaded end of the pullout bar was measured using a linear displacement potentiometer. Loading was not discontinued until the free-end slip of the bar was more than double the slip at maximum pullout force. Only one of the more than 1,400 tested bars yielded before reaching its maximum pullout force. In that occurrence, pullout force plateaued and free-end slip ceased while the jack continued to extend. That result was not used in analysis, as the uniformity of bond stress could have been affected by yielding of the steel bar.

The pullout testing configuration made it possible to pull out each bar with minimal additional confining pressure, without damaging the surrounding concrete, and without causing dynamic loading effects. An Optim MEGADAC data acquisition system was utilized for all data collection. Time, load, and slip were instantaneously displayed by the acquisition system and were viewable during testing, which made it possible to monitor and record load and free-end slip. The research team was thus immediately made aware of equipment malfunction, bar yielding, or testing completion.

Based on small-scale trial pullout testing, a relationship between bond strength and concrete compressive strength was determined to estimate the necessary minimum yield strength

of the rebar (68 ksi) and maximum compressive strength of the concrete (12,000 psi) that would prevent steel yielding during testing. This relationship was corroborated by research results from Khayat (1997) and Stocker and Sozen (1970). These strengths were taken into consideration when selecting concrete mixture proportions, which are described in Section 2.3.5, and when choosing to use deformed bars instead of seven-wire strand.

2.3.4.4 Compressive Strength Assessment

Standard 6-inch-diameter by 12-inch-high cylinders were cast for each mixture. They were used for compressive strength testing at each of the following ages: two days, to coincide with form removal and UPV testing; thirteen days, to coincide with pullout testing; and twenty-eight days, to establish a standard compressive strength for each mixture. SCC cylinders were cast in a single lift by pouring the concrete from a five-gallon bucket in a steady motion, filling the molds in 3 ± 1 seconds. No rodding or consolidation was used, but the outside of each mold was lightly tapped with a rubber mallet to remove any air pockets caught against the inside of the mold walls.

Molds were removed from the cylinders at the same time as form removal, at two days. The cylinders were then left adjacent to the walls so that they would be exposed to similar laboratory drying and curing conditions.

2.3.4.5 Hardened Visual Stability Testing and Digital Image Analysis

Hardened visual stability testing and digital image analysis of the 72 in. walls cast with SCC-3 and SCC-4 were conducted following completion of UPV and pullout testing. While coring was not available during the casting of SCC-1 and SCC-2 due to time and equipment constraints, the Auburn University researchers added coring during the testing of SCC-3 and SCC-4 once resources became available for it. Four-inch-diameter cores removed from the top and bottom of the 72 in. walls. Only 72 in. walls were cored because of time, effort, and storage constraints, as the coring and analysis took an extended amount of time.

Coring of large-scale elements provides a direct, visual means of determining the uniformity of hardened concrete. Visual assessment of the HVSI is standardized by AASHTO PP-58 (AASHTO 2012), and numerous researchers (Johnson et al. 2010; Khan and Kurtis 2010; and Lange et al. 2008) have utilized digital image analysis of specimens to study hardened uniformity of SCC.

2.3.4.5.1 Coring Configuration

Coring for this project was conducted using a commercially-available coring apparatus with a diamond-embedded 4.0-inch-diameter coring barrel. This coring barrel diameter was selected in light of the orientation of the cores, which is shown in Figure 2.13. As shown in the figure, the cores were extracted parallel to the direction of casting near the middle of the wall thickness. One core was always taken at the middle of the width of the wall (in the 40-inch direction), and the other was taken approximately 8 in. to one side of this core. Thus, the cores paralleled two of the five vertical UPV measurement lines and bisected vertical pullout specimen lines. This coring orientation had several advantages:

- The cores were directly in line with UPV measurement locations, which, like in the UPV measurements, should limit interference from nearby pullout specimens,
- No planes through the cylinder exposed regions of concrete near the broad faces of the walls (where preferred aggregate alignment and formwork friction could affect apparent uniformity),
- Cores with a height-to-width ratio of 2:1 in the direction of casting were able to be acquired as recommended by AASHTO PP-58 (AASHTO 2012), and
- The 2:1 height-to-width aspect ratio of the cores in the direction of casting allowed more accurate inspection of any height-based trends in segregation.

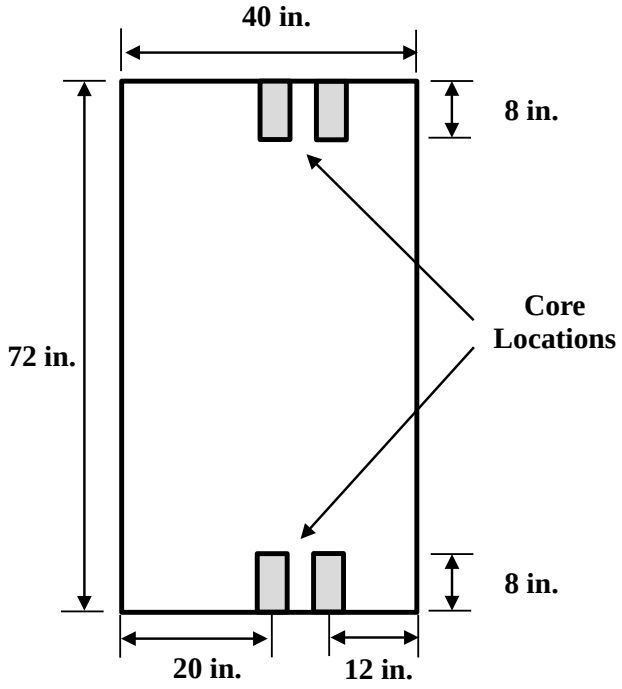

Figure 2.13: Core extraction locations

Following their extraction, the cores were cut vertically along a randomly selected plane that passed through the center of the core. While this cutting direction differed from that used by Johnson et al. (2010) (they cut cores into circular discs), it was the direction specified for assessment of the HVSI according to AASHTO PP-58 (2012). A randomly selected plane was deemed acceptable for two reasons: 1) any randomly selected plane should expose an approximately equal distribution of constituents given the orientation of the cores, and 2) AASHTO PP-58 gives no guidance on this topic.

Four cores were extracted from each wall (two from the top and two from the bottom of each), which yielded eight potentially assessable surfaces upon cutting. However, within each core, the two surfaces were only separated by the thickness of the saw blade used to separate them. Thus, they may not be independent samples, so only one randomly selected surface from each exposed pair was used in all testing. The same surface was used for HVSI and DIA testing in order to assess potential relationships between the tests.

2.3.4.5.2 Assessment of the Hardened Visual Stability Index

AASHTO PP-58 (2012) suggests that, when using cores to determine the HVSI, the cores be taken from the top-cast portion of concrete. Therefore, only two surfaces were evaluated per SCC-3 and SCC-4 mixture. Four individuals were trained to assess the HVSI by review of information in AASHTO PP-58 and Section 2.2.2.3 and by assessment of cores not used for this research. They were each then allowed to independently assess all of the specimens collected from SCC-3 and SCC-4. The individuals were shown the specimens in a random order, and they were given no indication of the other fresh or hardened results measured in each represented mixture.

2.3.4.5.3 Digital Image Assessment

Digital image assessment was the final hardened concrete test method conducted for each concrete mixture. The fifty-two specimens (four from each of eleven SCC and two VC walls) were prepared for DIA using the following procedure:

1. The surfaces were coarsely sanded using a concrete grinding stone in order to remove surface irregularities left by the concrete saw,
2. They were then finely sanded using a silica-based 100-grit sandpaper in order to remove any fine-to-moderate surface scratches left by the grinding stone,
3. Contrast between the cement and aggregate was enhanced by spraying the surfaces with phenolphthalein diluted to a 1:1 ratio with ethyl alcohol, and
4. Dust and residue were then removed by wiping the specimens with a 300-grit abrasive sponge.

The above procedure is in line with recommendations discussed in Section 2.2.2.4. After completing the above steps, the specimens were scanned in RGB color at 300 dpi using a commercially-available flatbed scanner. All subsequent analysis was conducted with the assistance of *ImageJ*, an open-source digital image editing software package. The primary hardened property analyzed with DIA was coarse aggregate surface area percentage. This measurement was chosen because

- Researchers could visually confirm, in the actual specimens, any digitally identified coarse aggregate,
- Coarse aggregate content is simpler to assess and simpler to interpret than coarse aggregate gradation (Johnson et al. 2010), and
- DIA was affected differently by mixture variation than UPV measurements, which depend on a wide range of factors (air content, localized *w/cm*, relative strength of paste to aggregate, etc.).

In order to assess coarse aggregate content in the region, coloration thresholds, image refinement algorithms, and particle size filters and were applied to each image. The red, green, and blue thresholds for binary conversion had to be varied to meet the unique properties of each image. This variability is well-documented in Section 2.2.2.4, and it precluded the use of standardized color thresholds. The results of RGB conversion were always confirmed by visual comparison to the physical specimen being studied, as shown in Figure 2.14.

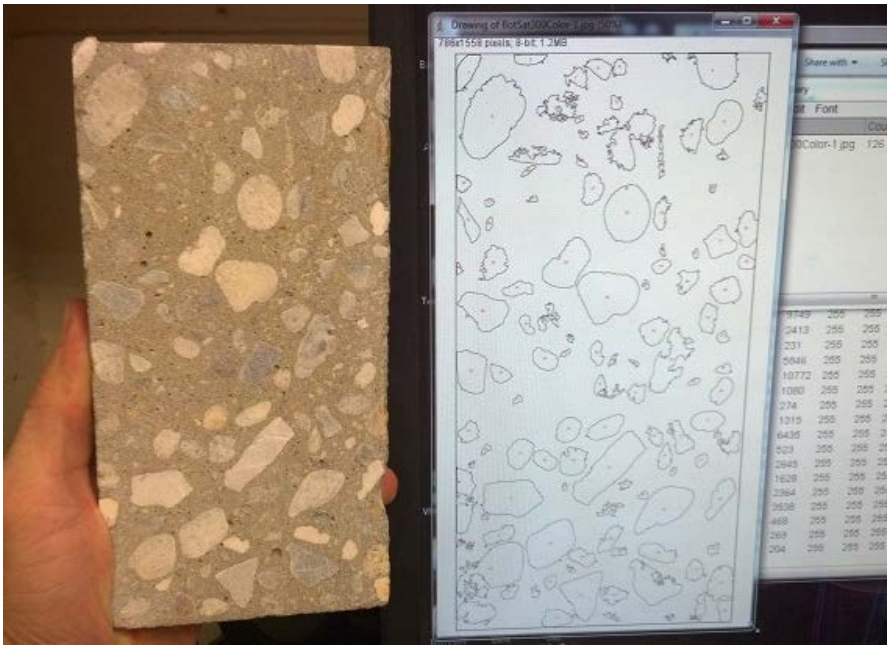

Figure 2.14: Comparison of actual specimen to digital identification of coarse aggregate

Areas of less than a 10-pixel (0.033 in.) diameter were filled to match their surroundings, as shown in Figure 2.15. Removal of these particles, or despeckling of the image, only affects air voids and scanner static. Despeckling smoothed and heightened the contrast between coarse aggregate and their surroundings. Also, as cross-sectional area measurements were based on total highlighted pixels, more accurate area measurements were obtained by despeckling of coarse aggregate (which would have no internal voids).

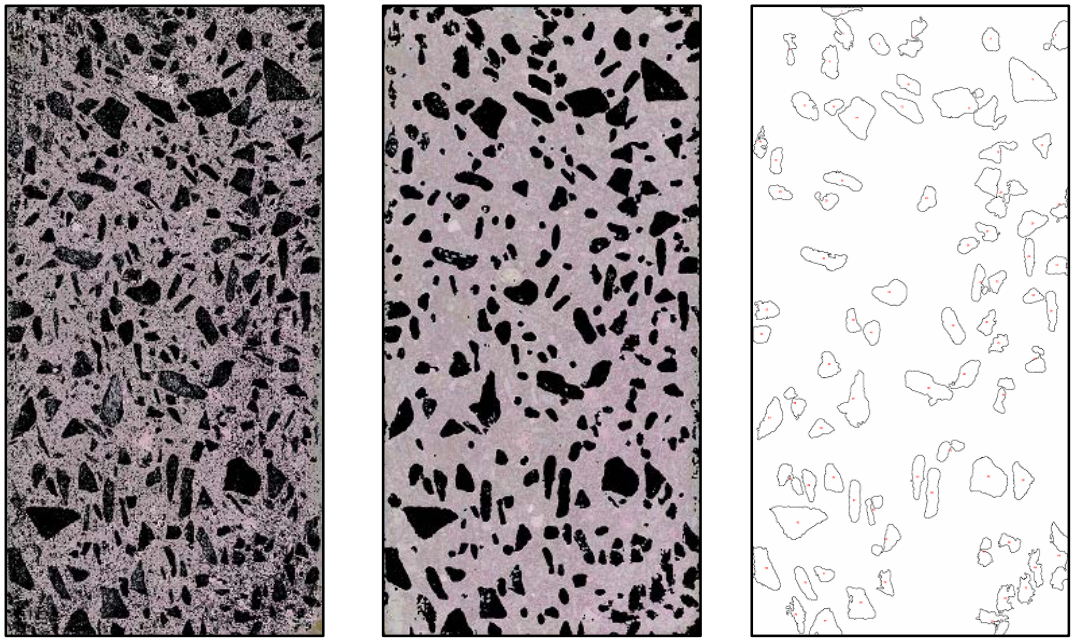

Figure 2.15: Scanned image of concrete (*left*) after binary conversion, (*middle*) after despeckling of image, and (*right*) after identification of coarse aggregate particles

The minimum area which would be identified as coarse aggregate was 2700 pixels. This corresponded to an area of 0.03 in.^{2}, which equals 75% of the sieve-opening area of a No. 4 sieve. According to ASTM C33 (2011), no less than 95% of fine aggregate passes the No. 4 sieve. The researchers decided to use 75% of that area to identify coarse aggregate because angular coarse aggregate whose average diameter is less than that of a No 4 sieve opening may still be retained. It was also in line with the practices of Fang and Labi (2006) and Shen (2007).

After these thresholds were applied, a preprogrammed algorithm of *ImageJ* was used to find the percentage of the image highlighted as coarse aggregate. This process was applied to all four specimens per mixture.

2.3.5 Mixtures and Raw Materials

Two of the self-consolidating concrete mixtures used for this research, SCC-1 and SCC-2, were based on mixture proportions developed by Schindler et al. (2007) for precast, prestressed applications. To expand the applicability of the results to mixtures that could be expected in SCC construction, an additional two, SCC-3 and SCC-4, were developed by augmenting the coarse aggregate portion of SCC-1 and SCC-2. SCC-3 used the same aggregate type (crushed limestone typical of Alabama precast, prestressed construction) but a reduced total aggregate fraction. SCC-4 was very similar to SCC-3, except that it used uncrushed siliceous river gravel.

Each of these primary mixtures was accompanied by several mixtures that were deliberately adjusted to obtain varying levels of stability. Vibrated concrete was also proportioned to mimic the early-age strength characteristics of each primary SCC mixture while exhibiting workability suitable for precast, prestressed applications. A total of twenty-four concrete mixtures were used—twenty SCC mixtures and four VC mixtures.

2.3.5.1 Mixture Design

SCC-1 was proportioned to achieve relatively higher strength but less flowability, and SCC-2 was proportioned to achieve moderate strength and higher flowability. SCC-3 was proportioned to mimic both SCC-1 and SCC-2, but with a total aggregate fraction of approximately 60%. This aggregate content was selected to provide contrast to SCC-1 and SCC-2, both of which contained aggregate fractions above 65%, and to clearly meet the limitations of the rapid penetration test (ASTM C1712 2009), which was developed for use only in mixtures with less than 65% total aggregate volume. SCC-4 was very similar to SCC-3, except that it used uncrushed siliceous river gravel.

From each of these four primary mixtures, other mixtures of the same cementitious content, aggregate content, and aggregate proportioning were created with varying stabilities. The stability was adjusted by changing the water content, HRWRA dosage, or VMA dosage, or by changing a combination of them. The majority of the mixtures were proportioned with stabilities whose acceptance would be marginal. This is the apparent stability at which the use of quantitative, less subjective fresh concrete stability tests should be most beneficial.

Four VC mixtures were selected as control mixtures to mimic each primary SCC mixture. The control mixtures employed a higher *w/cm*, lower *s/agg*, and different coarse aggregate gradation than the SCC mixtures. These changes were selected because VCs typically employ a larger gradation of stone (¾ in.) and lower *s/agg* than recommended for SCC. Still, the following were expected: that each mixture's slump and early-age compressive strength would be relevant to the represented SCC, and their proportions relative to each other would mirror the differences

between the SCCs. A hydration-stabilizing admixture was used in all mixtures. This dosage was not varied, and it was the minimum effective dosage recommended by the manufacturer. The proportions used are shown in Table 2.3 at the end of Section 2.3.

2.3.5.2 Raw Materials and Proportions

Materials used for this project were all locally available. Lafarge Type I portland cement was used because Type III portland cement is characterized by rapid setting and early-age strength gains. This could have jeopardized the researcher's ability to initiate all fresh tests while the concrete was still in the dormant period, and the use of Type III portland cement offered no long-term benefits over Type I portland cement in terms of testability.

Some of the mixtures (all SCC-2 mixtures and approximately half of SCC-3 and SCC-4 mixtures) incorporated a 30% replacement of Type I portland cement with Class C fly ash. This offered the possibility of producing concrete with a different characteristic workability and reaction to adjustments in stability modifiers (water, HRWRA, and VMA). The coarse aggregate used for SCC-1, -2, and -3 matched the No. 78 gradation crushed limestone used in earlier studies of SCC conducted at Auburn University. SCC-4 was proportioned with No. 67 (¾ in. NMSA) uncrushed river gravel. It was selected to expand the applicability of the fresh and hardened property assessment and because it offered the possibility of producing a concrete with a different fresh behavior.

Crushed limestone for SCC-1, -2, and -3, as well as matching VC control mixtures VC-1, VC-2, and VC-3, was supplied by Vulcan Materials of Calera, Alabama. Uncrushed river gravel for SCC-4 and VC-4 was supplied by Martin-Marietta Materials of Shorter, Alabama. Fine aggregate was well-graded natural sand taken from the ready-mixed concrete plant's general supply.

Table 2.3: Concrete mixture proportions

Mixture ID	Cement (pcy)	Fly Ash (pcy)	Water (pcy)	*w/cm*	Coarse Agg. (pcy)	Fine Agg. (pcy)	*sand/ total agg*	*total agg. vol.* (%)	HRWRA (oz/cwt)	VMA 1 (oz/cwt)	VMA 2 (oz/cwt)
VC-1	640	0	270	0.42	1,977	1,167	0.37	67.6	11	0	0
SCC-1A	750	0	270	0.36	1,680	1,342	0.44	66.9	6	2	0
SCC-1B	750	0	310	0.41	1,680	1,342	0.44	67.1	6	2	0
SCC-1C	750	0	295	0.39	1,680	1,342	0.44	62.8	11	2	0
SCC-1D	750	0	270	0.36	1,680	1,342	0.44	60.8	9	0	0
VC-2	450	190	290	0.45	1,935	1,125	0.37	67.4	2	0	0
SCC-2A	475	200	270	0.40	1,663	1,360	0.45	64.8	11	0	0
SCC-2B	475	200	270	0.40	1,663	1,360	0.45	66.4	12	0	0
SCC-2C	475	200	270	0.40	1,663	1,360	0.45	67.6	13	0	2
SCC-2D	475	200	290	0.43	1,663	1,360	0.45	66.7	5	0	0
SCC-2E	475	200	270	0.40	1,663	1,360	0.45	66.5	9	0	2
VC-3	655	0	240	0.37	1,970	1,205	0.38	69.5	4	0	0
SCC-3A	900	0	330	0.37	1,545	1,220	0.46	61.0	8	3	0
SCC-3B	900	0	350	0.39	1,545	1,220	0.46	60.1	6	0	3
SCC-3C	900	0	330	0.37	1,545	1,220	0.46	60.4	10	0	0
SCC-3D	550	240	330	0.42	1,605	1,160	0.42	62.3	7	3	0
SCC-3E	550	240	350	0.44	1,605	1,160	0.42	60.9	8	0	2
SCC-3F	550	240	330	0.42	1,605	1,160	0.42	60.8	8	0	0
VC-4	465	195	275	0.42	1,875	1,100	0.36	67.1	11	0	0
SCC-4A	910	0	360	0.40	1,485	1,143	0.43	59.5	6	0	4
SCC-4B	910	0	335	0.37	1,485	1,143	0.43	59.5	8	0	0
SCC-4C	560	240	335	0.42	1,500	1,235	0.45	62.1	5	0	2
SCC-4D	560	240	360	0.45	1,500	1,235	0.45	61.5	8	0	0
SCC-4E	560	240	335	0.42	1,500	1,235	0.45	62.0	6	0	3

Notes: HRWRA = Glenium 7500, VMA 1 = Rheomac 362, and VMA 2 = Rheomac 450

2.4 PRESENTATION AND ANALYSIS OF RESULTS

2.4.1 Concrete Production

Using the proportions shown in Table 2.3, twenty-four concretes were produced and tested with five fresh concrete stability and four hardened concrete uniformity test methods. Because of the varied proportions, as well as because of fluctuations in batching, mixing, handling, and ambient conditions, the concretes achieved different fresh and hardened properties. Some of these properties are shown in Table 2.4.

When comparing Table 2.3 and Table 2.4, mixtures that were proportioned to be very similar exhibited different fresh and compressive strength behaviors. The research team assumes that this inconsistency was the result of batching fluctuation at the ready-mixed concrete plant. This suspicion was supported by evidence of incorrect batching (wrong aggregate or gradation) observed upon receipt of some batches; batches that were obviously incorrect were rejected, while others of questionable proportioning were included. Minor inconsistency from specified proportions was deemed acceptable because the proportions used in each mixture were less important than the resulting stability of each. In other words, fluctuations from the proportions listed in Table 2.3 do not affect the viability of the data collected.

Table 2.4: Fresh properties and compressive strengths of concrete mixtures

Mixture ID	Fresh Concrete Properties				Compressive Strength, f_c (psi)		
	Slump Flow (in.)	T_{50} (sec.)	Total Air (%)	Unit Wt. (lb/ft^3)	2 day	13 day	28 day
VC-1	5.5[1]	-	4.0	149.5	4,680	6,700	7,440
SCC-1A	27.5	2.3	2.0	152.8	4,690	7,110	7,390
SCC-1B	25.5	6.9	1.7	150.8	5,230	8,030	8,460
SCC-1C	27.0	1.5	5.5	144.2	4,340	6,320	6,780
SCC-1D	26.0	1.3	9.5	138.5	3,200	4,790	5,190
VC-2	7.0[1]	-	2.3	148.9	2,460	5,000	5,390
SCC-2A	28.0	1.5	6.0	144.6	2,510	5,010	5,530
SCC-2B	27.5	2.1	3.6	148.5	1,820	4,160	4,410
SCC-2C	26.0	8.0	1.8	148.8	2,620	5,300	5,880
SCC-2D	25.5	1.5	2.3	145.2	2,200	4,370	5,060
SCC-2E	26.0	4.0	3.5	145.3	2,720	4,890	5,290
VC-3	3.5[1]	-	4.1	150.9	3,330	5,240	6,590
SCC-3A	28.5	1.6	1.3	156.3	4,620	6,050	7,060
SCC-3B	29.5	3.8	1.6	157.1	3,840	5,500	6,970
SCC-3C	26.75	2.1	2.3	157.6	5,910	7,220	8,390
SCC-3D	30.0	1.4	1.2	155.6	3,070	4,840	6,180
SCC-3E	30.5	2.9	2.3	157.1	2,770	3,990	5,980
SCC-3F	27.0	1.9	3.7	158.1	6,680	8,380	10,190
VC-4	7.0[1]	-	3.3	158.9	2,520	4,220	5,760
SCC-4A	28.0	4.5	1.3	151.3	2,070	3,350	4,740
SCC-4B	25.25	2.0	3.0	156.2	6,150	7,360	8,450
SCC-4C	27.5	3.3	1.5	154.6	4,200	5,930	7,070
SCC-4D	26.75	1.4	1.1	153.2	1,610	2,700	3,780
SCC-4E	28.0	4.1	1.6	154.2	3,210	4,740	6,100

Note: [1] = conventional slump

2.4.2 Fresh Concrete Stability Tests

Summary results of the five fresh concrete stability tests conducted on each mixture are presented in Table 2.5. All results shown are those obtained while utilizing standard test

procedures; alternatively-timed results of the sieve stability and rapid penetration tests are discussed later. Complete test data used to calculate fresh results are reported in Appendix A of Keske (2014).

Table 2.5: Fresh concrete stability test results

Mixture ID	VSI	Segregation Index (%)	Rapid Penetration (in.)	Sieve Fraction (%)	Rate of Settlement (%/hr)	Maximum Settlement (%)
SCC-1A	2	5.6	0.26	N.A.	0.15	0.60
SCC-1B	0.75	0.0	0.20	6.5	0.15	0.35
SCC-1C	1.25	8.4	0.12	8.2	0.11	0.03
SCC-1D	1.25	17.5	0.33	15.8	0.02	0.01
SCC-2A	1.75	8.0	0.35	13.8	0.05	0.02
SCC-2B	3	20	0.30	30.5	0.25	0.14
SCC-2C	1.75	3.0	0.30	9.0	0.12	0.09
SCC-2D	1.25	11.1	0.10	5.2	0.25	0.13
SCC-3A	1.75	15.4	0.08	5.2	0.20	0.17
SCC-3B	1.5	6.5	0.04	4.4	0.32	0.23
SCC-3C	0	2.9	0.24	2.8	0.14	0.15
SCC-3D	2	24.9	0.16	11.9	0.35	0.49
SCC-3E	1.25	3.9	0.04	5.2	0.35	0.49
SCC-3F	0.5	4.6	0.16	1.9	0.12	0.08
SCC-4A	2	21.3	0.43	21.3	0.22	0.49
SCC-4B	0.25	8.0	0.04	8	0.10	0.07
SCC-4C	0.5	24.1	0.20	17.6	0.28	0.32
SCC-4D	2.5	26.7	0.12	21.1	0.59	0.86
SCC-4E	1.5	19.6	0.16	21.6	0.29	0.29

Note: N.A. = not available because sieve fraction result was recorded incorrectly

In Table 2.5, each fresh test result represents the average of two tests conducted simultaneously, except that VSI values are always the average from two consecutive tests, and rapid penetration depth values for SCC-1 and SCC-2 mixtures are the average of two consecutive tests. For consistency, it was deemed best to have a single operator conduct both repetitions of the VSI test. The conversion of rapid penetration testing from consecutive-sample testing to simultaneous-sample testing was described in Section 2.3.3.1—extended testing of SCC-3 and SCC-4 required the use of separate samples, and the standard rest period required

for the rapid penetration test appeared to occasionally affect the VSI test during the testing of SCC-1 and SCC-2.

Visual stability index values other than the discrete values discussed earlier (0, 0.5, 1, 1.5, 2, or 3) indicate average values in instances in which the two VSI tests yielded different results. Although the two samples were obtained from the same sampling container, identical test results were not guaranteed. The research team took measures to avoid between-user variability (see Section 2.3.3.1), so occurrence of nonmatching VSI test results is simply a possible result of the test method.

The acrylic settlement plate of one surface settlement test apparatus sank unevenly into the test sample during placement of SCC-1A and SCC-4D, which nullified the result obtained from that apparatus during the respective cycles. This problem probably occurred because the SCC being tested was so unstable that the thin acrylic plate was unevenly engulfed as it settled. Each time, the result of the second surface settlement test indicated unacceptably high segregation according to the recommendation of Khayat and Mitchell (2009), which reinforces the possibility that failure of the first apparatus was due to the use of a highly segregating mixture and not testing error.

Results of the sieve stability and rapid penetration tests taken at alternative (abbreviated or delayed) times are presented in Table 2.6. These alterative measurements were taken to evaluate the applicability of abbreviating the sieve stability test or prolonging the rapid penetration test. These alternatives were considered following completion of the first phase of this testing and were, thus, only measured in the eleven SCC-3 and SCC-4 mixtures. The test procedures were unaltered except by changing the rest period required prior to placement of the settlement probe in the rapid penetration test or pouring of a sample onto the sieve and pan in the sieve stability test. Therefore, only test usability, in the form of total test time required, was affected by the change.

Table 2.6: Alternatively timed rapid penetration and sieve stability test results

Mixture ID	Rapid Penetration (in.)			Sieve Fraction (%)			
	80 sec.[1]	5 min.	10 min.	15 min.[1]	10 min.	5 min.	80 sec.
SCC-3A	0.08	0.08	0.04	5.2	5.1	8.1	7.7
SCC-3B	0.04	0.08	0.08	4.4	7.4	6.4	7
SCC-3C	0.24	0.16	0.20	2.8	3.3	2.7	2.4
SCC-3D	0.16	0.12	0.12	11.9	11.2	10.4	13.5
SCC-3E	0.04	0.08	0.04	5.2	7.5	4.9	5.8
SCC-3F	0.16	0.08	0.00	1.9	4.7	3.5	3.8
SCC-4A	0.43	0.39	0.16	21.3	24.5	16	20.4
SCC-4B	0.04	0.08	0.04	8	12.5	12.7	12.6
SCC-4C	0.20	0.16	0.16	17.6	18.6	16.5	16.3
SCC-4D	0.12	0.16	0.12	21.1	21.1	20	19.2
SCC-4E	0.16	0.24	0.12	21.6	25.4	18.3	17.5

Note: [1] = time specified by governing standard

2.4.2.1 Correlations between Fresh Concrete Stability Results

Five standardized fresh concrete stability test results were obtained for each concrete, along with multiple additional, alternatively-timed fresh test results for SCC-3 and SCC-4. Each concrete's results were compared to each other in order to identify any correlations between the fresh stability test methods. Because the alternatively-timed results were only obtained for approximately half of the concrete mixtures, analysis of their results is presented separately in a later subsection.

Table 2.7 is a correlation matrix that shows the linear-regression coefficients of determination (R^2) between each fresh stability test when comparing all twenty SCC mixtures. Sieve stability and rapid penetration test results are those obtained after the standard rest times so that all twenty results would be comparable. A nonlinear model was also applied to each relationship, but no test relationship's R^2-value significantly improved by its use. In the table, R^2-values are highlighted to show relative strength—the smallest bold value is at least 50% greater than all non-highlighted R^2-values, thus indicating a division of relative correlation strength.

Table 2.7: Fresh concrete stability result linear-regression coefficients of determination

Test Result	VSI	Seg. Index	Rapid Pen.	Sieved Fraction	Rate of Settlement	Max. Settlement
Maximum Settlement	0.14	0.14	0.00	0.08	**0.60**	-
Rate of Settlement	0.16	0.26	0.00	0.08	-	
Sieved Fraction	**0.43**	**0.56**	0.28	-		
Rapid Penetration	0.06	0.05	-			
Segregation Index	0.24	-				
VSI	-					

In the table, the linear correlations having the greatest R^2-values were the correlations between the sieve stability test and the VSI and column segregation tests, as well as the test correlation between rate of settlement and maximum settlement determined from the surface settlement test. These three strong correlations are discussed further in Sections 2.4.2.2 through 2.4.2.4. The rapid penetration test and surface settlement test do not exhibit a reasonable correlation with the VSI, column segregation test, sieve stability test, or each other.

To conduct a more refined comparison of the fresh concrete stability results, consideration had to be given to potential variables that could subdivide the twenty SCC mixtures. In the previously shown comparisons of all twenty mixtures, strong correlations indicate that the compared fresh tests appear to be universally related within the range of mixtures tested. While universal relation is preferable, fresh tests that exhibit situational, but equally strong relationships can still be of value in a quality assurance setting, where certain variables are known. Distinct subdivisions that were introduced through the selection of the twenty mixtures shown in Table 2.3 include

- Coarse aggregate NMSA, in which two groups existed (fifteen ½ in.-NMSA mixtures and five ¾ in.-NMSA mixtures),
- Total aggregate volume, in which groupings would depend upon an arbitrary delineation of total aggregate volume (such as 65%, a limitation employed in ASTM C1712), and
- A combination of coarse aggregate NMSA and total aggregate volume, in which the grouping of ½ in.-NMSA mixtures (fifteen mixtures) was sufficiently large enough to subdivide by total aggregate volume.

The only other feasible variable, *w/cm*, cannot be independently evaluated. Batching variations such as those described in Section 2.4.1 make identification of exact in-situ *w/cm* impossible, both during this research and during typical quality assurance testing. Thus, division of fresh test results by *w/cm* is not feasible. Similar difficulty exists in determining the exact total aggregate volume except when considering the *target* total aggregate volume. The total aggregate volume varied during this research because of variation in batching and in-situ air content, but the four primary mixtures were proportioned to exhibit distinctly different target total aggregate volumes. SCC-1 and SCC-2 were proportioned for a target total aggregate volume of 67%, while SCC-3 and SCC-4 were proportioned for a target of 60%.

The researchers chose to proportion mixtures for two distinct target-aggregate-volume groups for two reasons: 1) the applicability of the rapid penetration test criteria was unclear in the SCC-1 and SCC-2 mixtures due to their relatively high total aggregate volumes (Keske et al. 2013b), and 2) different stability behavior occurs in mixtures of distinctly different aggregate volumes (Bonen and Shah 2004; Koehler and Fowler 2008; and Shen 2007). For this analysis, a 65% delineation for target total aggregate volume was chosen in consideration of ASTM C1712 (2009) and to approximately evenly divide the twenty SCC mixtures (nine greater than 65%, eleven less than 65%)

Table 2.8 consists of linear-regression coefficients of determination (R^2) between each fresh concrete stability test when subdivided by coarse aggregate NMSA, target total aggregate volume, or, among the ½ in.-NMSA mixtures, a combination of NMSA and aggregate volume. All possible two-test comparisons are presented (10 combinations) except those involving the maximum settlement determined from the surface settlement test. Reasons for its exclusion are discussed further in Section 2.4.2.4. In the table, R^2-values are highlighted in bold that meet the following criteria:

- A statistically significant difference, at a 90% confidence interval (CI), is observed between the classes of linearly correlated fresh results, and
- The R^2-value for at least one class improved by greater than 0.10 versus the R^2-value calculated from the twenty-mixture comparison of the same relationship.

Table 2.8: Fresh concrete stability R^2-values for subdivided results

Fresh Result Comparison	Method of Subdivision					
	Coarse Agg. NMSA		Total Agg. Volume		½ in.-NMSA by Agg.	
	½ in. NMSA	¾ in. NMSA	> 65% Agg.	< 65% Agg.	> 65% Agg.	< 65% Agg.
VSI & Seg. Index	**0.37**	**0.43**	0.26	0.41	0.26	0.59
VSI & Rapid Pen.	0.02	0.16	0.12	0.01	0.12	0.00
VSI & Sieved Fraction	**0.62**	**0.63**	0.77	0.27	0.77	0.58
VSI & Rate of Set.	0.07	0.55	0.15	0.54	0.15	0.55
Seg. Index & Rapid Pen.	0.03	0.15	0.08	0.12	0.08	0.00
Seg. Index & Sieved Fraction	0.39	0.73	**0.54**	**0.72**	**0.54**	**0.80**
Seg. Index & Rate of Set.	0.05	0.64	0.03	0.31	0.03	0.16
Rapid Pen. & Sieved Fraction	0.35	0.33	0.36	0.22	0.36	0.00
Rapid Pen. & Rate of Set.	0.00	0.00	0.00	0.00	0.00	0.00
Sieve Fraction & Rate of Set.	0.00	0.39	0.04	0.24	0.04	0.48

Notably, almost all relationships that met the criteria listed above were those that were already identified as “strong correlations” when comparing all twenty SCC mixtures. The significance of those correlations (sieve result versus both VSI and column segregation result) is discussed in subsequent sections. The only other comparison that yielded statistically significant, different class relationships was the one between column segregation index and VSI. The relationship between those two tests, subdivided by coarse aggregate NMSA, is shown in Figure 2.16.

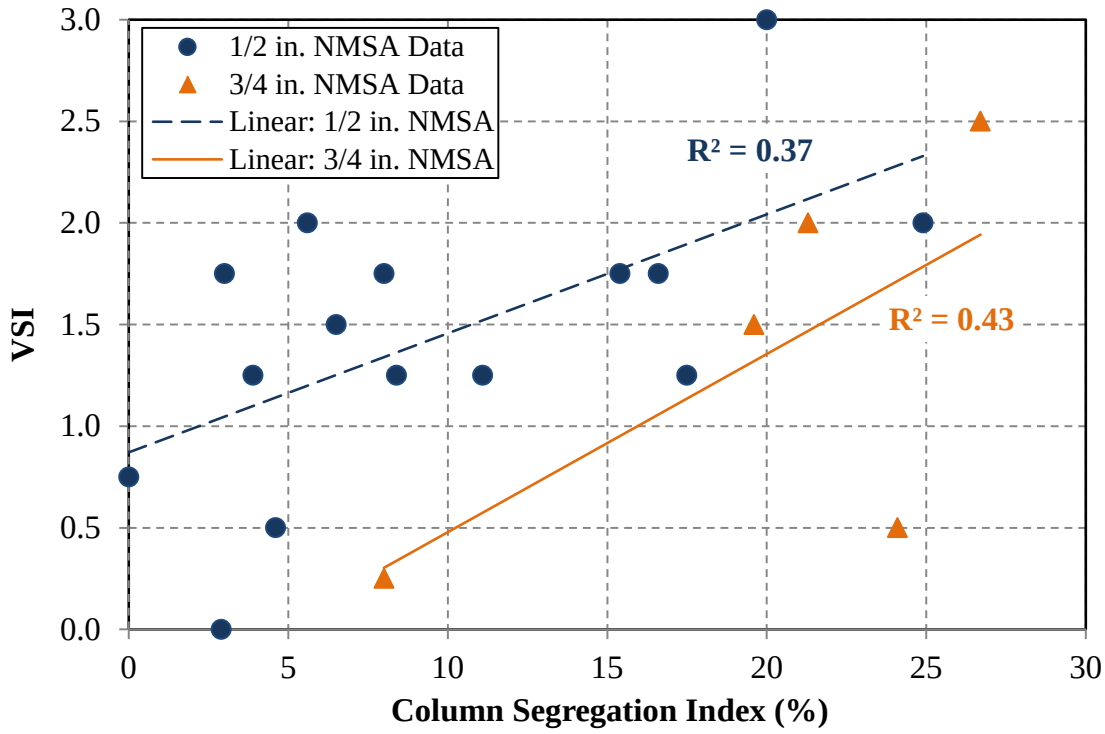

Figure 2.16: Comparison between column segregation index and VSI (mixtures subdivided by coarse aggregate NMSA)

In the figure, the VSI exhibits the same range of results within each NMSA class, but the segregation index is generally shifted right within the ¾ in.-NMSA class, indicating that only column segregation results are affected by NMSA. This shift may be complicated because the ¾ in.-NMSA class is also entirely of the lower total aggregate content class; it is unlikely that the shift is due to total aggregate content, though, when considering the lack of difference by aggregate content within the ½ in.-NMSA class.

2.4.2.2 Correlation between Sieve Stability and VSI Results

The correlations between the sieve stability test and the VSI were all relatively strong (R^2 = 0.43, 0.62, and 0.63 for all mixtures, ½ in.-NMSA, and ¾ in.-NMSA mixtures, respectively). The subdivided relationships are shown in Figure 2.17.

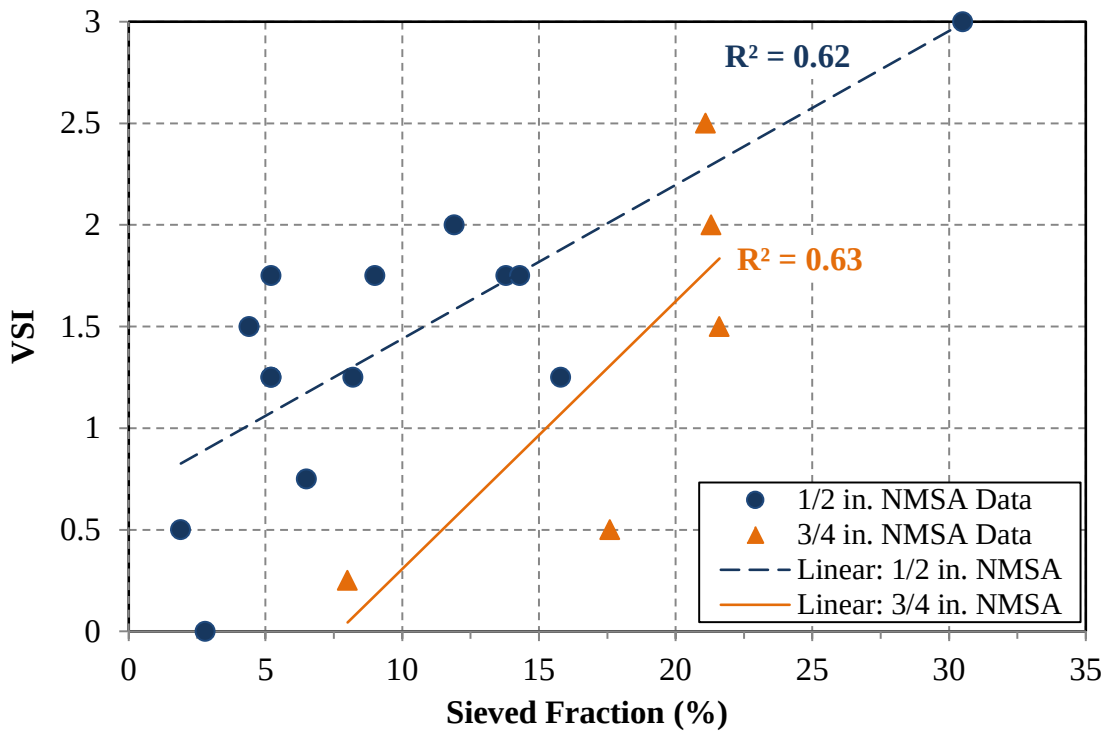

Figure 2.17: Comparison between sieved fraction and VSI results (mixtures subdivided by coarse aggregate NMSA)

Several conclusions are justified from these correlations. When assessed by trained technicians, the VSI test results are relatable to the more time-consuming but less subjective sieve stability test. Conversely, the sieve stability test is a well correlated and objective alternative to the VSI test for determining stability acceptance. Also, the sieve stability test is clearly affected by coarse aggregate NMSA—while assigned VSI values have the same range for each class, sieve stability results for the entire ¾ in.-NMSA class are shifted right by approximately +7.5%.

This shift in sieved fraction results may be complicated because the ¾ in.-NMSA class is also entirely of the lower total aggregate content class; that the shift is due to total aggregate content is unlikely, though, when considering the lack of difference by aggregate content within the ½ in.-NMSA class. Instead, the shift is likely related to the mechanism of segregation described by Bonen and Shah (2005): larger coarse aggregate has a lower surface-area-to-volume ratio, so less cohesion exists between aggregate and mortar to resist separation. This segregation mechanism appears to distinctly affect the sieve stability test, in which SCC is forcibly separated by a sieve; whether the mechanism also affects in-situ stability is evaluated in Section 2.4.3 and 2.4.4.

2.4.2.3 Correlation between Sieve Stability and Column Segregation Results

The correlations between the sieve stability and the column segregation tests were all relatively strong (R^2 = 0.56 for all mixtures, and 0.54–0.80 when subdivided). The relationships, subdivided by coarse aggregate NMSA and total aggregate volume, are shown in Figure 2.18. Three classes are created by this subdivision, as all ¾ in.-NMSA mixtures were also of a single target aggregate volume.

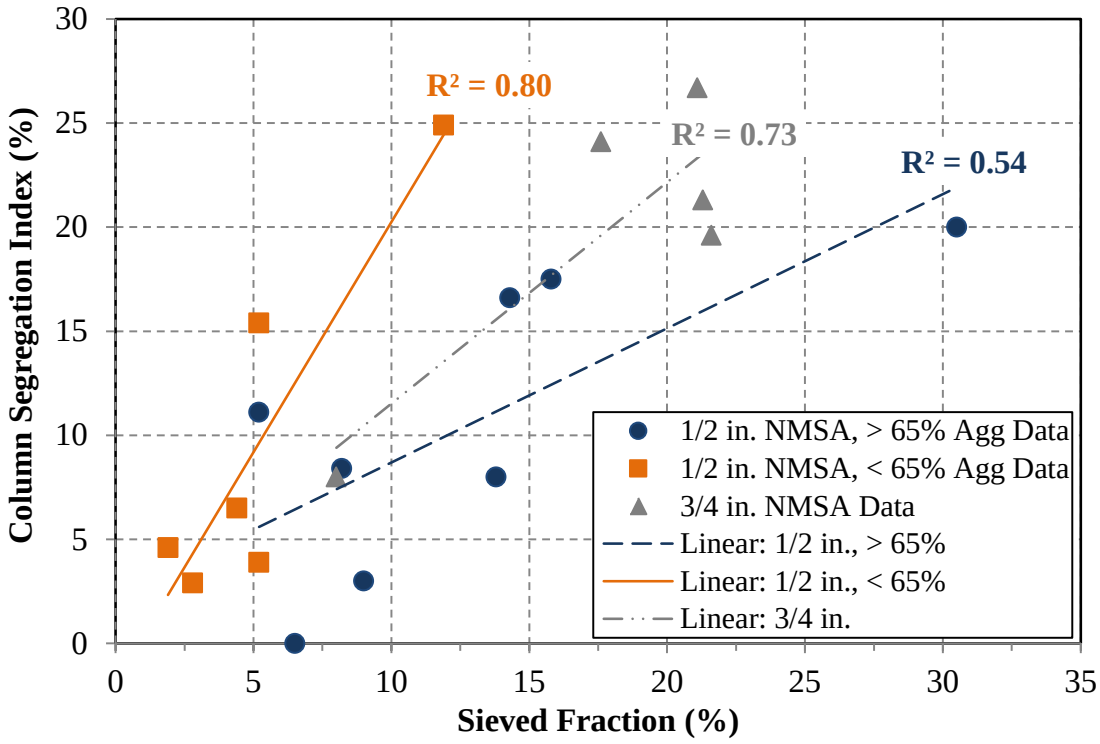

Figure 2.18: Comparison between sieved fraction and column segregation index results (mixtures subdivided by coarse aggregate NMSA and total aggregate volume)

Several conclusions are justified from these correlations. The linear-regression correlation coefficient between sieve stability and column segregation results found during this research is of similar magnitude to the relationship found by Kohler and Fowler (2010). As they (Kohler and Fowler 2010) determined, the sieve stability test is, therefore, a viable alternative to the column segregation test, especially considering its increased technician-friendliness that was described by Keske et al. (2013b).

Evaluation of the relationship between the column segregation test and other fresh stability tests for new SCC mixtures (Bui et al. 2007; Khayat and Mitchell 2009) may be warranted, but its relevance is moot considering the alternatives available. The VSI may be subjective, but it correlates well with the column segregation test (see Section 2.4.2.1) and is

distinctly quicker to conduct. The sieve stability test is equally objective, and it also requires less time and effort to conduct.

2.4.2.4 Correlation between Rate and Maximum Surface Settlement

The relationship between the rate of settlement and maximum settlement from the surface settlement test exhibited the largest linear-regression R^2-value of any fresh test comparison (R^2 = 0.60). This correlation is shown in Figure 2.19 and is of similar strength to the relationship found by Hwang et al. (2006).

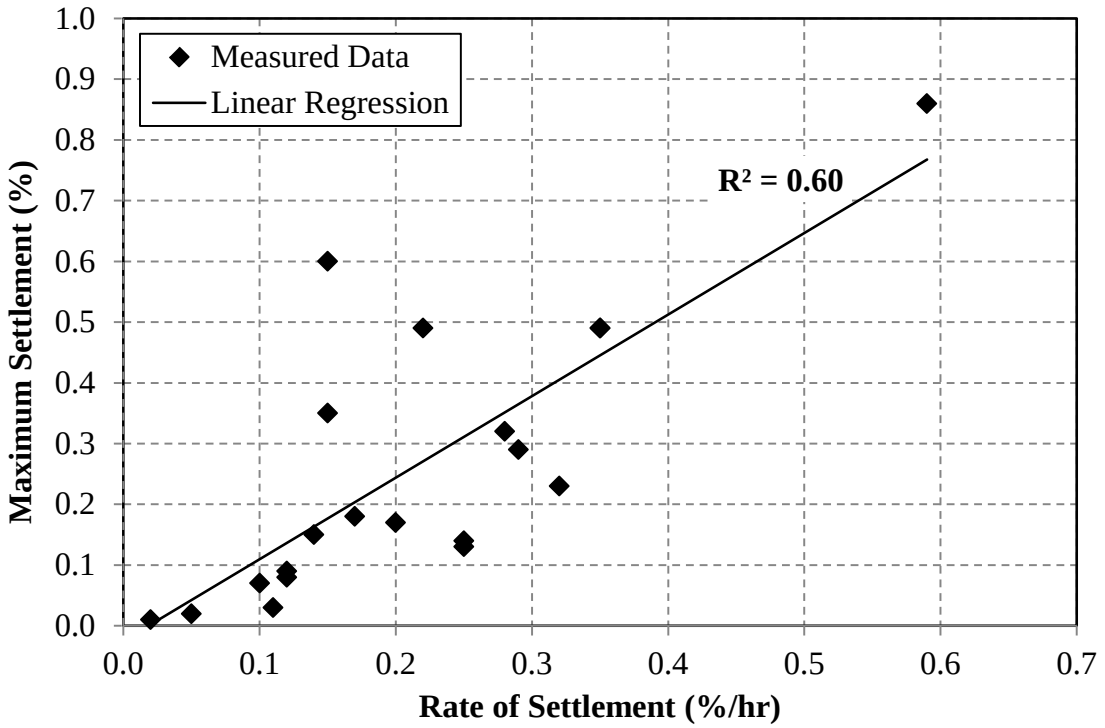

Figure 2.19: Comparison between rate of settlement and maximum settlement results from the surface settlement test (all available mixtures)

Subdivided relationships between rate and maximum settlement results are shown in Figure 2.20. The R^2-value of each was improved dramatically when applying a nonlinear-regression model, while the all-mixture comparison was not, which is why only nonlinear regression models are shown below in Figure 2.20.

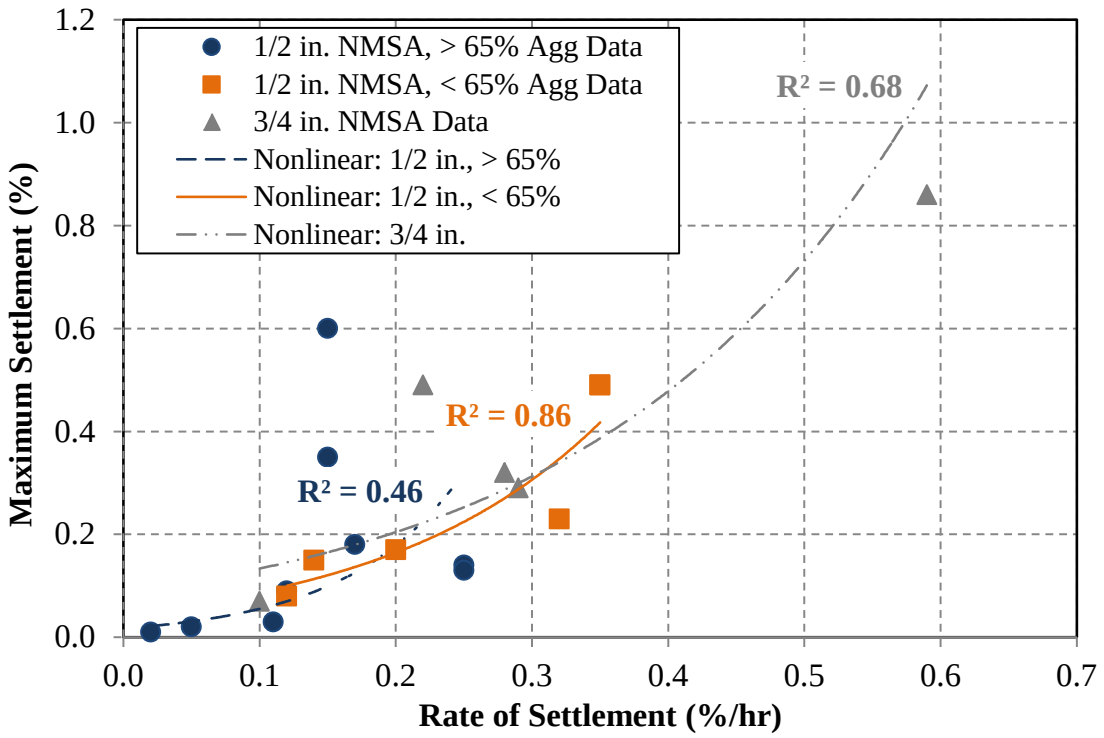

Figure 2.20: Comparison between rate of settlement and maximum settlement results (mixtures subdivided by coarse aggregate NMSA and total aggregate volume)

While all subdivisions have high R^2-values when applying a nonlinear regression model, the three subdivided correlations are not noticeably different from each other. Thus, the recommendation that the rate of settlement result be used in lieu of the maximum settlement result (Hwang et al. 2006; Keske et al. 2013b) is confirmed. This is also the reason that subdivided maximum settlement results were excluded from Table 2.8—measurement of the rate of settlement in place of the maximum settlement should always be sufficient.

2.4.2.5 Sieve Stability Test—Abbreviated-Rest Period Testing

The results of the alternatively-timed sieve stability test, which are shown in Table 2.6, were compared in a similar fashion as the relationships previously described: using all available SCC mixtures (eleven) and by subdividing by coarse aggregate MSA. Subdivision by aggregate volume was not possible, as all evaluated mixtures were of the 60% target-aggregate-volume class. Eleven-mixture comparisons of the standard 15 min. results to each abbreviated-time result are illustrated in Figure 2.21. For reference, a dashed line is shown to illustrate unity (when 15 min. results are compared to themselves). Subdivided relationships are not shown because they did not meet the criteria established for Table 2.8 and discussed in Section 2.4.2.1 (for improved R^2 and statistically significant difference).

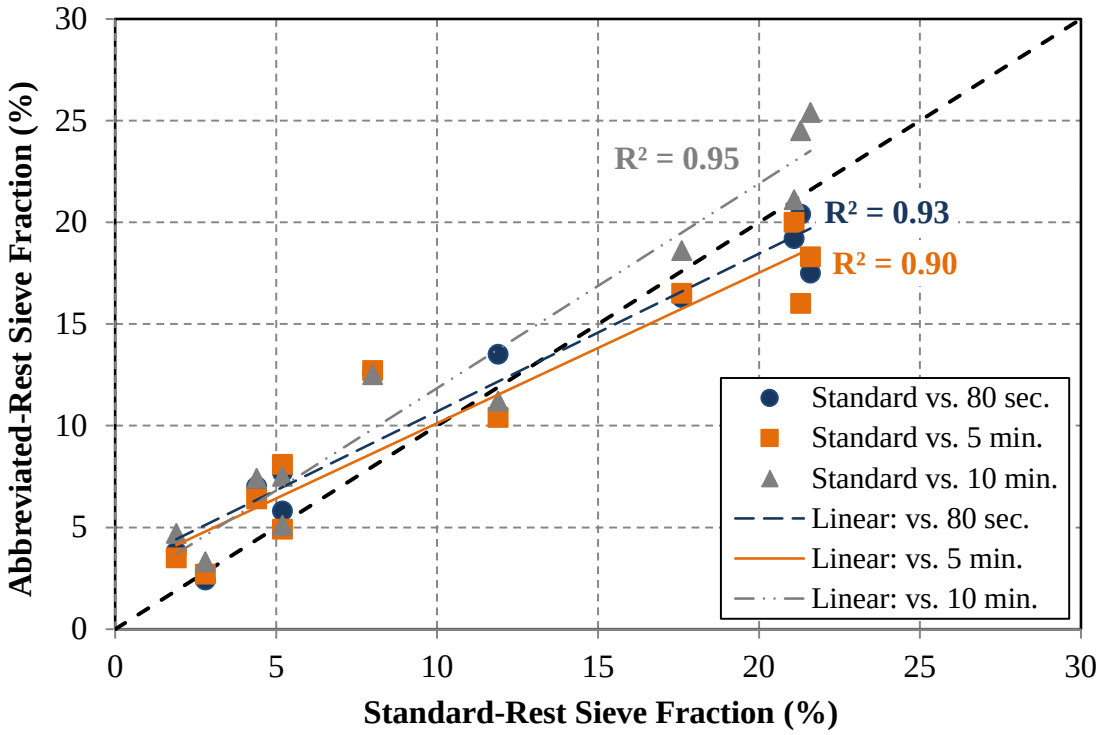

Figure 2.21: Comparison between sieve fraction results obtained after standard 15-min. rest period and after abbreviated rest periods

Several observations are drawn from the linear relationships shown in Figure 2.21. First, all comparisons have very strong R^2-values relative to the other fresh test comparisons, and all relationships also exhibit R^2-values exceeding those cited by Hwang et al. (2006) to recommend rate of settlement testing during the surface settlement test. Second, the change in the relationship (deviation from unity) resulting from abbreviating the rest period appears to lack a pattern, as the correlations do not systematically change between intervals.

The use of an abbreviated rest time for the sieve stability test is warranted based on these observations. Utilization of an eighty-second rest period should be acceptable because, all other considerations being equal, the use of the shortest rest period that provides accurate results is most practical. The relationship is of similar strength (based on R^2) to the other alternatively timed relationships, and the change in its slope (change in 80 sec. values relative to 15 min. results) can be conservatively accounted for in determining test acceptance criteria.

2.4.2.6 Rapid Penetration Test—Extended-Rest Period Testing

The results of the alternatively-timed rapid penetration test, which are shown in Table 2.6, were compared in a similar fashion as the alternatively-timed sieve stability results: using all available mixtures (eleven) and by subdividing by coarse aggregate NMSA. Eleven-mixture comparisons of the standard 80 sec. results to all extended times are illustrated in Figure 2.22. Subdivided relationships are not shown because they did not meet the criteria established for Table 2.8 and discussed in Section 2.4.2.1 (for improved R^2 and statistically significant difference).

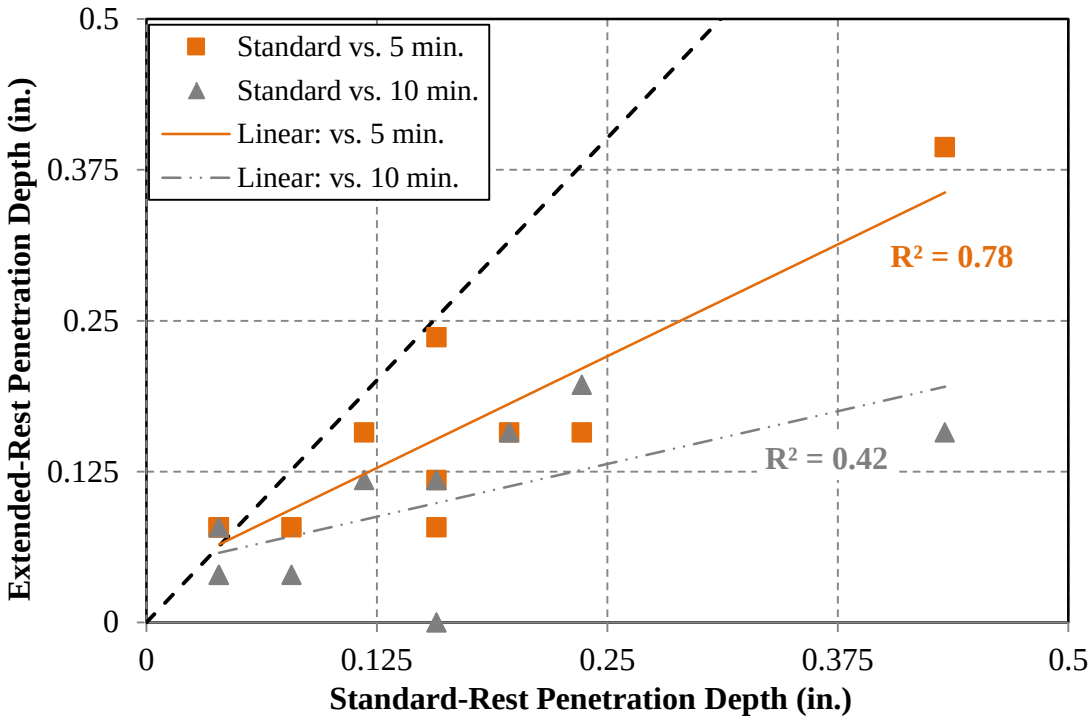

Figure 2.22: Comparison between rapid penetration results obtained after 80-second rest period and after extended rest periods

Several observations are drawn from the linear relationships shown in Figure 2.22**.** First, the comparison between results obtained after 5 min. and 80 sec. exhibited a notably higher R^2-value than the comparison between10 min. and 80 sec. results. This indicates that test variability observed after the standard rest period may be improved by extending the rest period—stronger correlation, like the comparison to 5 min. results, would indicate that test patterns are more consistent. Second, the change in the relationship (deviation from unity) indicates that penetration depth consistently decreases as a result of prolonging the rest period prior to testing.

Based on these observations, results obtained after a rest period of ten minutes should be compared independently to other measures of concrete fresh stability and in-situ uniformity.

When compared to the other tests, though, all 10 min. rapid penetration relationships exhibited R^2-values less than or equal to the values corresponding to 80 sec. results. Comparison of 10 min. values to hardened concrete uniformity results are discussed later.

2.4.3 In-Situ Concrete Uniformity Tests

In-situ hardened concrete uniformity test results (UPV, pullout, HVSI, and DIA testing results) obtained during this research are presented in Table 2.9. The way these values were determined for each test is discussed in the following subsections. In the last subsection, correlations between these hardened concrete uniformity results are presented and discussed.

Table 2.9: Hardened concrete uniformity test results

Mixture ID	UPV Segregation Index	Top-Bar Effect	HVSI	Coarse Agg. Dist. Index
VC-1	1.036	1.28	-	-
SCC-1A	1.073	1.24	-	-
SCC-1B	1.039	1.56	-	-
SCC-1C	1.034	1.16	-	-
SCC-1D	1.038	1.09	-	-
VC-2	1.066	1.75	-	-
SCC-2A	1.042	1.27	-	-
SCC-2B	1.114	2.80	-	-
SCC-2C	1.030	1.30	-	-
SCC-2D	1.056	2.05	-	-
SCC-2E	1.034	1.56	-	-
VC-3	1.034	1.29	0.75	1.141
SCC-3A	1.042	1.22	0.38	1.085
SCC-3B	1.043	1.19	0.13	1.167
SCC-3C	1.023	1.08	0.25	1.190
SCC-3D	1.069	1.98	0.38	1.241
SCC-3E	1.066	1.85	0.38	1.296
SCC-3F	1.022	1.16	0.38	1.164
VC-4	1.054	1.47	0.63	1.065
SCC-4A	1.061	1.70	0.75	1.146
SCC-4B	1.029	1.09	1.00	1.468
SCC-4C	1.051	1.20	2.75	1.148
SCC-4D	1.050	1.71	1.88	1.426
SCC-4E	1.043	1.25	1.50	1.357

2.4.3.1 Ultrasonic Pulse Velocity Testing

The five UPV measurements in each row of measurements (discussed in Section 2.3.4.2) were averaged to determine an average UPV for that height. Surface defects and human error in either testing or recording of measurements occasionally caused outliers in the determined pulse velocities within a wall. Outliers were identified as any pulse velocity greater than three standard deviations away from the average of the other four velocities at a given height. Outliers, which

were removed prior to further evaluation of results, were found in less than 11% of measurements.

Complete UPV data for each wall and mixture are reported in Appendix A of Keske (2014). Measured velocities tended to decrease with increasing height, but the fastest and slowest velocities were not always measured at the very top or bottom of each wall. Many properties affected by segregation, including distribution of air voids, aggregate, and excess water, can affect the measured UPV, and these properties do not necessarily fluctuate linearly. Therefore, although the UPV measurements in a wall may not consistently vary over the wall's height, the maximum and minimum velocities likely indicate the level of non-uniformity within the wall.

To quantify the UPV non-uniformity, a "UPV segregation index" was determined for each wall and mixture by dividing the maximum row-average UPV by the minimum. The UPV segregation indices for each wall and mixture are shown in Figure 2.23 and are presented in Appendix A of Keske (2014). Since the UPV segregation indices presented in Figure 2.23 do not vary consistently with wall height, the largest magnitude UPV segregation index for each mixture was used for all analyses. These mixture-maximum UPV segregation indices are presented in Table 2.9.

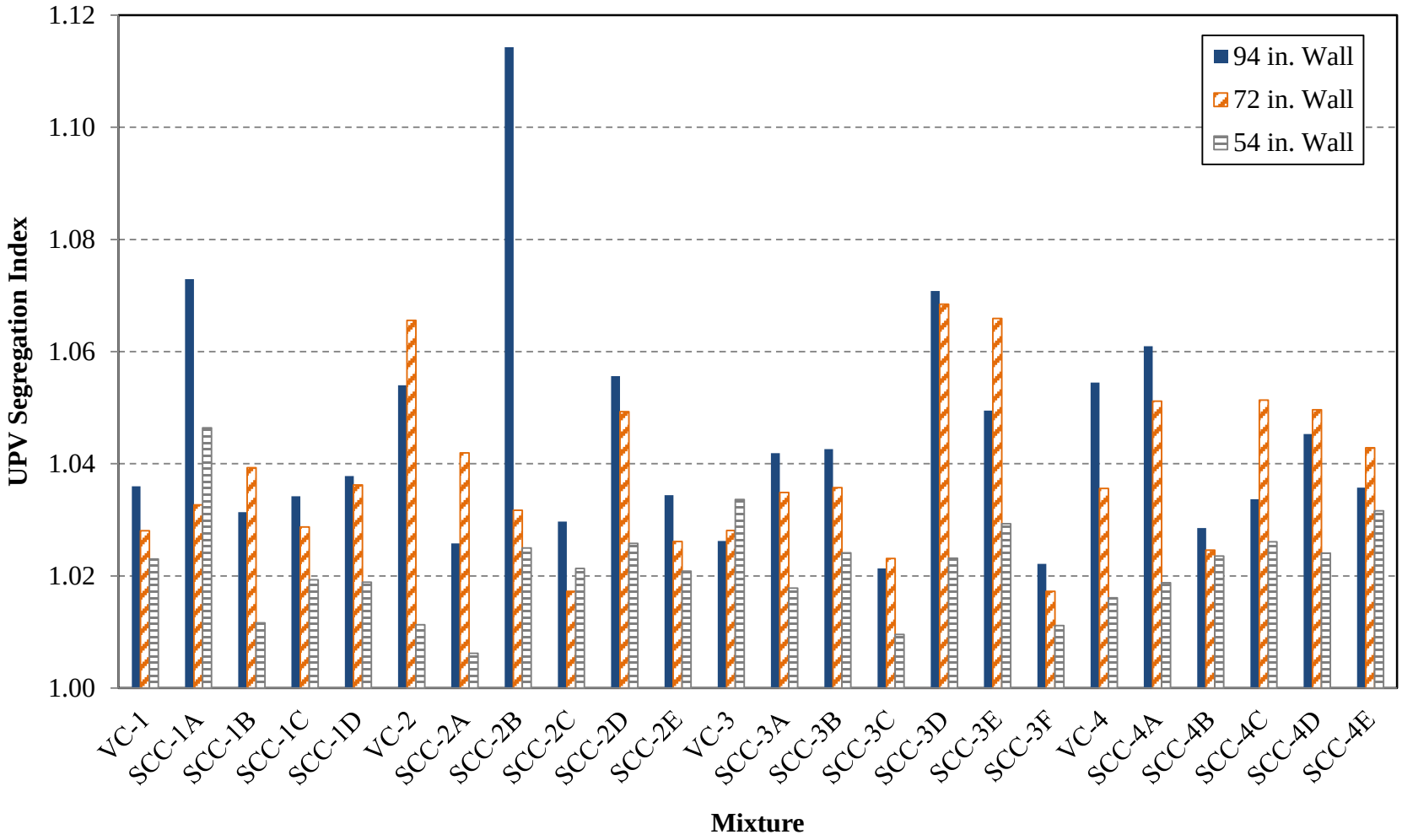

Figure 2.23: UPV segregation indices by wall height and mixture

2.4.3.2 Pullout Testing

The average pullout force was determined for the eight bars closest to each other at the top and bottom of each wall. Eight-bar groups were used because of the inherent scatter involved with short-embedment pullout testing and because the eight bars at each location were much closer to each other than to the other groups of eight. During the first phase of this research, Keske et al. (2013b) also tested a third group of eight bars at the approximate mid-height of each wall. They did not find a consistent pullout strength pattern between the three groups. Its use was abandoned prior to the second phase of testing for this reason, and because its exclusion allowed a 33% reduction in the number of pullout specimens needed for each mixture.

Similar to the earlier discussion regarding UPV outliers, pullout testing outliers were identified and removed from consideration. Outliers were identified as any value greater than two standard deviations away from the average of the other seven results in a given group. Outliers were found in less than 12% of measurements, which was similar to the percentage found during UPV testing.

Complete pullout force data for each wall and mixture are reported in Appendix A of Keske (2014). In accordance with the convention of Khayat and Mitchell (2009) and others (Khayat et al. 1997; Stocker and Sozen 1970), the top-bar effect was calculated by dividing the pullout force in the bottom group of bars by the pullout force of the top group (but never taken less than 1.00). The top-bar effects for each wall and mixture are summarized in Figure 2.24 and are presented in Appendix A of Keske (2014). Because the top-bar effects presented in Figure 2.24 do not vary consistently with wall height, the mixture-maximum top-bar effect was used as the pullout benchmark result for all analyses. These values are summarized in Table 2.9.

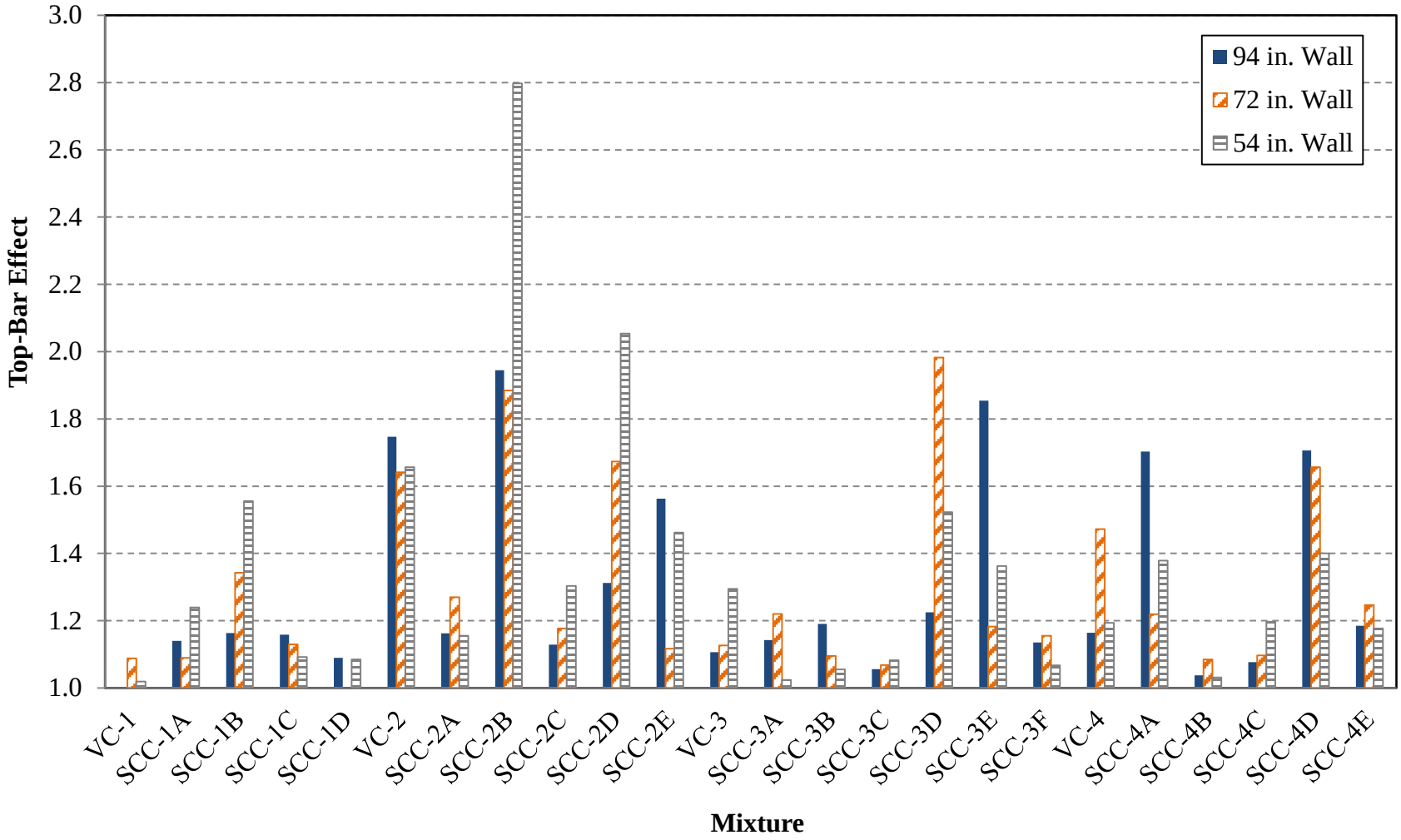

Figure 2.24: Top-bar effects by wall height and mixture

2.4.3.1 Hardened Visual Stability Index Testing

The HVSI values assigned to the 72 in. walls cast with SCC-3, SCC-4, VC-3, and VC-4 are presented in **Table 2.**10, as are the averages of the four results for each specimen and eight results for each concrete mixture that were assigned by four independent operators. Specimen identification is based on the location from which cores were taken from walls (see Figure 2.13). Each test operator was able to independently assess the HVSI as discussed in Section 2.3.4.5, and the order of evaluation of a mixture's two specimens (reorganized in **Table 2.**10 for clarity) was completely random.

In the table, no two results for a given specimen differed by greater than 1, but differences of that magnitude were frequent. The difference occasionally changed an individual specimen's stability classification as determined according to AASHTO PP-58 (2012)—three of twenty-six specimens were assigned an HVSI of 2 by one operator and HVSI of 1 by another (recall that HVSI values of 0 or 1 indicate acceptable concrete uniformity while HVSI values of 2 or 3 indicate unacceptable concrete uniformity). This indicates that the subjective nature of HVSI assessment may affect its value in determining uniformity acceptance of placed concrete.

Table 2.10: Hardened visual stability index results

Mixture ID	Specimen	HVSI Values by Operator				Specimen Average HVSI	Mixture Average HVSI
		Op. A	Op. B	Op. C	Op. D		
VC-3	Center	0	1	1	1	1	0.75
	Side	0	1	1	1	1	
SCC-3A	Center	1	1	0	0	1	0.38
	Side	0	1	0	0	0	
SCC-3B	Center	0	1	0	0	0	0.38
	Side	0	0	1	1	1	
SCC-3C	Center	0	0	0	1	0	0.13
	Side	0	0	0	0	0	
SCC-3D	Center	1	0	0	1	1	0.38
	Side	0	0	0	1	0	
SCC-3E	Center	0	0	0	1	0	0.25
	Side	1	0	0	0	0	
SCC-3F	Center	0	1	0	1	1	0.38
	Side	0	0	0	1	0	
VC-4	Center	0	1	1	1	1	0.63
	Side	0	0	1	1	1	
SCC-4A	Center	3	2	2	3	3	2.75
	Side	3	3	3	3	3	
SCC-4B	Center	1	1	1	1	1	0.75
	Side	0	0	1	1	1	
SCC-4C	Center	3	3	3	3	3	1.88
	Side	1	0	1	1	1	
SCC-4D	Center	2	1	1	2	2	1.00
	Side	0	0	1	1	1	
SCC-4E	Center	1	1	1	2	1	1.50
	Side	2	1	2	2	2	

When each specimen's result was rounded to the nearest integer (as would be assigned) specimens within each pair frequently exhibited differing HVSI values—seven of thirteen mixture pairs exhibited non-matching results, and three of the seven nonmatching pairs would contraindicate acceptability of in-situ concrete uniformity. The two specimens from each mixture in this research were cast simultaneously and 8 in. apart; while distance from the point of filling and topping-off of walls could have affected the results, the variation indicates that HVSI specimens collected from the same parent specimen can be significantly different. Therefore, care should be taken in formulating an HVSI testing protocol and acceptance criteria for determination of in-situ concrete uniformity acceptance.

While the two specimens for a given mixture were *assessed* independently, the two samples could not be considered independent because only one 'parent' specimen of concrete was cored to retrieve the two HVSI specimens. A mixture-average HVSI was necessary for this

reason. Its use also mimicked the practices utilized during collection of fresh concrete stability results from two apparatuses. Therefore, the eight-assessment mixture average (the rightmost column of **Table 2.**10) was chosen as the benchmark HVSI result for all analyses.

Comparing the HVSI results of the SCC-3 and SCC-4 mixtures, it appears that almost all SCC-3 mixtures exhibited acceptable HVSI uniformity, while very few SCC-4 mixtures did. This contradicts the previously presented findings in Sections 2.4.2 (fresh concrete stability testing), 2.4.3.1 (UPV testing), and 2.4.3.2 (pullout testing), which all indicate that each series achieved a wide range of stability and hardened uniformity results. This discrepancy could be either the result of the subjective nature of the HVSI test or the result of different identification of in-situ concrete uniformity. While SCC-3 and SCC-4 mixtures were proportioned to achieve the same target total aggregate content, SCC-3 achieved that target through the use of more, but smaller, coarse aggregate particles. Further analysis was conducted to determine whether this difference led to improved stability, or just the subjective *appearance* of improved stability. This analysis is discussed in the following section.

2.4.3.2 Digital Image Analysis Testing

2.4.3.2.1 Coarse Aggregate Distribution Index

The cores used for HVSI testing, as well as an equal number taken from the bottom face of each 72 in. wall, were further evaluated using DIA as described in Section 2.3.4.5. Four specimens were analyzed from each mixture, and individual and average coarse aggregate cross-sectional areas are presented in Table 2.11.

As shown in the table, wall-end pairs (top-cast or bottom-cast) exhibited similar coarse aggregate percentages—no pair differed by more than 9% coarse aggregate area. Notably, variation within bottom-cast pairs was frequently as large as within top-cast pairs. This suggests that the variation between HVSI results of adjacent cores is not due only to filling point distance and topping-off variation. HVSI and DIA variation are more likely a result of the heterogeneous nature of concrete, in which apparent coarse-aggregate content can vary widely between samples taken from the same parent specimen.

Table 2.11: Coarse aggregate distribution index results

Mixture ID	Specimen	Coarse Agg. %		Average		Coarse Agg. Dist. Index
		Top-Cast Concrete	Bot.-Cast Concrete	Top-Cast Concrete	Bot.-Cast Concrete	
VC-3	Center	16.3	14.4	13.9	15.8	1.141
	Side	11.4	17.2			
SCC-3A	Center	16.7	17.9	16.5	17.9	1.085
	Side	16.3	17.8			
SCC-3B	Center	23.5	26.1	23.4	27.3	1.167
	Side	23.3	28.6			
SCC-3C	Center	13.8	17.6	14.0	16.7	1.190
	Side	14.2	15.8			
SCC-3D	Center	12.9	20.5	14.9	18.5	1.241
	Side	16.9	16.5			
SCC-3E	Center	23.9	30.3	21.0	27.2	1.296
	Side	18.1	24.1			
SCC-3F	Center	16.8	21.3	17.8	20.7	1.164
	Side	18.8	20.1			
VC-4	Center	31.2	39.8	33.5	35.7	1.065
	Side	35.8	31.5			
SCC-4A	Center	28.0	34.6	30.5	35.0	1.146
	Side	33.0	35.3			
SCC-4B	Center	25.2	34.4	22.7	33.3	1.468
	Side	20.3	32.3			
SCC-4C	Center	23.1	27.2	23.5	27.0	1.148
	Side	24.0	26.9			
SCC-4D	Center	15.0	23.0	18.7	26.6	1.426
	Side	22.4	30.3			
SCC-4E	Center	33.9	39.8	29.3	39.8	1.357
	Side	24.7	39.8			

Because of the between-specimen variability, each wall-end pair was averaged. Within each mixture (both materials), the average bottom-cast coarse aggregate content always exceeded top-cast content. In line with the practice utilized to determine top-bar effects, top- and bottom-cast percentages were converted to a single, analyzable result by dividing the bottom-cast coarse aggregate percentage by the top-cast percentage. This "coarse aggregate distribution index," which indicates the difference in coarse aggregate percentage between locations in large specimens, was used as the DIA benchmark result for all analyses. Coarse aggregate distribution index results are summarized in **Table 2.**9.

2.4.3.2.2 Digital Image Analysis of Top-Cast Cores

In addition to the DIA analysis necessary to tabulate coarse aggregate indices, the cores used for HVSI testing were further evaluated using DIA to study the quantifiability of the HVSI test (which is subjective in nature, like the VSI). To do so, a method was used similar to those used by Johnson et al. (2010) and ASTM C1610: the 8 in. top-cast cores were divided into 2 in. quartiles, and the coarse aggregate percentage in the bottom quartile was divided by that in the top. This "core segregation index," which is shown in **Table 2.**12, was then compared to the HVSI results shown in **Table 2.**9.

Table 2.12: Core segregation index results

Mixture ID	Specimen	Coarse Agg. %		Average		Core Segregation Index
		Top Quartile	Bottom Quartile	Top Quartile	Bottom Quartile	
VC-3	Center	13.0	18.7	10.6	15.0	1.421
	Side	8.2	11.4			
SCC-3A	Center	15.5	20.9	16.3	18.8	1.156
	Side	17.0	16.7			
SCC-3B	Center	28.5	20.6	27.3	21.3	1.000
	Side	26.2	21.9			
SCC-3C	Center	14.8	18.6	14.6	17.3	1.179
	Side	14.5	16.0			
SCC-3D	Center	10.8	18.4	14.9	19.5	1.309
	Side	19.0	20.7			
SCC-3E	Center	12.3	23.7	19.0	25.1	1.320
	Side	25.7	26.4			
SCC-3F	Center	23.7	15.2	20.8	20.1	1.000
	Side	17.9	25.0			
VC-4	Center	31.5	33.0	34.9	36.3	1.041
	Side	38.2	39.6			
SCC-4A	Center	36.7	30.7	34.4	36.9	1.073
	Side	32.1	43.1			
SCC-4B	Center	16.2	26.0	22.7	27.4	1.209
	Side	29.1	28.8			
SCC-4C	Center	8.6	30.2	13.0	28.3	2.172
	Side	17.5	26.5			
SCC-4D	Center	5.6	17.2	16.9	20.9	1.236
	Side	28.2	24.7			
SCC-4E	Center	15.3	33.5	24.2	40.7	1.686
	Side	33.0	48.0			

2.4.3.3 Alternative Approaches for Result Determination

Alternative approaches were considered when choosing how to compare the UPV, pullout, and DIA measures to each other and to each fresh concrete stability test result. In additional to simple ratios of maximum results to minimum results, UPV results were alternatively tabulated as the ratio of the maximum UPV difference divided by the average of all measurements. This was considered because of the inconsistency between measurement location and pulse velocity. However, the alternative did not significantly affect the relationships found. This alternative was not possible when considering pullout or DIA testing, as only two finite groups were compared—the ratio of top to bottom measurements is directly proportional to their difference divided the average of the two.

While mixture-maximum UPV segregation index and top-bar effect results identify the most severe heterogeneity present among multiple walls, *average* uniformity values for each mixture were considered because of the inconsistency between wall height and uniformity shown in Figure 2.23 and Figure 2.24. However, these alternatives did not significantly affect the relationships found. As discussed in Section 2.4.3.1, this alternative was not possible when considering HVSI or coarse aggregate distribution index results, as only one wall from each mixture was tested.

Alternative DIA samples were analyzed in accordance with the DIA research practices of Johnson et al. (2010). They concluded that segregation most significantly affects the top and bottom one inch of a given specimen, so the top inch of each top-end pair was compared to the bottom inch of the top-end pair, as well as to the bottom inch of the bottom-end pair. Neither of these alternatives significantly affected the relationships found. While this contradicts the findings of Johnson et al. (2010), the results may not be directly comparable since they analyzed circular sections taken from a plane parallel to the top-cast surface, while the sections considered here were rectangular sections taken from a plane normal to the top-cast surface.

Alternative DIA samples were also analyzed in accordance with the DIA research practices of Khan and Kurtis (2010). They evaluated a simple percentage difference in coarse aggregate content between top- and bottom-cast specimens, so the same was evaluated for the mixtures tested for this research. This alternative did not significantly affect the relationships found. Again, the importance of the lack of correlation is unclear. Khan and Kurtis (2010) only found significant differences between sections from different longitudinal locations within a large specimen and not over height at a given longitudinal location, so the same was expected of this research, in which longitudinal flow was negligible.

2.4.3.4 Correlations between Hardened Test Results

Table 2.13 is a correlation matrix that shows the linear-regression coefficients of determination (R^2) between each hardened uniformity test when comparing *all available* mixtures. The comparison between UPV segregation index and top-bar effect includes twenty-four mixtures, while all comparisons involving the HVSI or coarse aggregate distribution index consist of thirteen mixtures; VC results were included in these comparisons, as the comparisons do not concern fresh concrete stability test results. A nonlinear model was also applied to each relationship, but no R^2-value was improved by more than 0.10 through the use of a nonlinear model. In the table, some R^2-values are highlighted that indicate significantly stronger correlations—the smallest bold value is at least 50% greater than all non-highlighted R^2-values, thus indicating a division of relative correlation strength. Additionally, the core segregation index (see Section **2.4.3.2**) was only compared to the HVSI, as it was only calculated to evaluate the quantifiability of the HVSI test.

Table 2.13: Hardened concrete uniformity result linear R^2

Test Result	Core Segregation Index	Coarse Agg. Dist. Index	HVSI	Top-Bar Effect	UPV Segregation Index
UPV Segregation Index	N.A.	0.00	0.01	**0.69**	-
Top-Bar Effect	N.A.	0.02	0.00	-	
HVSI	**0.64**	0.09	-		
Coarse Agg. Dist. Index	N.A.	-			

Note: N.A. = Not applicable, per above discussion

In the table, the linear hardened concrete uniformity test correlations having the greatest R^2-values were the correlations between UPV segregation index and top-bar effect and between the HVSI and core segregation index. These relationships are shown in Figure 2.25 and Figure 2.26.

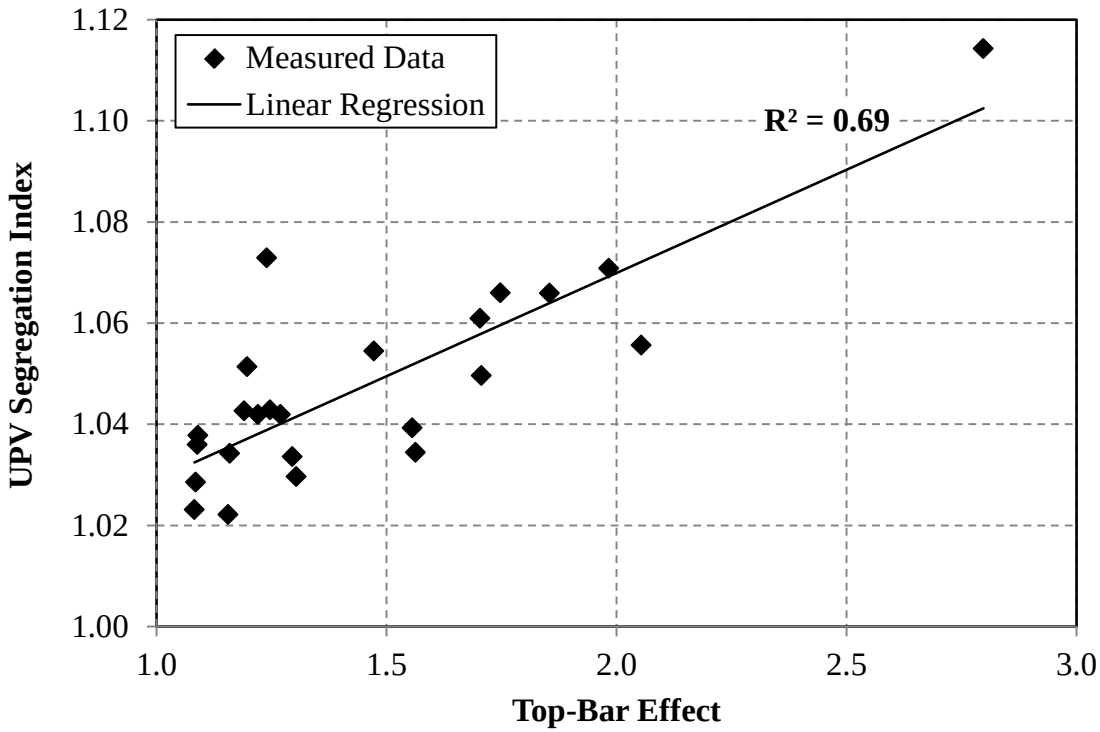

Figure 2.25: Comparison between top-bar effect and UPV segregation index

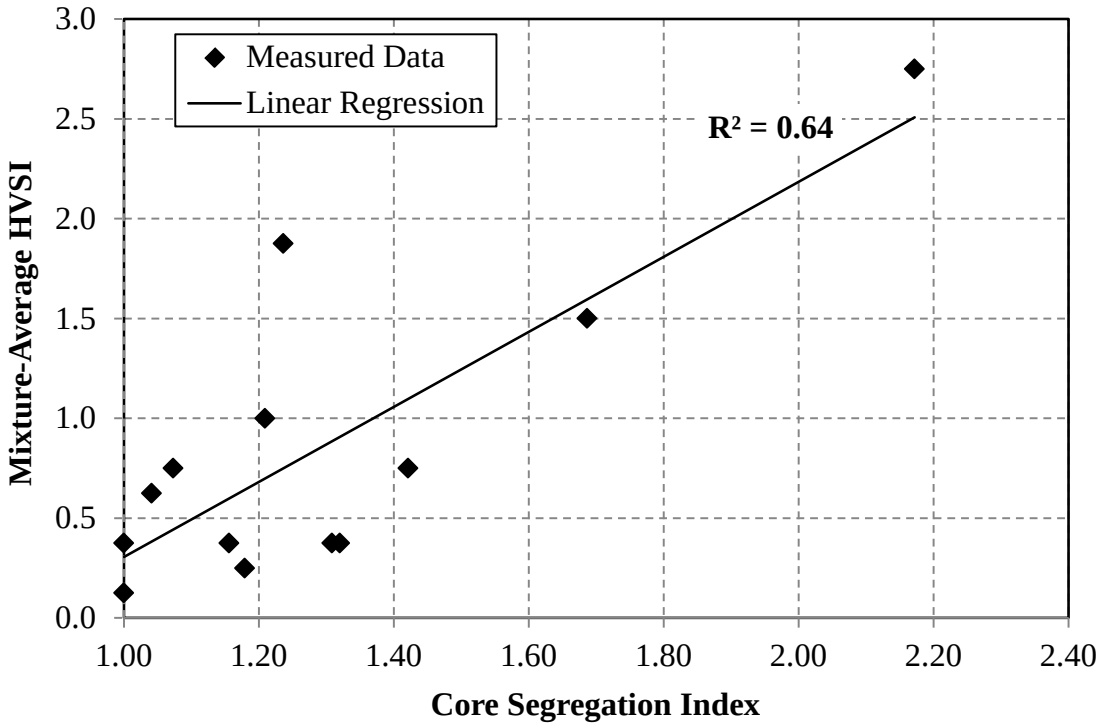

Figure 2.26: Comparison between core segregation index and HVSI

Several conclusions are drawn from the relationships presented in these figures. The types of in-situ non-uniformity identified by the UPV (air void stability, aggregate gradation, localized w/cm, etc.) appear to also affect the bond between concrete and horizontally-embedded reinforcement. This is in line with the findings of Castel et al. (2006), Esfahani et al. (2008), and Khayat et al. (1997), who all found that weakened bond surfaces develop as a result of irregular constituent dispersion. Also, the HVSI is correlated to less subjective, quantifiable results of DIA. This also confirms that SCC-3, which was proportioned with a ½ in.-NMSA aggregate, exhibited greater coarse aggregate uniformity than SCC-4, as uniformity was identified using both standardized HVSI procedures and quantifiable DIA.

Notably from Table 2.13, the HVSI and coarse aggregate distribution index do not exhibit a reasonable correlation with the UPV segregation index, top-bar effect, or each other. Several conclusions are warranted by these findings:

- Segregation appears to affect mechanical properties identified by UPV and pullout testing (air void stability, aggregate gradation, localized *w/cm*, bond to reinforcement) differently than properties identified by HVSI or DIA testing (coarse aggregate content and distribution, paste-layer depth),
- Segregation appears to affect mechanical properties quantified by the HVSI (localized coarse aggregate content and distribution, paste-layer depth) differently than properties quantified by the coarse aggregate distribution index (differences in coarse aggregate content between testing locations),
- Mixtures exhibiting acceptable uniformity according to the HVSI and coarse aggregate distribution index may not exhibit acceptable UPV and pullout uniformity, or vice versa.

Additionally, the HVSI is strongly correlated to the core segregation index (for top-cast cores) but not to the coarse aggregate distribution index (measure of variability between top-cast and bottom-cast cores). This suggests that the HVSI may be insufficient for identifying differences in coarse aggregate content within large specimens. Alternatively, a larger sampling of cores for HVSI evaluation may be necessary considering the large HVSI and DIA variation observed between adjacent cores from the same specimen (see Section 2.4.3.1 and 2.4.3.2).

To conduct a more refined comparison of the hardened concrete uniformity results, consideration was given to the same potential variables as during fresh stability result evaluation: coarse aggregate NMSA, target total aggregate volume, and, among the ½ in.-NMSA mixtures, a combination of the NMSA and aggregate volume. However, no correlations between measures of hardened concrete uniformity were improved by subdivision of their results. The strong correlations between the UPV segregation index and top-bar effect and between the HVSI and core segregation index were not statistically different between groups, and no other correlations involving the HVSI or coarse aggregate distribution index were improved.

From these results, it is concluded that the relationship between the UPV segregation index and top-bar effect (and between the types of in-situ non-uniformity identified by them) was consistent across the studied concrete mixtures. Also, concretes of different coarse aggregate gradations can be evaluated with the HVSI with equal capability, although the relevance of results to in-situ concrete uniformity is unclear.

2.4.4 Correlations between Test Results

Table 2.14 consists of linear-regression coefficients of determination (R^2) between each fresh stability and hardened uniformity test result when comparing *all available* SCC results (comparisons to the UPV segregation index and top-bar effect include twenty mixtures, while comparisons to the HVSI and coarse aggregate distribution index consist of eleven mixtures). In the table, R^2-values are highlighted to show relative strength—the smallest bold value is at least 50% greater than all non-highlighted R^2-values, thus indicating a division of relative degree of correlation strength.

Table 2.14: Linear correlation R^2-values between fresh concrete stability and hardened concrete uniformity test results (all available SCC results)

Hardened Uniformity Test Result	Fresh Concrete Stability Test Result					
	VSI	**Seg. Index**	**Rapid Pen.**	**Sieved Fraction**	**Rate of Settle.**	**Max. Settle.**
UPV Seg. Index	**0.47**	0.16	0.04	**0.39**	0.15	0.15
Top-Bar Effect	**0.38**	0.12	0.01	0.23	0.20	0.07
HVSI	0.00	**0.41**	0.02	**0.51**	0.13	0.12
Coarse Agg. Dist. Index	0.00	0.00	0.00	0.09	0.10	0.09

Highlighted in the table, the linear test correlations having the greatest R^2-values were the correlations relating the VSI to the UPV segregation index and top-bar effect and relating the sieved fraction to the UPV segregation index and HVSI. The only other strong correlation was between the segregation index (column segregation test result) and HVSI. The rapid penetration test and surface settlement test do not exhibit a reasonable correlation with any hardened concrete uniformity test results, at least when comparing all available mixtures.

A nonlinear model was also applied to each relationship, but no R^2-value was improved by more than 0.10 through the use of a nonlinear model. Furthermore, extended-rest rapid penetration results were evaluated per the discussion of Section 2.4.2.6. However, no correlations between the rapid penetration test and any measure of in-situ stability were improved by use results obtained after a 10 min. rest period.

To conduct a more refined comparison of the results, consideration had to be given to potential variables that could subdivide the SCC mixtures. In light of the discussion of Section 2.4.2, the results were subdivided three ways: by NMSA (½ in. or ¾ in.), target total aggregate volume (greater or less than 65%), and, among the ½ in.-NMSA mixtures, a combination of the NMSA and aggregate volume. The third subdivision, consisting of a combination of NMSA and target total aggregate content, is only evaluated for relationships involving the UPV segregation index and top-bar effect. All mixtures evaluated using the HVSI and coarse aggregate distribution index (SCC-3 and SCC-4 mixtures) had the same target total aggregate content. Therefore, relationships involving the HVSI and coarse aggregate distribution index are only subdivided by NMSA.

Complete tables of subdivided comparisons between concrete test results are given in Appendix A of Keske (2014). For the sake of brevity, only relationships that are significantly affected by subdivision of test results are presented in Table 2.15. Significance is identified by the following criteria:

- A statistically significant difference, at a 90% confidence interval (CI), is observed between the classes of linearly correlated fresh results,
- The R^2-value for at least one class changed by greater than 0.10 versus the R^2-value calculated from the all-mixture comparison of the same relationship, and
- The change in R^2-values for the subdivided groups affects whether the relationship is identified as a relatively strong correlation (as discussed in reference to Table 2.14).

Table 2.15: Linear correlation R^2-values between fresh and hardened concrete test results (SCC groups significantly affected by result subdivision)

Result Comparison	All-Mix. R^2	Method of Subdivision					
		NMSA		Total Agg.		½ in.-NMSA, Agg	
		½ in. NMSA	¾ in. NMSA	> 65% Agg.	< 65% Agg.	> 65% Agg.	< 65% Agg.
Top-Bar Effect & Sieve Frac.	0.23	0.38	0.46	-	-	-	-
Top-Bar Effect & Rate of Set.	0.20	-	-	-	-	0.70	0.62
UPV Seg. Index & Sieve Frac.	0.39	0.50	0.64	-	-	-	-
UPV Seg. Index & Rate of Set.	0.15	-	-	-	-	0.37	0.84
HVSI & Sieve Frac.	0.51	0.08	0.03	N.A.	N.A.	N.A.	N.A.
HVSI & Seg. Index	0.41	0.13	0.31	N.A.	N.A.	N.A.	N.A.

Notes: - = correlation does not meet significance criteria for inclusion; N.A. = no available data for correlation

The most significant relationship changes (whether favorable or unfavorable) revealed by the subdivision of results involve the sieve stability test, surface settlement test, and HVSI. Those changes are discussed further in Sections 2.4.4.2 through 2.4.4.4. Conclusions can also be drawn based on the relationships *not* included in Table 2.15, as their exclusion indicates what correlations, or lack thereof, shown in Table 2.14 are *not* significantly affected by subdivision of results. Notably absent are relationships involving the VSI, rapid penetration test, and coarse aggregate distribution index. These relationships are discussed in Sections 2.4.4.1 and 2.4.4.4. No correlation between fresh stability and in-situ uniformity of concrete was significantly improved through the use of a nonlinear regression model.

2.4.4.1 Visual Stability Index Correlations

The VSI exhibited the strongest correlation to both the UPV segregation index and top-bar effect of any fresh concrete stability test, at least when considering all available mixtures (twenty SCC mixtures). These relationships are shown in Figure 2.27 and Figure 2.28.

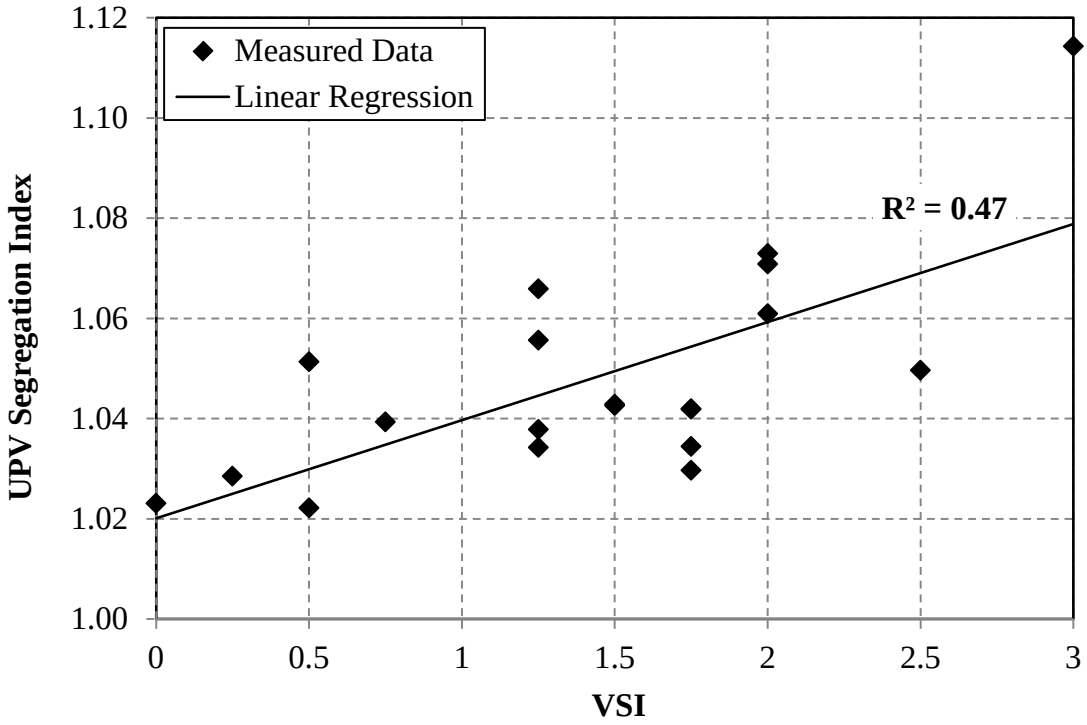

Figure 2.27: Comparison between VSI and UPV segregation index

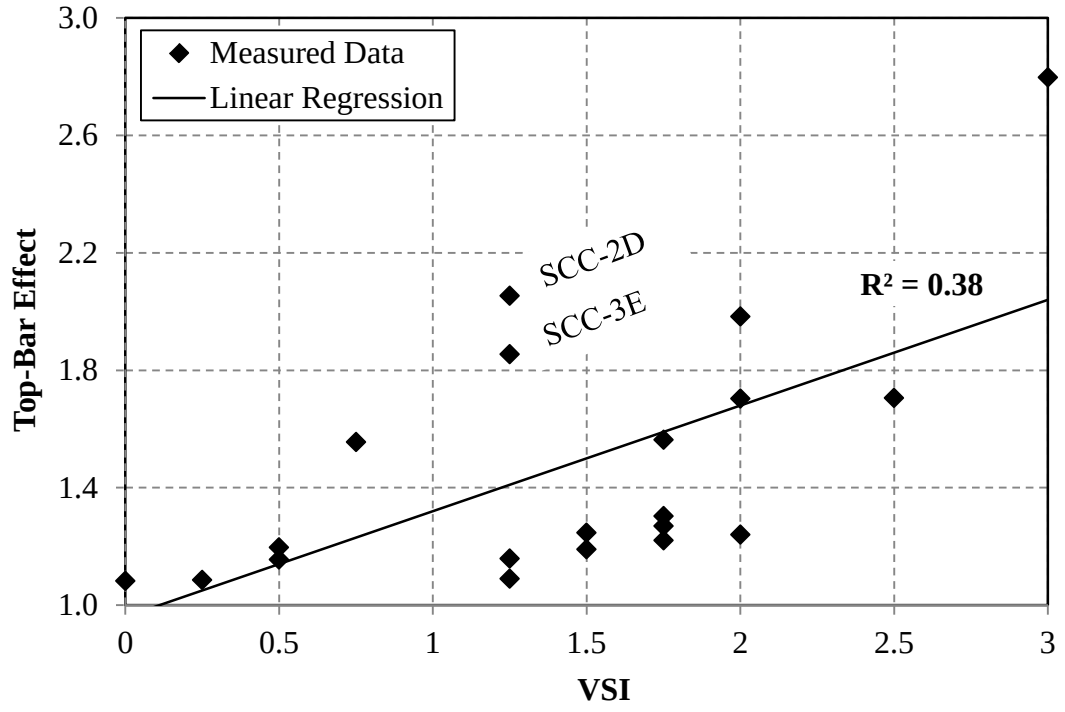

Figure 2.28: Comparison between VSI and top-bar effect

The VSI was found to be relatable to less subjective fresh concrete stability tests (see Section 2.4.2.2), and the relevance of its results to in-situ concrete uniformity is confirmed by Figure 2.27 and Figure 2.28. Important in both of those figures is that the relationships were not significantly different between classes subdivided by coarse aggregate NMSA, target total aggregate content, or, among the ½ in.-NMSA mixtures, by a combination of both. This suggests that the VSI is a viable fresh concrete stability test method for evaluation of SCC stability in a wide variety of SCC mixtures. The consistency of its results in a variety of situations should prove valuable during its use.

2.4.4.2 Sieve Stability Test Correlations

The sieve stability test exhibited the second strongest fresh concrete stability correlation to both the UPV segregation index and top-bar effect, even before subdividing its results by NMSA. Recall from Section 2.4.2.2 that the sieve stability test appears to be noticeably affected by coarse aggregate NMSA. This dependence is confirmed by the results presented in Table 2.15. Upon subdivision by coarse aggregate NMSA, the correlations between the sieve stability test and UPV segregation index are stronger than those of all other fresh test comparisons to the UPV segregation index. Likewise, its correlations to the top-bar effect are approximately as strong as the all-mixture comparison of the VSI to top-bar effect. Relationships between the sieve stability test and the two measures of in-situ concrete uniformity are shown in Figure 2.29 and Figure 2.30.

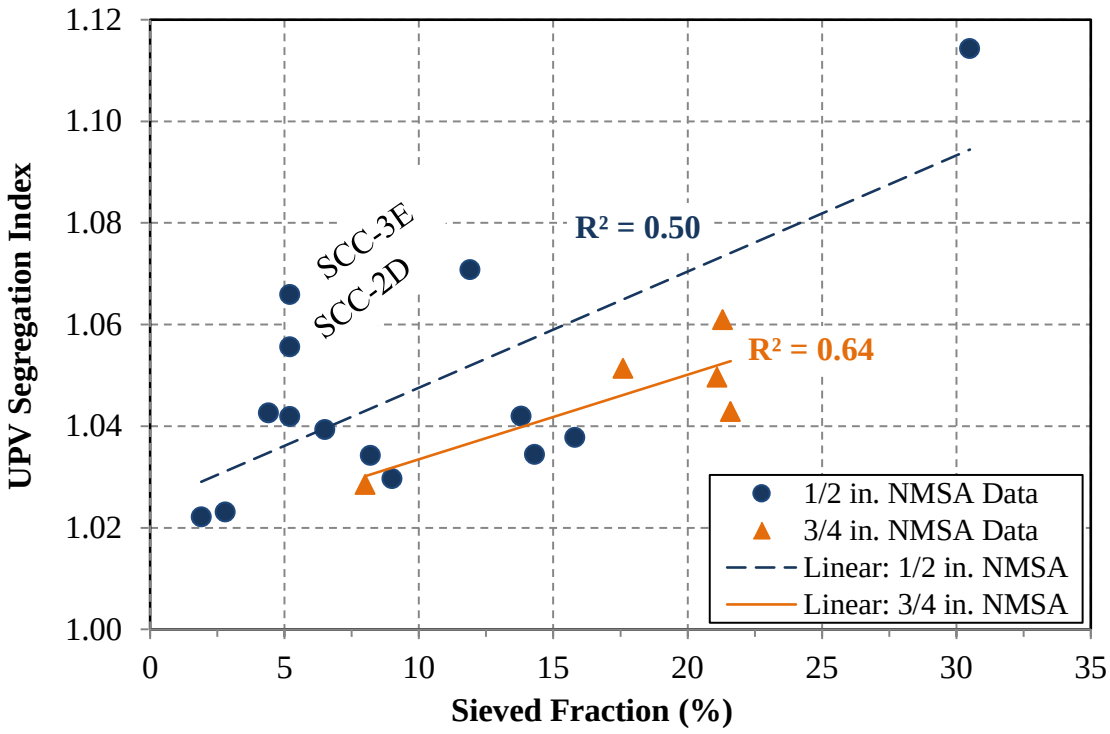

Figure 2.29: Comparison between sieved fraction and UPV segregation index (mixtures subdivided by coarse aggregate NMSA)

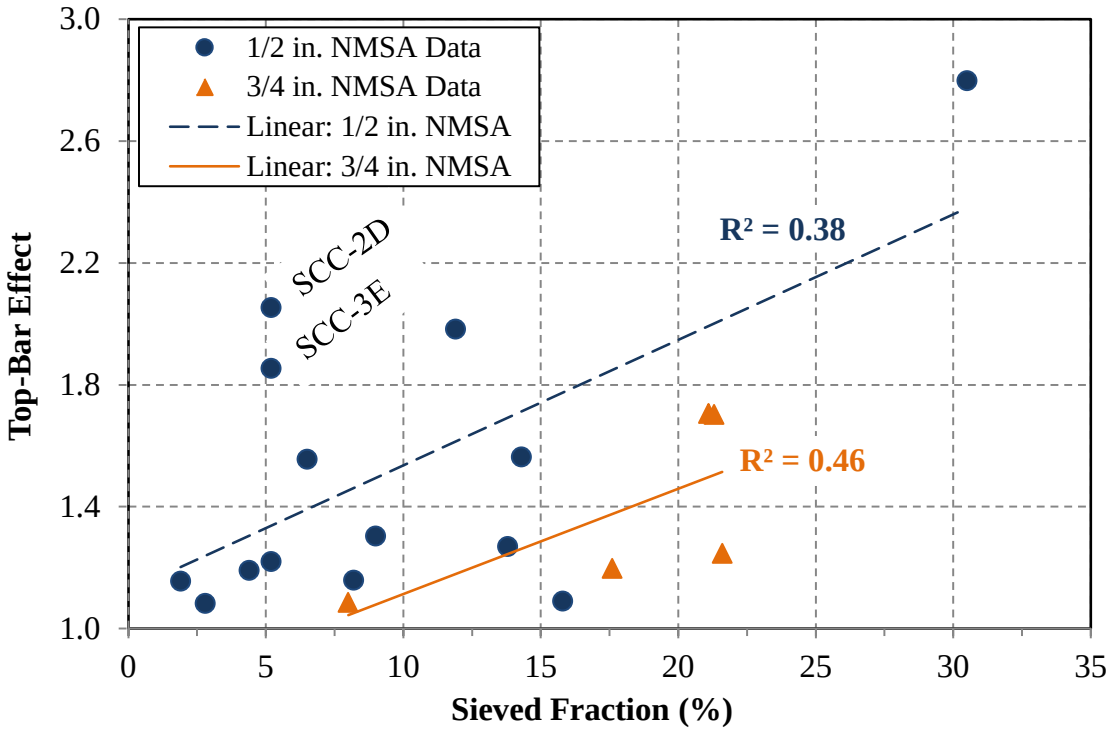

Figure 2.30: Comparison between sieved fraction and top-bar effect (mixtures subdivided by coarse aggregate NMSA)

The relevance of sieve stability results to in-situ concrete uniformity is clear in Figure 2.29 and Figure 2.30, but with results that are distinctly affected by coarse aggregate NMSA. Like its subdivided relationships with the VSI (see Section 2.4.2.2), the sieve stability relationships to both UPV and pullout uniformity indicate that larger sieve fractions occur in ¾ inch-NMSA SCC. The shift toward larger results appears to affect only the sieve stability result and not the UPV segregation index or top-bar effect, which indicates that the shift is more likely a result of the fresh concrete stability test method than different in-situ uniformity between NMSA classes. In other words, SCC mixtures of a ¾ inch-NMSA exhibit the same range of in-situ uniformity results as SCC mixtures of a smaller coarse aggregate gradation, but with consistently higher sieve stability results.

In light of the discussion of this section, the strong apparent correlation between the sieve stability test and the HVSI found over all available mixtures had to be evaluated after subdividing the results by NMSA. The subdivided results, which are presented in Table 2.15, are also illustrated in Figure 2.31.

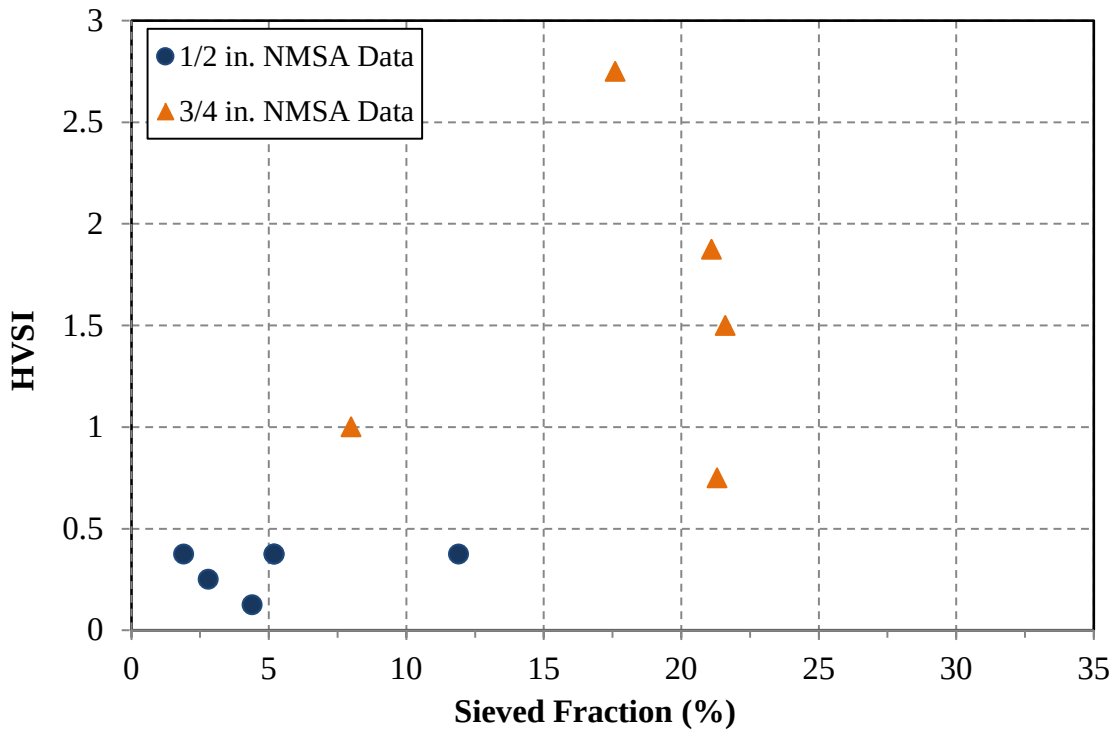

Figure 2.31: Comparison between sieved fraction and HVSI (mixtures subdivided by coarse aggregate NMSA)

It is concluded from the figure and Table 2.15 that the strong apparent correlation between the sieve stability test and HVSI is a coincidental result of the particular data collected for this research. Within each coarse-aggregate-NMSA class, the sieve stability result and HVSI

result do not correlate well; instead, a linear trend is accidentally created upon combining the two classes. Notably, distinct improvement and relative strength of sieve stability correlations to the UPV segregation index, top-bar effect, and VSI upon subdivision lead to two conclusions: 1) the sieve stability test is relatable to hardened concrete uniformity as evaluated by multiple in-situ measures, but 2) the HVSI likely exhibits too much variability to be of value to assess the impact of segregation.

2.4.4.3 Surface Settlement Test Correlations

The surface settlement test (rate of settlement or maximum settlement) did not exhibit relatively strong correlation to any measure of in-situ concrete uniformity when comparing all available results. Upon subdivision by coarse aggregate NMSA, though, the correlations between the rate of settlement and UPV segregation index are at least as strong as those of all other fresh test comparisons to the UPV segregation index. Likewise, correlations between rate of settlement and top-bar effect are the strongest of all comparisons between concrete stability and in-situ uniformity, when subdivided by coarse aggregate NMSA. Relationships between the rate of settlement and the two measures of in-situ concrete uniformity are shown in Figure 2.32 and Figure 2.33.

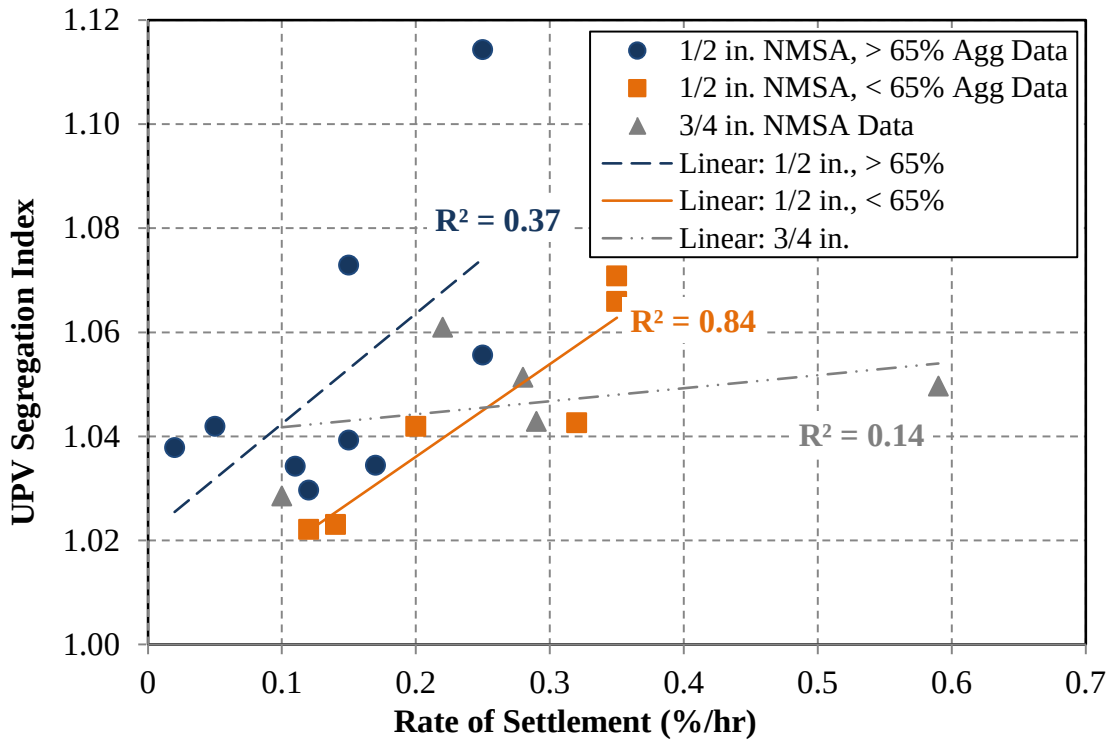

Figure 2.32: Comparison between rate of settlement and UPV segregation index (mixtures subdivided by coarse aggregate NMSA and total aggregate volume)

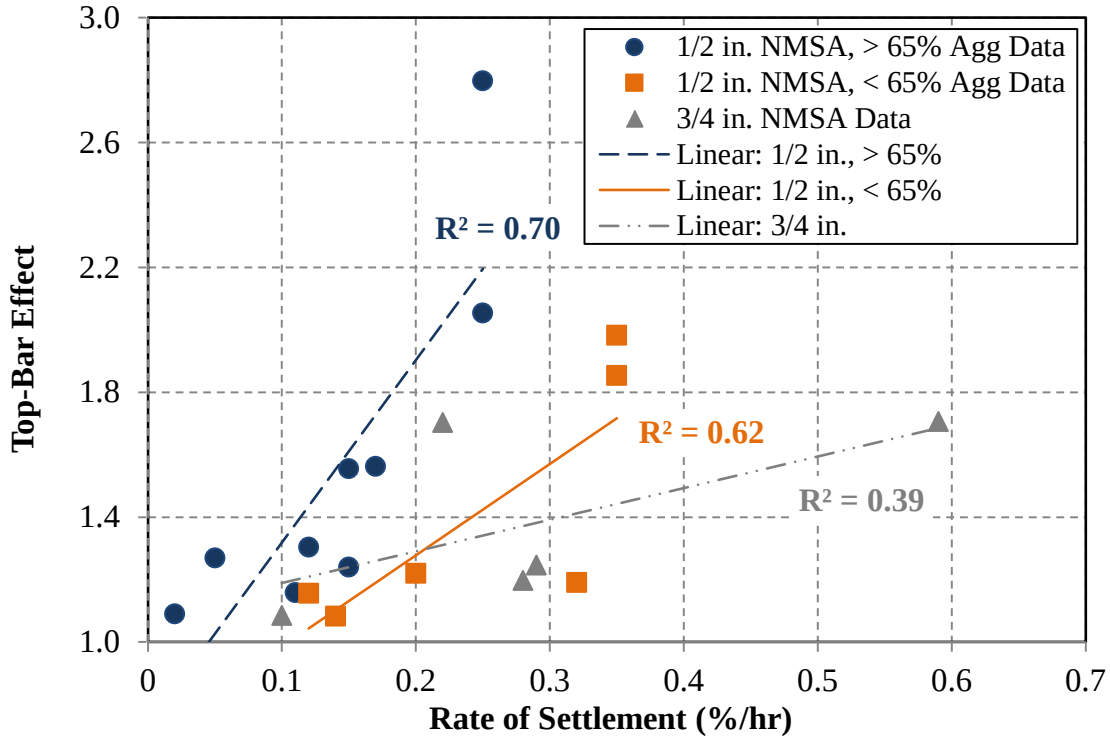

Figure 2.33: Comparison between rate of settlement and top-bar effect (mixtures subdivided by coarse aggregate NMSA and total aggregate volume)

The relevance of rate of settlement results to in-situ concrete uniformity is clear in Figure 2.32 and Figure 2.33, but with distinctly different settlement results in different classes of mixtures. There also appears to be a larger difference between the different target-aggregate-volume classes of ½ in.-NMSA results than between the two NMSA classes of a lesser target aggregate content. This is not in full agreement with the findings of Khayat and Mitchell (2009), who found that mixture NMSA predominately affects the results of this test. The results agree with the findings of Khayat (1999), Khayat et al. (2000), and Sonebi and Bartos (2002), though, who all found that the test can be affected by coarse aggregate content and binder content. Comparing target-aggregate-volume classes of the ½ in.-NMSA mixtures, the mixtures of a lesser target aggregate content clearly yield larger rates of settlement. This agrees with the findings of Bonen and Shah (2004), Koehler and Fowler (2008), and Shen (2007), who indicate that an aggregate lattice structure present in mixtures with larger total aggregate volume should reduce coarse aggregate settlement.

Similar to the discussion of the previous section (regarding sieve stability results), the shift toward larger rate of settlement results appears to affect only the fresh concrete stability test and not the UPV segregation index or top-bar effect. In other words, mixtures of a lesser total aggregate volume exhibit the same range of in-situ uniformity results as those of a larger aggregate volume, but with consistently higher rates of surface settlement.

2.4.4.4 Fresh Concrete Stability and Hardened Concrete Uniformity Tests Exhibiting Weak Correlations

The column segregation and rapid penetration tests did not exhibit relatively strong correlations to any measure of hardened concrete uniformity. Each of these tests was conducted on all twenty SCC mixtures prepared for this research, and performance was poor in all subdivisions of mixtures. Furthermore, rapid penetration test results obtained after extended rest periods correlated equally poorly with measures of in-situ uniformity in eleven tested SCC mixtures.

The only potentially viable correlation was between the segregation index (column segregation test) and the HVSI when comparing all mixtures. Subdivision of results by coarse aggregate NMSA was warranted, though, by the findings discussed in Section 2.4.2, in which the column segregation test appears to be affected by coarse aggregate NMSA. It was further necessary in light of the poor correlations found between the sieve stability test and HVSI upon subdivision of results. The sieve stability test and column segregation test appear to be equally affected by mixture NMSA (see Section 2.4.2.3), and both tests exhibit a strong correlation to the HVSI when comparing all results. Segregation index and HVSI results are plotted in Figure 2.34 and shown in Table 2.15, with results subdivided by coarse aggregate NMSA.

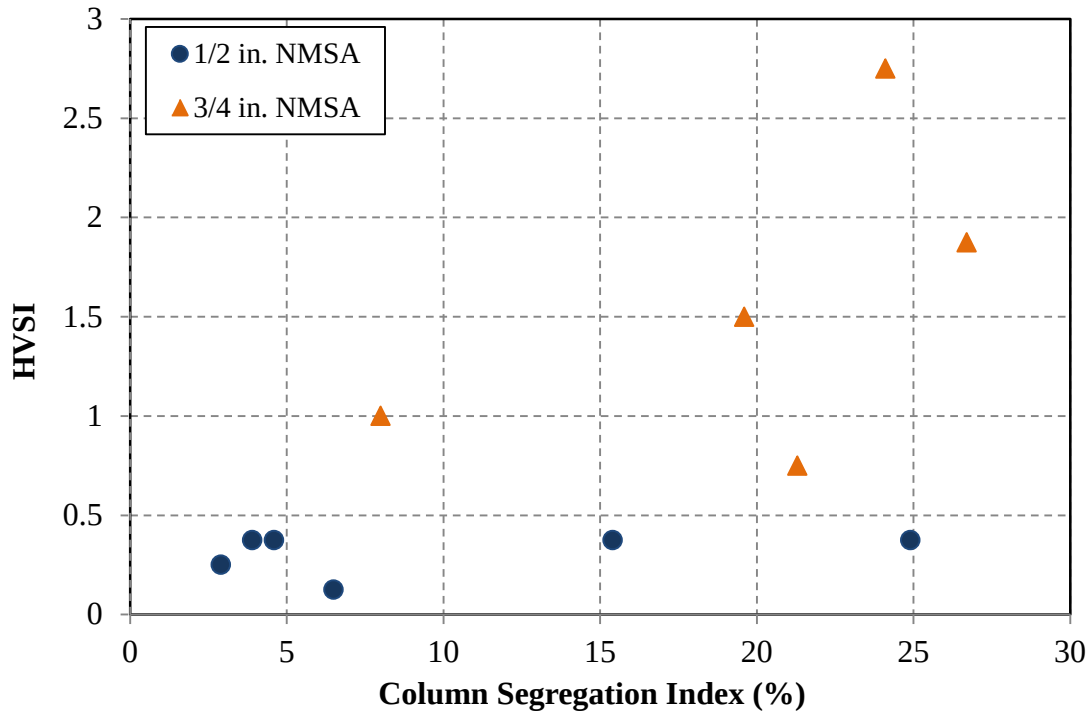

Figure 2.34: Comparison between column segregation index and HVSI (mixtures subdivided by coarse aggregate NMSA)

Like the correlation between sieve fraction and HVSI, the segregation index and HVSI data presented in Figure 2.34 and Table 2.15 indicate that the correlation between segregation fraction and HVSI is a coincidental result of the particular data collected for this research.

While the HVSI may indicate important forms of segregation (paste-layer depth and coarse aggregate content and distribution), it appears to exhibit too much variability to effectively study in-situ concrete uniformity when assessed as done in this research. Similarly, no fresh concrete stability test exhibits a strong correlation to the coarse aggregate distribution index determined through the use of DIA, whether when considering all available results or subdivided results. The core segregation index (see Section 2.4.3.2) does correlate well to the HVSI, though, which suggests that lack of correlation to fresh concrete stability tests is a result of the variability of the coring process and not an inability of fresh tests to identify stability. In other words, while several fresh concrete stability tests consistently correlate to measures of in-situ uniformity, a larger collection of cores (for HVSI or DIA analysis) would be necessary to effectively evaluate a mixture's in-situ uniformity.

2.4.5 Stability Testing Protocol and Criteria

2.4.5.1 Test Method Recommendations

The use of the VSI, sieve stability test, and surface settlement test in determining SCC stability is warranted from the discussions presented in Sections 2.4.2 and 2.4.4. In summary from those sections, these tests are recommended for use because

- The VSI is the only fresh concrete stability test that is well-correlated to hardened concrete uniformity as measured by both UPV and pullout testing when considering all available data, thus making it the most versatile fresh concrete stability test evaluated,
- The sieve stability test exhibits the strongest correlations to hardened concrete uniformity as measured by both UPV and pullout testing when accounting for coarse aggregate NMSA, thus making it the most accurate fresh concrete stability test when coarse aggregate NMSA is known, and
- The surface settlement test (rate of settlement) exhibits the strongest correlation to hardened concrete uniformity as measured by pullout testing when considering target total aggregate volume, thus making it the most valuable fresh concrete stability test when aggregate content is known to equal greater or less than 65% of total volume.

Further conclusions concerning the use of these tests, summarized from Sections 2.4.2 and 2.4.4, include that

- The use of an abbreviated rest period of eighty seconds during the sieve stability test is warranted based on strong correlation between the abbreviated results and those taken after the standard, fifteen-minute rest period,
- Sieved fractions measured after a rest period of eighty seconds are comparable to results obtained after a rest period of fifteen minutes, but differences may be conservatively accounted for during acceptance criteria determination, and
- Measurement of the rate of settlement determined over the 5-min. interval between (10:00–15:00) is sufficient for stability assessment by the surface settlement test, based on strong correlation between the rate of settlement and maximum settlement determined during the test.

Based on these conclusions, the testing protocol recommended by Keske et al. (2013b) is confirmed, except that the use of an abbreviated rest time with the sieve stability should be used during testing. Thus, the use of the VSI and *abbreviated* sieve stability test are recommended for use in on-site quality assurance, while the surface settlement test (rate of settlement) is recommended for mixture prequalification in a laboratory setting. The VSI test provides quick feedback and should be the first test used to screen a load of SCC for quality

assurance. If the VSI result exceeds acceptable limits (discussed in the next subsection), then the slower sieve stability test can provide a quantitative result for final determination of batch acceptance or rejection.

Different limiting VSI and sieve fraction values have been previously recommended; regardless, using the sieve stability test result can remove undesirable subjectivity from batch acceptance decisions in borderline VSI situations. This approach requires simultaneous initiation of the VSI and sieve stability tests, but the sieve stability test may be discontinued if the SCC exhibits a clearly acceptable VSI result. The two test methods are strongly correlated, and this simple approach provides a quantitative means for field quality assurance testing.

2.4.5.2 Test Result Recommendations

In accordance with the practice of Keske et al. (2013b) and Khayat and Mitchell (2009), acceptance criteria for these three tests were determined based on limiting measured top-bar effects to less than 1.4. This top-bar-effect limit is based on the top-bar factor applied by AASHTO (2013) and ACI 318 (2011), and its use for acceptance criteria determination is further discussed in Section 2.2.3.2. The rounded fresh stability test results beneath which the tested concrete should not exhibit a top-bar effect greater than 1.4 are summarized in Table 2.16. Also, a UPV segregation index limit of 1.045 was utilized based on the relationship between top-bar effect and UPV segregation index discussed in Section 2.4.3.4. The two in-situ measures are strongly correlated, so fresh concrete stability criteria based on the UPV segregation index should affirm the criteria determined based on the top-bar effect.

Table 2.16: Fresh concrete stability test acceptance criteria

Fresh Test		In-Situ Measurement		Recommended Test Criteria
Result	**Result Subdivision**	**UPV Seg. Index = 1.045**	**Top-Bar Effect = 1.4**	
VSI	All	1.35	1.35	≤ 1.0
Sieved Fraction	½ in. NMSA:	9.2[1]	8.5[1]	≤ 7.5%[2]
	¾ in. NMSA:	17.3[1]	18.0[1]	≤ 15%[2]
Rate of Surface Settlement	> 65% Agg.:	0.130	0.122	≤ 0.12 %/hr
	< 65% Agg.:	0.267	0.269	≤ 0.27 %/hr

Notes: [1]=based on results 15 min. test results; [2] = recommended for use with abbreviated version of test (using 80 sec. rest period)

The linear regression model shown in Figure 2.28 for the relationship between the VSI and top-bar effect identifies a top-bar effect of 1.4 at a VSI value of approximately 1.35. This is confirmed by the model for the relationship between the VSI and UPV segregation index. Therefore, a VSI limitation of 1.0 is recommended in Table 2.16, as it conservatively accounts for the subjectivity of the VSI test method and matches the recommendation of Khayat and Mitchell (2009). A VSI of 1.0 is also generally effective at identifying mixtures that exhibited acceptable uniformity. However, final determination of SCC stability acceptance in mixtures of questionable uniformity (those exhibiting a VSI greater than 1.0) should be based upon a more quantitative test method such as the sieve stability test.

The linear regression models shown in Figure 2.30 for the relationships between the sieved fraction and top-bar effect identify a top-bar effect of 1.4 at distinctly different sieved fractions, depending on coarse aggregate NMSA. These results are confirmed by the relationships between sieved fraction and UPV segregation index. Thus, the recommendations for sieved fraction acceptance criteria reflect the distinction:

- A sieved fraction limitation of 7.5% is shown for ½ in.-NMSA SCC because 10% matches the maximum sieved fraction recommended by EPG (2005) for highly demanding applications (vertical construction with confinement or lengthy flow), and a conservative reduction is acceptable for the abbreviated sieve stability test procedure discussed earlier, while
- A sieved fraction limitation of 15% is shown for ¾ in.-NMSA SCC because it matches the maximum sieved fraction recommended by EPG (2005) for Class 2 applications (vertical construction with limited confinement and travel distance), and Class 2 or less demanding class status is probable where ¾ in.-NMSA SCC can be utilized.

Selection of a slightly conservative allowable sieved fraction should account for potential increases in the variability of results taken after an 80-sec. rest period. It should also account for the prevalence of higher coarse aggregate fractions in precast, prestressed SCC. As coarse aggregate fraction increases, the portion of SCC that *can* fall through the sieve (mortar) decreases; consequently, the sieve stability test yields smaller sieved fraction results in these situations regardless of the actual segregation potential between mortar and coarse aggregate.

Similarly, the linear regression models for the relationships between the rate of settlement and top-bar effect identify a top-bar effect of 1.4 at distinctly different rates of settlement, with a lower allowable rate of settlement seen in SCC of a larger total aggregate fraction. These results are confirmed by the relationships between rate of settlement and UPV segregation index. Thus, the recommendations for surface settlement rate acceptance criteria reflect the distinction:

- A settlement rate limitation of 0.12 %/hr is shown for high-aggregate-volume SCC because it matches the maximum rate recommended by Khayat and Mitchell (2009) for SCC of greater than ½ in. NMSA, and use of the most conservative published result is warranted based on measured in-situ concrete uniformity results, while
- A rate limitation of 0.27% is shown for low-aggregate-volume SCC because it matches the maximum rate recommended by Khayat and Mitchell (2009) for SCC of ½ in. or smaller NMSA, and its use is warranted based on measured in-situ concrete uniformity results.

Two SCC mixtures—SCC-2D and SCC-3E—exhibited questionable VSI results (1.25 for each) and sieved fraction results that would be acceptable (5.2% for each) but unacceptable UPV segregation indices and top-bar effects (see Figure 2.28–Figure 2.30). They also exhibited rates of surface settlement that would be unacceptable according to the above recommendations (see Table 2.5). The discrepancy between these results confirms that the use of conservative VSI and sieved fraction acceptance criteria are appropriate based on this research and that the surface settlement test is the most accurate of the evaluated fresh concrete stability test methods. Confounding factors and the nature of fresh concrete stability testing make it difficult to isolate the cause of the error; considering that these mixtures exhibited among the highest *w/cm* of any tested SCCs (0.43 and 0.44) and a 30% SCM replacement rate (see Table 2.3), these particular mixtures may also be less indicative of SCC for precast, prestressed applications than others whose test results were more consistent.

The recommended rate of settlement and sieved fraction acceptance criteria may seem to contradict the recommendations of Khayat and Mitchell (2009) presented in NCHRP 628. They recommended a smaller acceptable surface-settlement rate limit for SCC of a larger NMSA (which may be subject to greater segregation potential), while the criteria recommended in Table 2.16 indicate a larger acceptable limit for SCC of a low total aggregate volume or larger NMSA. The results of this research indicate that SCC of a lesser aggregate volume or larger coarse aggregate gradation yields larger fresh concrete stability values (indicating less stability) but *equally acceptable* hardened in-situ concrete uniformity. While use of a larger total aggregate fraction or smaller coarse aggregate NMSA may reduce aggregate settlement, they do not prevent other forms of SCC segregation.

2.5 SUMMARY AND CONCLUSIONS

2.5.1 Summary

The research described in this chapter was undertaken as part of a larger research project funded by ALDOT to study the behavior of SCC used in the production of precast, prestressed bridge girders. This laboratory phase was undertaken to address the assessment of fresh SCC stability, as this is a concern that may limit the use of SCC in precast, prestressed applications. Five fresh concrete stability tests were selected for further study:

- ASTM C1611 Visual Stability Index (described in Section 2.2.1.1),
- ASTM C1610 Column Segregation Test (described in Section 2.2.1.2),
- ASTM C1712 Rapid Penetration Test (described in Section 2.2.1.3),
- Sieve Stability Test (described in Section 2.2.1.4), and
- Surface Settlement Test (described in Section 2.2.1.5).

To assess these tests, they were conducted concurrently with the casting of three concrete walls with heights of 54, 72, and 94 inches. Walls were cast and fresh concrete stability tests were conducted on a total of twenty mixtures, twenty of which were SCC. The twenty SCC mixtures were divided into four approximately equal groups by coarse aggregate size (½ in.-NMSA or ¾ in.-NMSA), total aggregate volume, and workability. Each mixture was adjusted to exhibit different fresh behavior and stability. The adjustments to stability were controlled by varying water content, HRWRA content, VMA content and type, or a combination of the variables.

The four VC mixtures were proportioned similarly to the SCC mixtures but using a higher *w/cm*, lower *s/agg*, and larger aggregate gradation typical of VC used in precast, prestressed applications. Only in-situ uniformity tests were conducted on VC mixtures, as the fresh concrete stability test methods could only be assessed in SCC mixtures.

Four test methods were selected to measure in-situ uniformity of the concrete walls: ultrasonic pulse velocity (UPV) testing, pullout bond testing, visual stability testing of hardened concrete cores (HVSI), and digital image analysis (DIA) of aggregate content in hardened specimens. UPV testing was used primarily to identify changes in overall uniformity of concrete, including changes in air void distribution and aggregate distribution. Pullout testing was conducted on eight-specimen groups of deformed steel bars cast horizontally through the walls at the bottom and top of each. This method was used primarily to identify changes in bond uniformity.

UPV segregation indices were determined for each wall and mixture based on the ratio of the fastest average pulse velocity to the slowest. The largest UPV segregation index for each mixture was used for comparative purposes. A top-bar effect was determined for each wall and mixture based on the ratio of the pullout strength of the bottom group of bars to the strength of the

top group of specimens cast into each wall. The largest top-bar effect for each mixture was used for comparative purposes.

Following completion of UPV and pullout testing, four cores were taken from each 72 in. wall. Top-cast cores were evaluated using the HVSI, which identifies paste-layer depth and variation in the distribution and content of aggregate. DIA testing was then conducted on top- and bottom-cast cores to provide a quantitative measure of aggregate content in the top and bottom of each 72 in. wall. This quantitative measure, the coarse aggregate distribution index, was determined by dividing the coarse aggregate content in the bottom-cast cores by that of the top-cast cores.

Results from the five fresh concrete stability tests were then compared with each other and with the results of each in-situ hardened concrete uniformity test. The observations and conclusions made during the collection and analysis of these results are summarized in Section 2.5.2. The recommendations made based on this research are given in Section 2.5.3.

2.5.2 Research Observations and Conclusions

2.5.2.1 Fresh Concrete Stability Tests

- Fresh stability tests were compared to each other when using all available SCC test results (twenty results) and when using results from the same subdivision (by coarse aggregate NMSA, total aggregate volume, or both). While the VSI exhibited the same range of results within all subdivisions, the other fresh tests were affected by one or more of the studied mixture variables.
- The strongest correlations between fresh tests were those between the sieve stability, VSI, and column segregation tests (three paired correlations), and between the rate of settlement and maximum settlement determined from the surface settlement test. Only the fresh-test correlation between the rate of settlement and maximum settlement was *not* affected by at least one of the studied mixture variables.
- The rate of settlement determined during the surface settlement test correlated well with the maximum settlement found during the same test (R^2 = 0.60) when compared using a linear regression model. Correlations between results subdivided by coarse aggregate NMSA or total aggregate volume were equally strong (based on magnitude of R^2-value) when using a nonlinear model.
- The sieve stability test correlated well with the VSI, but with different sieved fraction results when results were divided by coarse aggregate NMSA (R^2 = 0.62 and 0.63 among ½ in. and ¾ in.-NMSA mixtures). The VSI exhibited the same range of test results

among both subdivisions, which suggests that the sieve stability test yields larger sieved fraction results when testing ¾ in.-NMSA SCC than when testing ½ in.-NMSA SCC.

- The sieve stability test correlated well with the column segregation test, but with different relationships when considering relationships divided by coarse aggregate content (R^2 = 0.54 and 0.72 among mixtures with greater than or less than 65% total aggregate volume fraction). This was true even among mixtures of the same NMSA (R^2 = 0.54 and 0.80 among ½ in.-NMSA SCC of different total aggregate volumes). This suggests that both tests are similarly affected by SCC segregation.
- The rapid penetration test did not show any reasonable correlations to other fresh concrete stability tests, whether considering all results or those subdivided into categories of NMSA or total aggregate volume.
- Sieve stability test results obtained after abbreviated rest periods of eighty seconds, five minutes, and ten minutes all correlated well with those obtained after the standard fifteen-minute rest period (R^2 = 0.93, 0.90, and 0.95, respectively). The abbreviated-rest results were approximately equal to the standard-rest results and did not vary consistently with rest period.

2.5.2.2 Hardened Concrete Uniformity Tests

- The HVSI assessed according to AASHTO PP-58 (AASHTO 2012) ranged from 0 to 3 in eleven SCC mixtures and was less than or equal to 1 in two VCs. ½ in.-NMSA mixtures exhibited lower HVSI values (indicating better uniformity), although adjacent samples from the same wall exhibited HVSI values that differed by as much as 2 (on a 0–3 scale). Therefore, large variability in the HVSI may be a result of the heterogeneous nature of as-placed concrete.
- The coarse aggregate distribution index (ratio of coarse aggregate in bottom sample to top sample) assessed with digital image analysis of cores ranged from 1.085 to 1.468 in eleven SCC mixtures and equaled 1.065 and 1.141 in two VCs. Variability between adjacent cores, at both the top and bottom of each wall, was as significant as that identified by the HVSI. Therefore, large variability in this type of core assessment is likely a result of the heterogeneous nature of as-placed concrete.
- The UPV segregation index and top-bar effect are strongly correlated (R^2 = 0.69), but the HVSI and coarse aggregate distribution index do not exhibit a reasonable correlation with the UPV segregation index, top-bar effect, or each other. The HVSI correlates well with the core segregation index (R^2 = 0.64), a quantifiable measure of the coarse aggregate uniformity in the top-cast samples that were also tested according to the HVSI. This

indicates that the core aggregate distribution can be quantified, although the significance of this measurement is unclear.

- Mixtures exhibiting acceptable uniformity according to the HVSI and coarse aggregate distribution index may not exhibit acceptable UPV and pullout uniformity, or vice versa.

2.5.2.3 Relationships between Fresh Concrete Stability and Hardened Concrete Uniformity Test Results

- When comparing all available SCC results, the only relatively strong relationships were those relating the VSI to the UPV segregation index and top-bar effect (R^2 = 0.47 and 0.38, respectively) and the sieve stability test to the UPV segregation index (R^2 = 0.39). Only the relationships between the VSI and measures of hardened concrete uniformity were unaffected by the subdivision of mixture results by coarse aggregate NMSA or total aggregate volume.
- Relationships between the sieve stability test and both UPV segregation index and top-bar effect were significantly improved by the subdivision of results by coarse aggregate NMSA (R^2 range = 0.38–0.64). This confirms that the sieve stability test is affected by coarse aggregate NMSA but is well correlated to measures of in-situ hardened concrete uniformity when considering that variable.
- Relationships between the rate of settlement and both UPV segregation index and top-bar effect were significantly improved by the subdivision of results by total aggregate volume, and the subdivided correlations were among the strongest between any fresh concrete stability test and these measures of hardened concrete uniformity (R^2 range = 0.37–0.84). This confirms that the rate of settlement from the surface settlement test is affected by total aggregate volume but is well correlated to measures of in-situ hardened concrete uniformity when considering that variable.
- The column segregation and rapid penetration tests were not well correlated to any measure of in-situ hardened concrete uniformity, and the HVSI and coarse aggregate distribution index were not well correlated to any measure of fresh concrete stability.
- SCC of a lesser total aggregate volume or larger coarse aggregate NMSA may exhibit larger fresh stability test results (suggesting less stability), but in-situ hardened uniformity of concrete made with these mixtures can be equal to that of SCC of a larger total aggregate volume or smaller coarse aggregate NMSA, as well as that of a variety of VCs.

2.5.3 Recommendations

2.5.3.1 Test Method Recommendations

- The VSI correlates well with quantitative measures of fresh concrete stability and several measures of in-situ hardened concrete uniformity, and its results are not affected by coarse aggregate NMSA or volume fraction. It is, therefore, the most versatile fresh concrete stability test studied, so it is valuable in determining SCC stability despite its subjective nature.
- The sieve stability test is quantitative in nature and correlates well with measures of fresh concrete stability and in-situ hardened uniformity. Its results are affected by coarse aggregate NMSA, in which larger sieved fractions may occur in SCC of a larger coarse aggregate NMSA. The sieve stability test is, therefore, a preferred test method for SCC stability when coarse aggregate NMSA is known.
- The results obtained from the sieve stability test after an abbreviated eighty-second rest period strongly correlate to those obtained after a standard fifteen-minute rest period, so the use of the abbreviated eighty-second rest period is recommended to provide accelerated results which will be best to use for job-site quality assurance testing.
- The sieve stability test correlates well with the column segregation test regardless of mixture subdivision by coarse aggregate NMSA or total aggregate volume, and it is more convenient, so it should always be used in place of the column segregation test for determination of SCC stability.
- The surface settlement test (rate of settlement) is quantitative in nature and correlates well with measures of in-situ hardened concrete uniformity. Its results are affected by total aggregate volume, in which larger rates of settlement may occur in SCC of a lesser total aggregate volume. The surface settlement test is, therefore, a preferred test method for SCC stability when the approximate total aggregate volume is known.
- The rate of settlement and maximum settlement measured by the surface settlement test are strongly correlated, so the use of only the rate of settlement in place of the maximum settlement is recommended for improved test convenience.
- The use of the rapid penetration test, column segregation test, HVSI, and DIA of cores are not warranted by the results of this research. Reasons for their poor performance are unclear, although high test variability is suspected.

2.5.3.2 Stability Testing Protocol and Criteria

During mixture prequalification in a laboratory setting, the rate of settlement determined during the surface settlement test should be used alongside the sieve stability test to determine SCC mixture stability. The two measures, both of which provide a quantitative result and relate well with in-situ measures of hardened concrete uniformity, are differently affected by mixture composition and should together provide comprehensive identification of mixture stability. The rate of surface settlement should be limited to less than 0.12 %/hr and 0.27 %/hr for SCC with greater than and less than 65% total aggregate volume, respectively. The sieved fraction should be limited to 7.5% and 15% for ½ in. and ¾ in.-NMSA SCC, respectively.

Because it provides quick feedback, the VSI test should be the first test used to screen a load of SCC for quality assurance during full-scale production. If the VSI result exceeds 1.0, then the sieve stability test can provide a quantitative result for final determination of batch acceptance or rejection while removing undesirable subjectivity from batch acceptance decisions in borderline VSI situations. The sieve stability result at which to determine acceptance may vary by application, mixture, and reinforcement type, but, when evaluating SCC for precast, prestressed applications, sieved fractions of 7.5% and 15% should be acceptable for ½ in. and ¾ in.-NMSA SCC, respectively. This approach requires simultaneous initiation of the VSI and sieve stability tests, but the sieve stability test may be discontinued if the SCC exhibits a VSI less than or equal to 1.0. Despite the additional effort, this approach is simple and provides a quantitative means for field quality assurance testing.

CHAPTER 3: TIME-DEPENDENT DEFORMABILITY OF PRECAST, PRESTRESSED CONCRETE

3.1 INTRODUCTION

Self-consolidating concrete can exhibit different time-dependent deformation tendencies than VC of the same compressive strength or intended use because it frequently incorporates different constituent proportions than VC. Time-dependent deformation of concrete is considered in two parts: creep, or the time-dependent increase in strain under a sustained compressive load, and shrinkage, or the time-dependent, load-independent contraction due to drying and hydration of concrete.

Drying shrinkage occurs as water escapes concrete due to a difference between its internal humidity and the surrounding relative humidity. Shrinkage due to the chemical hydration of portland cement, which can occur even in concrete exposed to 100% relative humidity, is referred to as autogenous shrinkage. It is impossible to distinguish between autogenous and drying shrinkage in a particular concrete without exposing matching specimens to both 100% relative humidity and ambient relative humidity conditions, so the two are frequently grouped together and termed “free shrinkage” (Neville 1996; Mindess et al. 2003). Furthermore, creep has been found to increase in concrete exposed to both sustained stress and drying at the same time. While creep can thus be classified as basic creep or drying creep, it is common practice to ignore the distinction and consider creep to equal the deformation under load in excess of the sum of the initial elastic strain and accumulated free shrinkage strain (Mehta and Monteiro 2006).

While the underlying mechanisms are complicated, the effects of creep and shrinkage are direct—they induce concrete length change. Depending on restraint and loading conditions, this can lead to stress development, cracking, and changes in deflections in concrete structures. In prestressed members, these length changes also result in a change in length of the prestressing tendons which directly relates to maintenance of prestress force—prestress force decreases as the strands and the surrounding concrete contract. Because of this dependence, accurate prediction of long-term time-dependent deformation is crucial in the design of prestressed structures (Khayat and Mitchell 2009).

Many of the deformation prediction models currently in use are based on outdated research and were formulated using assumptions that may no longer be valid in current practice. The applicability of these models to SCC behavior is especially questionable. To address this, the AUHRC team evaluated time-dependent deformability of the SCC and VC used to construct the Hillabee Creek Bridge. This evaluation was completed using specimens cast during production days SCC-B, SCC-C, SCC-E, VC-B, and VC-F, thus including batches of the same

mixtures that had been produced under varied exposure conditions. The primary objective of this work was to evaluate the acceptability and relative predictability of precast, prestressed SCC and VC time-dependent deformability. To extend the previous work related to this topic reported by Keske et al. (2015), adjustments that could be made to the existing time-dependent material models were also sought during this work.

3.2 LITERATURE REVIEW

Volumetric change of concrete over time is an inherent property of the material, and it is influenced by a variety of factors that are interdependent. From ACI 209 (1992), some of these influences include

- Concrete composition including paste content, *w/cm*, and aggregate type,
- Environmental conditions such as ambient humidity, in which less contraction is experienced when a higher relative humidity is maintained,
- Geometric member properties including volume-to-surface-area ratio (*V/S*), in which decreasing *V/S* leads to increasing deformation, and
- Stress state, in which stress concentrations or inelastic-level stresses cause less predictable deformation responses.

In this research, the primary differences between the studied SCC and VC involve only the first of these—changes in mixture materials and proportions incorporated to yield self-consolidating behavior. While the other factors are significant, they were approximately the same for both materials. Specimens of SCC and VC were always geometrically identical, they were each loaded proportionally to f_c, and they were all exposed to very similar ambient conditions in the field or in controlled environmental conditions maintained for standardized assessment.

Differences in volumetric-change behavior can be evaluated either by observing structural behaviors that are affected by the volumetric change or by measuring volumetric changes in representative samples. Literature concerning the time-dependent *material* behavior of concrete is reviewed in the following sections, and the effect of time-dependent deformation on structural performance of full-scale girders is discussed in Chapter 4.

3.2.1 Creep and Shrinkage of Self-Consolidating Concrete

In concrete, irreversible decreases in volume over time take place in the paste phase (cementitious material and water), while aggregate experiences almost no volumetric change and acts to restrain the contraction of the paste (Mehta and Monteiro 2006; Mindess et al. 2003; Neville 1996). Thus, greater time-dependent volumetric change is expected in concrete mixtures with greater paste volumes (Neville 1996; Mehta and Monteiro 2006). This dependence on paste

volume has been widely cited as the main reason that SCC may exhibit more time-dependent deformation than VC (EPG 2005; *fib* 2010; Koehler et al. 2008; Naito et al. 2005; Ziehl et al. 2009).

Results have been inconsistent concerning the influence of SCMs, such as fly ash and slag cement, on time-dependent deformability. Some researchers (Khayat 1999; Raghavan et al. 2002; Schindler et al. 2007) found deformability to be reduced through the use of SCMs, while others (Horta 2005; Khayat and Mitchell 2009) found that it was increased. The effects of SCMs at least partly relate to the delayed strength gain associated with their use (Mehta and Monteiro 2006; Mindess et al. 2003). Compliance (strain per unit of stress) has been found to be inversely proportional to the strength of concrete at the time of load application over a wide range of strengths. Because SCMs such as slag cement tend to delay strength gain, concrete made with SCMs may exhibit greater early-age deformability (Peirard et al. 2005; Ziehl et al. 2009). Pierard et al. (2005) further found that slag cement (which was utilized in this project) also affects the load-independent free shrinkage behavior of concrete by delaying and prolonging drying.

The effect of aggregate on time-dependent deformability is two-fold: increasing aggregate content coincides with a reduction in the paste volume of the concrete (thus indirectly reducing the potential for time-dependent deformation), and it directly relates to the stiffness of the material. Its contribution to E_c was discussed in detail in Chapter 3 of Keske et al. (2015), and its effect on creep and shrinkage is similar—use of stiff aggregate restrains the volumetric deformation of the material (Mehta and Monteiro 2006). Therefore, SCC is expected to exhibit greater deformability when the volume of stiff coarse aggregate is reduced in the mixture (Khayat and Mitchell 2009; Koehler et al. 2007; Zia et al. 2005).

Similar to the effect of *s/agg* on E_c, Koehler et al. (2007) and Schindler et al. (2007) found that *s/agg* had essentially no effect on time-dependent deformability. Trejo et al. (2008), who worked with Koehler et al. (2007), hypothesize that the effect of *s/agg* on time-dependent deformability is minimized when elastic properties of the coarse and fine aggregates are similar. Ziehl et al. (2009) further found that SCC time-dependent properties were improved by the use of a larger *s/agg* because a weak coarse aggregate was incorporated in all mixtures tested during that research. Conflicting with these findings, Khayat and Mitchell found that increasing *s/agg* directly contributed to increased free shrinkage but had minimal effect on creep behavior.

Mehta and Monteiro (2006) and Neville (1996) conclude that f_c is strongly related to creep and shrinkage, both for direct and indirect reasons. Higher f_c may be achieved through the use of a lower *w/cm* or by other means, such as by increasing the content of high-quality aggregate. Reducing *w/cm* reduces water availability (which directly reduces creep and shrinkage), while the effects of increasing aggregate content have previously been discussed. Specifically regarding shrinkage, reducing *w/cm* increases autogenous shrinkage while reducing drying shrinkage. Thus, the effects of these changes on total free shrinkage depends upon the mixture.

Many underlying factors affect f_c, and it is difficult to change one mixture variable without affecting others. For example, reducing the *w/cm* while keeping the cement content constant reduces the paste *volume* (because less water is used). This volumetric reduction (at a constant cement content) is offset by increasing the aggregate content. Because mixture proportioning can be varied in many ways to produce concretes of similar mechanical properties (f_c or E_c), findings regarding SCC creep and shrinkage versus those of vibrated concrete have been inconsistent. The current European Model Code (*fib* 2010) notes in Sections 5.1.9.4.3 and 5.1.9.4.4 that SCC may exhibit 10–20% greater creep deformation and 20% greater shrinkage due to its increased paste content but that "deformations are within the scatter band for ordinary structural concrete, which is defined to be ±30%." This accepted level of precision is important when considering the accuracy of the prediction models described in in the following sections.

3.2.2 Creep Prediction Methods

Four current creep prediction models were selected for evaluation in this research. They include the model proposed by the ACI Committee for Creep and Shrinkage in Concrete (ACI 209 1992), the current model from Section 5.4.2.3.2 of *AASHTO LRFD* 6th Edition (AASHTO 2013), the SCC-specific adaptation of the AASHTO provisions developed by Khayat and Mitchell (2009), and the current model used in the European Model Code (*fib* 2010). These are referred to as the ACI 209, AASHTO 2013, NCHRP 628, and MC 2010 models, respectively, in the following subsections.

Several other creep prediction models, including older versions of the models used by AASHTO and *fib*, exist in the literature. These models were excluded from this report for several reasons:

1. They are outdated and are not regularly specified (especially among codes in which a more recent version of the same model has been implemented),
2. They are of little value to ALDOT, the chief sponsor of this research for whom these findings were prepared, due to the prevalence of the *AASHTO LRFD* specification, and
3. They were found to be no more accurate during other past studies of Alabama SCC creep conducted by Kavanaugh (2008) and Kamgang (2013).

3.2.2.1 ACI 209

The ACI Committee for Creep and Shrinkage of Concrete (ACI 209) has recommended the same creep prediction model since publishing its report on the topic in 1992 (*Prediction of Creep, Shrinkage, and Temperature Effects in Concrete Structures*). The prediction method yields an ultimate creep coefficient, v_u, which is adjusted to account for mixture properties, loading age, specimen geometry, and environmental conditions. Defined as the ratio of creep strain to initial

elastic strain resulting from the application of load, the ultimate creep coefficient is computed by the following equation:

$$v_u = 2.35(\gamma_{la}\,\gamma_\lambda\,\gamma_{vs}\,\gamma_\psi\,\gamma_s\,\gamma_a) \quad (3\text{-}1)$$

Where

γ_{la} is the loading age correction factor,
γ_λ is the relative humidity correction factor,
γ_{vs} is the volume-to-surface-area ratio correction factor,
γ_ψ is the fine aggregate percentage correction factor,
γ_s is the slump correction factor, and
γ_a is the air content correction factor.

The correction factors seen in Equation 3-1 are applied to the standard ultimate creep coefficient (2.35 in the equation) to account for conditions other than standard concrete composition and conditions. The derivations of these correction factors are given in ACI 209 (1992) and are discussed in relation to this project by Ellis (2012). Notable among them are γ_ψ and γ_s, which could have specific implications for SCC. Of the four creep prediction methods evaluated in this research, ACI 209 is the only method that specifically accounts for fine aggregate content or slump (water content).

Fine aggregate content was directly accounted for using the mixture proportions of the utilized SCC and VC (discussed in Keske et al. 2015). Meanwhile, the ACI 209 creep prediction method was developed before the introduction of HRWRA (and HRWRA-induced slumps or slump flows). Therefore, slump values had to be adjusted to account for the high admixture-induced slumps that occurred in these prestress-suitable mixtures. In past AUHRC research (Kamgang 2013; Kavanaugh 2008), an equivalent wet slump of 0.0 in. was chosen for SCC mixtures and a slump of 0.5 in. was chosen for prestress-suitable VC mixtures when determining the slump correction factor.

In addition to v_u, ACI 209 accounts for the growth in creep over time using a time-rate function. To ascertain the predicted creep coefficient for intermediate times of interest—such as at the time of girder erection—the ultimate creep coefficient is multiplied by a time parameter, v_t, that accounts for the time elapsed since the load was applied:

$$v_t = \frac{t^{0.6}}{10 + t^{0.6}} \quad (3\text{-}2)$$

In Equation 3-2, t is the length of time after loading (in days). After determining the creep coefficient at a given time, $v_u(t)$, the creep strain, ε_{cr}, for a constant load is predicted by multiplying $v_u(t)$ by the initial elastic strain due to that load.

3.2.2.2 AASHTO 2013

The current *AASHTO LRFD* creep prediction method (AASHTO 2013) was first implemented in the 2005 version of the *AASHTO LRFD Bridge Design Specifications*. This method may be used to determine the effects of creep on the loss of prestressing force in bridges that are not segmentally constructed, as discussed in Section 5.9.5.4 of the provisions and in Chapter 4 of this report. It is applicable for specified concrete strengths up to 15,000 psi, and the predicted creep is influenced by the magnitude and duration of the load applied, the maturity of the concrete at loading, and the relative humidity of the concrete. The *AASHTO LRFD* creep coefficient, $\psi(t,t_i)$, is computed using the following equation:

$$\psi(t,t_i) = 1.9(k_{hc}\, k_s\, k_f\, k_{td})t_i^{-0.118} \quad (3\text{-}3)$$

Where

k_{hc} is the relative humidity correction factor,
k_s is the volume-to-surface area ratio correction factor,
k_f is the concrete strength correction factor,
k_{td} is the time development correction factor, and
t_i is the age of the concrete at the time of load application (days).

The time development correction factor, k_{td}, can be used for both precast and cast-in-place concrete components and for accelerated and non-accelerated curing conditions because it is assumed that the load is applied after curing ends. This parameter is given by the following equation:

$$k_{td} = \frac{t}{61 - 4f'_{ci} + t} \quad (3\text{-}4)$$

In Equation 3-4, t is the amount of elapsed time (in days) since application of the sustained load. While the formulation of the above correction factors is different than those of the ACI 209 model, the principles are similar—they account for conditions other than the standard conditions in which the model was calibrated, and they include mixture and exposure conditions typically known by the engineer during design. After determining the creep coefficient, the predicted strain due to creep, ε_{cr}, is obtained by multiplying $\psi(t,t_i)$ by the elastic strain that would result from a given load.

3.2.2.3 NCHRP 628

The NCHRP 628 model was developed as part of the National Cooperative Highway Research Program (NCHRP) Project 18-12 (Khayat and Mitchell 2009). Objectives of the project were to develop guidelines for the use of SCC in precast, prestressed concrete bridge elements and to recommend relevant changes to *AASHTO LRFD Bridge Design* and *Construction Specifications*.

This model uses the AASHTO 2013 model format; however, it contains a specific modification for SCC, *A*, that depends upon cement type. Thus, the creep coefficient, $\psi(t,t_i)$, is computed according to the following equation:

$$\psi(t,t_i) = 1.9(k_{hc}\, k_s\, k_f\, k_{td})t_i^{-0.118}A \quad (3\text{-}5)$$

In Equation 3-5, *A* equals 1.19 for SCC incorporating Type I/II cement and 1.35 for SCC incorporating Type III cement with a 20% fly ash replacement (Class F fly ash was used during that project). All other factors are the same as those described following Equations 5-3 and 5-4.

While the *A* correction factor accounts for the use of SCC, it was only calibrated for two specific cementitious classes, neither of which was used in this project. Based on the proportions of the utilized mixtures (discussed in Keske et al. 2015), it was judged that the combination of cementitious materials used to make the SCC in this study is closer to the latter cementitious combination. This cementitious class was also chosen in past AUHRC research (Kamgang 2013) involving concrete mixtures similar to those used in this project.

3.2.2.4 MC 2010

MC 2010 is the latest version of the CEB-FIP Model Code (*fib* 2010), and it is applicable for concretes with f_c up to approximately 18,000 psi. Like the other methods, the MC 2010 method yields an ultimate creep coefficient, φ_o, that includes a coefficient to account for development of creep over time after loading, β_c. The creep coefficient at any intermediate time, $\varphi(t,t_o)$, is computed from

$$\varphi(t,t_o) = \varphi_o[\beta_c(t,t_o)] \quad (3\text{-}5)$$

In Equation 3-5, *t* is the age of concrete at the moment considered (in days) and t_o is the age of concrete at loading. Notably, t_o is based on the maturity-adjusted age at loading considering the curing history to which the concrete was exposed prior to loading. The creep development coefficient, β_c, is similar in nature to Equation 3-2, except that it is also a function of relative humidity. Both φ_o and β_c also incorporate factors to account for compressive strength, maturity-adjusted age at loading, and cement class, all of which are discussed in detail by Ellis (2012).

3.2.3 Shrinkage Prediction Methods

The four references described above also include unique shrinkage prediction models that were evaluated in this research. Like in the previous section, these are referred to as the ACI 209, AASHTO 2013, NCHRP 628, and MC 2010 shrinkage models, respectively, in the following subsections. More specifically, the AASHTO 2013 provisions allow the use of any one of several methods to predict shrinkage behavior, but the "AASHTO 2013" model assessed comes from Section 5.4.2.3.3 of the provisions. In addition to these four, a fifth model was investigated that is

based on a widely accepted European code—the *Eurocode 2: Design of Concrete Structures* (2004). The "Eurocode 2" method was convenient to investigate because the code incorporates the same creep prediction method as the MC 2010 but a slightly different shrinkage prediction method. It could thus produce a different prediction for total time-dependent strain.

Several other shrinkage prediction models, including older versions of the models used by AASHTO and *fib*, exist in the literature. These models were excluded from this report for several reasons:

1. They are outdated and are not regularly specified (especially among codes in which a more recent version of the same model has been implemented),
2. They are of little value to ALDOT, the chief sponsor of this research for whom these findings were prepared, due to the prevalence of the *AASHTO LRFD* specification, and
3. They were found to be no more accurate during other past studies of Alabama SCC conducted by Kavanaugh (2008).

3.2.3.1 ACI 209

Like the ACI 209 creep prediction method, the shrinkage prediction is based on determining an ultimate value, $(\varepsilon_{sh})_u$, that is modified for intermediate times by a time development factor. Thus, the ultimate shrinkage strain is computed by the following equation:

$$(\varepsilon_{sh})_u = 780(10)^{-6}(\gamma_\lambda\, \gamma_{vs}\, \gamma_\psi\, \gamma_s\, \gamma_a\, \gamma_c) \tag{3-6}$$

Where

γ_λ is the relative humidity correction factor,
γ_{vs} is the volume-to-surface-area ratio correction factor,
γ_ψ is the fine aggregate percentage correction factor,
γ_s is the slump correction factor,
γ_a is the air content correction factor, and
γ_c is the cement content correction factor.

The adjustment factors shown above, which are applied for the same purposes as those in Equation 3-1, are calculated using equations discussed further by Ellis (2012) and are applied to the standard ultimate shrinkage strain (-780 με in the equation). In addition to the slump (water content) correction and fine aggregate percentage correction factors, the cement content correction factor, γ_c, is of interest particularly for SCC. Among the five shrinkage prediction models evaluated in this research, the ACI 209 method is the only method that specifically accounts for cement content; only some of the other methods even account for *type* of cementitious material. No guidance is given concerning the use of SCM, so the use of total powder content (portland cement plus SCMs) is feasible.

To ascertain the predicted shrinkage strain for intermediate times of interest such as at the time of girder erection, the ultimate shrinkage is multiplied by a time parameter, $(\varepsilon_{sh})_t$, that accounts for the time elapsed since the concrete was exposed to drying:

$$(\varepsilon_{sh})_t = \frac{t}{X + t} \tag{3-7}$$

In Equation 3-7, t is the length of time after initial curing (in days), and X depends on the type of curing (accelerated or non-accelerated). For concrete exposed to accelerated curing for 1–3 days, $X = 55$. No guidance is given for accelerated curing times less than 1 day. This was of importance to the evaluated data, as initial curing was frequently of a shorter duration (average release age of 22 hours; see Keske et al. 2014 for further fabrication data). After determining the time correction factor using Equation 3-7, the shrinkage strain at time t, $\varepsilon_{sh}(t)$, is predicted by multiplying the ultimate shrinkage strain by the time factor.

3.2.3.2 AASHTO 2013

The current *AASHTO LRFD* shrinkage prediction method may be used to determine the effects of shrinkage on the loss of prestressing force in bridges that are not segmentally constructed, as discussed in Section 5.9.5.4 of the provisions and in Chapter 4 of this report. Like the ACI 209 shrinkage model, the model involves calculation of an ultimate shrinkage strain, $(\varepsilon_{sh})_u$, that is modified for intermediate times by a time development factor. The ultimate strain is computed using the following equation:

$$\varepsilon_{sh} = 480(10)^{-6}(k_{hs}\, k_s\, k_f\, k_{td}) \tag{3-8}$$

Where

k_{hs} is the relative humidity correction factor,
k_s is the volume-to-surface area ratio correction factor,
k_f is the concrete strength correction factor, and
k_{td} is the time development correction factor.

Of the above factors, all except k_{hs} are calculated according to the same equations as used for the AASHTO 2013 creep prediction model. All are described further by Ellis (2012). After determining the ultimate shrinkage strain, the predicted shrinkage strain at intermediate times is calculated as in the AASHTO 2013 creep prediction method.

3.2.3.3 NCHRP 628

The NCHRP 628 shrinkage prediction model was developed by modifying the pre-2005 *AASHTO LRFD Bridge Design Specifications*. It is recommended specifically for shrinkage predictions of

SCC for precast, prestressed applications. The strain due to shrinkage at any time, *t*, after drying exposure is calculated for accelerated-cured concrete according to Equation 3-9:

$$\varepsilon_{sh} = 560(10)^{-6}(k_s\, k_h)(\frac{t}{55+t})A \quad (3\text{-}9)$$

Where

k_s is the size factor,
k_h is the relative humidity factor,
t is the drying time (in days) after initial curing, and
A is the cement factor for SCC only, equaling 0.918 for Type I/II cement or 1.065 for Type III cement plus 20% fly ash replacement.

In the above correction factors, k_s is used to account for *V/S*. The time-adjustment factor shown in Equation 3-7 is integrated as would be necessary when computing shrinkage at intermediate times using the ACI 209 shrinkage model. All factors are discussed in detail by Ellis (2012).

3.2.3.4 MC 2010

The current *Model Code* shrinkage prediction model has been in use since 1999, when the *fib* revised the MC 90 shrinkage prediction method. The total shrinkage of concrete predicted using the MC 2010 method is given by

$$\varepsilon_{sh}(t, t_c) = \varepsilon_{cas}(t) + \varepsilon_{cds}(t, t_c) \quad (3\text{-}10)$$

Where

ε_{cas} is the autogenous shrinkage strain,
ε_{cds} is the drying shrinkage strain,
t is the age of concrete at the moment considered (days), and
t_c is the age of concrete at the beginning of drying (days).

The derivations of these components are given in the MC 2010 code (*fib* 2010) and are discussed in relation to this project by Ellis (2012). In the derivations, autogenous shrinkage is not dependent on the concrete maturity when initial curing ends, relative humidity, or *V/S*, but it is dependent on the concrete strength at twenty-eight days. Both it and the drying shrinkage component are modified by the cement *type*, with distinction between slow-hardening cements, normal-to-rapid hardening cements, and rapid-hardening high-strength cements.

3.2.3.5 Eurocode 2

Like the MC 2010 model, the Eurocode 2 shrinkage prediction model distinguishes between autogenous shrinkage and drying shrinkage. The model is similar to the one employed by MC 2010, except with some different correction factors that are described by Ellis (2012). Distinctions described further in the referenced report include that

- Drying shrinkage is determined through direct application of *V/S* in the MC 2010 model but as a function of notional cross-sectional size (cross-sectional area divided by the length of perimeter exposed to drying) in the Eurocode 2,
- Numerical factors to account for cement type are slightly different between the models, although the same three cement classes are delineated—slow-hardening, normal-to-rapid hardening, or rapid-hardening high-strength cement, and
- Autogenous shrinkage calculated according to the Eurocode 2 model considers the compressive strength specified at any concrete age, *t*, but it is calculated using the mean 28-day f_c within the MC 2010 model.

3.3 EXPERIMENTAL PROGRAM

3.3.1 Measurement of Time-Dependent Strain in Cylindrical Specimens

Much of the experimental work pertaining to this research program has been described elsewhere by Keske et al. (2015) and Ellis (2012). Important information from those sources is summarized by the following:

- Cylinders were produced for time-dependent deformation testing during five production days: SCC-B, SCC-C, SCC-E, VC-B, and VC-F, thus including concrete placed in all four spans of the completed bridge.
- All cylinders were tested for time-dependent deformation in accordance with ASTM C512 (2002) and were stored in a temperature- and humidity-controlled environment from the time of initial loading until when they were tested for late-age strength and elasticity (as described by Keske et al. 2015).
- The exact placement location of the sampled batches within the girders could not be determined. Samples taken at the midpoint of each production day were assumed to be representative of the majority of concrete placed during that day.
- Three curing regimes were implemented: match curing based on the measured temperature at the center of the bottom bulb of the girders, steam-curing in the recesses of the formwork followed by temperature- and humidity-controlled storage, and steam-curing followed by approximately one year of ambient-exposure similar to that experienced by the girders.

- A single SCC and a single VC mixture were used throughout girder production and each set of cylinders (within and between production days) was exposed to a different curing and exposure history.
- In addition to concrete cylinders, free shrinkage prisms were produced for testing according to ASTM C157 (2008) from production groups SCC-E, VC-E, and VC-F. Additional free shrinkage prisms were produced during the placement of concrete in each span of the deck of the bridge over Hillabee Creek.

Assessment of time-dependent deformation according to ASTM C512 (2002) *Standard Test Method for Creep of Concrete in Compression* consists of two parts: measurement of the free shrinkage of unloaded cylindrical concrete specimens and measurement of the *total deformation* of companion cylinders exposed to the same drying conditions plus a known sustained compressive stress. Load-induced strain is then determined by subtracting the measured shrinkage strain in the unloaded cylinders from the measured total strain in the loaded cylinders. Finally, creep strain is then determined by subtracting the initial elastic strain from the calculated load-induced strain. These quantities are presented graphically in Figure 3.1.

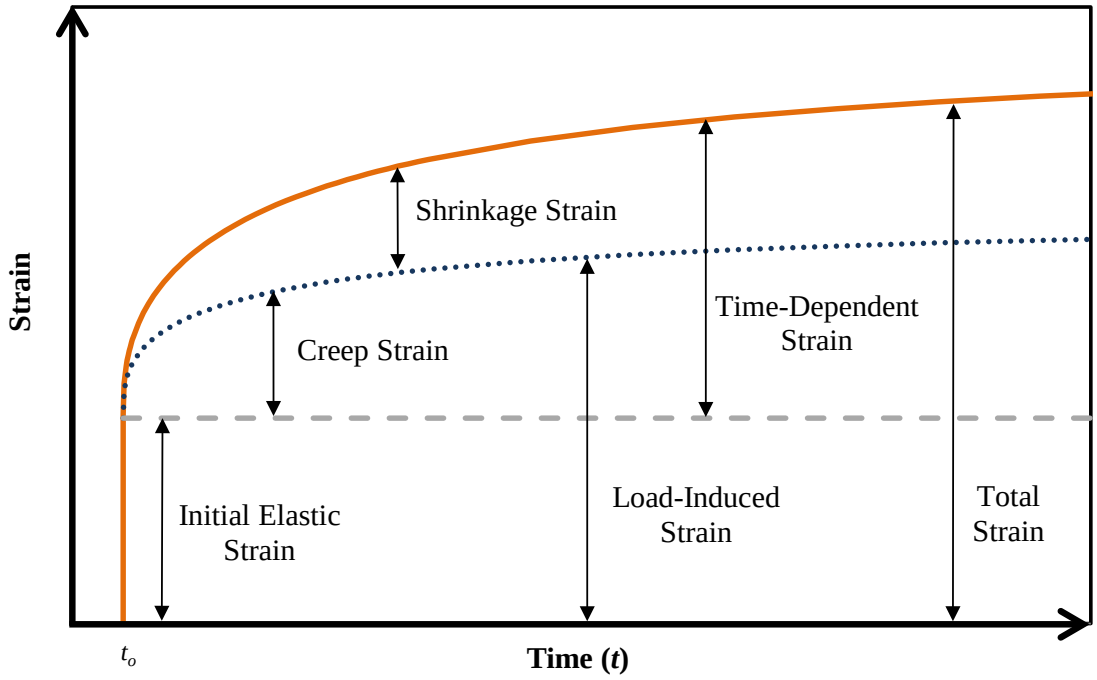

Figure 3.1: Components of strain in unrestrained concrete

During testing according to ASTM C512 (2002), it is difficult to precisely distinguish between instantaneous elastic strain and rapidly evolving creep strain at the beginning of testing

because it may take several minutes to execute the cylinder loading process. For reference, notice that time-dependent strain evolves most rapidly at early ages in the above figure. Therefore, the initial measurement of load-induced strain that is obtained once the total load is applied can include a creep component that is impossible to accurately quantify (ACI 209 2008).

3.3.1.1 Preparation of Test Specimens

In addition to the cylinders for evaluation of strength and E_c, cylinders were cast for measurement of time-dependent deformation according to ASTM C512 (2002), *Standard Test Method for Creep of Concrete in Compression*. These cylinders were always obtained during the second round of fresh concrete sampling to coincide with the majority of strength-cylinder production, and they were produced and stored alongside the other cylinders until approximately three hours before the girders were demolded and detensioned. At that time, all cylinders for time-dependent deformation testing were transported two hours to the laboratory in an insulated container which was used to allow a graduate temperature decrease from the elevated temperature in the bed to standard laboratory conditions. They were transported at this time so that some would be loaded to coincide with detensioning of the full-scale girders.

Approximately half of the cylinders that were used for time-dependent deformation testing were cured in the plant using a match-curing apparatus, as discussed further by Ellis (2012). The match-curing apparatus was temperature-controlled to match the internal temperature of the bottom bulb of a girder on the bed. The match-cured cylinders were frequently exposed to a different temperature history than steam-cured cylinders from the same production day. Two examples of the difference are shown in Figure 3.2 which illustrate that the difference was not consistent between production groups. In other words, match-cured cylinders were sometimes heated more and sometimes heated less than the companion tarp-cured cylinders.

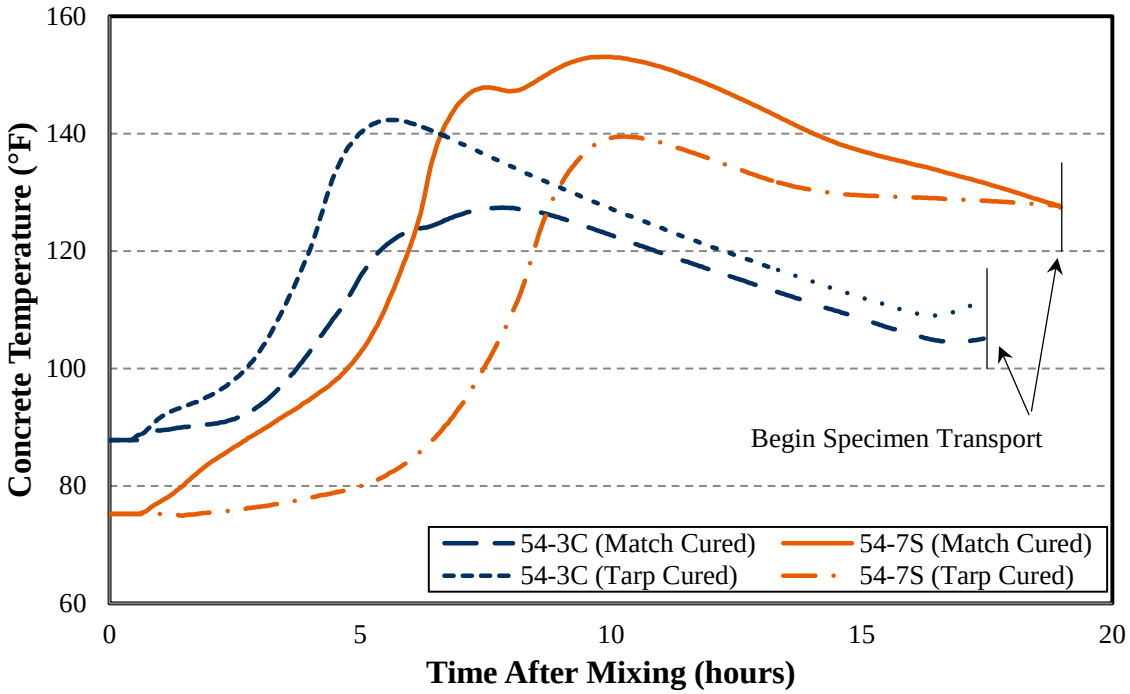

Figure 3.2: Measured temperature histories of cylindrical specimens used in time-dependent deformation testing

Once at the laboratory, the cylinders were demolded and prepared for creep loading and shrinkage testing. To ensure that the concrete cylinders were flat and smooth on their ends, a concrete grinder was used to achieve a smooth, level surface meeting the planeness requirements of ASTM C512. After both ends of each cylinder were ground, demountable, mechanical (DEMEC) strain-measurement points were attached to the specimens. After the DEMEC targets were installed, most of the specimens were placed into a climate-controlled room which maintains a humidity of 50% ± 10%. Here, the specimens were exposed to controlled drying and temperature conditions and, where applicable, sustained compressive loading until they all reached three years of age.

The appropriate sustained load (40% of f_c) was determined by testing two additional cylinders and calculating their average compressive strength. Match-cured sets of cylinders were loaded at the time of prestress transfer (to most closely match the behavior of the girders), and steam-cured sets were loaded at approximately twenty-six hours (always after the match-cured cylinders). An additional set of steam-cured cylinders were stored in ambient conditions until approximately when the deck was cast over the girders; mechanical-property results from these cylinders were reviewed in Chapter 3 of Keske et al. (2015), but time-dependent behavior of these cylinders is included here because these results relate to the predictability of long-term time-dependent deformation.

In addition to cylinders, rectangular prisms measuring approximately 11.25 in. long with a 3 in. square cross section were prepared according to ASTM C157 (2008) during SCC production group E and during VC production groups E and F for unrestrained shrinkage evaluation. After being steam-cured alongside the girders until girder form removal, the prisms were taken to the laboratory to be air-cured in a climate-controlled room which maintains a humidity of 50% ± 10%. They were stored there and regularly measured until July of 2013, following completion of all in-field deformation measurements and live-load testing.

3.3.1.2 Reporting of Measured Time-Dependent Strain

Experimental determination of the creep coefficient, which is traditionally defined as the ratio of creep strain to initial elastic strain, is particularly sensitive to slight inaccuracies in the initial strain measurement (ACI 209 2008). Because of this, creep effects were assessed in this report primarily by considering the total load-induced deformation attributable to a sustained load. A standard measure of this phenomenon is the compliance, $J(t,t_i)$. Compliance represents the total load-induced strain (elastic strain *plus* creep strain) at age t per unit of uniaxial stress due to a load maintained since loading age, t_i. ACI 209 (1992) defines it as follows:

$$J(t,t_i) = \frac{Total\ Strain - Shrinkage\ Strain}{Applied\ Stress} \tag{3-11}$$

Compliance values allow for a more accurate comparison of creep results because they are normalized for applied load levels (ACI 209 1992), but the use of J implicitly emphasizes some concrete material properties and de-emphasizes others. Because it includes the initial elastic strain component, J is dependent upon E_{ci}—initial compliance *should* equal the inverse of E_{ci} since no time-dependent change would occur during theoretically instantaneous loading. Consequently, concrete with a higher E_{ci} exhibits less initial (elastic) compliance, regardless of the creep it may experience. In this way, J may de-emphasize the creep component—a material with high initial deformation but less creep deformation still exhibits a larger J than one with lower relative initial deformation, at least until later ages.

The reporting of J instead of measured creep strain also makes it impossible to compare the magnitude of creep strain to the magnitude of shrinkage strain. This is not of concern during this analysis, as it would be inappropriate to directly compare the measured creep strain, load-induced strain, or total strain in SCC and VC. Each set of cylinders exhibited a different f_{ci} and E_{ci} and was loaded to a different *force*, so compliance results are only comparable because they are normalized for stress.

3.3.1.3 Batch-Specific Considerations and Specimen Nomenclature

The basic nomenclature used in this research is shown below in Figure 3.3.

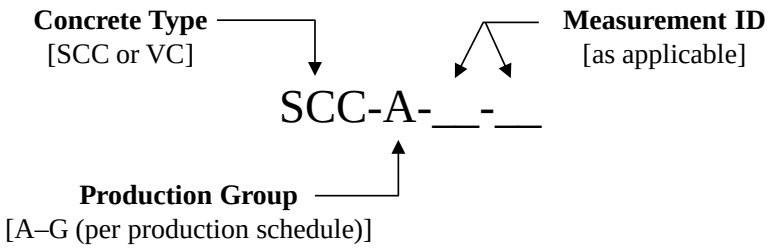

Figure 3.3: Production group identification scheme

In addition to the basic nomenclature, identification suffixes were necessary for identification of the specimens produced for this testing. Cylinders were loaded at up to three different ages (at transfer, at approximately twenty-six hours, and at approximately one year), so the first identifier is based on the order of loading: -1, -2, or -3, respectively. Thus, two sets of cylinders were tested from SCC-B (SCC-B-1 and SCC-B-2), while three sets were tested from the other four referenced production groups. Additionally, free-shrinkage prisms are denoted with a "-P" suffix, as they were treated independently and were all tested using standardized practices.

The match-curing apparatus used to cure some of the SCC-B-1 cylinders did not function correctly. The cylinders affected by this malfunction were not marked, so the maturity of the SCC-B-1 group is unclear. Consequently, this group is excluded from all prediction method analyses and calibrations discussed in Section 3.4. The second set of cylinders tested from production day SCC-B was unaffected by this malfunction, and they continue to be labeled SCC-B-2 through this report for continuity.

Additionally, two other sets of cylinders were not loaded to the intended target load, so these two sets are henceforth denoted as SCC-E-2U and VC-F-2U to indicate that they were under-loaded. These two sets are excluded from the analysis and calibration of load-dependent deformation predictions because the precision of the measurements would be disproportionately significant in these cylinders. Curing and drying of these sets was effectively controlled and free shrinkage measurement is load-independent, so the sets are still included in the analysis and calibration of shrinkage prediction models.

The aged-then-loaded cylinders (denoted "-3" where applicable) were exposed to uncontrolled ambient conditions for one year before being tested for time-dependent deformability. Consequently, the free shrinkage behavior of these sets was not expected to conform to any prediction methods. Because of the potential for variation due to the uncontrolled curing conditions, these aged-then-loaded cylinders were analyzed only to assess whether compliance responses are comparable or as predictable if loads are applied at a later age.

Gardner and Tsuruta (2004) and Yue and Taerwe (1993) found that, when the sustained load in concrete changes (as would be the case when adding a deck over girders), the

subsequent creep can be predicted by superimposing functions that describe the creep response to each load. Consequently, these aged-then-loaded cylinders provided valuable insight into whether the evaluated (or calibrated) creep prediction functions could be used for such later-age superposition of predictions.

3.3.2 Prediction of Time-Dependent Strains

3.3.2.1 Application of Prediction Methods

All of the referenced creep prediction models yield a creep coefficient based on the model-specific inputs reviewed in Section 5.2 (such as applied stress, f_c, relative humidity, age at the time of loading, etc.). This creep coefficient can then be applied to the elastic deformation corresponding to the applied stress to determine the creep strain. In light of the chosen reporting convention, conversion of these strains to predicted compliance values was necessary before they could be compared to the measured values obtained according to the testing method described earlier.

To most accurately evaluate the prediction models, it was necessary to base the predictions on measured concrete properties and exposure conditions whenever possible. The measured, utilized properties are shown in Table 3.1 at the end of this section. Thus, predictions of the time-dependent behavior of these full-scale cylinders were based on the following procedures:

- Elastic strain was calculated by dividing the actual applied stress by the measured E_{ci} of companion cylinders tested in accordance with ASTM C469 (2010).
- Creep strain was predicted by multiplying the predicted creep coefficient by the elastic strain calculated above.
- Compliance was predicted by dividing the sum of the creep strain (predicted by the model) and elastic strain (calculated using E_{ci}) by the actual applied stress as in Equation 3-11.
- Shrinkage predictions, which were compared directly to measured shrinkage strains, were based on the measured geometric, material, and exposure properties of the tested cylinders (V/S, relative humidity, etc.).
- Total-strain predictions consisted of the sum of the predicted creep strain (based on the predicted creep coefficient), elastic strain (based on measured E_{ci}), and predicted shrinkage; these total-strain predictions were compared directly to the total strain measured in the creep-loaded cylinders.

3.3.2.2 Testing and Model-Specific Considerations

Prediction of compliance required application of the predicted creep coefficient to the elastic response calculated using the E_{ci} tested in cylinders according to ASTM C469 (2010). However, to accelerate the initiation of time-dependent deformation testing, only f_{ci} was evaluated in the laboratory-tested group of specimens while f_{ci} and E_c were evaluated in cylinders at the plant as part of the assessment presented in Keske et al. (2015). Because E_c is widely considered to be proportional to the square root of f_c, E_{ci} of the specimens loaded for time-dependent deformation testing was estimated according to the following equation:

$$(E_{ci})_{lab} = (E_{ci})_{field} \frac{\sqrt{(f_{ci})_{lab}}}{\sqrt{(f_{ci})_{field}}} \tag{3-12}$$

In Equation 3-12, the properties of field-tested specimens (denoted with a "field" subscript) that were used to estimate E_{ci} of the laboratory-tested specimens are reported in Keske et al. (2015). Laboratory- and field-tested cylinders were always produced from the same batch of concrete, and efforts were made to minimize differences in their temperature histories. Comparisons of field- and laboratory-tested compressive strengths can be made in Keske et al. (2015). Each creep and shrinkage prediction model incorporates correction factors to account for different nonstandard material and exposure conditions. Pertinent assumptions and choices are summarized below, and additional information is contained in the thesis prepared by Ellis (2012):

- Factors based on cement content were assumed to be based on total powder content, which included a replacement of Type III cement with slag cement during this research.
- Factors based on cement type in the NCHRP 628 models were chosen based on the "Type III + 20% Fly Ash" classification used in those models. Consequently, *A*-values of 1.35 and 1.065 were utilized when evaluating SCC creep and shrinkage according to these models.
- The "rapid-hardening high-strength cement" classification used in the MC 2010 and Eurocode 2 models was chosen based on the ACI 209 (2008) recommendation for its use when evaluating concrete proportioned with Type III cement.
- Slump correction factors were chosen based on the slump achievable without the use of HRWRA, which was approximated to equal 0.0 inches for the SCC and 0.5 inches for the VC used during this research.
- Concrete aging and curing were assumed to begin at the time at which the water and cementitious material were mixed at the plant, and the end of initial curing was assumed to occur when the cylinders were removed from their cylinder molds. Initiation of drying was assumed to coincide with the end of initial curing.

Notably, while ACI 209 (2008) recommends the use of the "rapid-hardening high-strength cement" factors in the European models when evaluating concrete proportioned with Type III cement, Section 5.1.9.4 of the MC 2010 provisions states that the use of SCMs (fly ash, specifically) may affect the applicability of the factors. SCMs may have contradictory effects: delayed hydration may directly increase early-age creep and reduce shrinkage, but overall creep and shrinkage may also be affected as an indirect result of the relative reduction in portland cement content (*fib* 2010).

The European models incorporate ages that have been adjusted to reflect the actual maturity of accelerated-cured specimens, while the other models account for accelerated curing through the use of alternative factor derivations in conjunction with chronological ages. The methodology used to determine temperature-adjusted ages is discussed by Kamgang (2013) and Kavanaugh (2008), and considerations specific to this research are discussed by Ellis (2012). Chronological and temperature-adjusted ages are shown in **Table 3.**1 alongside the other measured and calculated inputs needed to apply the assessed prediction models. In the table, the inputs are as follows:

t_{cure} is the length of initial curing

t_i is the concrete age at which the load was applied, from the time of initial mixing

t_i - t_{cure} is the length of time from initiation of drying to the application of load

$t_{i,T}$ is the temperature-adjusted age at loading

$t_{m,T}$ is the age at loading modified for temperature and cement class

f_{ci} is the compressive strength at prestress transfer

f_{c28} is the compressive strength at twenty-eight days

E_{ci} is the estimated elastic modulus at transfer based on Equation 3-12

C is the total cementitious content

S is the adjusted slump (in.), and

F is the applied and sustained compressive force.

Table 3.1: Inputs used in creep and shrinkage prediction calculations

Specimen ID	Measured Times			Adjusted Times		Mixture Properties			Measured Properties			
	t_{cure} (days)	t_i (days)	$t_i - t_{cure}$ (days)	$t_{i,T}$ (days)	$t_{m,T}$ (days)	C (lb/yd^3)	*Fines* (%)	*Air* (%)	f_{ci} (ksi)	f_{c28} (ksi)	E_{ci} (ksi)	F (kips)
SCC-B-2	0.99	1.15	0.15	4.55	9.57	892	48	3.0	8.93	10.8	6,450	102
SCC-C-1	0.89	0.99	0.10	3.86	8.78	892	48	4.2	7.88	10.18	6,050	88
SCC-C-2	0.91	1.12	0.21	3.10	7.84	892	48	4.2	7.49	10.18	5,900	86
SCC-C-3	0.91	350	349	352	355	892	48	4.2	10.91	10.91	6,300	127
SCC-E-1	0.75	0.84	0.09	3.26	8.04	895	47	4.3	7.06	10.77	5,550	84
SCC-E-2U	0.78	1.09	0.31	3.60	8.47	895	47	4.3	7.68	10.77	5,800	35
SCC-E-3	0.78	337	336	340	342	895	47	4.3	11.67	11.67	6,500	127
VC-B-1	0.81	0.90	0.09	2.41	6.86	820	38	4.5	7.11	9.67	6,350	81
VC-B-2	0.85	1.06	0.21	3.06	7.79	820	38	4.5	8.12	9.67	6,750	88
VC-B-3	0.85	355	354	357	360	820	38	4.5	12.10	12.10	6,850	135
VC-F-1	0.77	0.86	0.10	2.39	6.83	833	38	3.1	7.98	11.05	6,650	91
VC-F-2U	0.79	1.14	0.35	2.83	7.48	833	38	3.1	8.88	11.05	7,050	34
VC-F-3	0.79	331	330	333	336	833	38	3.1	11.79	11.79	7,450	134

3.4 PRESENTATION AND ANALYSIS OF RESULTS

Results and discussion relevant to the objectives of this chapter are presented in this section. First, measured time-dependent deformations are compared at concrete ages up to three years. Then, measured deformations are compared to those predicted using the methods described earlier. The statistical methodology chosen to avoid bias in these comparisons is also given. Finally, modifications to the reviewed models are proposed, and the modified models are reviewed for accuracy relative to the measured data.

3.4.1 Comparison of Measured Time-Dependent Deformation

3.4.1.1 Compliance and Creep

In this section, the dependence of J on E_{ci} is especially important considering the SCC evaluated during this research. The evaluated SCC regularly exhibited a lower E_{ci} than that of the companion VC, which was expectable considering the changes required to induce self-consolidating behavior in the SCC (see Keske et al. 2014 for further discussion). With this in mind, comparisons of J should be useful relative to precast, prestressed applications, as prestress losses are related to both the initial elastic shortening and time-dependent deformation of the surrounding concrete.

Compliance of the assessed mixtures is presented in Figure 3.4. Pertinent results from this data are then summarized in Table 3.2 below the figure. The data necessary to create this figure and table are presented in the dissertation prepared by Keske (2014). In both the figure and table, only cylinders that were cured and tested according to ASTM C512 are presented; other, non-standard results are discussed later.

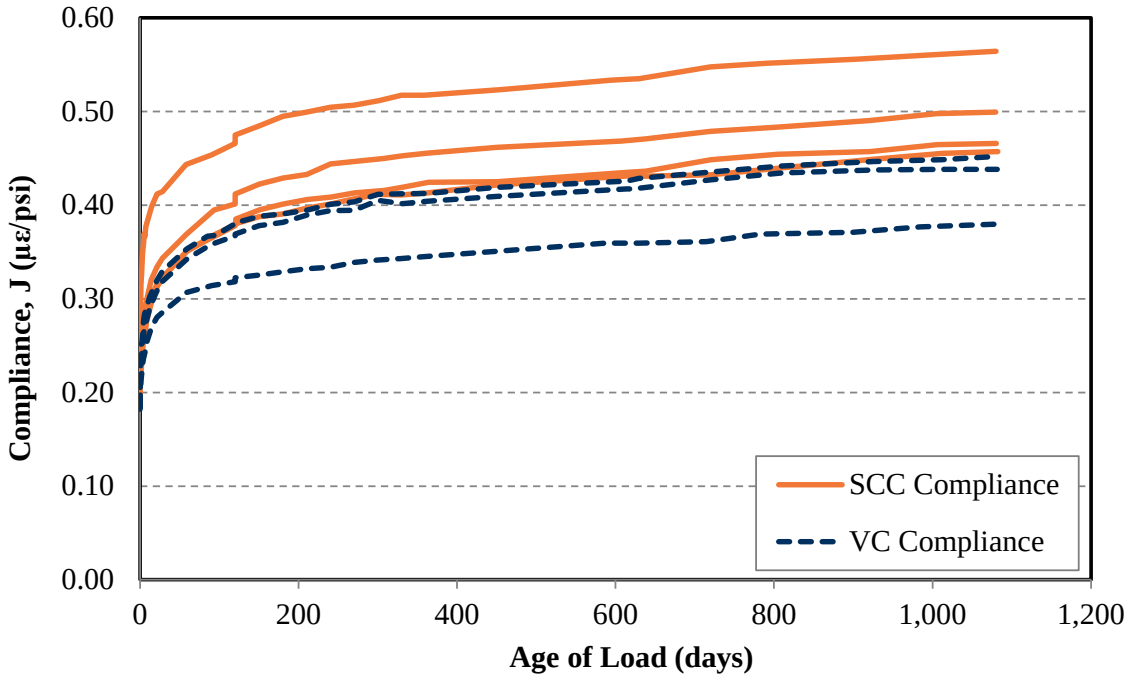

Figure 3.4: Measured compliance in specimens tested according to ASTM C512

Table 3.2: Compliance, *J*, of SCC and VC tested in accordance with ASTM C512

ID	Compliance (με/psi)			
	Initial	56-Day	1-Year	3-Year
SCC-B-2	0.20	0.35	0.41	0.46
SCC-C-1	0.21	0.37	0.46	0.50
SCC-C-2	0.19	0.35	0.42	0.47
SCC-E-1	0.25	0.44	0.52	0.56
SCC Avg.	*0.21*	*0.38*	*0.45*	*0.50*
VC-B-1	0.18	0.34	0.40	0.44
VC-B-2	0.18	0.35	0.41	0.45
VC-F-1	0.19	0.31	0.34	0.38
VC Avg.	*0.18*	*0.33*	*0.38*	*0.42*

In the table, *J* is presented for concrete ages at initial loading, fifty-six days, and three years. These three ages were chosen considering important ages in the life of precast, prestressed girders:

1) Initial *J* should relate to the concrete behavior at prestress transfer,

2) Fifty-six days is a reasonable estimate of the time at which most precast, prestressed girders are erected,
3) One-year is the approximate age at which the deck was cast in place over the girders, and
3) Three-years is the best available estimate of the long-term service behavior of the tested mixtures.

The SCC cylinders exhibited *J* of approximately 15% more than in companion VC cylinders at all ages. This closely resembles the 10–15% reduction in E_{ci} discussed in the previous report prepared by Keske et al. (2015). The reduction could be expected between any two concretes that differ in mixture proportions, so the difference in *J* should be expected of these evaluated mixtures. As noted previously, though, elastic effects could mask any differences in time-dependent deformation growth. Thus, isolation of time-dependent creep effects on *J* required consideration of the difficulties inherent to the testing process that were described in Section 3.3.1.

Considering that unmeasurable time-dependent effects resulting from creep testing would be approximately equal and random between all tests, creep compliance effects, *C*, were calculated according to Equation 3-13:

$$C = \frac{J(t, t_i) - J(t_i)}{J(t_i)} \tag{3-13}$$

Where

$J(t,t_i)$ is the measured compliance at time *t* due to a load sustained since time t_i, and

$J(t_i)$ is the measured initial compliance as shown in Table 3.2.

Importantly, *C* is presented in the same form as the creep coefficient determined according to each of the models described in Section 3.2 (such as v_u in ACI 209 or ψ in AASHTO 2013), but it is only used in this work for comparisons of *measured* results and not for comparisons of measured and predicted results. In other words, the *C* values reported below in Table 3.3 are not relatable to predicted creep coefficients because they all include an unknown amount of time-dependent effects. Measured *C* results at concrete ages of fifty-six days, one year, and three years are presented below, as are the average ratios of SCC results to VC results at these ages.

Table 3.3: Creep compliance effects, *C*, of SCC and VC cylinders

ID	Creep (Equation 3-13)			SCC / VC		
	56 Days	1 Year	3 Years	56 Days	1 Year	3 Years
SCC-B-2	0.75	1.05	1.30			
SCC-C-1	0.76	1.19	1.38			
SCC-C-2	0.84	1.21	1.47			
SCC-E-1	0.76	1.08	1.24			
SCC Avg.	*0.81*	1.14	*1.38*	0.98	1.03	1.04
VC-B-1	0.89	1.22	1.44			
VC-B-2	0.94	1.28	1.50			
VC-F-1	0.63	0.79	1.00			
VC Avg.	*0.83*	1.11	*1.33*			

Based on the information presented in Table 3.3, the SCC cylinders appear to exhibit comparable creep as the VC cylinders (less than 5% different, on average). This difference is trivial considering the 30% variability of creep in "ordinary structural concrete" alluded to by the MC 2010 provisions. The individual-specimen results also highlight the between-batch variability inherent to this type of measurement. The variability between SCC specimens was no greater that the variability between VC specimens, thus further suggesting that the creep of the tested SCC and VC mixtures was practically the same.

In addition to the results obtained in accordance with ASTM C512, compliance was also measured in the under-loaded specimens and aged-then-loaded specimens. These results are included in Keske (2014). The compliance of the under-loaded specimens was very similar to those shown above (as expected because *J* is normalized for load), as were *C* (determined according to Equation 3-13) and the ratio of SCC creep to VC creep. However, only one set of SCC specimens (SCC-E-2U) and one set of VC specimens (VC-F-2U) were under-loaded, so these comparisons are limited.

Meanwhile, the aged-then-loaded specimens all exhibited much less creep than the cylinders loaded at earlier ages (approximately one-half of *C* exhibited by the standard specimens). The reduction in *C* was expectable because of the increase in the age of the concrete at the time of load application—the aged concrete should have experienced a large amount of drying (reduction of available water) and decrease in porosity, which would reduce its creep potential. The number of alternatively tested cylinders was limited, but the difference in creep of the aged-then-loaded cylinders was more pronounced (SCC *C* was 20% greater than vibrated concrete *C*). Considering the variability of this type of testing, these results are

reasonable and suggest that any differences between these two concretes were minor and expectable in response to the differences in mixture proportioning of the two.

From these alternatively tested cylinders, it can also be concluded that differences in load-dependent behavior are expectable in response to differences in applied stress (if less than 40% of f_c) or age at the time of initial loading (up to one year). Within each concrete type, under-loaded cylinders exhibited comparable compliance and creep, and aged-then-loaded cylinders exhibited expectably reduced compliance and creep. SCC did not appear to be differently affected by either of these conditions.

3.4.1.2 Free Shrinkage

Free shrinkage results of the assessed mixtures are presented in Figure 3.5; the data necessary to create this figure are presented in Keske (2014). Pertinent results from this data are then summarized in Table 3.4 below the figure. Only results from cylinders that were cured and tested according to ASTM C512 are presented in the figure and table. As previously discussed, the shrinkage behavior of the under-loaded specimens was independent of their response to loads, so they are included in this section. Values are presented for concrete ages of fifty-six days and three years because they should be representative of erection-age and long-term behavior, and values measured at a concrete age of seven days are included to compare rates of shrinkage growth.

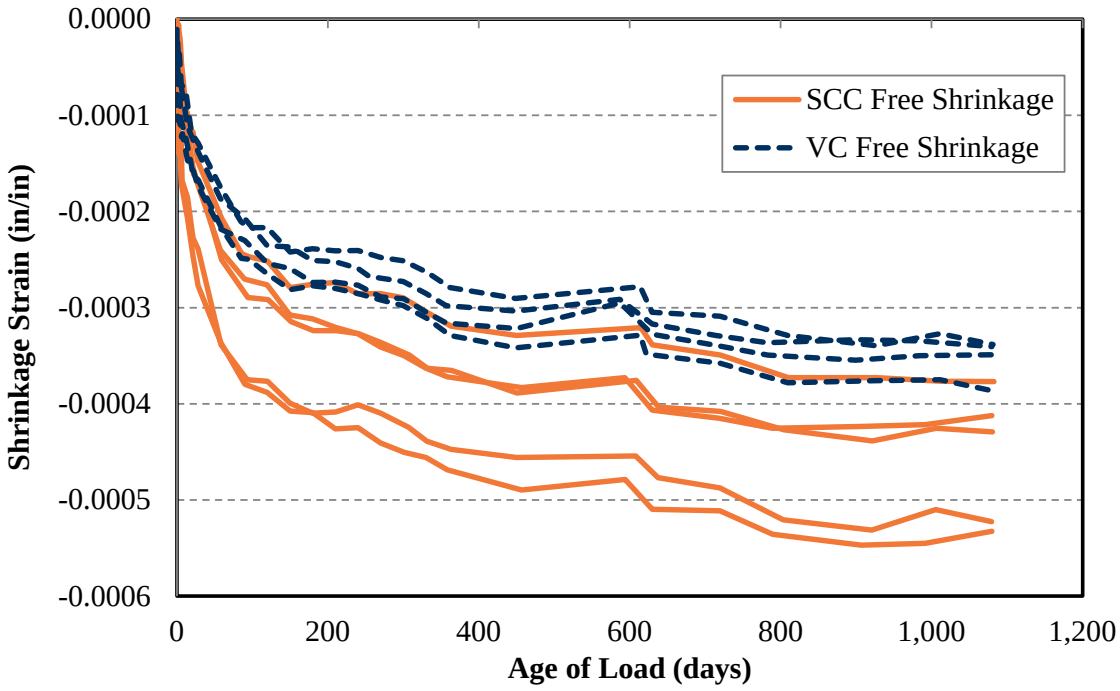

Figure 3.5: Measured shrinkage in specimens tested according to ASTM C512

Table 3.4: Shrinkage of SCC and VC tested in accordance with ASTM C512

ID	Measured Shrinkage (με)			Ratios		
	7-Day	56-Day	3-Year	56-Day/ 7-Day	3-Year/ 56-Day	3-Year/ 7-Day
SCC-B-2	-150	-210	-380	1.40	1.82	2.53
SCC-C-1	-170	-340	-520	2.00	1.54	3.06
SCC-C-2	-100	-250	-430	2.50	1.72	4.30
SCC-E-1	-180	-340	-530	1.89	1.59	2.94
SCC-E-2U	-90	-240	-410	2.67	1.72	4.56
SCC Avg.	*-140*	*-270*	*-450*	*2.09*	*1.68*	*3.48*
VC-B-1	-120	-220	-390	1.83	1.78	3.25
VC-B-2	-80	-180	-340	2.25	1.91	4.25
VC-F-1	-120	-220	-350	1.83	1.60	2.92
VC-F-2U	-80	-190	-340	2.38	1.82	4.25
VC Avg.	*-100*	*-200*	*-350*	*2.07*	*1.78*	*3.67*

The SCC cylinders exhibited approximately 30% more shrinkage than in companion VC cylinders at all ages shown in the table. While this difference is expectable due to the increase in paste content in the SCC and is in line with other findings (*fib* 2010; Khayat and Mitchell 2009), it is practically significant when considering that the two mixtures exhibited comparable f_c and E_c (see Keske et al. 2014 for additional information regarding mechanical properties). Statistical significance was also confirmed: shrinkages at concrete ages of fifty-six days and three years were significantly different at a 90% CI and 95% CI, respectively.

The ratios presented in the table were given to compare shrinkage growth rates. Shrinkage growth is complicated because autogenous and drying shrinkage strains evolve at different rates over time, but the proportion of shrinkage that occurs before erection (assumed to occur at approximately fifty-six days) is of particular interest. Based on the ratios shown in Table 3.4 and the data shown in Figure 3.5, the SCC and VC appear to exhibit very similar shrinkage growth, with the most rapid changes occurring in the first fifty-six days. Shrinkage doubled between seven days and fifty-six days but did not double again between fifty-six days and three years. This pattern was practically identical in the SCC and VC and strengthens the conclusions regarding time-dependent behavior reported by Keske et al. (2015).

Rectangular prisms for unrestrained shrinkage evaluation were prepared according to ASTM C157 (2008) during SCC production day E and during VC production days E and F. They were also produced during the casting of each span of the deck over the Hillabee Creek Bridge. Measured results are summarized in Table 3.5 in terms of length change—percentage length

change is the recommended result format of the test, and it is directly comparable to the specifications set forth for this project.

Table 3.5: Length-change of SCC and VC prisms tested in accordance with ASTM C157

ID	28-Day (%)	56-Day (%)	1-Year (%)	2-Year (%)	3-Year (%)
SCC-E-P	-0.029	-0.034	-0.049	-0.058	-0.060
VC-E-P	-0.016	-0.021	-0.033	-0.042	-0.044
VC-F-P	-0.026	-0.035	-0.054	-0.066	-0.066
Deck-1-P	-0.045	-0.052	-0.058	-0.068	-
Deck-2-P	-0.044	-0.050	-0.057	-0.064	-
Deck-3-P	-0.055	-0.058	-0.067	-0.075	-
Deck-4-P	-0.044	-0.047	-0.054	-0.060	-

Note: - = not tested

All girder-concrete prisms met the specifications set forth for this project (less than 0.04% length change at twenty-eight days). Variability between the girder-concrete prisms was high, but the data in the above table illustrate an important concept: the unrestrained shrinkage of the high-strength concrete utilized in these girders was consistently less than of that of the cast-in-place concrete used in the bridge deck.

3.4.2 Comparisons of Measured Values to Predicted Values

In this section, measured deformations are compared to those predicted by the models described earlier. While a direct comparison of the evaluated mixtures was warranted in the previous section because these two mixtures are direct companions in an in-service bridge, evaluation of the *predictability* of time-dependent deformation is of wider value in advancing the understanding of SCC. Within each model, each set of specimens would be expected to exhibit different creep and shrinkage even if exposed to the same compressive stress and ambient conditions. Therefore, the ability of the various models to correctly identify measured differences is important.

Before comparing these predicted and measured values, the statistical methodology chosen to avoid bias in these comparisons is given first, in the next section. Comparisons are then presented in separate sections for compliance (and creep), shrinkage strain, and total strain prediction.

5.1.1.1 Analysis Methodology

Results obtained from the assessment of time-dependent deformation according to ASTM C512 can be compared to predicted values in two general ways: by comparing the values at discrete, important ages (such as at girder erection or for ultimate long-term behavior) or by comparing every predicted and measured value over a particular region of measured behavior (such as only until erection or over the entire measured lifetime). Both methods of comparison are useful to this research, although for different reasons. Differences at discrete, important ages are evaluated because they are relevant for engineering purposes; differences between the trends are more relevant for understanding the behavior of the concrete over time.

Differences between predicted values ($Y_{Predicted}$) and measured values ($Y_{Measured}$) at discrete ages are evaluated according to Equation 3-14. By arranging the equation as shown, negative errors indicate that a given model under-predicts the magnitude of the result (compliance, shrinkage, or total strain) at a given time, while positive errors indicate that a given model over-predicts the magnitude of the measured result at that time.

$$Error\ (\%) = 100\left[\frac{Y_{Predicted} - Y_{Measured}}{Y_{Measured}}\right] \tag{3-14}$$

In comparisons of error percentages, the preferred range of error was selected as ±20% based on statements by Gardner and Lockman (2001) concerning creep and shrinkage prediction:

> A model that could predict the shrinkage within 15% would be excellent, and a prediction within 20% would be adequate. Obviously for compliance, the range of expected agreement would be worse because compliance is not measured but calculated by subtracting a large number (shrinkage) from another large number (total deformation).

In addition to error percentages at discrete ages, it was useful to utilize a single-parameter comparison tool to evaluate the overall accuracy of the prediction models. Results are collected on a nonlinear calendar according to the ASTM C512 guidelines (every day for the first week, then weekly for the first month, then monthly for the first year, and then quarterly or less frequently thereafter), which may bias common single-parameter forms of assessment such as the simple sum-of-squares error calculation. Several statistical indicators are presented in the ACI 209 (2008) *Guide for Modeling and Calculating Shrinkage and Creep in Hardened Concrete* that can overcome this bias. In general, these indicators are calculated by dividing measured results into groups and weighting the groups statistically.

Of those presented in the ACI 209 (2008) guide, the model proposed by Bazant and Panula (1978) was selected for use during this assessment. The indicator from their model, the BP coefficient of variation, ω_{BP}, was developed by parsing measured data into logarithmic

decades (0 to 9.9 days, 10 to 99.9 days, etc.) and weighting the measurements based on the number of measurements in each decade relative to the total number of measurements and decades. Calculation of ω_{BP} is described further in Appendix E of Keske et al. (2015).

In addition to assessment of the existing models, adjustments to the models, which are described further in Section 3.4.3, were determined by minimizing ω_{BP}. In all applications of ω_{BP}, one exception was deemed acceptable: measured results were last obtained at a concrete age of three years (approximately 1,095 days), but the use of a fourth logarithmic decade (from 1,000 to 10,000 days) consisting only of this last set of readings would have been questionable. Therefore, the last measurement for each cylinder set was included in the third logarithmic decade of measurements (alongside data from 100 to 1,000 days), and only three logarithmic decades were used.

3.4.2.1 Comparisons of Measured and Predicted Compliance

Errors between predicted and measured compliance for each reviewed prediction model are presented in Table 3.6. The data necessary to derive this table are presented in Keske (2014). Per the discussion of the previous subsection, ω_{BP} gives the best indication of the overall accuracy of the various models, while error percentages are presented to indicate the margin of error in compliance at concrete ages of fifty-six days (an approximation of the age at erection) and three years (the last age at which strains were measured, which is the closest estimate of long-term behavior). ω_{BP} results are always positive, with results closer to zero indicating better accuracy; a positive average error percentage indicates an over-predicted compliance.

Table 3.6: Error comparisons for existing compliance prediction models

Compliance Prediction Model	ω_{BP}		Error % at 56 days		Error % at 3 years	
	SCC	VC	SCC	VC	SCC	VC
ACI 209	0.122	0.118	-7	-4	-7	1
AASHTO 2013	0.168	0.169	-9	-6	-14	-8
NCHRP 628	0.155	0.169	8	-6	5	-8
MC 2010[1]	0.121	0.074	-9	-3	-10	0

Note: Similar to model used in Eurocode 2

Several conclusions are warranted based on the results shown in Table 3.6. They include that

- All models were reasonably accurate for predicting compliance,
- While SCC compliance was slightly less predictable using the existing models, all average SCC and VC predictions were within 15% and 10% of actual results, respectively, at concrete ages of up to three years.

As previously discussed in Section 3.4.1.1, compliance is directly dependent upon E_{ci}, and the correlation may disguise differences in creep behavior. However, since measured E_{ci} was used to calculate the initial elastic strain to which predicted creep coefficients were applied in this analysis, the data presented in Table 3.6 directly indicate the predictability of the *creep* of the assessed SCC and VC. Therefore, it is concluded that, when using measured properties, all referenced creep predictions are reasonably accurate, on average, for evaluation of Alabama concrete for precast, prestressed applications as they are currently specified. The prediction of creep in the assessed SCC was slightly less accurate, but the error is insignificant considering the variability discussed in Section 3.4.1.1.

3.4.2.2 Comparisons of Measured and Predicted Shrinkage

Errors between predicted and measured shrinkage for each reviewed prediction model are presented in Table 3.7 using the same parameters as in the previous subsection (ω_{BP} and error percentages at fifty-six days and three years). Also like in the previous subsection, data used to derive this table are presented in the dissertation prepared by Keske (2014).

Table 3.7: Error comparisons for existing shrinkage prediction models

Shrinkage Prediction Model	ω_{BP}		Error % at 56 days		Error % at 3 years	
	SCC	VC	SCC	VC	SCC	VC
ACI 209	0.532	0.633	24	42	35	47
AASHTO 2013	0.212	0.433	10	46	-4	19
NCHRP 628	0.859	1.163	51	87	65	94
Eurocode 2	0.565	0.963	49	100	24	58
MC 2010	0.393	0.727	14	54	24	58

Several conclusions are warranted based on the results shown in Table 3.7:

- Prediction of the shrinkage of the assessed SCC and VC was far less accurate than prediction of their compliance,
- The AASHTO 2013 shrinkage model was markedly more accurate than the other models at predicting shrinkage in the assessed mixtures (in terms of ω_{BP} and percent error), especially in SCC,
- On average, the prediction models tended to over-predict shrinkage at all ages, especially in VC, and

- The only model that was reasonably accurate for SCC shrinkage prediction (AASHTO 2013) was also somewhat accurate for VC shrinkage prediction (within 20% at a concrete age of three years).

Notably, the time-dependent shrinkage deformation of Alabama concrete for precast, prestressed applications was also over-predicted in past AUHRC projects (Kavanaugh 2008; Levy et al. 2010), especially in mixtures proportioned with slag cement. Thus, the mixture proportions of the SCC and VC utilized in this project, which included a similar usage of slag cement, could partially explain the over-prediction of the shrinkage of the tested SCC and VC.

3.4.2.3 Comparisons of Measured and Predicted Total Strains

In the comparisons of measured SCC results to measured VC results, a direct comparison of total strain was not warranted because each specimen exhibited a different f_{ci} and E_{ci}. Note that, in this section, each specimen's total strain is only compared to the total strain predicted for that particular specimen. This could prove useful because an engineer is likely to use one reference's prediction models (AASHTO 2013 or MC 2010, for example) for both creep and shrinkage prediction.

Errors between predicted and measured total strain for each reviewed prediction model are presented in Table 3.8 using error percentages at fifty-six days and three years. The BP coefficient of variation was not accessed in this comparison, as the results are compared only to illustrate the relative magnitude of prediction errors that would occur under common engineering circumstances—during the use of a single reference's creep and shrinkage models.

Table 3.8: Error comparisons for total deformation predicted by existing references

Compliance Prediction Model	Error % at 56 days		Error % at 3 years	
	SCC	VC	SCC	VC
ACI 209	-3	3	2	11
AASHTO 2013	-7	2	-13	-1
NCHRP 628	15	9	17	14
Eurocode 2	1	13	-3	13
MC 2010	-5	6	-3	13

Several conclusions are warranted based on the results shown in Table 3.8. They include that

- The total deformations of the tested SCC and VC were reasonably predictable using any of the referenced models (within 20% of measured results at concrete ages of fifty-six days and three years, on average),
- Use of the AASHTO 2013 creep and shrinkage models led to the most under-predicted total strain predictions, while use the NCHRP 628 models led to the most over-predicted total strain predictions,
- Use of the ACI 209, Eurocode 2, or MC 2010 models led to the most accurate prediction of total SCC strain (within 5% of measured strains at concrete ages of fifty-six days and three years, on average), and
- Use of the AASHTO 2013 models led to the most accurate prediction of total VC strain (within 2% of measured strains at concrete ages of fifty-six days and three years, on average).

While use of any single reference's creep and shrinkage predictions led to accurate total strain prediction in both materials, the occurrence is only coincidental to these particular concretes. The references that most under-predicted compliance also tended to most over-predict shrinkage; only the current *AASHTO LRFD* models reasonably predicted both compliance and shrinkage. Still, the AASHTO 2013 (Section 5.4.2.3.2 of the code) model most under-predicted SCC compliance, and the AASHTO 2013 shrinkage model (Section 5.4.2.3.3 of the code) was only accurate (within 20% of measured results) concerning VC behavior at the late concrete age of three years. Therefore, mixture-specific corrections to all of the referenced models could be useful to provide more accurate prediction of each component of time-dependent strain.

3.4.3 Adjustments to Prediction Models

In Section 3.4.2 almost all compliance models were found to slightly under-predict measured results, almost all shrinkage models over-predicted measured results, and almost all single-reference predictions of total strain became reasonably accurate by negating the errors in the compliance and shrinkage models. In this section, all compliance and shrinkage models except those proposed by NCHRP 628 are calibrated and compared, and the errors between the revised predictions and the measured results are compared. The NCHRP 628 recommendations are excluded from this evaluation because they already exist only as mixture-specific corrections to the AASHTO models and a similar calibration format was selected for this evaluation. Also recall that the Eurocode 2 provisions for compliance are not explicitly reviewed, as they are the same as those employed by the MC 2010 compliance prediction method.

3.4.3.1 Calibration of Prediction Methods

Calibration of the prediction methods required two choices: 1) selection of the type of correction to apply, and 2) selection of the error measurement to minimize. Concerning the former, the nature of the compliance and shrinkage prediction models allows for adjustment of the ultimate value, the time rate-of-growth function applied to predict the value at intermediate times, or both. Some potential ways of adjusting the models include

- Application of a multiplicative constant that affects the ultimate value within a prediction method (see *A* of Equation 3-5),
- Adjustment of one or more of the existing test- or property-dependent factors that affect the ultimate value (see $t_i^{-0.118}$ in Equation 3-3 regarding loading age or the factors in Equation 3-5 regarding relative humidity or compressive strength), or
- Adjustment of the time-adjustment factor, such as by changing either the constant or exponent within Equation 3-2.

Adjustment of both the ultimate value and time-adjustment function could yield very accurate predictions. However, adjustment of even one parameter could provide practical improvements given the inherent scatter in compliance and shrinkage measurements shown in Figure 3.4 and Figure 3.5. Furthermore, adjustments should only be made in a manner that reflects the experimental variables that were evaluated. Considering that this research consisted of a one-to-one comparison of two concretes incorporating similar local materials (one SCC and one VC), only linear scaling of the existing ultimate creep coefficient and shrinkage strain predictions was warranted. This method of adjustment could provide a reasonably accurate prediction that would be simple and efficient to implement; the scalar adjustment factor could also be directly compared between methods.

Meanwhile, all of the specimens were exposed to very similar curing histories prior to loading (except the four sets of cylinders left in ambient conditions for one year), which would limit the applicability of any time rate-of-growth factor adjustments. Adjustments to the rate-of-growth constants and exponents would also be difficult to compare between models because the factors vary in formulation—see Equation 3-2 and Equation 3-4, for example. While these factors affect the slope of the time-dependent relationships, they do not affect the ultimate predicted values.

Thus, each prediction model was adjusted according to the general form of Equation 3-15 in a similar fashion as the application of *A* to the AASHTO provisions that was recommended by Khayat and Mitchell (2009) in Equations 5-5 and 5-9. In Equation 3-15, the best-fit adjusted prediction of the creep coefficient or shrinkage strain ($Y_{Adjusted}$) equaled the value predicted using the existing model ($Y_{Predicted}$) multiplied by a constant to account for local Alabama materials and conditions (A_{AL}).

$$Y_{Adjusted} = A_{AL}(Y_{Predicted}) \tag{3-15}$$

Application of A_{AL} to the predicted shrinkage strain was straightforward—by definition, shrinkage increases from an initial value of zero strain, so A_{AL} represented a direct amplification or reduction of the predicted shrinkage strain to better align those predictions with the measured results. Meanwhile, compliance predictions were developed in this program by applying the *predicted creep coefficient* to the elastic strain calculated using the actual elastic stiffness (E_{ci}) measured in companion cylinders according to ASTM C469. Thus, A_{AL} is applied to the predicted creep coefficient—specifically *not* the predicted *J*. Only a creep coefficient is predicted according to each of the reviewed methods, so only that coefficient should be adjusted to account for the time-dependent behavior of concrete produced using local Alabama materials and proportions.

As the goal of this research was to advance the understanding of long-term SCC behavior in precast, prestressed girders, best-fit adjustment factors were determined by minimizing ω_{BP} over the entire lifetime of measured results. The fit of the entire time-dependent model is improved in an unbiased fashion by minimizing ω_{BP}, so the adjusted prediction models should give the best overall predictions of the time-dependent behavior of the assessed concretes.

3.4.3.2 Adjustment Factors

A nonlinear numerical solver was used to determine the best-fit A_{AL} for each dataset shown in Table 3.2 and Table 3.4. The factors unique to each specimen group, which are shown by Keske (2014), were evaluated statistically using a two-sample t-test to determine if different adjustments would be necessary for SCC and VC. P-values from that analysis, which are also included reported by Keske (2014), indicate that 1) no compliance adjustment factor was significantly different between materials at a 90% confidence interval (CI), while almost all shrinkage adjustment factors were significantly different between materials at a 95% CI. The only shrinkage adjustment factor not significantly different between SCC and VC was the one applied to the ACI 209 shrinkage prediction model.

After statistically determining if the adjustment factors should be separated by material type, values were averaged to determine a best-fit A_{AL} for each method and (when applicable) material as shown in Table 3.9 and Table 3.10. For practicality, the magnitude of each adjustment factor was also considered because adjustments that would only minimally affect the existing prediction methods would be impractical to implement. Consequently, only adjustments exceeding a threshold minimum change of ± 20% from the existing model are highlighted in bold in the tables based on the statement by Gardner and Lockman (2001) concerning the practical accuracy of time-dependent deformation predictions.

Table 3.9: Evaluation of statistically admissible compliance adjustment factors

Compliance Prediction Model	Adjustment Factor, A_{AL}			Change from Existing (%)		
	SCC	VC	All	SCC	VC	All
ACI 209	-	-	1.11	-	-	11
AASHTO 2013	-	-	**1.21**	-	-	**21**
MC 2010	-	-	1.12	-	-	12

Note: - = not statistically admissible

Table 3.10: Evaluation of statistically admissible shrinkage adjustment factors

Shrinkage Prediction Model	Adjustment Factor, A_{AL}			Change from Existing (%)		
	SCC	VC	All	SCC	VC	All
ACI 209	-	-	**0.72**	-	-	**-28**
AASHTO 2013	0.97	**0.75**	-	-3	**-25**	-
Eurocode 2	**0.74**	**0.56**	-	**-26**	**-44**	-
MC 2010	0.83	**0.63**	-	-17	**-37**	-

Note: - = not statistically admissible

After determining the average adjustment factors, practically applicable adjustments (bold values in the tables) were applied to every dataset. A trend was observed in the adjusted values—SCC compliance was regularly under-predicted, while VC compliance was regularly over-predicted. Furthermore, each adjusted compliance model was less accurate at predicting SCC compliance than at predicting VC compliance.

Thus, while the bold-highlighted compliance adjustment factors in Table 3.9 may not have been statistically significantly different between materials, distinguishing between materials could provide *practical* refinements to the predictions. In light of this, the compliance adjustment factors for Alabama SCC and VC were reconsidered separately. These adjustment factors are shown in Table 3.11, in which those that met a threshold minimum change of ± 10% are highlighted in bold. While a threshold change of ± 20% was used earlier based on the discussion of Gardner and Lockman (2001), a 10% threshold was selected for use with Table 3.11 such that practical adjustments would provide the best estimate of time-dependent behavior achievable within the precision of this testing.

Table 3.11: Evaluation of practically admissible compliance adjustment factors

Compliance Prediction Model	Adjustment Factor, A_{AL}			Change from Existing (%)		
	SCC	VC	All	SCC	VC	All
ACI 209	**1.15**	1.04	-	**15**	4	-
AASHTO 2013	**1.25**	**1.14**	-	**25**	**14**	-
MC 2010	**1.19**	1.03	-	**19**	3	-

Note: - = not practically combinable

The adjustment factors in Table 3.9 through Table 3.11, and their statistical significance, correlate closely with the findings presented in Sections 3.4.1 and 3.4.2. The existing prediction methods were reasonably accurate but would slightly under-predict measured creep, thus necessitating adjustment factors close to but greater than 1.0. Meanwhile, the existing shrinkage prediction models over-predicted average measured results, especially in VC, thus regularly necessitating shrinkage adjustment factors less than 1.0.

The only shrinkage prediction adjustment factor that was statistically and practically similar in SCC and VC was the one applied to the ACI 209 shrinkage prediction model. Material-specific reconsideration of the ACI 209 shrinkage adjustment factor was therefore not necessary. This was also acceptable considering that the ACI 209 shrinkage model already incorporates factors for slump (water content), fine aggregate percentage, and air content, all of which differentiate concrete mixtures.

3.4.3.3 Assessment of Recommended Adjustments

Based on the analysis and discussion presented in the previous subsection, the following adjustment factors presented in Table 3.12 are recommended for application according to Equation 3-15. In the table, adjustments to compliance models are based on the practically significant factors determined for each material, and adjustments to shrinkage models are based on the statistically and practically significant results shown in Table 3.10. All adjustments are considered to be accurate to ±0.1. No greater precision of these recommendations is warranted considering the inherent variability of experimentally measured creep and shrinkage results.

Table 3.12: Recommended creep and shrinkage prediction adjustments, A_{AL}

Material	Prediction Type	Reference			
		ACI 209	AASHTO 2013	Eurocode 2	MC 2010
SCC	Creep	1.1	1.2	1.2	1.2
	Shrinkage	0.8	1.0	0.8	0.8
VC	Creep	1.0	1.1	1.0	1.0
	Shrinkage	0.7	0.8	0.5	0.6

Note: 1.0 = no change recommended

Use of the above recommended values should allow for accurate prediction of time-dependent deformation in concrete produced in Alabama, especially concrete made using crushed dolomitic limestone, a relatively low *w/cm*, and replacement of some portland cement with slag cement. Specifically, the use of A_{AL} for prediction of shrinkage in Alabama concrete should be especially useful considering the pattern of reduced time-dependent free shrinkage observed in similar concrete mixtures during past AUHRC projects (Kavanaugh 2008; Levy et al. 2010).

The difference between the recommended SCC and VC adjustment factors does not precisely match the measured differences in creep and shrinkage (measured SCC creep and shrinkage were approximately 5% and 30% greater than those of the companion VC, respectively). Two variables may explain this discrepancy: 1) the exact adjustment factors shown in Table 3.10 and Table 3.11 were rounded to determine the recommended results considering their practical precision, and 2) the solutions that minimized ω_{BP} may have been affected by differences in the rate of time-dependent deformation growth.

After applying the recommended A_{AL} adjustments to the datasets shown in Table 3.2 and Table 3.4, errors were evaluated versus the existing-model errors shown in Table 3.6 (compliance), Table 3.7 (shrinkage), and Table 3.8 (total deformation). These adjusted-model errors are summarized below in Table 3.13 through Table 3.15. In the below tables, the NCHRP 628 models are not shown because the models were not adjusted—recall that they only differed from other existing models by a mixture-specific constant, A, that was evaluated similarly to A_{AL} in this research.

Table 3.13: Error comparisons for adjusted compliance prediction models

Compliance Prediction Model	ω_{BP}		Error % at 56 days		Error % at 3 years	
	SCC	VC	SCC	VC	SCC	VC
ACI 209	0.108	0.118	-2	-4	-2	-1
AASHTO 2013	0.143	0.160	0	1	-2	-2
MC 2010	0.093	0.074	1	-3	1	-1

Table 3.14: Error comparisons for adjusted shrinkage prediction models

Shrinkage Prediction Model	ω_{BP}		Error % at 56 days		Error % at 3 years	
	SCC	VC	SCC	VC	SCC	VC
ACI 209	0.279	0.236	-1	-1	8	3
AASHTO 2013	0.212	0.199	10	17	-4	-5
Eurocode 2	0.210	0.209	4	0	-13	-21
MC 2010	0.215	0.160	-9	-8	-1	-5

Table 3.15: Error comparisons for total deformation predicted by adjusted references

Total Deformation Prediction Model	Error % at 56 days		Error % at 3 years	
	SCC	VC	SCC	VC
ACI 209	-3	-4	1	1
AASHTO 2013	1	2	-5	-2
Eurocode 2	0	-3	-2	-4
MC 2010	-2	-4	0	-1

The overall accuracy of the compliance prediction models was only moderately improved with respect to ω_{BP} by applying the recommended adjustments. However, the error percentages at concrete ages of fifty-six days and three years were noticeably improved: average model errors ranged -14% to +1% in the existing models, but average adjusted-model errors were no greater than 4% at fifty-six days or 2% at three years. Notably, the only errors greater than 2% at either age were in predictions of VC *J* for which no changes were applied to the existing models (ACI 209 and MC 2010). A graphical sample of the improvement in *J* prediction is illustrated in Figure 3.6 below.

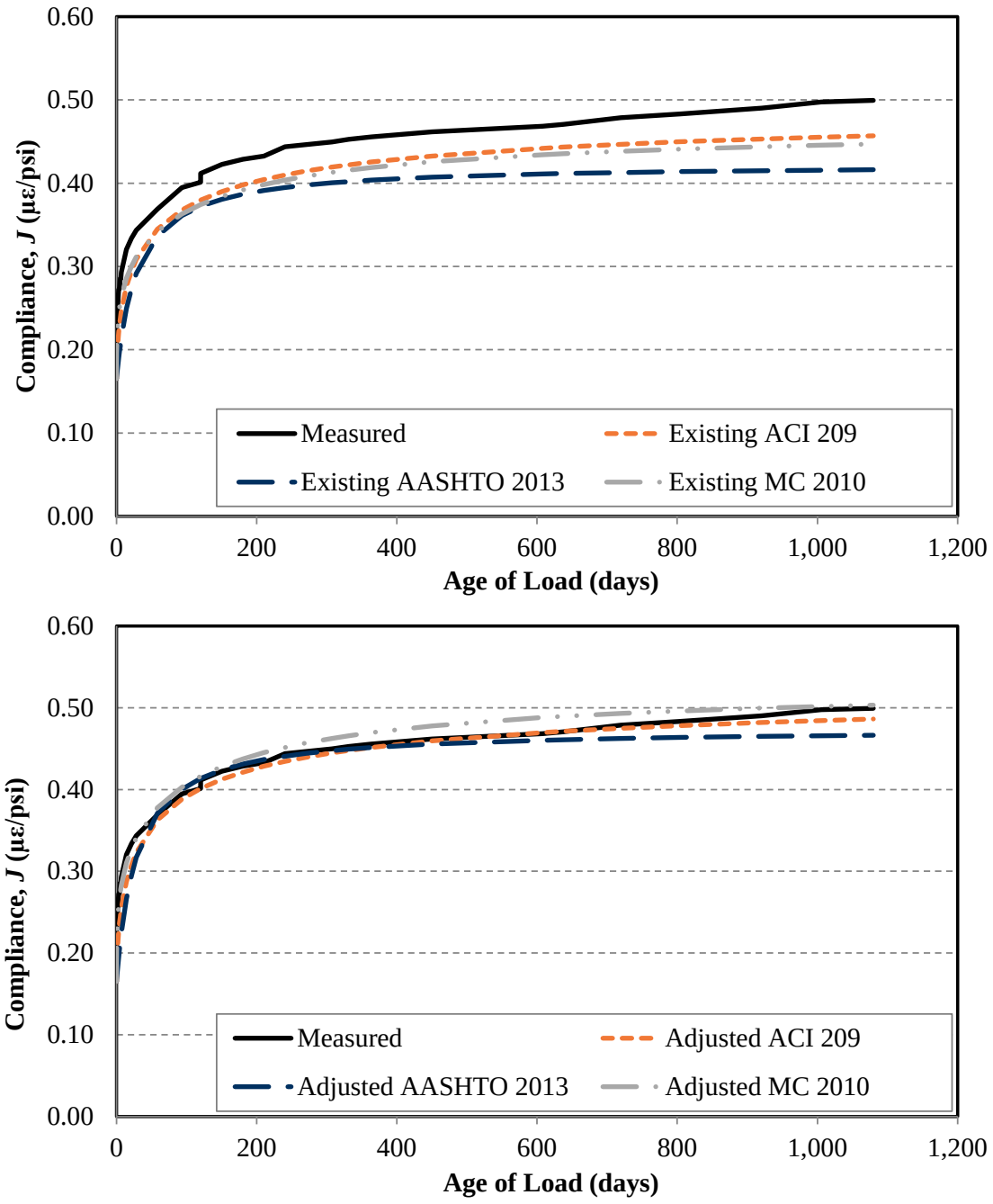

Figure 3.6: Comparison of measured SCC-C-1 data to (*top*) existing and (*bottom*) adjusted compliance prediction models

Based on the results summarized in Table 3.13 and illustrated in Figure 3.6, use of the ACI 209, AASHTO 2013, or MC 2010 models in conjunction with their respective adjustment factors should provide reasonably accurate prediction of compliance in SCC and VC similar to the mixtures employed in this project.

The accuracy of the shrinkage prediction models was more greatly improved with respect to ω_{BP} by applying the recommended adjustments. The BP coefficient of variation was reduced by an average of 66% in all cases except the use of the AASHTO 2013 shrinkage model to predict SCC shrinkage, for which no changes were recommended. The error percentages at concrete ages of fifty-six days and three years were noticeably improved: average model errors ranged up to +114% in the existing models, but average adjusted-model errors were no greater than 17% at fifty-six days or 21% at three years. A graphical sample of the improvement in shrinkage prediction is illustrated in Figure 3.7.

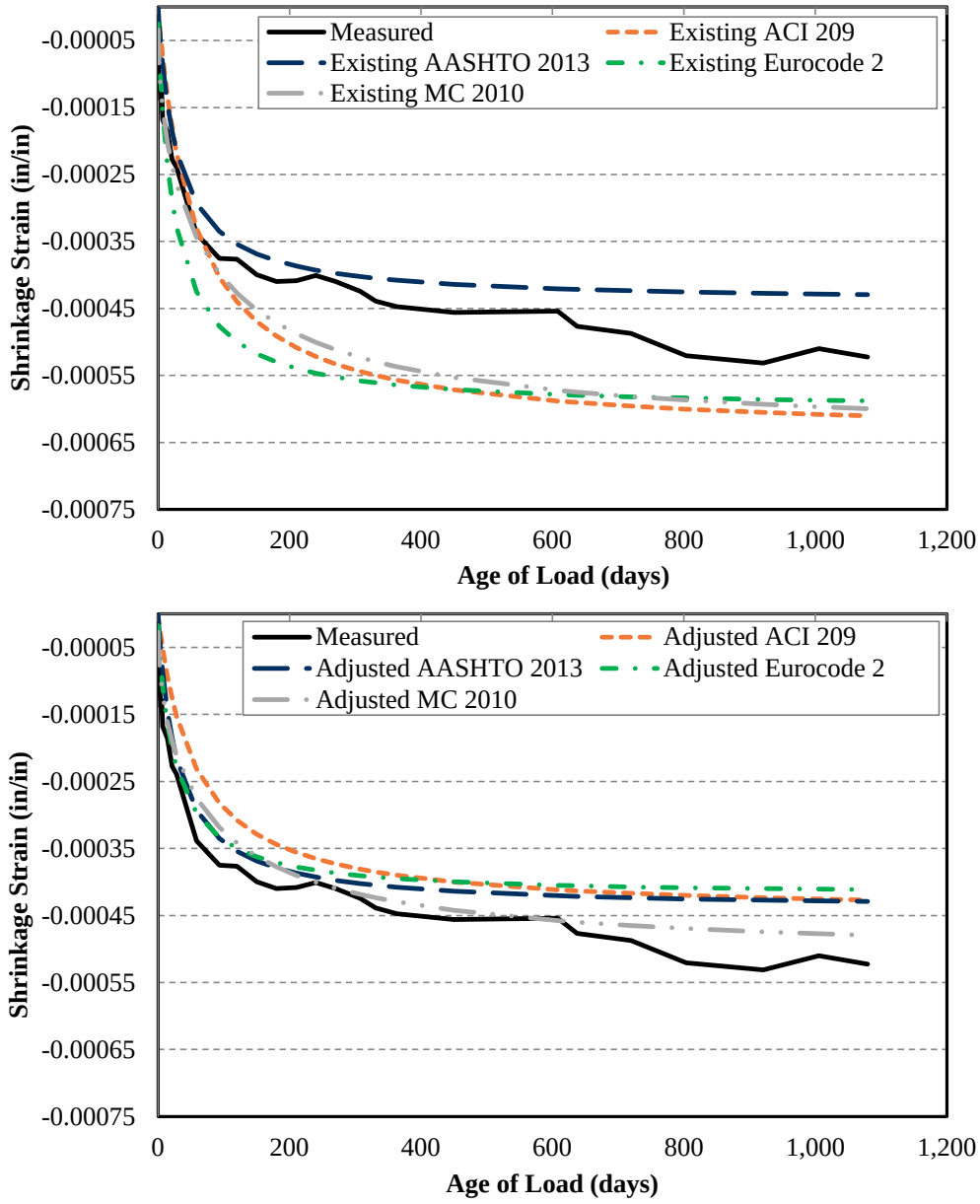

Figure 3.7: Comparison of measured SCC-C-1 data to (top) existing and (bottom) adjusted shrinkage prediction models

While the ω_{BP} and error percentages were still greater in the adjusted shrinkage prediction models than in the adjusted *J* models, the larger errors are likely related to the scatter of the measured shrinkage data shown in Figure 3.5. Based on the 20% preferred error margin discussed in this chapter, such variability is expectable of this type of testing. Consequently, all of the shrinkage prediction models are considered reasonably accurate for the prediction of free shrinkage of concretes similar to those studied in this project, once including the recommended adjustment factors.

Once the recommended creep and shrinkage adjustment factors were incorporated into each reference's models, all references—ACI 209, AASHTO 2013, Eurocode 2, and MC 2010—provided accurate total strain predictions, on average. No average total strain predictions exhibited more than 5% error, and the largest errors (AASHTO 2013 considering SCC and Eurocode 2 considering VC) were in the models in which one of the components of time-dependent strain was acceptable as currently modeled. In all models, the most important improvement afforded by the use of the recommended adjustment factors is that the components of the total strain were accounted for appropriately through their use.

In addition to the specimens evaluated in the previous section, adjusted *J* was assessed in the specimens that were under-loaded and that were aged then loaded. Results concerning these specimens are reported in Keske (2014). As when comparing the measured results in Section 3.4.1.1, the adjusted predictions of compliance for the under-loaded specimens were as accurate as in the standard-tested specimens.

Compliance in the aged-then-loaded specimens was less predictable than in those tested according to ASTM C512, but all adjusted predictions were within 20% of measured results at concrete ages of fifty-six days and two years. Compliance ω_{BP} was comparable in the aged-then-loaded cylinders (0.074–0.131 versus 0.074–0.160 in the early-age loaded cylinders). These results indicate that the time-dependent behavior of the tested concretes was predictable even in exceptional applications of the adjusted prediction models.

3.5 SUMMARY AND CONCLUSIONS

3.5.1 Summary

To better understand the time-dependent deformability of SCC used in precast, prestressed applications, the SCC and VC used to construct the Hillabee Creek Bridge girders were tested for compliance, free shrinkage, and total strain deformation. This evaluation was completed using concrete from five production days (three SCC and two VC production days), and specimens were loaded at up to three ages for a total of thirteen evaluated specimen sets. By testing multiple batches of the same mixtures that had been produced under similar but varied exposure

conditions, valuable insights were gained regarding the time-dependent deformability of prestressed-suitable SCC and VC made using materials and practices common in Alabama.

SCC time-dependent deformation was evaluated both in relation to the companion VC used in the bridge and in relation to various current prediction models proposed by ACI 209 (ACI 209 1992), AASHTO (AASHTO 2013), NCHRP (Khayat and Mitchell 2009), and *fib* (*fib* 2010). The ACI 209, AASHTO 2013, and MC 2010 models were then calibrated to fit the measured data where practical to improve their accuracy. The observations and conclusions made concerning the measured deformability of SCC and VC used in the Hillabee Creek Bridge girders are summarized in Section 3.5.2, including conclusions regarding the applicability of these existing and calibrated prediction methods. The recommendations made based on this research are then given in Section 3.5.3.

3.5.2 Observations and Conclusions

3.5.2.1 Measured Compliance and Shrinkage

- Measured SCC compliance was approximately 15% greater than that of the equivalent-strength companion VC. The increased compliance of the SCC was likely related to its reduced stiffness (SCC E_{ci} was approximately 10-15% less than that of the companion VC).
- Compliance growth (creep) of SCC was comparable to that of VC; average measured SCC creep approximately 5% greater than that of the companion VC. Any difference was expectable in response to the differences in mixture proportions and was considered practically insignificant considering the inherent variability of creep testing.
- Creep in both under-loaded and aged-then-loaded specimens was reasonably predictable: under-loaded specimens exhibited similar creep to standard-tested specimens, and aged-then-loaded specimens exhibited expectably reduced creep due to their advanced age at the time of initial loading. This suggests that creep behavior is predictable under varied loading and aging conditions and between materials.
- Measured SCC free shrinkage was approximately 30% greater than that of the equivalent-strength companion VC. The increased shrinkage of the SCC was likely related to its increased paste volume and reduced aggregate content.
- Shrinkage growth of SCC was comparable to that of VC when compared over a range of time periods. In both concretes, the free shrinkage doubled between concrete ages of seven days and fifty-six days but did not double again between fifty-six days and three years.
- High variability was observed in the shrinkage measurements of SCC and VC prisms tested in accordance with ASTM C157, but all specimens satisfied the requirement of the project that length change be no greater than 0.04% after twenty-eight days of drying.

Free shrinkage of the girder-concrete was consistently less than that of the concrete used in the deck over the bridge at Hillabee Creek.

3.5.2.2 Prediction of Compliance, Shrinkage, and Total Strain

- All of the reviewed creep prediction models—ACI 209, AASHTO 2013, NCHRP 628, and MC 2010—were reasonably accurate at predicting the compliance of SCC and VC at concrete ages of fifty-six days and three years.
- While SCC *J* was slightly less predictable using the existing models, predictions of SCC *J* were within 15% of measured results, on average, and those of VC *J* were within 10%, on average, at concrete ages of up to three years.
- Prediction of the shrinkage of the tested concretes was less accurate than prediction of their time-dependent compliance. On average, the prediction models tended to over-predict shrinkage, especially in vibrated concrete.
- Only the AASHTO 2013 shrinkage model was reasonably accurate at predicting shrinkage in the assessed mixtures; it was more accurate at predicting shrinkage of the tested SCC, in which the predicted shrinkage was within 10% of the measured result, on average.
- While use of any single reference's creep and shrinkage predictions led to accurate total strain prediction in both SCC and VC, the occurrence is only coincidental to these particular concrete mixtures and circumstances—each reference compensated for under-predicting *J* by over-predicting shrinkage.

3.5.2.3 Calibration of Compliance and Shrinkage Models

- Calibrations were made to the referenced prediction models using the format employed by Khayat and Mitchell (2009)—by applying a constant, A_{AL}, to the creep or shrinkage predicted at a given time. Each A_{AL} constant was solved to minimize ω_{BP}, thus optimizing the predictions for all measurements up to a concrete age of three years.
- Adjustments to SCC and VC creep predictions were not statistically different, but they were practically different and suggested an approximate 10% difference between the materials. Corrections to shrinkage predictions were statistically and practically different between materials and reflected the 30% difference in measured shrinkage.
- Compliance model fit as measured by ω_{BP} was only somewhat improved through the use of A_{AL}, while shrinkage model fit was markedly improved (reduction of ω_{BP} by up to 84% in material-specific shrinkage models).

- After applying A_{AL} corrections, average J predictions were accurate to within 5% of measured results at concrete ages of fifty-six days and three years. At the same ages, average shrinkage predictions were accurate to within 21% of measured results.
- After applying A_{AL} corrections, all references were used to determine total strain predictions that were accurate to within an average of 5% of measured results at multiple concrete ages.
- Use of A_{AL} corrections improved the correspondence of each predicted and measured total strain component, which should allow for more accurate prediction of time-dependent behavior in specimens other than cylinders tested in standardized conditions.

3.5.3 Recommendations

- Concerns about the increased compliance or creep of SCC should not restrict the implementation of SCC in precast, prestressed applications because increases were minor and expectable in response to mixture changes commonly used to achieve self-consolidating behavior.
- While many current provisions for creep and shrinkage were used to accurately predict total time-dependent strain of SCC or VC cylinders tested according to ASTM C512, no single reference yielded accurate prediction of both time-dependent strain components. Therefore, adjustment of the models to accurately reflect the separate creep and shrinkage behaviors of Alabama concrete are recommended.
- Prediction of Alabama SCC creep should be improved through the use of a multiplication factor of 1.1 with the ACI 209 model or 1.2 with the AASHTO 2013 or MC 2010 models.
- Prediction of Alabama VC creep according to the ACI 209 and MC 2010 models should be sufficiently accurate as currently specified; prediction of it according to the AASHTO 2013 guidelines should be improved through the use of a multiplication factor of 1.1 applied to the creep predicted using that model.
- Prediction of Alabama SCC free shrinkage should be improved through the use of a multiplication factor of 0.8 with the ACI 209, Eurocode 2, or MC 2010 model; it is already sufficiently predictable using the AASHTO 2013 model.
- Prediction of Alabama VC free shrinkage should be improved through the use of a multiplication factor of 0.7 with the ACI 209 model, 0.8 with the AASHTO 2013 model, 0.5 with the Eurocode 2 model, or 0.6 with the MC 2010 model.
- On average, the concrete tested during this research exhibited less shrinkage than predicted by current design provisions, although SCC free shrinkage was approximately 30% greater than that of the companion VC. The sensitivity of full-scale structural behavior to this difference in shrinkage behavior is evaluated in the next chapter.

CHAPTER 4: TIME-DEPENDENT BEHAVIOR OF GIRDERS

4.1 INTRODUCTION

In Chapter 3 of this report, the difference in the long-term creep behavior of SCC cylinders was shown to be minor and largely explainable by the differences in mixture proportions and hardened mechanical properties observed between the tested SCC and VC. The difference in load-independent free-shrinkage behavior of the tested SCC relative to that of the companion VC was also assessed. While increased paste content or other confounding variables (such as *s/agg*, coarse aggregate gradation, or chemical admixture use) led to approximately 30% greater unrestrained shrinkage in the SCC than in the vibrated concrete, the increase was expectable in response to such mixture changes, and both concretes exhibited less shrinkage than predicted using current models.

The primary long-term time-dependent structural performance characteristic evaluated in the Hillabee Creek Bridge girders was the effective prestress in the prestressed strands. This behavior directly relates to the creep and shrinkage properties evaluated in the previous chapter. Evaluation of long-term full-scale behavior is critical because existing full-scale evaluations of SCC have been limited, and their implications for SCC girders of the scale used in this bridge and made using Alabama materials and methods are unclear. Furthermore, existing evaluations have been limited in duration, which is of clear significance since time-dependent deformations were found in Chapter 3 to continue to evolve through a concrete age of three years.

Prediction of full-scale time-dependent behavior is frequently based on empirical formulas derived from the evaluation of representative cylinders. For this project, these small-specimen tests were conducted on some batches of concrete placed in the girders, so the measured material properties were directly used in the predictions. In this way, the predictability of full-scale behavior of SCC girders was assessed while using the most accurate material properties determined from testing representative cylinders.

To effectively evaluate full-scale time-dependent properties, measurements that reflect varying ambient conditions must be adjusted to account for differences in concrete temperature at the times of data collection. While variations due to ambient thermal conditions may be important, measurements obtained during this research were corrected relative to a standard reference temperature to isolate the long-term time-dependent changes due to creep and shrinkage from those due to transient thermal effects. Thus, it was useful to determine the coefficient of thermal expansion (CTE) of each mixture. This analysis was valuable because CTE is a load-independent material property that, like unrestrained shrinkage behavior, is affected by concrete proportioning (Neville 1996).

The work documented in this chapter was conducted to evaluate the acceptability of the full-scale time-dependent structural performance of the SCC girders used during Alabama's first full-scale implementation of SCC in an in-service precast, prestressed bridge. This evaluation required consideration of both the companion VC girders used in the bridge and the time-dependent behavioral provisions set forth in Sections 5.9.5.3 and 5.9.5.4 of the *AASHTO LRFD Bridge Design Specifications* (AASHTO 2013). The research team selected several tasks necessary to achieve the primary objective of this evaluation:

- Analyze and account for the effects of diurnal and seasonal changes in ambient temperature on apparent concrete strain measurements,
- Compute the long-term, time-dependent maintenance of prestressing force in the SCC and VC girders, and
- Compare the measured prestressing force in the girders to the amounts predicted using various *AASHTO LRFD* models and using design properties in place of measured properties.

4.2 LITERATURE REVIEW

4.2.1 Time-Dependent Behavior of Precast, Prestressed Girders

The two full-scale time-dependent behaviors most commonly assessed in precast, prestressed girders are camber and effective prestress. Incorrectly predicting the amount of prestress lost over the service life of a girder can have significant effects. Over-prediction of losses can result in the use of an unnecessarily large amount of prestressing in the girder, driving up the cost of that girder; under-prediction can lead to cracking and excessive deflections under service loads. Although under-prediction of prestress loss is not likely to affect flexural strength, it can lead to an over-estimation of concrete shear strength in the end regions of prestressed concrete beams. In a similar fashion, the significant over-prediction of camber can cause issues during the construction of the bridge and afterwards: the casting of a deck over girders with a smaller than expected camber requires an increased volume of deck concrete, which increases cost and superimposed dead loads. In extreme cases, low-camber girders may eventually sag under superimposed dead loads.

In light of the previous statements regarding over-prediction of camber, the property is most important at early ages around the time of deck construction. As long as the camber at the time of deck construction is adequately predicted, long-term cambers are not likely to be problematic. Camber decreases during the addition of the deck, but composite-bridge cambers are not typically specified. Only the minimum camber at shipment (greater than 0.5 in.) was

specified in the special provision of this project. However, estimates of initial camber and camber at the time of deck construction were provided on the construction plans.

Due to its self-weight, the deck reduces the precompression in the most heavily prestressed concrete (bottom flange) while simultaneously returning some of the effective prestress to the strands. Once the deck hardens and acts compositely with the girders, the composite section exhibits greater restraint against time-dependent deformation due to its increased flexural stiffness and also exhibits reduced load-induced time-dependent deformation because of the concrete decompression. Thus, the later-age camber behavior of individual girders is complex. This is especially true among girders joined by diaphragms and decking (as in this bridge) that are forced to act at least somewhat concordantly.

While the addition of the deck causes conservative load-dependent changes in effective prestress that are discussed further in Chapter 5, changes in load-independent strains may continue to significantly affect effective prestress (f_{pe}) afterwards. The two primary types of load-independent strain are those due to concrete volumetric shrinkage (predominantly drying and autogenous) and due to thermal effects (Mehta and Monteiro 2006). Considering the variables discussed in Chapter 3, any two concretes may exhibit different long-term effective prestress behavior even if they exhibit the same load-dependent behavior. The importance of continued load-independent strain increase is also evidenced by the results of Section 3.4.1, in which the unrestrained shrinkage of cylinders increased by an average magnitude of approximately 70% between concrete ages of fifty-six days and three years.

4.2.1.1 Prediction of Time-Dependent Deformations in Girders

Time-dependent behavior of precast, prestressed girders involves many variables, many of which are interdependent or change with time. The most important variables include f_c, E_c, and time-dependent creep and shrinkage properties of the material (Stallings et al. 2003; Storm et al. 2013). Changes in the above concrete properties over time were discussed in the previous chapter and in the Phase I report prepared by Keske et al. (2015), as were the differences expectable in response to changes in mixture proportioning. Barr et al. (2008) concluded that errors in the prediction of full-scale behavior are predominantly due to errors in the material-behavior prediction models, which is why the time-dependent behavior of representative cylinders continues to be evaluated.

Unlike the compliance testing discussed in Chapter 3, the compressive stress in full-scale precast, prestressed girders changes with time, both in response to changing external loads (such as the addition of a deck or diaphragms) and changing internal strains (due to creep, shrinkage, or thermal effects). Thus, an incremental time-step method is typically needed to predict the full-scale behavior of these girders. In previous research at the AUHRC including the

work presented by Keske et al. (2015), AUHRC researchers have used such a method based on compatibility, equilibrium, empirically defined material behaviors (elastic and time-dependent), and engineering beam theory.

The time-step method used in past AUHRC research involved evaluation of stress and strain in a user-defined number of time steps and cross sections using empirical time-dependent deformation models (such as those specified by AASHTO 2013). Because prestressing is applied eccentrically and external loads cause flexural stresses, prediction of time-dependent deformation required calculation of an axial strain component (at the centroid of the cross section) and curvature-based strain component (assuming that plane sections remain plane). Thus, time-dependent deformations were computed by incrementally evaluating the changes in strain over all of the time steps leading up to the time of interest—at midspan to determine f_{pe} and over a user-defined number of cross sections to determine camber.

Conversely, the *AASHTO LRFD* (2013) provisions include two approaches to estimate time-dependent losses: an approximate or a refined approach. The approximate approach yields a lump-sum long-term prestress loss, Δf_{pLT}, due to time-dependent effects. Alternatively, the refined method splits the estimation of long-term losses into two separate time periods: from the time of transfer to the time of deck casting (Δf_{pid}) and from deck casting onward (Δf_{pdf}). The refined method was based upon research by Tadros et al. (2003), which also aimed at extending applicability of the existing provisions to high-strength concrete.

While prediction of time-dependent growth of camber is affected by inclusion or exclusion of transfer length, strand debonding, and strand draping (Storm et al. 2013), these considerations should have almost no effect on the calculation of time-dependent *changes* in effective prestress away from these regions. Camber predictions were not evaluated during the work documented in this report, as pre-erection behavior was reported in the report regarding ALDOT project 930-738 (Keske et al. 2015), and composite-bridge cambers are difficult to predict.

4.2.1.2 Time-Dependent Deformation of Full-Scale SCC Girders

The importance and predictability of pre-erection camber was discussed in relation to this project by Keske et al. (2015)—SCC girders appeared to exhibit practically similar cambers and internal strains as companion VC girders prior to erection (initial and time-dependent growth). Any early-age differences appeared to be largely explainable by the differences in the mixture proportions of the two concretes. Pre-erection cambers were systematically over-predicted in the girders produced for the Hillabee Creek Bridge, even when using measured engineering properties. Keske et al. (2015) suggested that the prediction error was likely related to poor prediction of the time-dependent material deformability, as initial elastic responses were reasonably predictable.

Results from other full-scale research projects regarding SCC girder behavior have been mixed. Naito et al. (2005) and Ziehl et al. (2009) found that SCC girders exhibited greater elastic shortening due to the reduced stiffness of the SCC, but that the SCC girders exhibited less growth over time. Trent (2007) also found that SCC girders exhibited less prestress loss despite being of the same strength and stiffness as the companion VC. Thus, these researchers suggested that SCC exhibited improved resistance to time-dependent deformation.

Other researchers (Hamilton et al. 2005; Schrantz 2012; Zia et al. 2005) have found no difference between SCC and VC camber or camber growth. Still others have found that SCC exhibits slightly greater (Erkmen et al. 2008; Ozyildirim 2008) or less (Khayat and Mitchell 2009) camber relative to companion VC girders. Many (Erkmen et al. 2008; Khayat and Mitchell 2009; Ozyildirim 2008) found that differences could be explained by differences in the material properties measured in representative cylinders; Khayat and Mitchell (2009) specifically found that later-age SCC camber was reduced because of the increased volumetric shrinkage of the material.

It is difficult to directly compare structural properties of SCC and VC without accounting for differences in the tested materials. Erkmen et al. (2008) and Trejo et al. (2008) concluded that representative-cylinder data could be used to predict measured in-place performance of SCC girders with as much accuracy as when predicting VC girder behavior. Storm et al. (2013) suggest that the variability inherent to the production process (including the use of many discrete batches of concrete, differences in curing and ambient temperature, and release method) greatly affects behavioral predictions in all precast, prestressed concrete.

Hamilton et al. (2005), Staton et al. (2009) and Trejo et al. (2008) state that such construction variations may be more important than the difference between SCC and VC. Furthermore, several researchers have indicated that the accuracy of full-scale behavioral predictions is most significantly improved by the use of measured engineering properties in place of design properties, whether considering VC (Stallings et al. 2003; Storm et al. 2013) or SCC (Keske et al. 2014 and as discussed in this report).

4.2.2 Thermal Behavior of Concrete

Unrestrained concrete and steel each expand when heated and contract when cooled. The stress-free change in unit length per unit of temperature change is referred to as the coefficient of thermal expansion (CTE). It is used to describe the load-independent thermal strain (ε_T) response to a change in temperature (ΔT) according to Equation 4-1.

$$\varepsilon_T = CTE \times \Delta T \quad (4\text{-}1)$$

Concrete and steel exhibit different but very similar CTE: approximately 4.1–7.2 με/°F in concrete (average of 5.6 με/°F) and 6.1–6.7 με/°F in steel (FHWA 2011). Concrete and steel

interact favorably because they exhibit similar CTE, but the disparity between the two can vary widely due to the heterogeneous nature of concrete. Each component of concrete—cement, SCM, sand, coarse aggregate, and water—exhibits a different CTE, so the CTE of the composite material varies widely and is based entirely on the mixture proportions and interactions between the components. In general, CTE of concrete is based on the paste volume, cementitious material type, and aggregate type, with aggregate type having the most significant influence because aggregate represents the largest portion of the material volume (Mindess et al. 2003).

An increasing understanding of the large stresses that can develop in integral concrete structures (especially bridge decks and concrete pavements) due to thermal expansion led the AUHRC research team to evaluate CTE in concrete made using typical Alabama materials and proportions. In that research, Sakyi-Bekoe (2008) determined that Alabama concrete made using siliceous river gravel exhibited a greater CTE than concrete made with crushed dolomitic limestone—6.9 με/°F versus 5.5 με/°F, respectively. The difference was attributed to the distinctly different CTE of the coarse aggregates. Mindess et al. (2003) state that quartz and similarly siliceous aggregates exhibit the highest aggregate CTE of approximately 6.9 με/°F, while dolomite may exhibit a CTE as low as 3.0 με/°F. Furthermore, the mineralogy of a particular aggregate type can vary between quarries, with direct implications on the CTE of the aggregate (Emanuel and Hulsey 1977).

The second largest effect observed in the AUHRC study by Sakyi-Bekoe (2008) was *s/agg*, at least when evaluating the dolomitic-limestone concrete. Because natural sand typically contains a high percentage of silica, it exhibits a CTE more similar to that of siliceous river gravel. Thus, increasing the coarse aggregate content or reducing the *s/agg* reduced the CTE of concrete made with crushed dolomitic limestone (Sakyi-Bekoe 2008). Also, increasing total aggregate volume decreased CTE, but the effect of the variable was confounded in that work because *w/cm* was also increased, which would have the same effect on the concrete CTE.

CTE of hardened, saturated cement paste is approximately 10 με/°F, and it is affected by SCM replacement, *w/cm*, and (most importantly) degree of saturation (Mindess et al. 2003). The effects of SCMs and *w/cm* on paste CTE are generally considered to be minor except when comparing drastically different mixtures. In past AUHRC research, changing the *w/cm* from 0.32 to 0.44 typically decreased CTE by 3–10% (Sakyi-Bekoe 2008). Meanwhile, completely saturated concrete exhibits approximately the same CTE as oven-dried concrete, but concrete CTE increases by up to approximately 18% at partial saturation (maximum at approximately 70% relative humidity) (Neville 1996). More specifically, the CTE of the paste fraction has been observed to increase by 60–70% when exposed to approximately 50–70% relative humidity. This dependence is illustrated in Figure 4.1 from Neville (1996).

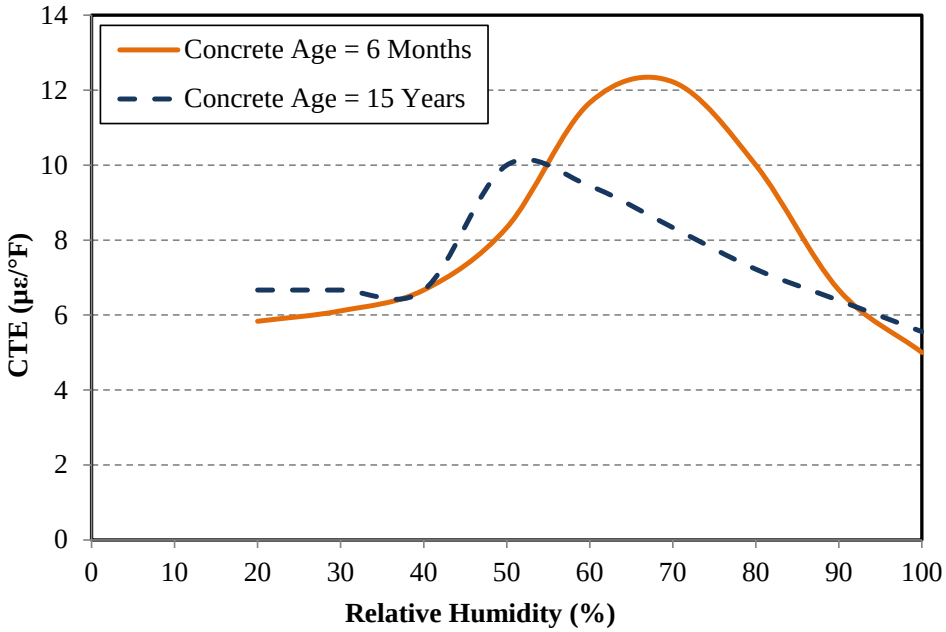

Figure 4.1: Variation of CTE of cement paste due to relative humidity (adapted from Neville 1996)

The effect of partial saturation on concrete CTE can also be interpreted from ACI 209 (1992) Equation 2-32, which is presented as Equation 4-2 below. In it, CTE (in με/°F) is estimated by an empirical formula with variables for concrete saturation (*x*) and coarse aggregate type (e_{agg}):

$$CTE = x + 1.72 + 0.72(e_{agg}) \quad (4\text{-}2)$$

In the equation, an e_{agg} value of 3.1 was recommended for limestone. The variable *x* was described as equaling 0.0 in saturated conditions and "0.83 to 1.11" in external beams exposed to gradual drying. Based on this equation, CTE of limestone-aggregate concrete at a partially saturated relative humidity is as much as 17% greater than at full saturation. Furthermore, a Mississippi DOT report on the effect of relative humidity on CTE found that concrete made with Alabama limestone exhibited up to 26% greater CTE at 75% relative humidity than at saturation (Al-Ostaz 2007).

Emanuel and Hulsey (1977) first recommended a volumetrically weighted calculation of CTE for concrete. This concept was recommended by FHWA (2011) as being second in accuracy only to the physical measurement of CTE according to AASHTO T 336 (AASHTO 2012). Volumetric calculation of CTE was also used by Sakyi-Bekoe (2008) to estimate CTE in Alabama concrete. In a general form, this relationship is illustrated by Equation 4-3 (Emanuel and Hulsey 1977):

$$CTE_{Concrete} = CTE_{Paste}\left(\frac{V_{Paste}}{V_{Total}}\right) + CTE_{FA}\left(\frac{V_{FA}}{V_{Total}}\right) + CTE_{CA}\left(\frac{V_{CA}}{V_{Total}}\right) \quad (4\text{-}3)$$

Where

V_{Paste} is the volume of the cementitious paste,

V_{FA} is the volume of the fine aggregate,

V_{CA} is the volume of the coarse aggregate, and

V_{Total} is the total volume of concrete that includes air content.

Based on Equation 4-3, the CTE of SCC is expected to be different than that of VC if it contains a greater paste volume (which exhibits a relatively larger CTE) and sand volume (frequently siliceous, which exhibits a larger CTE than dolomitic limestone coarse aggregate). Notably, this difference would be expected between *any* two concretes with varying proportions or different types of aggregate.

While SCC may exhibit a larger CTE than comparable VC due to its different mixture proportions, documentation of thermal effects in full-scale SCC girders has been limited. Specifically, Zia et al. (2005) found that thermal fluctuations in internal strain were greater in SCC girders than in companion VC girders despite being of the same elastic stiffness. They stated that, "under seasonal temperature changes, the stiffness of the SCC girders appeared to decrease more than the stiffness of the regular concrete girders." What their results more likely indicate is a difference in CTE—E_c does not change seasonally, but load-independent strains would be different at a given temperature if two concretes exhibit different CTEs.

Elsewhere, varying values of concrete CTE were assumed during analyses of measured SCC and VC results. Khayat and Mitchell (2009) assumed a concrete CTE of 6.4. με/°F in both the SCC and VC they utilized because of the high paste content and low *w/cm* of those mixtures. Trejo et al. (2008) assumed an SCC CTE of 5.6 με/°F because it would be very similar to assumed steel and strain-gauge CTEs of 5.0 and 5.6 με/°F, respectively. Meanwhile, Erkmen et al. (2008) assumed concrete and steel CTEs of 6.0 and 6.8 με/°F, respectively. All of these fell within the range published by the FHWA (2011) and described earlier, and none distinguished between the CTE of SCC and of VC.

4.3 EXPERIMENTAL PROGRAM

4.3.1 Bridge Description

The bridge selected for study has four spans—two outer spans each consisting of seven AASHTO-PCI BT-54 bulb-tees, and two inner spans each consisting of seven AASHTO-PCI BT-72 bulb-tees. One span of BT-54s and one span of BT-72s were made with SCC while the companion spans were constructed with VC girders. SCC girders support the first and second spans, while VC girders support the third and fourth spans, as displayed in Figure 4.2.

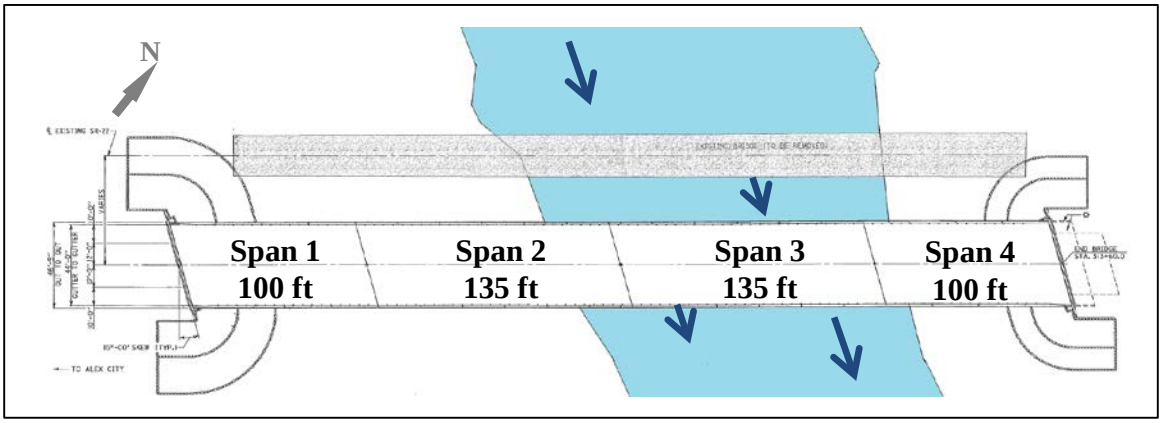

Figure 4.2: Plan view of the bridge over Hillabee Creek (Spans 1 & 2 are SCC girders)

Construction of the bridge over Hillabee Creek in Alexander City, AL, took place in the summer of 2011. The seven girders in each span are spaced at 6 ft-6 in. on center. The bridge has a 15° skew, and each girder-end face is skewed to this degree. The girders rest on neoprene bearing pads and are supported by reinforced cast-in-place VC bents and columns between spans and reinforced cast-in-place, VC abutments at each end of the bridge. The roadway has a transverse width of 44 ft between traffic barriers with a 7 in. thick, VC deck. After the girders were placed at the bridge site in early May of 2011, the bridge deck over each span was cast on four days during August of 2011. Finally, all barriers were slip-form cast in place on November 1, 2011.

Girder numbers are reversed in the SCC and VC spans as indicated in Figure 4.3 for reporting purposes. This was done so that SCC and VC girders with the same number represent a pair of girders that were instrumented and supported in a congruent configuration within the bridge. The girders were not produced sequentially in the order they would be placed at the bridge site, but they were instrumented with knowledge of their expected location in the bridge. Thus, this numbering scheme is used to clearly identify behaviors assessed at the bridge site including camber growth, long-term prestress losses, response to ambient conditions, and live-load response.

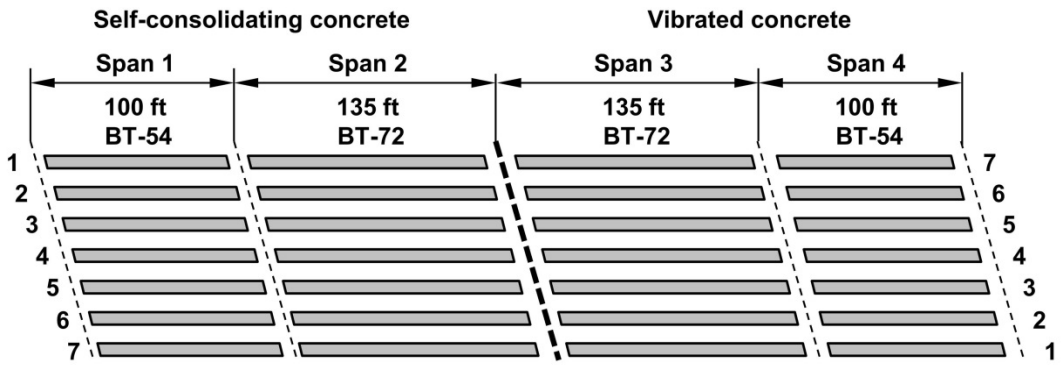

Figure 4.3: SCC and VC girders placed in the bridge over Hillabee Creek

4.3.1.1 Deck Design and Construction

The cast-in-place components added to the precast, prestressed girders at the Hillabee Creek bridge site consists of diaphragms between girders at girder ends and at intermediate locations, a 7 in. deck, and slip-formed, continuously-cast barriers. There is no structural continuity between any of the four spans due to the use of open deck and barrier joints at the end of each.

Cast-in-place VC diaphragms are located at the ends of each girder, at the midspan points of the girders in spans 1 and 4 (SCC and VC BT-54 spans), and at the quarterspan and midspan points of the girders in spans 2 and 3 (SCC and VC BT-72 spans). They were gradually and incrementally added between June 6 and June 21, 2011; their erection was not completed with a systematic pattern, either by span or between particular girders. Therefore, independent mobility of individual girders is assumed to have ceased around the time of diaphragm erection.

Diaphragm dimensions and reinforcement are configured according to ALDOT standard drawings (ALDOT 2012) and are described more thoroughly by Miller (2013). They are 8 in. thick and achieve composite action with the girders through rebar inserts through the webs of all girders. They achieve composite action with the deck through #5 stirrups and have a bottom face located 10.5 in. from the bottom face of the adjoined girders. All diaphragms are similar except that intermediate diaphragms span perpendicular to the girder-web faces and are staggered along the skew, while end diaphragms span parallel to the skew. The difference is shown in Figure 4.4.

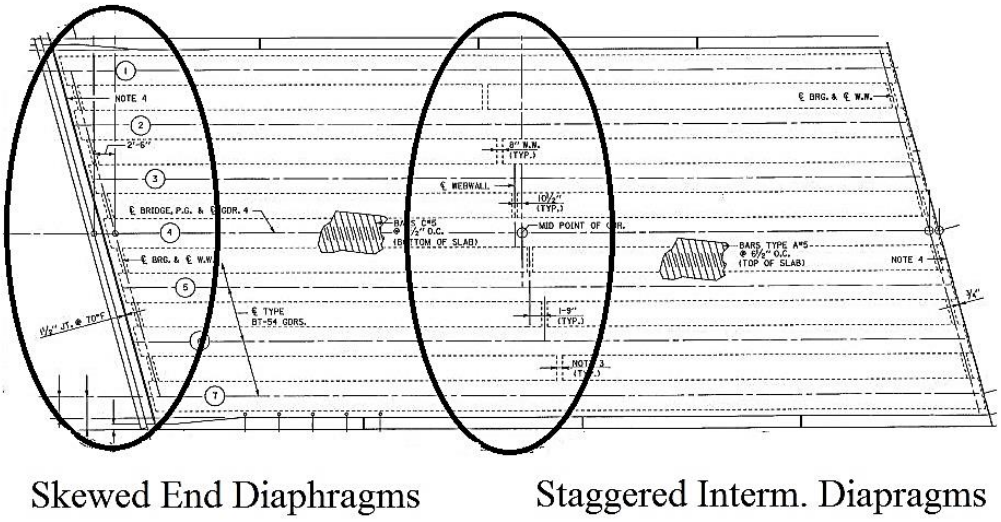

Figure 4.4: Typical diaphragm configuration for end and intermediate diaphragms

The bridge over Hillabee Creek has a 46 ft-9 in. deck with a 44 ft roadway surface width between the barriers. The bridge deck was cast on four separate days between August 3 and August 16, 2011. The 7 in. slab contains two layers of longitudinal, nonprestressed steel. The top layer contains #4 bars throughout while the bottom layer contains #5 bars. The deck also contains two transverse layers of nonprestressed steel. The top layer, consisting of #5 bars, rests upon the top longitudinal layer of steel and has 2 in. of clear cover to the upper deck surface. The bottom layer of steel consists of #5 bars located immediately *below* the bottom layer of longitudinal steel. It has at least 1 in. of clear cover to metal decking welded into place as permanent formwork for the deck; clear cover varies due to the differences in concrete build-up required to create a level upper deck surface atop cambered girders. Reinforcement was also tied into place to protrude from the deck where barriers would be added later.

Traffic barriers were slip-form cast over reinforcement protruding from the deck on November 1, 2011. The barriers, which conform to ALDOT standard drawings for continuously-cast barriers (ALDOT 2012), are not continuous between spans. They also contain saw-cut joint openings at every 25 ft in spans 1 and 4 (midspan and quarterspans) and at every 22.5 ft for spans 2 and 3 (midspan and at each sixth of the span). Therefore, while they achieve composite action with the deck, their effect on the flexural rigidity of the underlying girders (girders 1 and 7 of each span) is substantial but not precisely known because of the incremental control joints.

All cast-in-place elements were produced with the same concrete mixture, which is shown in Table 4.1. In total, approximately 740 yd^3 of this mixture were required to construct the cast-in-place deck and barriers.

Table 4.1: Mixture used in diaphragms, deck, and barriers of bridge over Hillabee Creek

Item	Cast-in-Place VC
Cement content (pcy)	496
Class C fly ash content (pcy)	124
Maximum Water content (pcy)	276
Maximum w/cm	0.45
SSD Coarse aggregate #67 (pcy)	1,870
Fine aggregate (pcy)	1,200
sand/total aggregate (by volume)	0.39
***Total aggregate volume* (%)**	0.67
Air-entraining admixture (oz/cwt)	0.2
WRA (oz/cwt)	3.0
Midrange WRA (oz/cwt)	5.0
Measured air content (%)	3.3
Measured unit weight (lb/ft^3)	147.2
Specified 28-day f'_c (psi)	4,000

The above mixture is distinctly different from both precast, prestressed concrete mixtures. Distinctly different characteristics include the use of:

- Type I/II cement with 20% Class C fly ash replacement (versus Type III cement with 15% slag cement replacement in girders) and
- Upper *w/cm* limit of 0.45 (versus consistent use of *w/cm* = 0.28–0.30 in girders)

While the #67 coarse aggregate was crushed limestone meeting the same gradation specification as that of the VC girders, properties of the aggregate varied due to differences between quarries. The use of a lower specific-gravity coarse aggregate and higher *w/cm* also yielded a lower unit weight, w_c, than in the precast, prestressed concrete. All chemical admixtures for the cast-in-place concrete were supplied by BASF Construction Chemicals, while all chemicals for the girders were supplied by Grace Chemicals.

4.3.2 Concrete Coefficient of Thermal Expansion Evaluation

Rectangular prisms discussed in Chapter 3 served a second purpose when the response of the composite bridge to diurnal heating was investigated by testing the apparent coefficient of thermal expansion (CTE) of prisms. These rectangular prisms exhibited marginally different cross-sectional properties than specified for CTE measurement according to AASHTO T 336-09—they exhibit a square cross section with sides equaling 3 in., while the standard specifies the use of a

cylindrical specimen with a diameter equaling four inches. Thus, the utilized specimens exhibited a smaller cross-sectional area and smaller *V/S*.

CTE was only tested in concrete from one girder-production group per material and two spans of the deck. As the need for this testing only became apparent well after the girders were cast, these were the only matching samples still available. Because of their similarity to the standard specimen used during testing according to AASHTO T 336-09, the testing of these prisms was deemed acceptable and necessary. Testing of the two deck samples indicated very low variability (the difference was less than 0.2 με/°F), thus suggesting that the method utilized should be applicable to all concrete of each material type. All testing was conducted after the girder concrete reached an age of three years, at which time the deck concrete was approximately two years old. At this age, deformations due to shrinkage that would occur during the testing interval were assumed to be minimal.

The prisms were tested using two methods. First, they were exposed to cycles of heating and cooling from 40–120°F using an environmental chamber to closely reflect the measured range of temperatures in the bridge. The apparatus used to measure the length change due to unrestrained shrinkage was then used to measure the length change due to thermal effects. After observing potentially significant differences between the materials, the specimens were then tested as described by AASHTO T 336-09. This required the ends to be sawn to shorten the prisms, as the test equipment requires a sample approximately 7.0 in. in length.

Recall from earlier that the unrestrained shrinkage prisms evaluated in Chapter 3 were used to assess the approximate CTE of the SCC-girder, VC-girder, and VC-deck concretes. These rectangular prisms exhibited marginally different cross-sectional properties than specified for CTE measurement according to AASHTO T 336-09—they exhibit a square cross section with sides equaling 3 in., while the standard specifies the use of a cylindrical specimen with a diameter equaling four inches. Thus, the utilized specimens exhibited a smaller cross-sectional area and smaller *V/S*.

4.3.3 Concrete Strain Evaluation

Vibrating-wire strain gauges (VWSGs) were installed in every girder in the bridge, as well as in the deck over every girder, at midspan. The VWSGs were installed at various locations over the height of the girders and at the mid-depth of the deck. The gauge locations and girder geometries were identical in companion SCC and VC girders, which allowed for the direct comparison of measured concrete-strains and temperatures.

Measured effective prestress (as determined by measuring changes in concrete strain) was also directly compared to the f_{pe} predicted according to the provisions of *AASHTO LRFD Bridge Design Specifications* (2013) Sections 5.9.5.3 and 5.9.5.4 concerning approximate and

refined estimation of time-dependent prestress losses, respectively. The refined estimation models presented in Section 5.9.5.4 are the models currently used by ALDOT for prestress-loss prediction that were also evaluated in Chapter 3 relative to results measured in representative cylinders. The direct implementation of the recommendations from that chapter was, consequently, also evaluated in these girders.

4.3.3.1 Vibrating-Wire Strain Gauges and Locations

VWSGs were placed to allow for strain comparisons between girders undergoing congruent loading once erected at the bridge. However, they were used throughout this research to measure time-dependent strains and temperatures. With reference to Figure 4.5, Figure 4.6, and Figure 4.3 below, girders along lines 4–7 were instrumented for "full-depth" strain and temperature measurement, while girders in lines 1–3 were instrumented only for bottom-flange concrete strain and temperature measurement. Thus, the VWSGs were placed so that they would be located (where applicable) at

- The midspan centroid of the bottom-flange prestressing strands located 6 in. from the bottom surface of the BT-54 girders and 8.8 in. from that of the BT-72 girders (all girders),
- One quarter of the web height above the bottom bulb as well as below the top flange (for full-depth measurements only),
- The centroid of the lightly stressed prestressing steel in the top flange (for full-depth measurements only), and
- A constant depth of 3.9 in. from the top surface of the deck, which varied in relation to the bottom of the girder due to differences in the girder haunch (every girder).

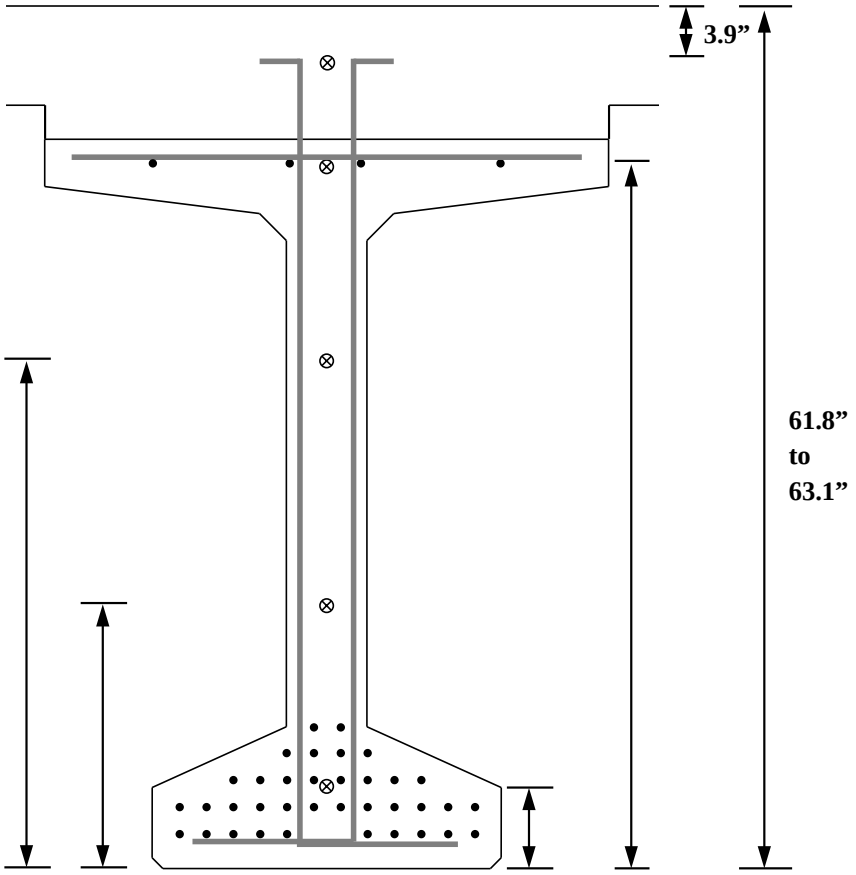

Figure 4.5: BT-54 VWSG configuration (where applicable)

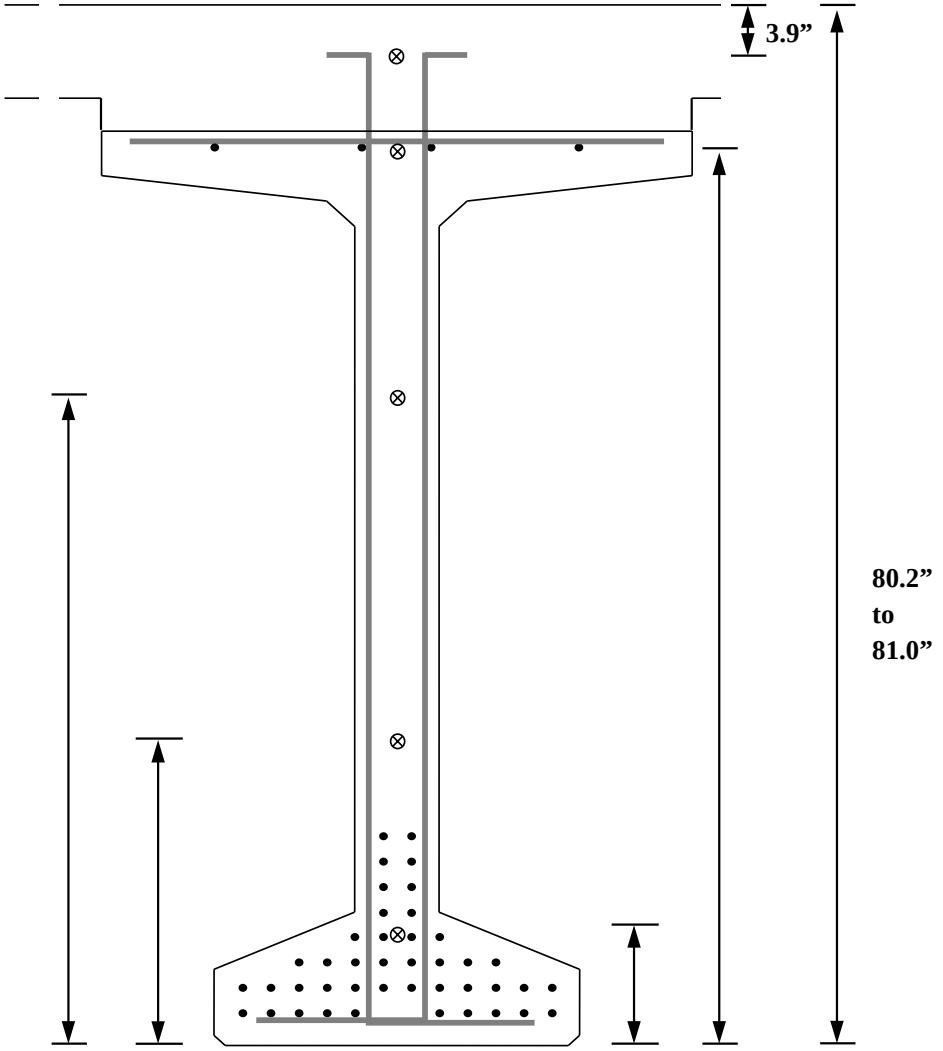

Figure 4.6: BT-72 VWSG configuration (where applicable)

Details concerning the manner in which the VWSGs were secured at the proper locations within each girder are discussed by Johnson (2012). In a fashion similar to that employed during girder fabrication, gauges cast into the deck were secured to the deck reinforcement using zip-ties. An example of this instrumentation is given in Figure 4.7.

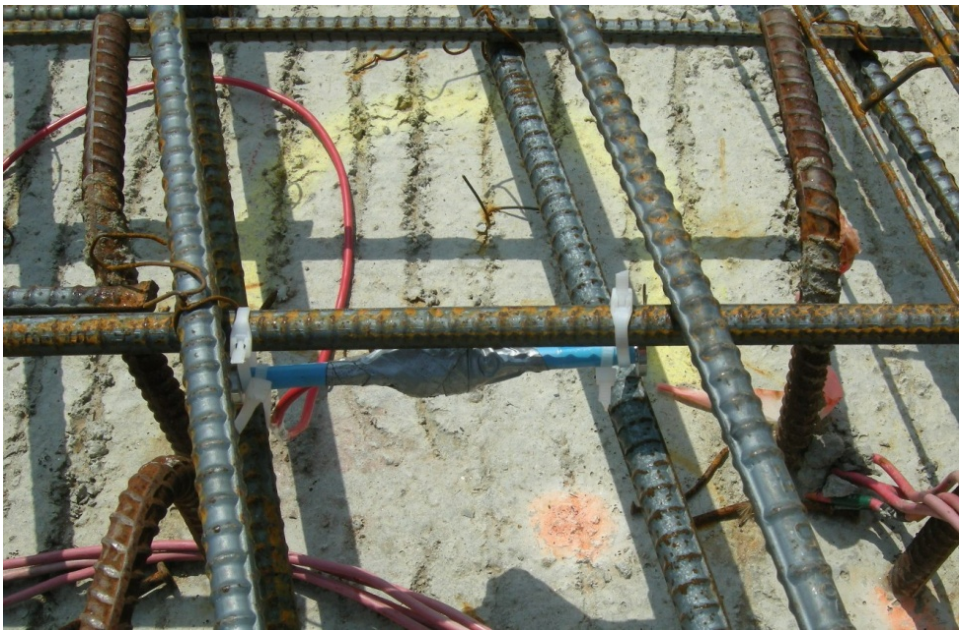

Figure 4.7: VWSG installed within deck reinforcement prior to casting

Two data acquisition systems were used in this research. These systems were described in detail by Johnson (2012). The process by which gauge strains are determined is found in Appendix B of the Geokon Instruction Manual (2010) that was included with the gauges; this process was also described by Johnson (2012). In all reported results, the measured strains have been corrected for the actual temperature of the gauge according to the process described by those two references.

4.3.3.2 Conversion of Concrete Strain to Effective Prestress

Prestress losses were not directly measured in this research. However, prestress losses were estimated based on the strain results from the VWSGs. Compatibility and the bond between the concrete and prestressing strand should mean that a strain change measured by the VWSG corresponds directly to a strain change in the prestressing strand at the level of the gauge. The stress in the prestressing steel remained well within the linear-elastic behavior range, meaning that a change in measured concrete strain would also correspond directly to a change in stress in the strand. Based on linear-elastic stress-strain behavior and compatibility, the effective prestress is thus determined as follows:

$$f_{pe} = E_p(\Delta\varepsilon_{c,cgp}) + f_{pbt} \tag{4-4}$$

In Equation 4-4, $\Delta\varepsilon_{cgp}$ is the change in concrete strain at the *cgp* since immediately prior to transfer (elastic plus time-dependent). It is directly measured using the VWSGs placed at each girder *cgp*; alternatively, its calculation according to the *AASHTO LRFD* (2013) provisions is

discussed in the next section. Several mechanisms can lead to unidentifiable loss of prestress in the strands—steel stress relaxation, seating of the strand chucks, friction at draped-strand hold-downs, and differential heating prior to concrete set. Most of these mechanisms only occur prior to strand release, and they may be compensated for by the producer or have not been found to be differently affected by the use of SCC (Erkmen et al. 2008). Meanwhile, time-dependent stress relaxation, or a reduction in steel stress without a corresponding change in strain, occurs over time and is difficult to accurately measure in the prestressing bed or once the steel is bonded to the concrete.

The elastic strain response to the release mechanism depends on the strand stress immediately *before* transfer (f_{pbt}), which is reduced by stress relaxation; furthermore, all subsequent predictions of time-dependent behavior depend upon the initial elastic response. Therefore, pre-release strand relaxation losses may be estimated according to Equation 4-5 (Stallings et al. 2003):

$$\Delta f_{p,R} = f_{pj}\left[\frac{\log(t_i)}{45}\right]\left[\left(\frac{f_{pj}}{f_{py}}\right) - 0.55\right] \quad (4\text{-}5)$$

Where

$\Delta f_{p,R}$ is the change in prestress force due to stress relaxation (ksi),
f_{pj} is the jacking stress (ksi),
f_{py} is the yield strength of the prestressing reinforcement (ksi), and
t_i is the time between jacking and prestress transfer (hours).

While it would actually differ over the height of the cross section due to curvature of the girder, effective prestress (and prestress loss) is only calculated at the center of gravity of the bottom-bulb prestressing steel, or *cgp*, during design. It is for this reason that VWSGs were placed at the approximate midspan *cgp* in every girder. Consequently, the measured concrete strains reported in Keske (2014) were used to directly calculate f_{pe} in the prestressing steel at various girder ages.

4.3.4 Concrete Temperature Evaluation

Thermistors attached to the VWSGs allowed development of a concrete temperature profile for use to correct strain measurements for thermal effects. By measuring both strain and temperature, the effects of concrete CTE on fluctuations in concrete strain were also directly assessed. Predictions of time-dependent internal strains and prestress losses are computed assuming a constant temperature throughout the girder cross section. However, the girders were stored outdoors and were exposed to varying environmental condition. The method described in

the following subsections was developed by Johnson (2012) to isolate and account for these ambient effects.

4.3.4.1 Specimen Simplification for Thermal-Effect Analysis

The first step in the process of accounting for the thermal gradients in the instrumented cross sections was to simplify the standard sections for improved ease of analysis. The simplified BT-54 and BT-72 sections are shown below in Figure 4.8 and Figure 4.9. These idealized shapes were dimensioned in order to very closely resemble the BT-54 section and BT-72 section in such geometric properties as the location of the centroid, the area of the cross section, and the moment of inertia of the cross section.

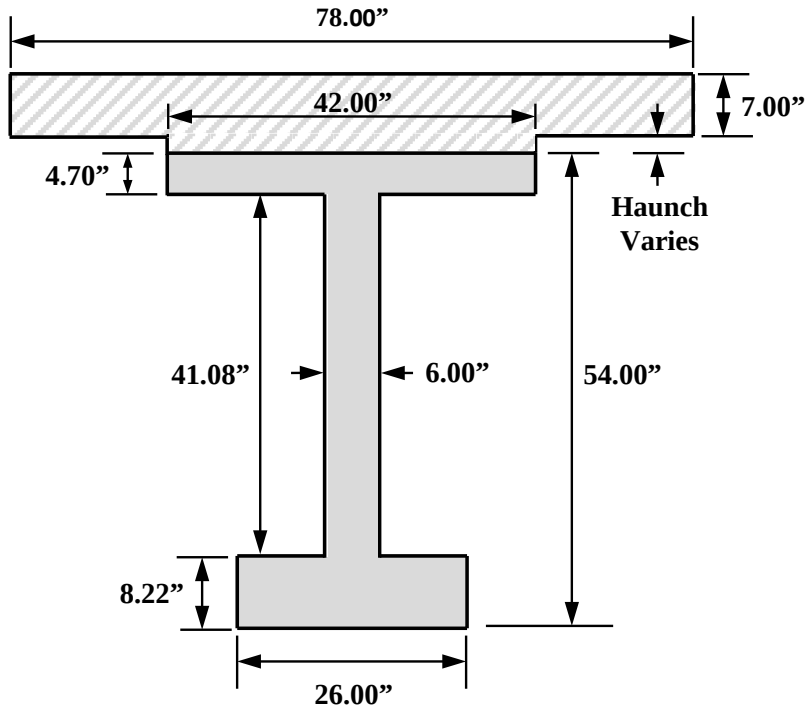

Figure 4.8: Simplified BT-54 composite section

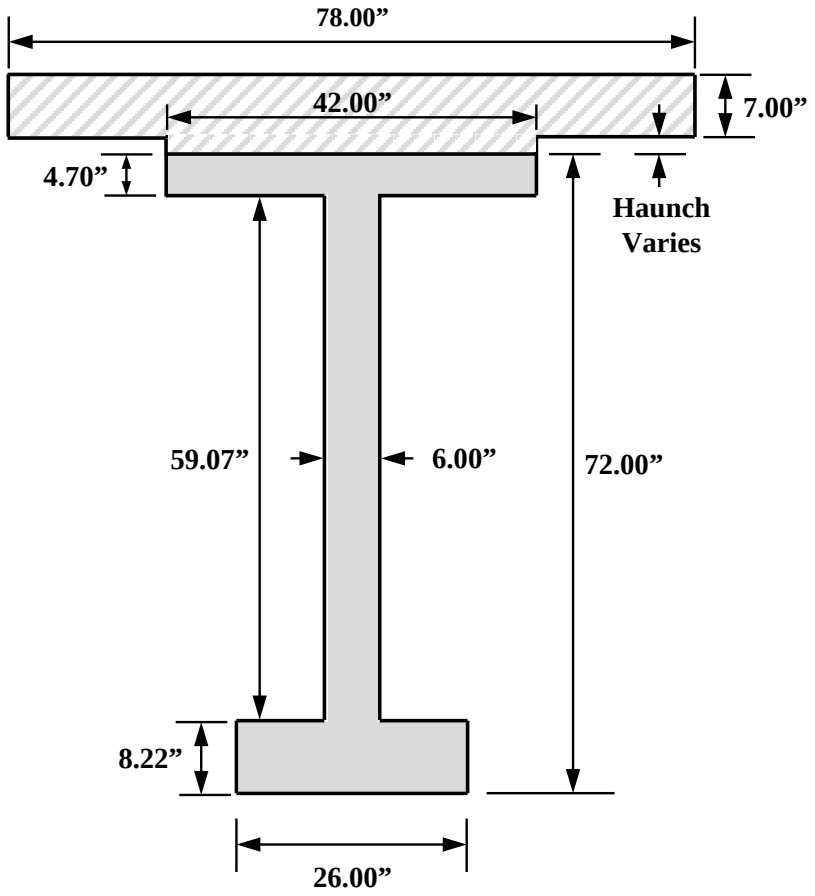

Figure 4.9: Simplified BT-72 composite section

The deck shown in the previous figures (cross-hatched areas) was only included in the simplified section during the analysis of composite behavior at the bridge. The effective width of the deck was determined in accordance with ACI 318 (2011) and equaled the girder-to-girder spacing—78 inches. Also, the haunch thickness noted in the figures varied between girders. It was measured in every instrumented girder using the camber measurement system described in Section 4.3.5.

With reference to the strain gauge locations shown in Figure 4.5 and Figure 4.6, it was necessary to assume a reasonable temperature profile between the discrete temperature measurements observed over the height of the girder and (when applicable) deck and haunch. The assumed temperature profile is presented graphically in Figure 4.10 and is described by the following:

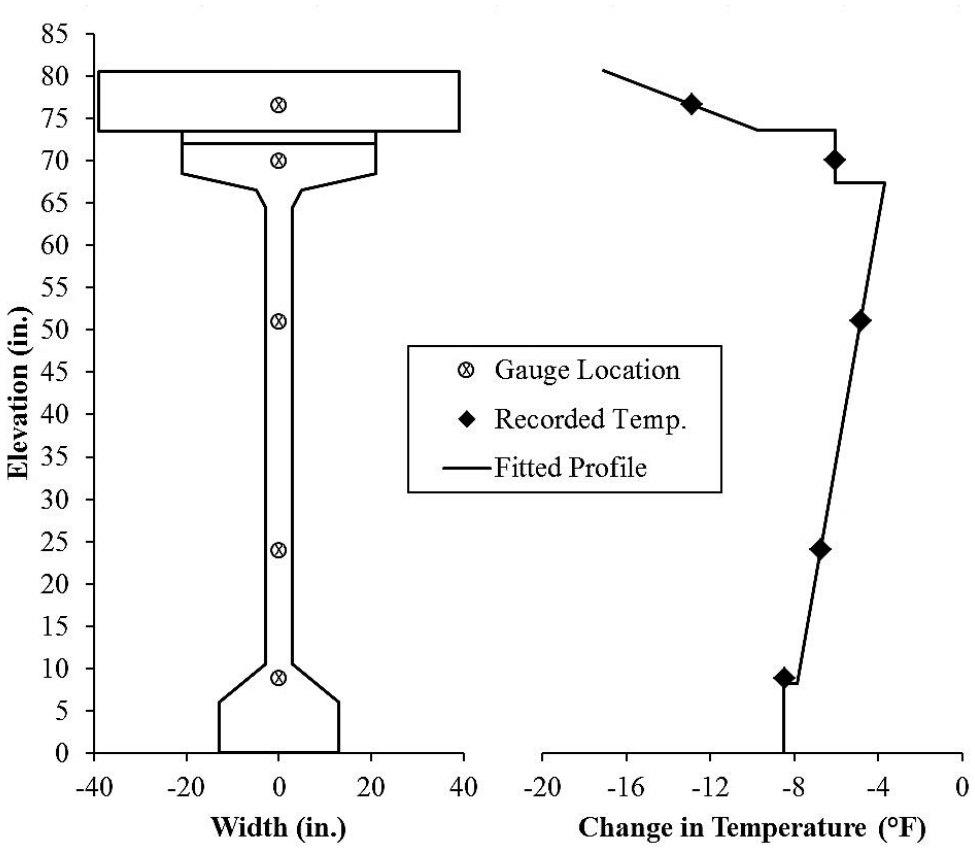

Figure 4.10: Example of idealized thermal gradient profile in BT-72

- The temperature was assumed to be uniform in each of the simplified bottom and top flanges. The utilized temperatures were those measured in the respective bottom- and top-flange thermistors;
- A linear temperature gradient was assumed to occur through the simplified web of the girder which was created by passing a straight line through the two measured web-thermistor temperatures. This linear gradient was projected to the heights of the constant-temperature simplified flanges regardless of whether the projected temperatures matched those of the flanges;
- The temperature in the haunch (when applicable) was assumed to be constant and equal to that of the simplified top flange; and
- A linear temperature gradient was assumed to occur through the thickness of the deck (when applicable). This linear gradient was developed by projecting a straight line through the measured deck temperature and the measured top-flange temperature.

Linear interpolation through the simplified web was understandable because two thermistors were installed in the web and were located well away from the flanges. It was also acceptable to disassociate the temperature of the web from those of the flanges because of the

small *V/S* of the web. It is plausible that the temperatures actually measured in the web would not always relate to the temperatures measured in the self-insulated volumes of the top and bottom flanges. Meanwhile, a constant haunch temperature was safe to assume because the haunch was exposed to very similar environmental conditions as the top flange and was in direct contact with it.

The linear gradient in the deck that was dependent upon projection to the top-flange gauge was chosen because the upper surface of the deck was exposed to more severe environmental conditions than the underside (due to sunlight, wind, or precipitation). It was acceptable to disassociate the temperature of the deck from that of the haunch because approximately half of the tributary width of the deck was not in contact with the haunch—the haunch was 42 in. wide, while a deck width of 78 in. was attributed to each girder. While a linear extrapolation of temperatures was imperfect compared to the actual thermal gradient in the deck, it was a better approximation than to assume a constant temperature like in the simplified flanges. Trial analyses were also conducted by Neal (2015) assuming alternative gradients in the segments (three segments in the non-composite section or five in the composite section); results from those models did not differ significantly from the profile chosen.

4.3.4.2 Method of Isolation of Thermal Effects

To account for thermal effects, the CTEs of steel and concrete were assumed to be equal in this analysis, which was in line with the method employed elsewhere for thermal strain corrections (Erkmen et al. 2008; Trejo et al. 2008). While there may have been a slight discrepancy between the two materials, the area of steel is small relative to the area of the concrete. It would also be difficult to isolate the differential restraint experienced due only to the difference in CTEs. Considering the piecewise approximation of thermal gradients employed and that lateral temperature gradients could also exist (such as where sunlight warms only one side of the girder), this assumption is within the precision of the process.

In order to make accurate comparisons to predicted time-dependent behavior, the measured strains needed to be adjusted so that they would represent what the measured strain would have been if the girder exhibited a constant reference temperature. This reference was chosen arbitrarily to equal 68°F. The process through which nonlinear thermal effects were calculated in this research was outlined regarding non-composite girder behavior by Johnson (2012) and Keske et al. (2015) and regarding composite deck-girder behavior by Neal (2015). In summary, the strains expected to result from a nonlinear temperature distribution consist of an axial component of strain change ($\Delta\varepsilon_{cen,t}$) and a change in curvature ($\Delta\phi_t$). From Keske et al. (2015), these components, which are derived by assuming plane sections remain plane and enforcing cross-section equilibrium, are described by Equations 4-6 and 4-7, respectively. To

compensate for these nonlinear thermal effects, $\Delta\varepsilon_{cen,t}$ and $\Delta\phi_t$ are then subtracted from all measured strain readings.

$$\Delta\varepsilon_{cen,t} = \frac{CTE \int \Delta T dA'}{A'} \quad (4\text{-}6)$$

Where

CTE is the coefficient of thermal expansion of concrete,

ΔT is the difference in the temperature gradient of the cross section from 68°F, which is determined from a piecewise linear approximation in this research, and

A' is the simplified cross-sectional area

And

$$\Delta\phi_t = \frac{CTE \int \Delta T y dA'}{I} \quad (4\text{-}7)$$

Where

y is the vertical distance from the simplified centroid, and

I is the simplified cross-sectional moment of inertia.

4.3.5 Camber Evaluation

The camber measurement instrumentation and methodology utilized prior to girder erection at Hillabee Creek was described in detail by Keske et al. (2015). In summary, the method involved the measurement of girder-end and midspan elevations using a prism rod and a total station. An imaginary line was then drawn through the end-points prior to release and a permanent offset at midspan (due to variations in top-flange thickness) was determined. Offsets of the midspan reading in all subsequent measurements were then interpreted as camber.

To provide a specific and consistent location for the prism rod placement, a hex-headed lag bolt was embedded in the top surface of the girders at each location for use as a surveying target. After the girders were erected at the bridge site, construction practices began to interfere with the collection of camber measurements using the above procedure. The bolts that were cast into the tops of the girders were no longer easily accessible and would eventually be enveloped by the deck. Therefore, a method was developed for camber measurement that would be accessible both before and after the deck was cast. The system devised by the research team involved surveying the underside of the girders, which was accomplished by use of the apparatus shown below in Figure 4.11.

Figure 4.11: Apparatus used to survey underside of girders during construction

The researchers designed the C-shaped apparatus shown in the figure to fit snugly around the bottom bulb and maintain a constant distance from the bottom surface of the girder to the prism. Thus, the spring-loaded rod-and-wheel system maintained constant contact with the bottom surface while the apparatus was pulled along the girder length to the desired location (girder-end or midspan). The apparatus effectively acted as a prism rod with a known, short length, which allowed surveying to continue during construction.

While the top-surface targets were still exposed, the girder thickness was determined at each end point and at midspan by consecutively measuring the underside elevation and top-surface elevation. Multiple girder-thickness readings were taken for each girder at each location to obtain average thicknesses for use in future calculations. Subsequent measurements obtained with the underside method of surveying were then translated to the corresponding embedded-target elevation by adding the location-specific girder thickness to the underside measured elevation. Throughout, camber calculation proceeded in much the same way as conducted by Johnson (2012) and Keske et al. (2015)

The placement location for the apparatus near midspan of each girder was approximate—the apparatus was always placed halfway between the staggered midspan diaphragms, which allowed for longitudinal-location precision of approximately ± 6 inches. The midspan location was approximately 40 ft above the vantage point of the researchers, who pulled the apparatus to the surveying point from the ground. Because of this, the precision of the total

station, and the distance from the total station to the prism, measured girder thicknesses varied by up to 0.10 in. in consecutive days of testing. While the use of an average girder thickness should have minimized the error, all readings obtained via the underside method of surveying must be considered with an appropriate understanding of their precision.

After the barriers were cast and the deck surface was grooved, construction traffic was reduced to a level so that surveying could continue from the top of the deck. After consecutively surveying the top of the deck and underside of the girder to determine total section thickness, the combined thickness of the deck and haunch were determined by subtracting the girder thickness from the total section thickness.

Upon determining the combined thickness of the deck and haunch at each location, haunch thickness was determined by subtracting the assumed depth of the deck, 7.0 inches. Errors in camber readings were compounded by the implementation of each new surveying method (underside and deck), and the value of camber measurements in girders that are mechanically joined by diaphragms and a deck is unclear, at least when attempting to evaluate the time-dependent behavior of individual girders. Therefore, the main purposes of this camber evaluation were to determine the change in camber due to the addition of the deck (reported in Chapter 5), the approximate camber after that addition (also reported in Chapter 5), and the haunch thickness needed for transformed-section analyses of time-dependent and elastic responses. Additional conclusions regarding the camber behavior of the composite bridge are discussed by Neal (2015).

4.3.6 Prediction of Prestress Losses using *AASHTO LRFD* (2013) Models

Prediction of prestress losses consisted of two components: elastic losses (or gains) due to changes in external loading and time-dependent losses due to concrete creep and shrinkage. In all calculations and predictions, the following engineering principles are assumed and employed: strain compatibility, linear-elastic stress-strain material behavior, internal equilibrium, and the assumption that plane sections remain plane. Also, engineering properties measured in representative cylinders (such as f_c or E_c) were used throughout this research; while transformed-section properties were also utilized, the stiffnesses used in to calculate these properties are reviewed in Chapter 5 because they relate more closely to the elastic response of the composite bridge.

Unlike the incremental time-step analysis documented in Keske et al. (2015) and mentioned in Section 4.2, the *AASHTO LRFD* (2013) provisions include two lump-sum approaches to estimate time-dependent losses: an approximate or a refined approach. The approximate estimation method is presented in Section 5.9.5.3 of the *LRFD* specifications, and the refined estimation method is presented in Section 5.9.5.4 of the code. The approximate

approach yields a lump-sum long-term prestress loss, Δf_{pLT}, due to time-dependent effects. Alternatively, the refined method splits the estimation of long-term losses into two separate time periods: from the time of transfer to the time of deck casting (Δf_{pid}) and from deck casting onward (Δf_{pdf}). The refined method was based upon research by Tadros et al. (2003), which also aimed at extending applicability of the existing provisions to high-strength concrete.

Both estimation methods were applied to predict the prestress of the girders produced for the Hillabee Creek Bridge. They are considered "standard precast, pretensioned members subject to normal loading and environmental conditions" as defined in Section 5.9.5.3 of the *AASHTO LRFD*, but the refined models of Section 5.9.5.4 may more precisely estimate time-dependent prestress losses based on measured conditions and material properties. Considerations involved in these prediction methods are discussed in the subsequent subsections.

Unlike the uniaxial compression testing described in Chapter 3, effective prestress in full-scale girders actively affects and is affected by time-dependent deformation. It is also affected by the elastic response of the concrete to external loads, including transfer and deck addition. Because the simplified and refined methods are only used to predict *time-dependent* losses, the prediction of total losses (for direct comparison to measured results) according to either method required calculation of these elastic responses. Therefore, the method used to calculate these elastic responses is discussed first.

4.3.6.1 Calculation of Instantaneous Elastic Change in Strain

At the time of transfer, the axial compression resulting from the applied prestressing force causes an axial shortening of the member. The strands simultaneously shorten, causing a prestress loss due to elastic shortening. AASHTO (2013) allows the designer to determine elastic shortening losses in a few different ways: gross-section approximation, iterative gross-section analysis, and a transformed-section analysis.

The transformed-section approach is more accurate than a gross-section approximation when measured engineering properties are known, and it removes the need for iteration that was involved in the analysis presented by Keske et al. (2015). Transformed properties could also be adjusted over time to reflect changes in concrete material properties or the addition of a concrete deck (during refined estimations), making this method convenient for the current research. The transformed-section approach used to determine the stresses in the concrete and prestressing steel immediately after transfer is summarized below:

$$f_{cgp} = -\frac{f_{pbt}A_{ps}}{A_{tr}} - \frac{f_{pbt}A_{ps}e_{tr}y_{tr}}{I_{tr}} + \frac{My_{tr}}{I_{tr}} \tag{4-8}$$

And

$$f_{pt} = f_{pbt} - n_p\left(\frac{A_{ps}}{A_{tr}} + \frac{e_{tr}^2 A_{ps}}{I_{tr}}\right) f_{pbt} + n_p \frac{M e_{tr}}{I_{tr}} \quad (4\text{-}9)$$

Where

f_{cgp} is the concrete stress at the *cgp* immediately after transfer,

f_{pbt} is the stress in prestressing steel immediately before transfer,

f_{pt} is the stress in prestressing steel immediately after transfer,

A_{ps} is the area of prestressed reinforcement,

A_{tr} is the transformed cross-sectional area (including replacement of reinforcement area with equivalent concrete area),

I_{tr} is the moment of inertia of the transformed section,

e_{tr} is the eccentricity of prestress force with respect to the centroid of the transformed area,

y_{tr} is the distance from the centroid of the transformed section to the location at which strain is determined, equaling e_{tr} is this equation,

n_p (equal to $\frac{E_p}{E_{ci}}$) is the modular ratio of prestressing reinforcement with respect to concrete, at transfer,

E_p is the modulus of elasticity of prestressed reinforcement,

E_{ci} is the modulus of elasticity of concrete at time of prestress transfer, and

M is the bending moment present at a given cross section immediately after transfer (usually due to self-weight of the girder)

By rearranging Equation 4-9, the elastic shortening loss Δf_{pES} is calculated as the difference between f_{pt} and f_{pbt}.

$$\Delta f_{pES} = -n_p\left(\frac{A_{ps}}{A_{tr}} + \frac{e_{tr}^2 A_{ps}}{I_{tr}}\right) f_{pbt} + n_p \frac{M e_{tr}}{I_{tr}} \quad (4\text{-}10)$$

The first term in Equation 4-10 represents the loss from the prestress transfer, while the second term represents the opposing effect of the self-weight bending moment on the cross section. As such, the elastic gains due to the addition of the diaphragms, deck, and barriers were directly calculated using the second term in the equation in conjunction with transformed properties determined using the material properties present at the time of that loading. This gain was then included in the calculations of time-dependent and total prestress losses as necessary.

4.3.6.2 Approximate Estimate of Long-Term Time-Dependent Losses

AASHTO LRFD (2013) Section 5.9.5.3 contains the expression derived by Al-Omaishi (2001) and Tadros et al. (2003) to estimate the total long-term losses due to shrinkage and creep. The prestress loss due to these combined long-term effects, Δf_{pLT}, is determined by Equation 4-11:

$$\Delta f_{pLT} = 10\frac{f_{pi}A_{ps}}{A_g}\gamma_h\gamma_{st} + 12\gamma_h\gamma_{st} + \Delta f_{pR} \quad (4\text{-}11)$$

Where

f_{pi} is the prestressing steel stress immediately prior to transfer (equivalent to f_{pbt} in this research),

A_g is the gross cross-sectional area of the non-composite girder,

γ_h is the correction factor for relative humidity of the ambient air,

γ_h is the correction factor for strength at the time of prestress transfer, and

Δf_{pR} is an estimate of steel relaxation loss taken as 2.4 ksi for low-relaxation strand.

The approximate estimate of time-dependent losses presented in *AASHTO LRFD* (2013) Section 5.9.5.3 and above was based on calibration with full-scale test results and with results of the refined method described in the next section, and it was found to give conservative results (Al-Omaishi 2001; Tadros et al. 2003). The estimate assumes that the member is fully utilized (level of prestressing is such that concrete tensile stress at full service loads is near the maximum limit), which is reasonable for I-beam construction (AASHTO 2013) such as used in this research.

As shown in relation to Equation 4-11, long-term losses due to steel relaxation after release, Δf_{pR}, are approximated as a lump-sum of 2.4 ksi. Note that this lump-sum does not include losses between the time of jacking and release, so its calculation is separate from that discussed in relation to Equation 4-5.

4.3.6.3 Refined Estimate of Losses from Release to Time of Deck Addition

AASHTO LRFD (2013) Section 5.9.5.4.2 contains the expressions derived by Tadros et al. (2003) to determine the losses due to shrinkage and creep from transfer to the time of deck addition. The prestress loss due to the shrinkage of girder concrete during this time period, Δf_{pSR}, is determined by Equation 4-12:

$$\Delta f_{pSR} = \varepsilon_{bid}E_pK_{id} \quad (4\text{-}12)$$

In which

$$K_{id} = \frac{1}{1 + \frac{E_p}{E_{ci}}\frac{A_{ps}}{A_g}\left(1 + \frac{A_g e_{pg}^2}{I_g}\right)\left[1 + 0.7\Psi_b(t_f, t_i)\right]} \quad (4\text{-}13)$$

And where

ε_{bid} is the concrete shrinkage strain of in the girder between the time of transfer and deck placement, per Equation 3-8,

K_{id} is the transformed-section coefficient that accounts for the time-dependent interaction between concrete and steel in the section being considered, for the time period prior to deck placement,

e_{pg} is the eccentricity of prestressing force with respect to the gross-section centroid of the girder (positive where it is below girder centroid),

I_g is the gross moment of inertia of the girder,

$\psi_b(t_f,t_i)$ is the girder creep coefficient at final time due to loading introduced at transfer, per Equation 3-3,

t_f is the final age considered (days), and

t_i is the age at transfer (days)

The prestress loss due to creep of the girder concrete between time of prestress transfer and deck placement, Δf_{pCR}, is determined by Equation 4-14:

$$\Delta f_{pCR} = \frac{E_p}{E_{ci}} f_{cgp} \Psi_b(t_d, t_i) K_{id} \quad (4\text{-}14)$$

Where

$\psi_b(t_d,t_i)$ is the girder creep coefficient at time of deck placement due to the loading introduced at transfer, per Equation 3-3, and

t_d is the age at deck placement (days).

In the previous equations, K_{id} is used to account for the restraint that would actually be present in the gross section due to the presence of steel reinforcement. Notably, this single calculation is based on *gross* section properties, not transformed section properties, because it directly accounts for the interaction between steel and concrete through the inclusion of a modular ratio in the denominator.

Losses due to relaxation of prestressing strands between the times of transfer and deck addition, Δf_{pR1}, are discussed in Section 5.9.5.4.2c of the provisions. According to those provisions, Δf_{pR1} may be calculated according to Equation 5.9.5.4.2c-1, which is shown below as Equation 4-15.

$$\Delta f_{pR1} = \frac{f_{pt}}{K_L}\left(\frac{f_{pt}}{f_{py}} - 0.55\right) \quad (4\text{-}15)$$

Where

Δf_{pR1} is the change in prestress force due to stress relaxation (ksi) between the times of transfer and deck addition,

f_{pt} is the stress in the steel immediately *after* release (ksi), and

K_L is a constant equal to 30 for low-relaxation strand.

Per the provisions of *LRFD* Section 5.9.5.4.2c, Δf_{pR1} may alternatively be assumed to equal 1.2 ksi for low-relaxation strand. Equation 4-15 was chosen over the assumed value to improve the accuracy of predictions that involved its use, specifically Equation 4-19 in the next section. While similar in format to Equation 4-5, Equation 4-15 does not require calculation of the time between release and deck addition. This information would not typically be known to the engineer during design, and Equation 4-15 is a simplification of an equation derived by Tadros et al. (2003) in which t_i and the age at deck addition are assumed to equal 0.75 days and 120 days, respectively (AASHTO 2013).

4.3.6.4 Refined Estimate of Losses from Time of Deck Addition Onward

AASHTO LRFD Section 5.9.5.4.3 contains the expressions derived by Tadros et al. (2003) to determine the losses due to shrinkage and creep from time of deck placement onward. The prestress loss due to shrinkage of girder concrete after the time of deck placement, Δf_{pSD}, is determined by Equation 4-16:

$$\Delta f_{pSD} = \varepsilon_{bdf} E_p K_{df} \quad (4\text{-}16)$$

In which

$$K_{df} = \frac{1}{1 + \frac{E_p}{E_{ci}}\frac{A_{ps}}{A_c}\left(1 + \frac{A_c e_{pc}^2}{I_c}\right)\left[1 + 0.7\Psi_b\left(t_f, t_i\right)\right]} \quad (4\text{-}17)$$

And where

ε_{bdf} is the shrinkage strain in the girder from the time of deck placement onward, per Equation 3-8,

K_{df} is the transformed-section coefficient that accounts for the time-dependent interaction between concrete and steel in the section being considered, from the time of deck addition to the final time considered,

e_{pc} is the eccentricity of prestressing force with respect to centroid of the composite girder-deck section (positive in common construction where the centroid of prestress is below girder centroid),

A_c is area of the section calculated using the gross composite concrete section properties of the girder and the deck and the deck-to-girder modular ratio (in.^{2}), and

I_c is the moment of inertia of the section calculated using the gross composite concrete section properties of the girder and the deck and the deck-to-girder modular ratio at service (in.^{4}).

Similarly, the prestress loss due to the creep of girder concrete from the time of deck placement onward, Δf_{pCD}, is estimated by Equation 4-18 in which a loss is positive and gain is negative.

$$\Delta f_{pCD} = \frac{E_p}{E_{ci}} f_{cgp}\left[\Psi_b(t_f, t_i) - \Psi_b(t_d, t_i)\right]K_{df} + \frac{E_p}{E_c}\Delta f_{cd}\Psi_b(t_f, t_d)K_{df} \quad (4\text{-}18)$$

In which

$$\Delta f_{cd} = \Delta f_{ce} + \frac{A_{ps}}{A_{tr}}(\Delta f_{p,id}) + \frac{A_{tr}e_{tr}^2}{I_{tr}}(\Delta f_{p,id}) \quad (4\text{-}19)$$

And where

$\psi_b(t_f,t_d)$ is the girder creep coefficient due to the additional loading at the time of deck placement, per Equation 3-3,

Δf_{cd} is the change in concrete stress at the *cgp* due to time-dependent losses between transfer and deck placement plus elastic gains due to the deck weight and superimposed loads (ksi), in which a compressive stress is positive and a tensile stress is negative,

Δf_{ce} is the elastic change in concrete stress at the *cgp* due to the deck weight and superimposed loads (ksi), in which a compressive stress is positive and a tensile stress is negative, and

$\Delta f_{p,id}$ is sum of Δf_{pSR}, Δf_{pCR}, and Δf_{pR1}.

After composite action is achieved, deck concrete shrinkage is restrained by the girder. Due to compatibility with the girder, the restrained deck shrinkage induces compression in the top of the girder. Because both net axial force and internal bending moment equal zero, this results in a downward deflection, an extension of the bottom flange, and a resulting gain in prestress due

only to the shrinkage of the deck, Δf_{pSS}. The *AASHTO LRFD* provisions account for this phenomenon by Equations 4-20 and 4-21:

$$\Delta f_{pSS} = \frac{E_p}{E_c} \Delta f_{cdf} K_{df} \left[1 + 0.7\Psi_b\left(t_f, t_d\right)\right] \quad (4\text{-}20)$$

In which

$$\Delta f_{cdf} = \frac{\varepsilon_{ddf} A_d E_{cd}}{\left[1 + 0.7\Psi_d\left(t_f, t_d\right)\right]} \left(\frac{1}{A_c} - \frac{e_{pc} e_d}{I_c}\right) \quad (4\text{-}21)$$

And where

Δf_{cdf} is the change in concrete stress at the *cgp* due to shrinkage of the deck concrete (ksi),

ε_{ddf} is the shrinkage strain of the deck concrete from the point of initial curing through the final time considered, per Equation 3-8,

A_d is the gross area of deck concrete (in.^{2}),

E_{cd} is the modulus of elasticity of deck concrete (ksi),

e_d is the eccentricity of the deck centroid with respect to the gross composite-section centroid (positive where deck is above girder), and

$\psi_d(t_f,t_d)$ is the creep coefficient of the *deck* concrete applied to loading introduced after deck placement (i.e. overlays, barriers, etc.), per Equation 3-3.

Losses due to relaxation of prestressing strands from the time of deck addition onward, Δf_{pR2}, are discussed in Section 5.9.5.4.3c of the *LRFD* provisions. As stated in that section, "research indicates that about one-half of the losses due to relaxation occur before deck placement; therefore the losses after deck placement are equal to the prior [Δf_{pR1}] losses." While total relaxation losses from the time of release onward are thus calculated by doubling Δf_{pR1}, this calculation does not include the pre-release relaxation losses that were discussed in relation to Equation 4-5.

4.3.6.5 Prediction Methodology Using the *AASHTO LRFD* (2013) Models

During the computation of transformed section properties for the analyses described in the previous subsections, non-prestressed reinforcement in the deck was not considered. This reinforcement would provide some minor additional flexural stiffness, but the *AASHTO LRFD* provisions do not require its inclusion. The restraint against deck shrinkage provided by this reinforcement is also unclear, which could slightly affect results.

Predictions of the time-dependent behavior of these full-scale girders using the simplified estimates from the *AASHTO LRFD* provisions were based on the following procedures:

- Elastic strain changes, and associated changes in prestress, due to transfer and the weight of the cast-in-place deck elements were calculated as shown in Section 4.3.6.1 and using the measured stiffness of representative cylinders. The accuracy of these calculations is assessed independently of the predictability of time-dependent effects, in Chapter 5.
- Total long-term time-dependent prestress losses were predicted using the method described in Section 4.3.6.2.
- Total predicted prestress losses consisted of the sum of the predicted time-dependent losses (based on the approximation method described in *AASHTO LRFD* Section 5.9.5.3) and calculated elastic changes (based on measured *E* at the time of each load application).

The computation of the complicated cross-sectional deformations of girders at different stages in the construction process requires an understanding of the fundamental engineering mechanics described earlier, as well as the creep and shrinkage models discussed in Chapter 3. Predictions of the time-dependent behavior of these full-scale girders using the refined method of the *AASHTO LRFD* provisions were thus based on the following procedures:

- Elastic strain change due to transfer was calculated as shown in Section 4.3.6.1 using the measured E_{ci} of companion cylinders tested in accordance with ASTM C469 (2010) and a calculated f_{pbt} of 200.4 ksi.
- Prestress losses due to creep, shrinkage, and relaxation from the time of transfer until the time of deck addition were predicted as discussed further in Section 4.3.6.3. The change in prestress due to the addition of the cast-in-place elements was calculated using 28-day concrete stiffness, as this value was the best available indicator of the elastic stiffness of the girder concrete at the time of deck construction. The accuracy of this calculation is also assessed independently of the predictability of time-dependent effects, in Chapter 5.
- Total prestress losses were calculated by the addition of the elastic losses at transfer, time-dependent losses from the time of transfer to the time of deck addition, elastic gains due to the weight of the deck, and time-dependent losses from the time of deck addition to the time considered (per Section 4.3.6.4).

While the main purpose of the Section 5.9.5.4 *AASHTO LRFD* provisions is the prediction of the lump-sum time-dependent prestress losses at the time of deck addition and at the latest time considered, the nature of the creep and shrinkage models used in those provisions allowed prediction of losses at intermediate times. Specifically, refer to Equation 3-4 of this report regarding k_{td}. Determination of this factor was explicitly required to calculate the lump-sum losses at deck addition and at the final age considered because the creep and shrinkage models

discussed in Chapter 3 predict an *ultimate* value that is modified for time through the use of k_{td}. Because it was used for these lump-sum calculations, k_{td} was also used at intermediate times so that measured results at these intermediate ages could be compared.

Application of Equation 3-4 to the refined-*LRFD* time-dependent loss predictions was complicated because the empirical equations presented in Chapter 4 consider different time periods for creep, shrinkage, and other factors (such as K_{id} and K_{df})—from initial time (t_i) to final time (t_f), t_i to time at deck construction (t_d), or t_d to t_f. The application of these time intervals to the models described in the previous subsections is further explained in the dissertation prepared by Keske (2014).

4.3.7 Nomenclature and Additional Considerations

4.3.7.1 Nomenclature and Use of Data

In order to distinguish the twenty-eight girders, a specimen identification system was implemented as shown in Figure 4.12. This numbering scheme is consistent with the nomenclature used in the report prepared by Keske et al. (2015) regarding fabrication and pre-erection behavior.

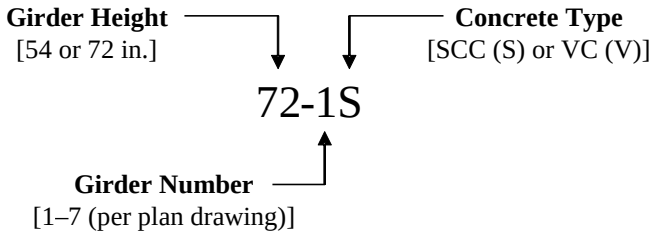

Figure 4.12: Girder identification scheme

As with the assessments of the other chapters, the exact placement location of the batches sampled for laboratory testing could not be isolated within the girders. Samples taken at the midpoint of each girder-production day and deck-casting day were assumed to be representative of the majority of concrete placed during those days. The use of production-group hardened mechanical properties is of imperfect accuracy for the prediction of individual-girder behavior that is actually measured in girders mechanically joined by diaphragms and a fully composite deck. However, it would be less accurate to incorporate measured results any differently. Essentially only three mixtures (for SCC girders, VC girders, and all cast-in-place elements) were used throughout production, but every element could have been subjected to different curing and ambient exposure histories. Furthermore, many of the behaviors assessed in this work were measured prior to the attainment of composite-bridge action, so it was best to

continue using these production-day-specific mechanical properties even after the girders achieved composite action. The precision of all comparisons should be considered in light of the inherent variability of concrete material testing and full-scale property measurement.

4.3.7.2 Prediction Application Considerations

Based on the literature reviewed in Section 4.2 and the discussions of Section 4.3, inputs had to be selected for implementation in the various equations required for this work. Many of the material-specific considerations were already discussed in Chapter 3, as the work of that chapter involved the concrete directly placed in these girders. Pertinent assumptions and choices are summarized below, and further explanations of these selections are reported by Ellis (2012), Johnson (2012), and Neal (2015):

- Gross section properties (V/S, A_g, I_g, etc.) were those specified in the *AASHTO LRFD* provisions (AASHTO 2013).
- A constant relative humidity of 70% was used during the modeling of time-dependent behavior of these girders based on Figure 5.4.2.3.3-1 of the *AASHTO LRFD* provisions (AASHTO 2013).
- Measured values of f_c and E_c that were used for time-dependent creep modeling were discussed previously by Keske et al. (2015) and in Section 4.3.6.
- Measured values of f_c for time-dependent shrinkage modeling were those measured at the earliest age after the end of curing (f_{ci} for the girders and 3-day compressive strengths measured in the deck spans).
- A constant deck thickness of 7.0 in. was assumed based on the project specifications. Deck thicknesses were only measured directly over girders, so haunch thickness was assumed to equal the difference between the measured total thickness and the assumed 7 in. deck thickness.
- Individually measured haunch thicknesses were used to determine composite-section properties for time-dependent analysis because only a few girders (with different transformed properties and potentially different haunches) were analyzed during this assessment—see Appendix G of Keske (2014) for measured haunch thicknesses.
- The modulus of elasticity of prestressed strand (E_p) was assumed to equal 28,600 ksi to match the previous work of this project.

During this project, strands were always stressed the day before placing the concrete; thus, the strands were stressed for approximately two days between jacking and release. Using Equation 4-5, the prestress loss due to pre-release steel relaxation was estimated to equal approximately 2.1 ksi. This estimate agrees well with measured pre-release stress relaxation

losses measured during previous AUHRC work (Boehm et al. 2010). Therefore, (f_{pbt}) was assumed to equal f_{pj} (202.5 ksi) minus the estimated relaxation loss. This f_{pbt}, 200.4 ksi, was used during all calculations of the f_{pe} of the girders.

During the determination of Δf_{ce} in Equation 4-19, 91-day deck properties were used to calculate the concrete stress response to the addition of the barriers. To account for their effect on elastic and time-dependent behavior, the weight of the two barriers was distributed evenly to the seven girders in the span, per the *AASHTO LRFD* (2013) recommendation for this distribution. While this distribution is only an approximation of the actual behavior, the girders that would be affected most by any discrepancy (girders in lines 1 and 7) were not evaluated in this work because these exterior girders are differently restrained and are exposed to more variable thermal exposure. The difference in time-dependent exterior-girder behavior may be important, but evaluation of it was beyond the scope of this work.

4.4 PRESENTATION AND ANALYSIS OF RESULTS

Results and discussion relevant to the assessment of full-scale time-dependent girder behavior are presented in this section, including evaluations of full-scale changes due to transient thermal conditions and due to time-dependent creep and shrinkage. The recommended modifications to the *AASHTO LRFD* (2013) material-deformation models that were proposed in Chapter 3 are also evaluated in this section. Strength and stiffness measurements were also necessary to compute the predictions of time-dependent behavior; the evaluation of these mechanical properties and their predictability are more relevant to the evaluation of elastic responses to construction and service loads, so f_c and E_c results are discussed in Chapter 5.

Transformed-section release properties for determination of f_{cgp} according to Equation 4-8 are shown in Appendix G of Keske (2014). The bending moments applied to determine the elastic responses for post-deck-addition time-dependent analysis, as well as the concrete ages corresponding to these loadings, are also included in the referenced appendix. While calculations of elastic responses to the transfer mechanism and the addition of the deck were necessary for this analysis of time-dependent behavior, further discussions of these elastic responses and their predictability relative to measured results are presented in Chapter 5.

4.4.1 Coefficient of Thermal Expansion

Results from CTE testing are presented below in Table 4.2. In the table, “Dry” and “Saturated” measurements reflect the two methods of measurement discussed in Section 4.3.7—using the apparatus usually used to measure unrestrained drying shrinkage (from ASTM C157) and tested

in accordance with AASHTO T 336, respectively. The calculated values were determined by proportional weighting of constituents using Equation 4-3.

Table 4.2: Comparison of coefficients of thermal expansion

Concrete	CTE (με/°F)				
	Measured		Calculated (Eq. 4-3)	Comparison	
	Dry	Saturated		*Dry/Calc.*	*Sat./Calc.*
SCC Girder	7.4	5.2	6.4	*1.15*	*0.81*
VC Girder	6.8	5.1	6.1	*1.12*	*0.83*
SCC/VC Girder	*1.08*	*1.03*	*1.05*	-	-
Deck	5.3	4.2	6.1	*0.87*	*0.70*
Girder Avg./Deck	*1.35*	*1.22*	*1.04*	-	-

The CTE of concrete can be as much as 30% greater at a relative humidity of approximately 50–70% than at 100% saturation (see Section 4.2.2), so the relatively higher dry-tested CTE results are expected. The humidity was not well controlled in the environmental chamber used for dry testing though, so dry-tested results should be considered mainly as an upper bound. Because AASHTO T 336 involves the testing of completely saturated concrete, the results determined from saturated testing should be considered as a lower bound of the ambient-humidity thermal behavior of the in-place girder concrete. The CTE of concrete is generally considered to be lowest at 100% relative humidity (Neville 1996). Meanwhile, estimates of the CTE values expected at ambient conditions were needed during this research to accurately account for thermal effects that occurred in the girders. The estimated, "apparent CTE" values selected to account for in-place thermal effects in the girders are discussed in Section 4.4.2.

The calculated results in the table were based on the mixture proportions described by Keske et al. (2015) and Table 4.1 and constituent-CTE values described by Sakyi-Bekoe (2008) and others (FHWA 2011; Mindess et al. 2003). The CTE values of constituent materials were as follows: 10.0 με/°F for hardened cement paste, 6.8 με/°F for siliceous natural-sand fine aggregate, and 3.3 με/°F for dolomitic limestone coarse aggregate. Because references to the effect of SCMs on paste CTE are limited and conclusions were mixed, only total cementitious content was considered in these calculated values. Also, calculations were volumetrically weighted while using measured air contents—4.0%, 3.7%, and 3.3% for SCC-girder, VC-girder, and VC-deck mixtures, respectively, per the referenced tables of proportions.

Two main trends are apparent in Table 4.2: 1) SCC appeared to exhibit a marginally higher CTE than its companion VC mixture (approximately 5%), and 2) the concrete used to construct the precast, prestressed girders for this project exhibited distinctly higher CTEs than the mixture used in the cast-in-place deck. The former trend is expected in response to the

differences in mixture proportioning recurrently discussed in this report; it was discussed previously in the report prepared by Keske et al. (2015).

The difference between the girder concrete and deck concrete was not as expectable based on the existing literature. All three mixtures utilized very similar coarse and fine aggregates, and the VC mixtures utilized very similar total aggregate fractions (67% and 68% for the girder and deck mixtures, respectively). As shown by the calculated results, this should have led the mixtures (especially VC mixtures) to exhibit comparable CTEs.

It was not possible to isolate the cause of the differences between the girder- and deck-concrete CTE values or between measured values and those recommended previously by Sakyi-Bekoe (2008) for Alabama concrete (5.5 με/°F at 100% saturation). Three causes are strongly suspected: SCMs, *w/cm*, and the inherent variability of aggregate mineralogy, even within the same general aggregate source. The previous AUHRC research did not include concrete of either this SCM replacement or *w/cm*. Furthermore, the girder and deck mixtures tested during this project, as well as those tested by Sakyi-Bekoe, could have exhibited different aggregate mineralogy. Because the main differences between the deck and girder mixtures (especially the VC mixtures) were SCM type (slag cement versus fly ash), SCM replacement rate, *w/cm* (0.29 versus 0.40), and mineralogy (within the same general aggregate type), one or more of these variables likely contributed to the differences.

Considering these results and the literature previously reviewed, it appears that the concrete used in the deck exhibited a reduced CTE, while the concretes used in the girders exhibited reasonably predictable CTEs. Furthermore, considering the range of the measured and recommended CTEs presented in this section, the CTE of the SCC-girder mixture is considered acceptably similar to that of the companion VC-girder mixture.

4.4.2 Measured Time-Dependent Responses

The primary time-dependent full-scale girder properties assessed in this report are the associated properties of internal concrete strain and effective prestress, f_{pe}. As previously discussed, changes in concrete strain since immediately prior to transfer are directly measured using VWSGs cast into the concrete at the *cgp*, and these strains are converted to effective prestress according to Equation 4-4. However, thermal effects also cause an apparent strain change, but such apparent changes do not necessarily correspond to a change in effective prestress because the steel and concrete both deform in response to changes in temperature. Therefore, to effectively compare measured strains, it is necessary to isolate transient thermal effects due to ambient conditions from long-term time-dependent changes due to creep and shrinkage.

In addition to isolating these effects, time-dependent transient thermal effects were considered to better understand the changes in girder behavior corresponding to diurnal and

seasonal thermal strain variation. To that effect, measured thermal strains were evaluated, and adjustments to account for them were applied to the measured $\Delta\varepsilon_{cgp}$ results prior to the evaluation of creep and shrinkage behavior. These thermal-effect considerations are discussed in Sections 4.4.2.1–4.4.2.3. Temperature-adjusted measured long-term responses are then discussed in Section 4.4.2.4

Camber is also affected by time-dependent concrete material properties and transient thermal effects, but its evaluation became difficult during erection, and its significance to long-term performance was less clear once composite action was achieved between the girders and deck. Meaningful conclusions concerning time-dependent changes in pre-erection camber were reported by Keske et al. (2015), those concerning long-term camber were reported by Neal (2015), and changes in camber in response to construction loads are discussed in Chapter 5.

In the subsequent analyses of Section 6.4, the results from only a few girders are presented. This was necessary because several gauges failed during the bridge construction process. Therefore, the analyses instead focus on a few robustly instrumented girders per span. This was deemed acceptable considering that all of the girders are mechanically locked together via diaphragms and a deck. The behavior measured in even a few girders should be representative of the entire span. Also, only interior girders are assessed because the exterior girders (girder lines 1 and 7) are differently restrained, potentially affected more greatly by the cast-in-place barrier, and are exposed to more variable thermal exposure. While the difference in exterior-girder behavior may be important, evaluation of it was beyond the scope of this work.

4.4.2.1 Significance of Thermal Effects

Measured changes in concrete strain due to transient thermal effects (corrected for gauge temperature but not concrete temperature) are illustrated in Figure 4.13, in which concrete strains noticeably fluctuate daily and seasonally. Also, using the simplified cross-sectional representations shown in Figure 4.8 and Figure 4.9 and the method summarized in Section 4.3.4.2, changes in girder strain due to transient thermal effects were isolated from those due to gradually changing creep and shrinkage deformations in the concrete material. This process, the effect of which can be evaluated by comparing “Measured Strain” and “Corrected Strain” results in the figure, is discussed in the next section.

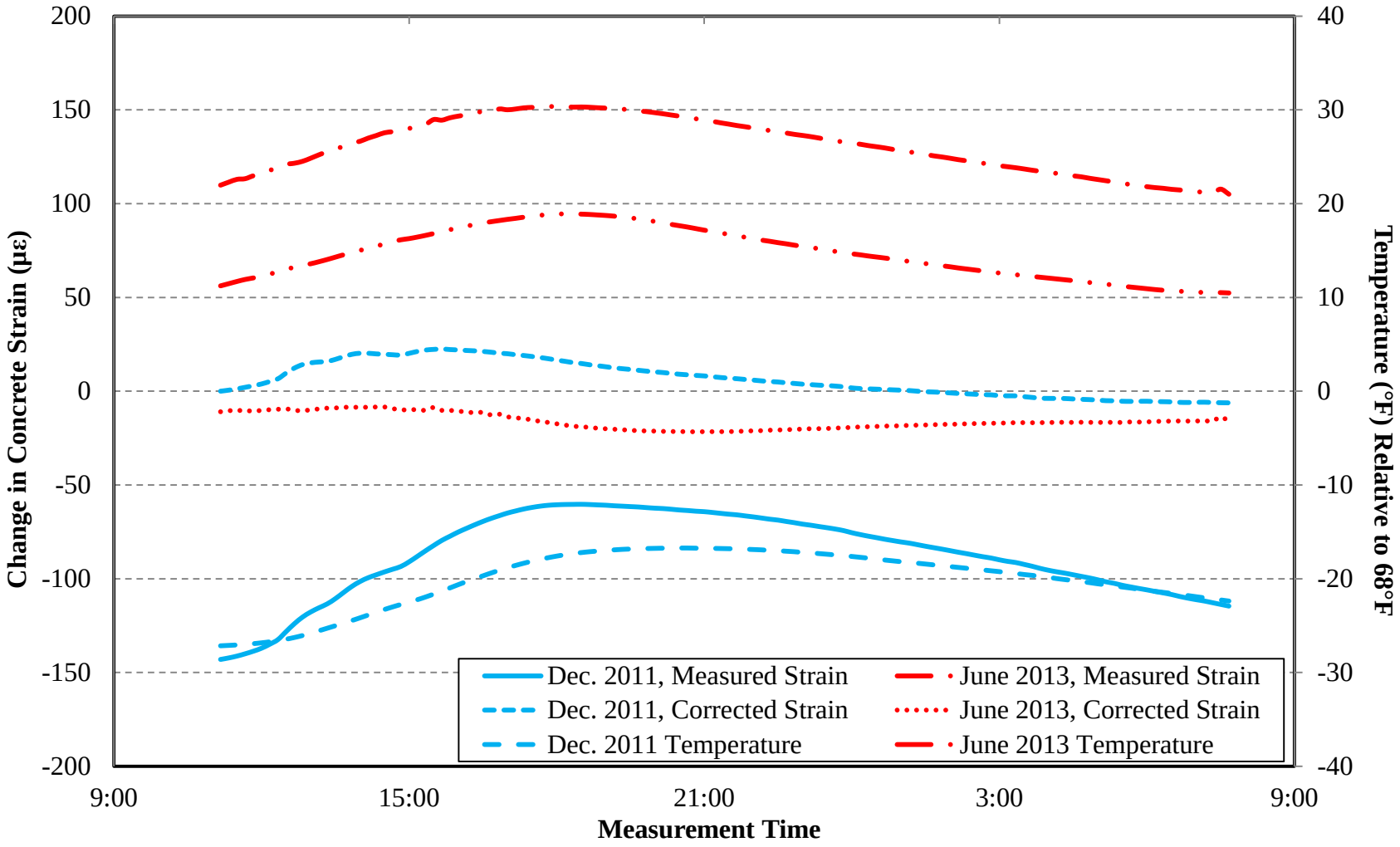

Figure 4.13: Concrete strains and temperatures at the center of gravity of prestress

From Figure 4.13, the temperature of the concrete has a distinct effect on the measured concrete strain. Measured concrete strains (corrected for gauge temperature but not for concrete temperature) changed by an average of 250 με between consecutive summers and winters. More specifically, measured concrete strains at the *cgp* varied seasonally by up to approximately

- 270 με in SCC BT-54s,
- 250 με in SCC BT-72s,
- 240 με in VC BT-54s, and
- 230 με in VC BT-72s.

While smaller in magnitude, diurnal strain changes also approached 100 με. While attempts were made to account for these variations prior to evaluation of time-dependent behavior, the magnitude of these diurnal and seasonal changes is noteworthy. Based on the relationship described by Equation 4-4, these measured concrete strain changes would equate to diurnal and seasonal changes in effective prestress of approximately 3.0 and 7.5 ksi. Since both the concrete and encapsulated steel can experience stress-independent deformations due to thermal effects, these apparent strain changes do not necessarily correspond to a change in effective prestress. Therefore, it is crucial to account for thermal effects before comparing time-dependent results to each other and to those predicted by the *AASHTO LRFD* provisions.

Comparison of the seasonal thermal effects shown above also confirms the earlier conclusion that the SCC and VC-girder CTEs are acceptably similar. The marginally increased CTE of SCC only led to slightly greater seasonal changes (approximately 25 με or 10% of the total), which is likely insignificant in this application. While internal stresses could develop between the perfectly bonded girders and deck, evaluation of the discrepancy was beyond the scope of this project.

Recall, too, that these thermal effects are transient in this linear-elastic structure while relaxation and other time-dependent losses are not. While thermal effects could affect long-term creep slightly, the primary conclusions warranted from the data in this section are that 1) it is crucial to account for thermal effects before attempting to evaluate long-term time-dependent changes in girder behavior and 2) the tested SCC and VC girders exhibited comparable thermal behavior. The implications of the difference were minor in this research because the girders were not thermally restrained (except internally); further research may be necessary, though, regarding the implications of this behavior in structures restrained against thermal movement (like continuous-span bridges).

4.4.2.2 Assessment of Thermal Correction Methodology

Ideally, the "Corrected" strains in Figure 4.13 would not vary at all diurnally. The slight gradients shown are acceptable when considering the errors relative to the actual differences in measured strain. From measured diurnal changes of up to approximately 100 με, the *maximum* diurnal difference in the corrected values shown in Figure 4.13 was 22 με. Not only is this difference distinctly smaller than in the measured results, but it is of similar magnitude to the difference observed between readings obtained approximately 1.5 years apart. Other sources of the slight errors have been discussed previously in Section 4.3.4:

- The idealized thermal gradient shown in Figure 4.10 may only coarsely model the actual thermal gradient present, as the actual gradient could be very complex and dependent upon the sunlight, precipitation, wind, or other environmental conditions present,
- Differences between the temperature at the external girder surface and that measured at the *cgp* would vary depending upon the same environmental conditions,
- Changes in relative humidity due to moisture fluctuation would affect the CTE of the concrete material (as discussed previously in Section 4.4.1), and
- The simplified cross-sectional properties are only an approximation of the actual girder dimensions.

In light of all of these potential sources of errors, it is concluded that the method presented here to account for thermal gradients is efficient; significant deviations in apparent strain were greatly reduced prior to evaluation of long-term time-dependent effects. Errors were also minimized during this work by regularly utilizing readings obtained at around dawn. At this time of day, the temperature gradient across the girder is usually the most constant, meaning that the entire cross section should be close to the same temperature. This is confirmed by viewing Figure 4.13—corrected values appeared to be changing the least from approximately 3:00–6:00 AM each day.

4.4.2.3 Determination of Apparent CTE for Isolation of Thermal Effects

As mentioned previously in Section 4.3.4.2, Johnson (2012) applied an assumed CTE of 6.0 με/°F in all corrections to account for internal temperatures and thermal gradients during the assessment of pre-erection behavior. As the girders aged and should have exhibited more gradual time-dependent changes in camber and effective prestress (after Johnson's work was completed), the inaccuracy of this assumed value became more apparent. Errors became especially apparent in trial attempts to account for thermal effects in the composite bridge, which provided the impetus for the CTE testing described in Section 4.4.1.

The appropriate *apparent* CTE values to implement in the thermal-adjustment calculations were chosen by evaluating the apparent change in f_{pe} and concrete strain of the temperature-corrected results, both in the non-composite girders and composite bridge section. Accurately corrected results should fluctuate the least in response to diurnal and seasonal thermal variation. This analysis, which is summarized in Appendix H of the dissertation prepared by Keske (2014), indicated that girder-CTE values of approximately 6.1–6.9 με/°F would be acceptable, with consistent improvement by differentiating between SCC and VC-girder values by approximately 0.5 με/°F. While this difference does not precisely match the difference in measured SCC and VC-girder CTEs shown in Table 4.2 (approximately 0.3 με/°F), it was acceptable considering the precision of these corrections and the potential sources of errors discussed in the previous subsection.

An apparent deck-concrete CTE of 5.6 με/°F was chosen for use during this apparent-CTE optimization because it was found to best minimize the diurnal and seasonal variation in deck strain. While this value is slightly greater than the upper-bound "dry-tested" deck CTE shown in Table 4.2 (5.3 με/°F), it was still less than the value calculated using Equation 4-3 that is shown in the table (6.1 με/°F). The upper-bound testing described in Section 4.4.1 could have also exhibited some variability because the humidity was not well controlled in the environmental chamber used for that testing. Use of a deck-concrete CTE of 5.6 με/°F was acceptable in consideration of both this variability and the previously mentioned potential sources of correction errors.

The appropriateness of the selected apparent CTE values was also confirmed graphically. An example of the effect of apparent CTE on the accuracy of the temperature correction procedure is presented in Figure 4.14, which was developed using the same measured SCC BT-72 results shown earlier in Figure 4.13. Figure 4.13 was developed using the apparent CTEs chosen for the SCC girders and VC deck (6.9 and 5.6 με/°F, respectively); comparison to the alternative girder-CTE values in Figure 4.14 reveals that selection of an appropriate apparent CTE increases the accuracy of the discussed thermal-gradient correction method.

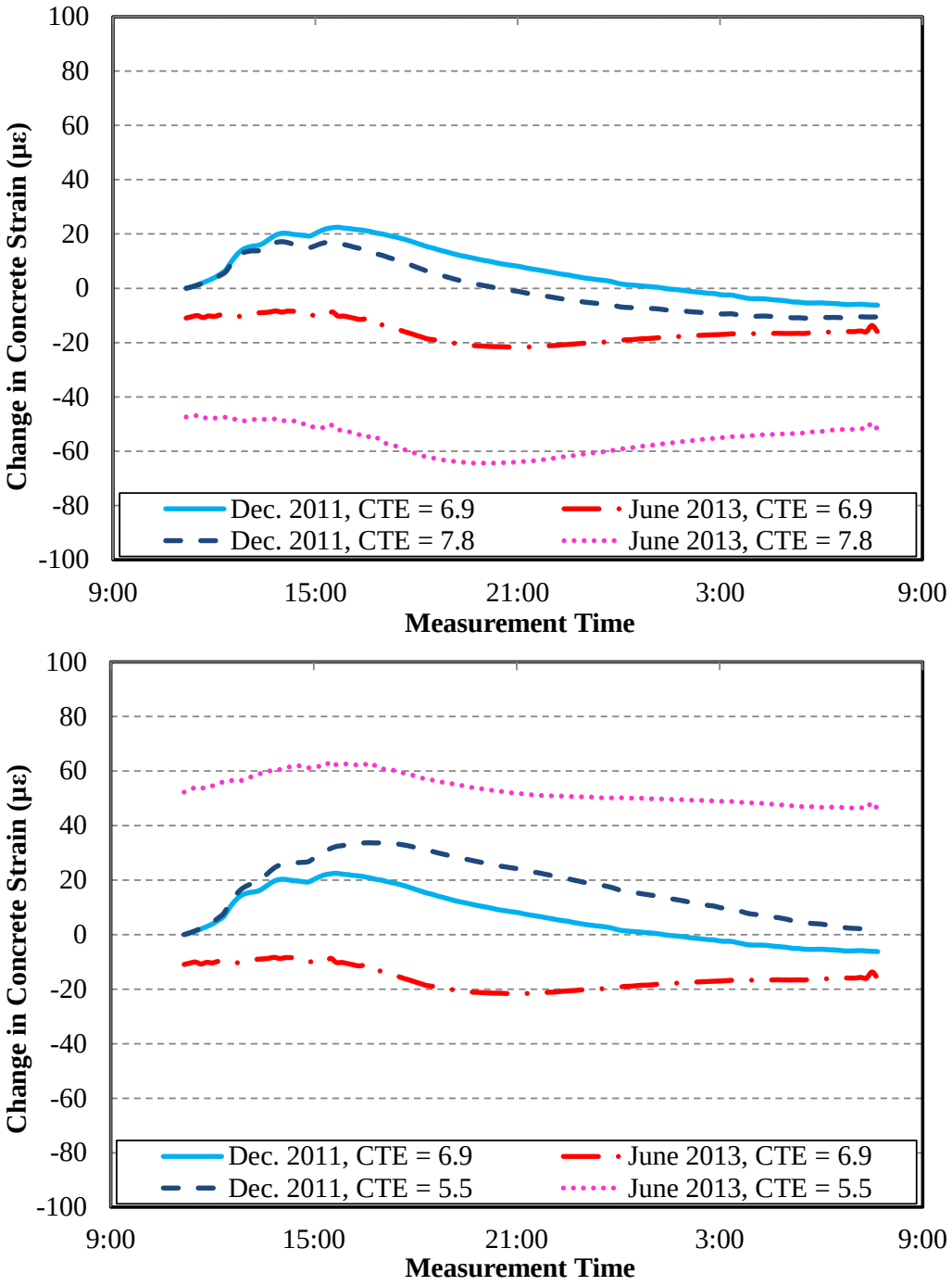

Figure 4.14: Comparison of SCC strains corrected for different apparent CTE values

Regardless of the selected CTE, differences were less severe than in the measured results—maximum diurnal variation equaled approximately one-third of the uncorrected variation (35 με in corrected results versus approximately 100 με in uncorrected results), indicating that the method is beneficial. Furthermore, the effect of CTE selection on the perceived amount of long-term time-dependent deformation is important. As the applied value varied from the chosen

apparent CTE of 6.9 με/°F, a greater portion of the measured change *between seasons* is mistakenly attributed to time-dependent effects.

In the bottom half of Figure 4.14, the CTE value recommended by Sayki-Bekoe (5.5 με/°F) is shown to be inappropriate, as its use would lead to the false conclusion that the change in concrete strain was *positive* between December, 2011 and June, 2013. By contrast, the use of a larger apparent CTE would indicate a greater amount of prestress loss during this timeframe. Measurements were obtained during multiple summers and winters, which confirmed that this was inappropriate—the same CTE values that indicated greater losses from winter to summer indicated greater gains from summer to the next winter. Thus, the appropriate apparent CTEs for use during analyses of long-term time-dependent behavior were confirmed to equal 6.9, 6.4, and 5.6 με/°F for the SCC girders, VC girders, and VC deck, respectively.

4.4.2.4 Measured Long-Term Time-Dependent Responses

After correcting for thermal effects as discussed in the previous section, measured concrete strains were converted to values of effective prestress, f_{pe}, by Equation 4-4. Total measured prestress losses were determined by subtracting f_{pe} from f_{pbt}. Measured total losses from the assessed girders are presented graphically in Figure 4.15 and Figure 4.16. To confirm the acceptability of the analysis of this limited number of girders, consider the limited variability between the presented results.

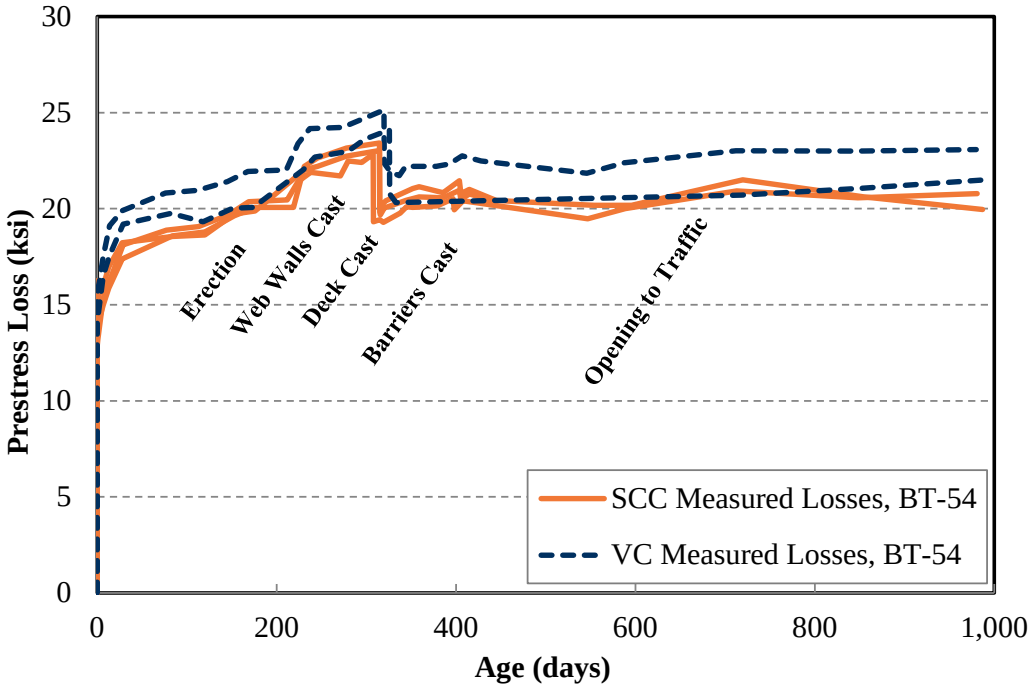

Figure 4.15: Total measured prestress losses in BT-54s

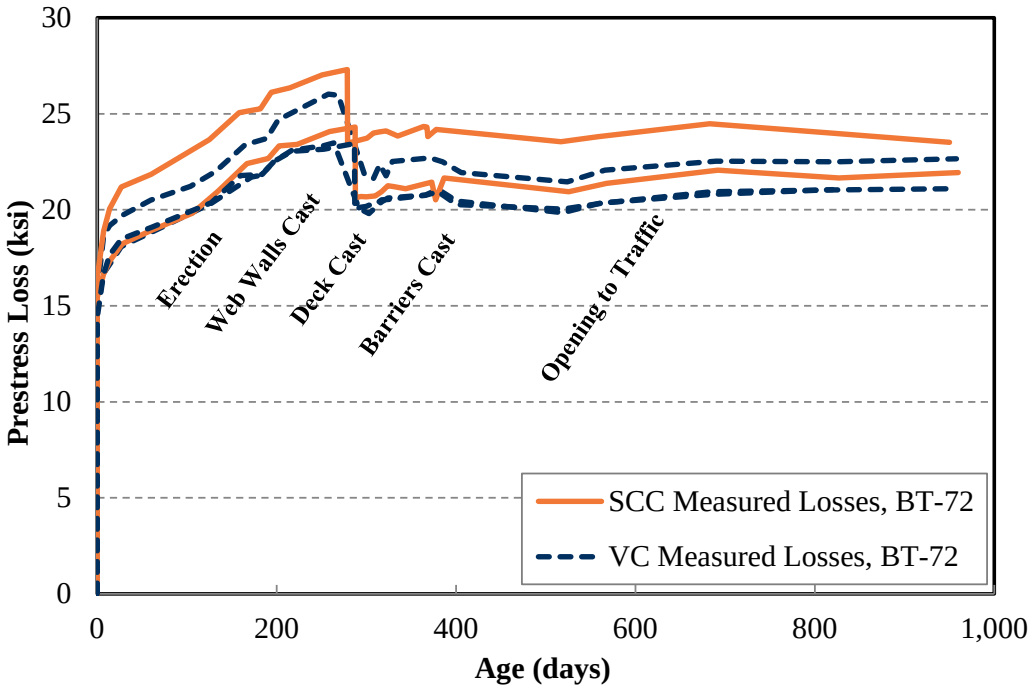

Figure 4.16: Total measured prestress losses in BT-72s

Several conclusions are warranted from the above figures, first among which is that the SCC girders appear to have accumulated essentially the same total measured prestress losses of approximately 22 ksi, or 11% of f_{pbt}, within the first 1,000 days. They also appear to have accumulated those losses in exactly the same manner over time. Additional conclusions regarding the response to construction loads are given in Chapter 5, including an assessment of the sudden decrease in prestress losses at approximately 300 days that resulted from the addition of the deck.

To further confirm the time-dependent results presented in Figure 4.15 and Figure 4.16, total prestress losses are also tabulated below in Table 4.3. Losses were evaluated at two critical ages: at the time of deck addition and at the latest age monitored.

Table 4.3: Total measured time-dependent prestress losses

Girder	Losses at Deck Add.		Losses at 1,000 Days		*SCC/VC*	
	(ksi)	(%f_{pbt})	(ksi)	(%f_{pbt})	*At Deck*	*At 1,000d*
54-4S	22.9	11.4%	20.8	10.4%		
54-5S	23.0	11.5%	-	-		
54-6S	23.4	11.7%	20.0	10.0%		
54-S Average	*23.1*	*11.5%*	*20.4*	*10.2%*	*0.94*	*0.93*
54-4V	25.1	12.5%	23.1	11.5%		
54-6V	24.1	12.0%	20.7	10.3%		
54-V Average	*24.6*	*12.3%*	*21.9*	*10.9%*		
72-4S	24.3	12.1%	21.9	11.0%		
72-6S	27.3	13.6%	23.5	11.7%		
72-S Average	*25.8*	*12.9%*	*22.7*	*11.3%*		
72-2V	26.0	13.0%	22.7	11.3%	*1.06*	*1.04*
72-3V	23.5	11.7%	-	-		
72-4V	23.4	11.7%	21.1	10.5%		
72-V Average	*24.3*	*12.1%*	*21.9*	*10.9%*		

Note: - = not tested due to gauge failure

The results shown above confirm the graphical results—SCC girders have experienced essentially no different time-dependent behavior during the first 1,000 days after they were cast. While these total losses include elastic losses and gains that are reviewed later, these results suggest that the SCC girders are behaving very similarly to their companion VC girders over time. The most important practical consideration may be the difference between SCC and VC losses as a percent of f_{pbt}: total differences at 1,000 days would equate to less than 1% of f_{pbt}, indicating

that the SCC and vibrated concrete are identical to within the precision of the application of this data.

Interestingly, this contradicts the findings presented in Chapter 3, in which SCC cylinders were found to exhibit approximately 15% greater compliance and up to 30% greater shrinkage than the companion VC cylinders at all concrete ages up to 1,000 days. While further conclusions are drawn by comparing these results to those predicted by the *AASHTO LRFD* provisions, these results alone are sufficient to conclude that the full-scale time-dependent behavior of these SCC girders is acceptably similar to that of the companion VC girders.

4.4.3 Comparisons of Measured Responses to Predicted Responses

While it was instructive to compare the measured responses of the SCC and VC girders because they have been placed in matching spans of an in-service bridge, it is equally or more important to evaluate the predictability of the measured girder responses after accounting for their unique material properties. In the following sections, measured responses are compared to those predicted using the simplified and refined *AASHTO LRFD* prediction methods, as well as to the refined *LRFD* prediction method once including the previously proposed modifications to account for local Alabama materials and methods (A_{AL}).

To make equitable comparisons of measured and predicted results, the way in which measured data are collected must be considered: as previously discussed in Section 4.3.3.2, only changes in concrete strain are measured by embedded VWSGs, and these strains are converted to prestress losses or effective prestress according to Equation 4-4. Therefore, *strain-independent* prestress losses due to stress relaxation occurred in the girders but were not measured. It was appropriate to *subtract* the predicted relaxation losses after release (Δf_{pR}) to account for this—in all comparisons, measured results are compared to *LRFD*-predicted results minus predicted relaxation losses (Δf_{pR}, Δf_{pR1}, or Δf_{pR2}, where applicable). Note that this does not affect the choice of f_{pbt}: pre-release relaxation losses are measurable in the prestressing bed prior to concrete placement (Boehm et al. 2010), and their inclusion is necessary to accurately assess elastic and time-dependent responses (Stallings et al. 2003).

4.4.3.1 Comparisons to *AASHTO LRFD* Simplified Prediction

The simplified approximate estimate of time-dependent losses described in the *AASHTO LRFD* (2013) provisions (Section 5.9.5.3) and in Section 4.3.6.2 of this report yields a lump-sum prediction of total long-term losses. As previously discussed, total predicted losses are determined by summing the predicted time-dependent losses due to creep, shrinkage, and relaxation and the elastic losses and gains due to transfer and superimposed weights. To make

equitable comparisons of measured and predicted results, measured and predicted results are presented in Table 4.4 and in Figure 4.17 after subtracting the predicted relaxation losses from the predicted total losses. In both the figure and table, losses at approximately 1,000 days (the last age at which strains were measured) are presented because they are the closest estimate of long-term behavior.

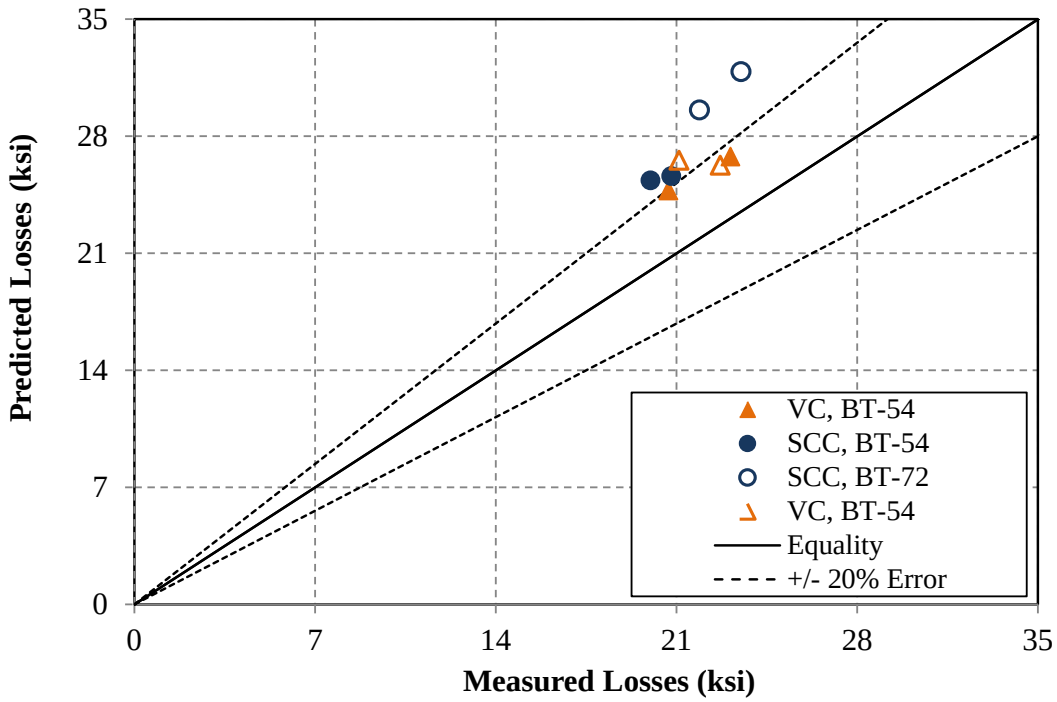

Figure 4.17: Comparison of measured and simplified predicted prestress losses

Table 4.4: Comparison of measured and simplified-LRFD predicted prestress losses

Girder	Measured Total (ksi)	Calculated Elastic (ksi)	Time-Dependent (ksi)	Total Predicted (ksi)	Measured/ Predicted Total
54-4S	20.8	8.4	17.3	25.6	0.81
54-5S	-	8.6	16.8	25.3	-
54-6S	20.0	8.6	16.8	25.4	0.79
54-S Average	*20.4*	*8.7*	*17.0*	*25.4*	*0.80*
54-4V	23.1	8.2	18.6	26.8	0.86
54-6V	20.7	7.7	17.1	24.7	0.84
54-V Average	*21.9*	*8.1*	*17.9*	*25.8*	*0.85*
72-4S	21.9	9.1	20.5	29.6	0.74
72-6S	23.5	9.2	22.6	31.9	0.74
72-S Average	*22.7*	*9.4*	*21.7*	*30.7*	*0.74*
72-2V	22.7	7.4	18.8	26.3	0.86
72-3V	-	8.0	18.5	26.5	-
72-4V	21.1	8.1	18.5	26.5	0.79
72-V Average	*21.9*	*8.0*	*18.7*	*26.4*	*0.83*

Note: - = not tested due to gauge failure

As shown in the figure and table, the simplified total-loss predictions were conservative, typically providing estimated losses that were approximately 20% larger in magnitude than the comparable measured losses. In terms of the difference in effective prestress, the average over-prediction of measured losses by approximately 5.4 ksi is reasonable, representing less than 3% of f_{pbt}. Consequently, the simplified provisions appear to be reasonably accurate for the prediction of long-term time-dependent losses, at least when using measured material properties

Also, the data presented in Figure 4.17 appear to indicate that SCC total losses were slightly more over-predicted, especially among SCC BT-72s—the average over-prediction equaled 8.0 ksi in SCC BT-72s, versus 4.5 ksi in VC BT-72s. This is likely because the only concrete material property incorporated in the simplified predictions is f_{ci}, and f_{ci} was found to be significantly affected by age at release in these girders (strengths varied up to 2,000 psi at release ages that varied by up to seven hours). Girders 72-4S and 6S were released at 20 and 18 hours, respectively, while 72-2V, 3V, and 4V were released at 23, 23, and 20 hours, respectively; while the measured results did not appear to be affected by this age variation, the simplified predictions were somewhat affected by it.

Without further evaluation of the accuracy of the elastic-deformation calculations shown in the table (which is included in Chapter 5), it is difficult to conclude whether the conservatism of

the simplified predictions stem more from these elastic-deformation calculations or from over-prediction of the time-dependent deformations. Evaluation of the refined *AASHTO LRFD* predictions may illuminate differences in the entire time-dependent behavior instead of only the ultimate time-dependent deformation value, which should be of value. Regardless, the data presented in this section confirm that the approximate estimate of time-dependent losses calculated using Section 5.9.5.3 of the *AASHTO LRFD* (2013) provisions provides a reasonable, conservative estimate of full-scale long-term behavior, at least when using measured material and exposure properties.

4.4.3.2 Comparisons to Existing *AASHTO LRFD* Refined Predictions

It was acceptable to present results in terms of prestress losses in the previous sections because these comparisons consisted of measured results or predicted lump-sum results. Per the discussion of Section 4.3.6.5, the *AASHTO LRFD* Section 5.9.5.4 refined estimates of time-dependent losses were used to evaluate the time-dependent behavior of the girders at all intermediate times. Thus, in this comparison, it was acceptable to present results in terms of effective prestress to better illustrate the magnitude of the difference between measured and predicted results.

The conversion of measured results to values of effective prestress was conducted per Equation 4-4; for comparison, predicted relaxation losses were subtracted from the refined-*LRFD* predictions before comparison (but after inclusion in the necessary prediction equations, such as Equation 4-19). These comparisons are made graphically in Figure 4.18 and Figure 4.19 for SCC and VC girders, respectively.

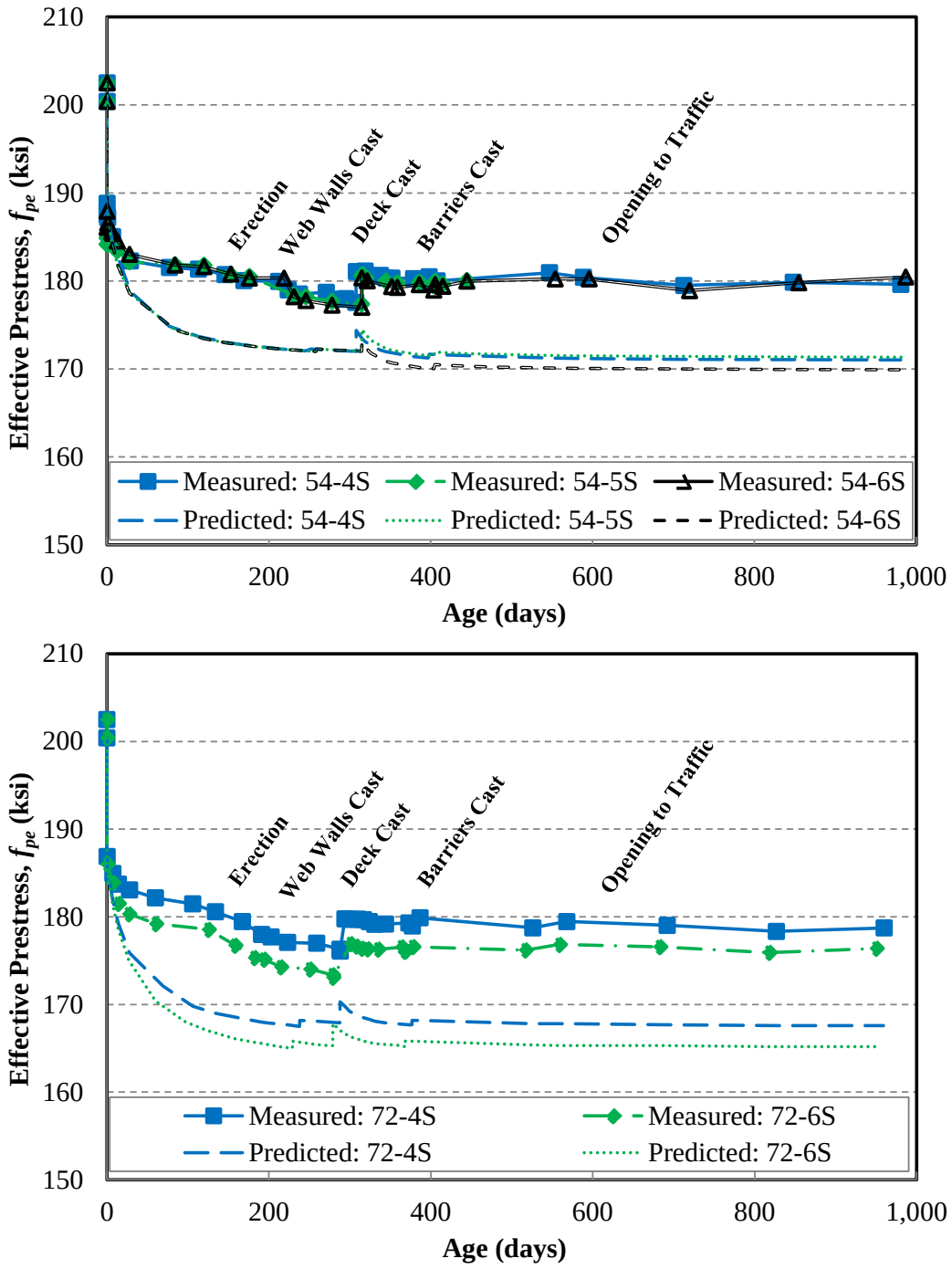

Figure 4.18: Comparison of measured and predicted effective prestress in SCC girders

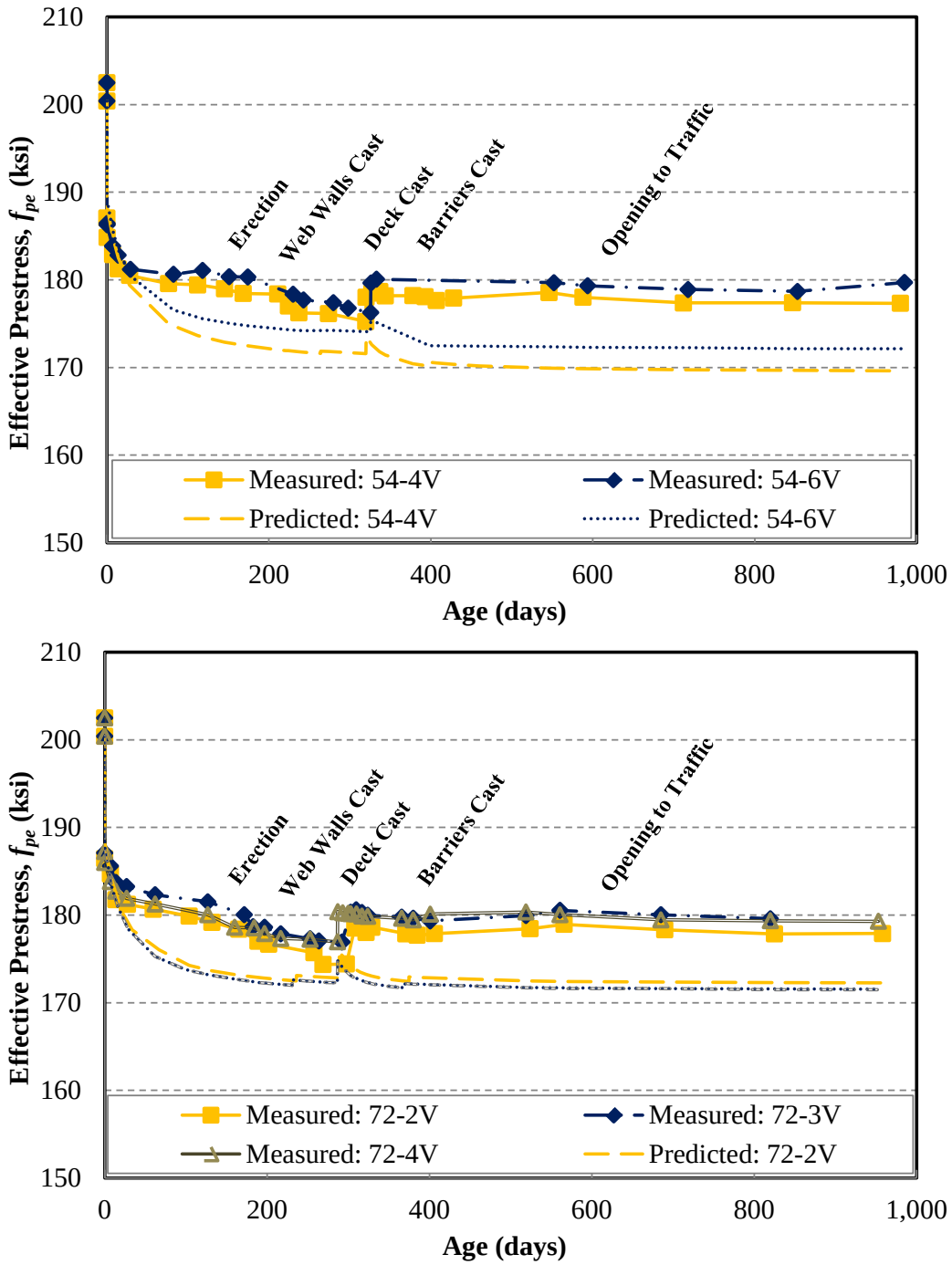

Figure 4.19: Comparison of measured and predicted effective prestress in VC girders

In the above figures, the SCC and VC girders appear to be behaving very similarly (maintaining approximately 179 ksi or 89% of f_{pbt} through 1,000 days), and the refined *LRFD* models appear only slightly less accurate for SCC performance than for VC performance. This observation was confirmed analytically, and pertinent results are summarized below in Table 4.5.

Table 4.5: Comparison of measured and refined-*LRFD* predicted effective prestress

Girder	At Deck Addition			At 1,000 Days		
	Predicted f_{pe} (ksi)	Measured f_{pe} (ksi)	Meas./ Predicted	Predicted f_{pe} (ksi)	Measured f_{pe} (ksi)	Meas./ Predicted
54-4S	172.0	177.5	1.03	171.0	179.6	1.05
54-5S	172.0	177.4	1.03	-	-	-
54-6S	172.0	177.0	1.03	169.9	180.4	1.06
54-S Average	*172.0*	*177.3*	*1.03*	*170.4*	*180.0*	*1.06*
54-4V	171.6	175.3	1.02	169.6	177.3	1.05
54-6V	174.1	176.3	1.01	172.1	179.7	1.04
54-V Average	*172.8*	*175.8*	*1.02*	*170.9*	*178.5*	*1.04*
72-4S	167.9	176.1	1.05	167.6	178.5	1.06
72-6S	165.3	173.1	1.05	165.2	176.9	1.07
72-S Average	*166.6*	*174.6*	*1.05*	*166.4*	*177.7*	*1.07*
72-2V	172.8	174.4	1.01	172.3	177.7	1.03
72-3V	172.3	176.9	1.03	-	-	-
72-4V	172.3	177.0	1.03	171.5	179.3	1.05
72-V Average	*172.5*	*176.1*	*1.02*	*171.9*	*178.5*	*1.04*

*Note: **-** = not tested due to gauge failure*

As shown in the table, all girders maintained greater effective prestress than predicted by the refined *AASHTO LRFD* (2013) model prior to deck addition and during the approximately 650 days after. The SCC girders appeared to maintain slightly greater prestress relative to that predicted, but all measured results were within 7% of predictions (approximately 11 ksi, or 5% of f_{pbt}). This suggests that the predictability of the SCC-girder behavior is acceptably similar to that of vibrated concrete and confirms that the behavior of girders constructed with either material is conservatively predictable according to the existing refined provisions of *AASHTO LRFD* (2013) Section 5.9.5.4.

While these measured and predicted results include instantaneous changes in prestress that are discussed later, the girders appear to be behaving conservatively because measured results more greatly exceed the prestress values predicted at approximately 1,000 days than immediately after the time of deck addition approximately 650 days earlier. Considering that effective prestress has plateaued in both measured results and predicted results, future time-dependent changes are expected to be minimal.

4.4.3.3 Comparisons of Measured Results to Refined Predictions Using A_{AL}

Recall from Chapter 3 that the total deformation of SCC and VC cylinders was reasonably predictable using the existing provisions, but only as a coincidence of the particular testing conditions—creep was under-predicted by the models while shrinkage was over-predicted. The adjustment factors for concrete produced using typical Alabama materials and proportions only moderately improved the total-deformation predictions but distinctly improved the individual time-dependent behaviors during that analysis. Thus, application of those A_{AL} factors to the refined *AASHTO LRFD* provisions for full-scale behavior could provide similar improvements.

To evaluate the recommendations of Chapter 3, the factors that were determined based on these utilized mixtures were directly implemented in the following previously described equations concerning the refined *AASHTO LRFD* predictions:

- Equation 4-12 regarding the shrinkage of the girder concrete prior to deck addition (ε_{bid}),
- Equation 4-13 regarding the interaction between shrinkage and creep prior to deck addition (K_{id}),
- Equation 4-14 regarding the creep of the girder concrete from the time of prestress release until the time of deck addition [$\psi_b(t_d,t_i)$],
- Equation 4-16 regarding the shrinkage of the girder concrete from the time of the deck addition onward (ε_{bdf}),
- Equation 4-17 regarding the interaction between shrinkage and creep after the deck addition (K_{df}), and
- Equations 4-18 and 4-20 regarding the additional creep of the girder concrete due to the deck addition [$\psi_b(t_f,t_d)$].

Recall that, in all of these applications, the A_{AL} factors were directly multiplied by the existing predictions of the creep coefficient (using A_{AL} equal to 1.2 in SCC and 1.1 in VC) and shrinkage strain (using A_{AL} equal to 0.8 in VC). Meanwhile, the shrinkage of the deck concrete was modeled using the existing provisions, as application of the A_{AL} factors was not justified. Pertinent comparisons of the existing and revised predictions to the measured results are summarized below in Table 4.6. To increase readability, only average values from the existing predictions are reproduced in the table.

Table 4.6: Comparison of measured and predicted effective prestress

Girder	At Deck Casting			At 1,000 Days		
	f_{pe} Predicted with A_{AL} (ksi)	Meas./ Predicted with A_{AL}	Meas./ Existing Prediction	f_{pe} Predicted with A_{AL} (ksi)	Meas./ Predict. with A_{AL}	Meas./ Existing Prediction
54-4S	170.2	1.04		169.5	1.05	
54-5S	170.2	1.04		-	-	
54-6S	170.2	1.04		169.8	1.06	
54-S Average	*170.2*	*1.04*	*1.03*	*169.7*	*1.06*	*1.05*
54-4V	174.5	1.01		171.5	1.05	
54-6V	171.9	1.02		174.0	1.04	
54-V Average	*173.2*	*1.01*	*1.02*	*172.7*	*1.04*	*1.04*
72-4S	165.7	1.06		165.9	1.06	
72-6S	162.9	1.06		163.3	1.07	
72-S Average	*164.3*	*1.06*	*1.05*	*164.6*	*1.07*	*1.07*
72-2V	173.1	1.01		174.0	1.03	
72-3V	172.5	1.03		-	-	
72-4V	172.5	1.03		173.1	1.05	
72-V Average	*172.7*	*1.02*	*1.02*	*173.5*	*1.04*	*1.04*

Note: - = not tested due to gauge failure

As shown in the table, the use of modifications calibrated with representative cylinders had minor but opposing effects on SCC and VC predictability. SCC performance was slightly more under-predicted by the adjusted models, while VC performance was slightly better predicted. After applying the A_{AL} factors, measured effective prestress in SCC girders was under-predicted by up to approximately 13 ksi, or 6.5% of f_{pbt}; VC effective prestress was conservatively and accurately predicted to within approximately 5 ksi, or 2.5% of f_{pbt}.

That the magnitude of the adjustment factors exceeded their effect suggests two possibilities: that the existing prediction models may have been accurate coincidentally because of the offsetting errors in creep and shrinkage or that the prediction models are insensitive to these parameters. In either case, application of the A_{AL} factors was acceptable, especially when considering VC girders.

Meanwhile, the inclusion of these adjustments to account for measured time-dependent cylinder behavior slightly reduced the accuracy of the already conservatively predicted SCC girder behavior. This suggests two possibilities: that the testing of representative samples may not well represent full-scale SCC performance or that full-scale SCC behavior is differently (more conservatively) affected by full-scale structural phenomena or ambient conditions. Both are

plausible and would lead to more conservative prediction of SCC behavior, but neither possibility could be directly assessed in this research.

4.4.4 Comparisons of Measured Responses to Design Predictions

In Section 4.4.2, measured full-scale SCC time-dependent responses were found to be reasonably similar to those measured in comparable VC girders. In Section 4.4.3, the behavior of SCC and VC girders was found to be conservatively predictable using either simplified or refined prediction models, at least when considering measured material properties. In previous AUHRC research, Stallings et al. (2003) and Johnson (2012) concluded that the use of design properties (such as f'_c) could lead to gross errors in the predictions, so a further analysis of this occurrence was warranted in this evaluation of full-scale behavior. In this way, differences in the measured SCC and VC responses, and differences in their predictability, are evaluated relative to the level of accuracy expectable in a typical design environment.

4.4.4.1 Comparisons to *AASHTO LRFD* Simplified Prediction

Only the specified f'_{ci} was necessary to calculate the lump-sum long-term prestress loss according to the simplified *LRFD* provisions discussed earlier. The same relative humidity (70%) was used in this prediction, and, as in all calculations of predicted/design and measured losses, relaxation losses were removed prior to comparison with measured results. Furthermore, f'_{ci} was used in conjunction with the most common estimate of E_c (equaling 57,000 $\sqrt{f'_c}$) to calculate the elastic portion of the prestress losses according to Equation 4-10. Total measured and predicted design losses are summarized in Table 4.7 below. In it, “Predicted” responses are the predictions that incorporated measured material properties, and “Design” responses are those based on design properties.

Table 4.7: Comparison of measured and simplified-*LRFD* design prestress losses

Type of Girder	Average Total Losses (ksi)			Ratios	
	Measured at 1,000 Days	Simplified-*LRFD*		Measured/ Predicted	Measured/Design
		Predicted	Design		
SCC BT-54	20.4	25.4	38.4	0.80	0.53
VC BT-54	21.9	25.8		0.85	0.57
SCC BT-72	22.7	30.7	37.5	0.74	0.61
VC BT-72	21.9	26.4		0.83	0.58

The results shown in the above table support the conclusion that the difference between measured long-term SCC-girder performance and measured VC-girder performance (less than 2 ksi of effective prestress) is insignificant relative to the difference between measured and assumed design responses (approximately 16–18 ksi). The difference in the *predictability* of measured responses (SCC-girder losses were approximately 3 ksi more over-predicted than were VC-girder losses using the simplified *LRFD* provisions) is also minor relative to the difference between design and measured responses.

This indicates that all measured full-scale prestress losses were equally and conservatively predictable relative to design, according to the simplified *AASHTO LRFD* provisions. It also confirms the conclusions of Stallings et al. (2003) and Keske et al. (2015): predictions can be highly conservative when using design properties in place of expected or measured properties. The difference between measured-property and design predictions, which ranged 7–13 ksi, represents up to approximately 6.5% of f_{pbt} and could be significant during design.

4.4.4.2 Comparisons to Existing *AASHTO LRFD* Refined Predictions

A number of assumptions were required to calculate the average refined estimates of design effective prestress. Like in the previous section, specified f'_{ci} was used, as was an assumed relative humidity of 70%; similarly, the specified $f'_{c,deck}$ (4,000 psi) was used, and all values of E_c were calculated using $57{,}000\sqrt{f'_c}$. Other assumed values were based on the average exposure conditions experienced by the girders such that differences between the design estimates and the measured-property predictions mainly illuminate differences between the *concrete material* properties. These assumed values included

- Average release times, t_i, of 0.99 days and 0.88 days for BT-54s and BT-72s, respectively,
- Average deck-addition times of 320 days and 280 for BT-54s and BT-72s, respectively, based on observed average times at deck addition,
- An average haunch thickness of 1.5 in. for all girders based on information presented in Appendix G of Keske (2014), and
- An average deck thickness of 7.0 in. for all girders based on the construction plans for this bridge.

As in Section 4.4.3.2, it is instructive to compare the predicted effective prestress graphically because the refined *AASHTO LRFD* estimates allow evaluation of the entire time-dependent maintenance of f_{pe}. Therefore, these comparisons are made in Figure 4.20 and Figure 4.21 for BT-54 and BT-72 girders, respectively. For clarity, only a few representative measured SCC and VC responses are presented; design responses are equally applicable to both, as they only vary by girder size (and not material) according to the *LRFD* provisions.

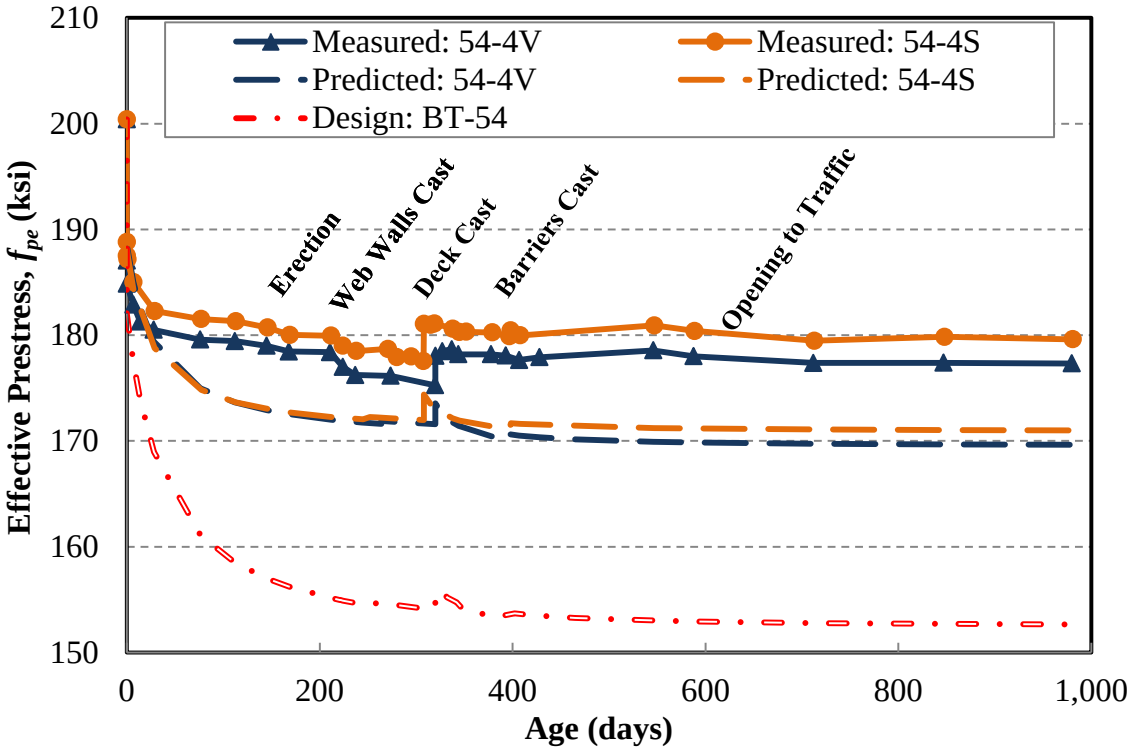

Figure 4.20: Comparison of measured and design effective prestress in BT-54 girders

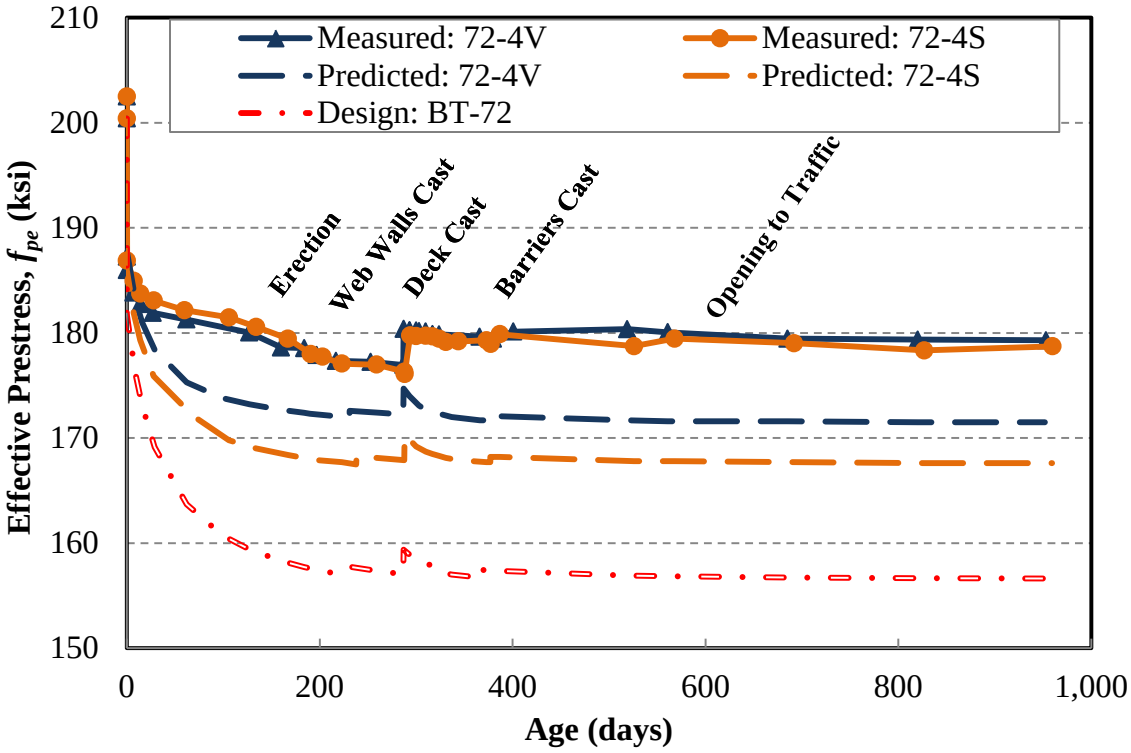

Figure 4.21: Comparison of measured and design effective prestress in BT-72 girders

In the above figures, differences are apparent between measured time-dependent behavior, predicted behavior based on measured mechanical properties, and design behavior based on specified properties. Especially among BT-54s, the design predictions appear to grossly under-predict f_{pe} (and over-predict prestress losses). These observations were confirmed analytically, and pertinent average results are summarized below in Table 4.8. Like before, "Predicted" responses are the predictions that incorporated measured material properties, and "Design" responses are those based on design properties.

Table 4.8: Comparison of measured and refined-*LRFD* design effective prestress

Type of Girder	Average 1,000-Day f_{pe} (ksi)			Ratios	
	Measured	Refined-*LRFD*		Measured/Predicted	Measured/Design
		Predicted	Design		
SCC BT-54	180.0	170.4	152.7	1.06	1.18
VC BT-54	177.3	169.6		1.05	1.16
SCC BT-72	177.7	166.4	156.6	1.07	1.13
VC BT-72	178.5	171.9		1.04	1.14

The findings shown in the above table support the conclusion that the difference between measured long-term SCC-girder performance and measured VC-girder performance (less than 2 ksi of effective prestress, on average) is insignificant relative to the difference between measured and assumed design responses (approximately 21–27 ksi different). Differences in the predictability of measured responses (SCC-girder f_{pe} was approximately 3 ksi more under-predicted than was VC-girder f_{pe} using the refined estimates) are also minor relative to the difference between design and measured responses.

This indicates that all values of f_{pe} determined from measured concrete-strain results were equally and conservatively predictable relative to the behaviors estimated using design properties and average construction times. It further confirms the conclusions of Stallings et al. (2003) and Johnson (2012): predictions can be highly conservative when using design properties in place of measured or expected material properties. The difference between measured-property and design long-term prestress predictions, which ranged approximately 10–18 ksi, represents up to approximately 9% of f_{pbt} and could be significant during design.

4.5 SUMMARY AND CONCLUSIONS

4.5.1 Summary

The work documented in this chapter was conducted to evaluate the long-term full-scale time-dependent structural performance of the SCC girders used to construct the bridge over Hillabee Creek, both in relation to the companion VC girders used in the bridge and in relation to currently employed predictions. The primary full-scale structural property evaluated was the long-term effective prestress in the prestressed strands. Additionally, to isolate transient thermal effects from long-term time-dependent effects, the CTE of the utilized concrete mixtures was evaluated. CTE tests were conducted on samples of concrete placed in the bridge; those results and the

results from other representative-specimen tests (E_c, compliance, and shrinkage) were then implemented in the models used to predict the full-scale responses.

By incorporating the measured material properties in this evaluation, the acceptability of the SCC-girder behavior, and ways in which it may be affected differently than that of VC girders by material properties, was thoroughly evaluated. Not only are such full-scale evaluations of SCC girders limited or nonexistent, but their implications for SCC girders of the scale used in this bridge and made using Alabama materials and methods are unclear. Also, no previously reported study of full-scale time-dependent behavior in SCC girders has approached the 1,000-day duration of this project, which is significant considering that time-dependent effects could continue to evolve through this time.

The work of this chapter was divided into several components: measurement of the apparent CTE of the tested SCC and VC, observation of the full-scale thermal effects due to diurnal and seasonal ambient effects, and evaluation of the full-scale time-dependent behavior of the girders, as well as the predictability of these responses. The observations and conclusions made concerning these topics are summarized in Section 4.5.2. The recommendations made based on this research are then given in Section 4.5.3.

4.5.2 Observations and Conclusions

4.5.2.1 Coefficient of Thermal Expansion

- In standardized testing and in testing conducted in ambient-humidity condition, specimens made with the girder concrete exhibited CTEs approximately 20% greater than in the concrete utilized to construct the cast-in-place bridge elements. The difference was not clearly explained by the mixture differences present, at least with respect to the existing literature.
- Because the main differences between the deck and girder mixtures were SCM type (slag cement versus fly ash), SCM replacement rate, *w/cm* (0.29 versus 0.40), and within-aggregate-type mineralogy, one or more of these variables likely contributed to the difference.
- In light of the difference between girder- and deck-mixture CTEs, SCC CTE was considered to be acceptably similar to that of the companion VC-girder mixture.

4.5.2.2 Thermal Responses of Full-Scale Girders

- Diurnal and, more significantly, seasonal thermal effects affected the apparent concrete strains measured in these girders (but would not affect effective prestress because steel

responds similarly to thermal effects); it was, therefore, crucial to account for these thermal effects before evaluating long-term time-dependent changes in concrete strain and steel prestress due to creep and shrinkage.

- The approach utilized to account for transient thermal effects was accurately used to isolate these effects from the effects of long-term time-dependent material deformation.
- Confirmation of the appropriate apparent CTE and accuracy of the applied method was achieved by comparing measured girder-strain results obtained at distinctly different concrete temperatures.

4.5.2.3 Measured Time-Dependent Behavior of Full-Scale Girders

- After accounting for thermal effects, SCC girders exhibited practically identical effective prestress as the companion VC girders throughout the first 1,000 days after casting. Differences in total losses between the materials equated to no greater than 1% of f_{pbt} at a concrete age of 1,000 days.
- The time-dependent structural behavior of the SCC girders contradicts the findings presented in Chapter 3—cylinders of SCC were found to exhibit up to 15% greater compliance and 30% greater unrestrained shrinkage at a concrete age of 1,000 days, but full-scale time-dependent behavior of SCC girders was essentially identical to that of the companion VC girders.
- f_{pe} determined from measured concrete-strain results was practically unchanged during the approximately 650 days after the casting of the deck, and the f_{pe} maintained since the addition of the deck exceeded that measured immediately prior to its addition. Based on these results, time-dependent changes in behavior (other than transient thermal effects) are expected to be minimal during the remainder of the service life of these girders (at least thirty years).

4.5.2.4 Prediction of Time-Dependent Behavior of Full-Scale Girders

- Use of the *AASHTO LRFD* (2013) provisions to approximate prestress-loss (Section 5.9.5.3 of the provisions) led to reasonably accurate predictions of total long-term losses when using measured material properties—all predictions were conservative but within approximately 6 ksi, or 3% of f_{pbt}, of measured results.
- Use of the *AASHTO LRFD* (2013) refined prestress-loss provisions (Section 5.9.5.4 of the provisions) led to under-predictions of effective prestress at multiple ages when using

measured material properties—all predictions were conservative but within approximately 11 ksi, or 5% of f_{pbt}, of measured results.

- The accuracy of the predictions was moderately improved in the VC girders when applying the A_{AL} adjustments recommended in Chapter 3 (under-predicted by less than 2.5% of f_{pbt} using adjusted models)
- The accuracy of the predictions was insignificantly reduced in the SCC girders when applying A_{AL}. Measured effective prestress in SCC girders was under-predicted by up to approximately 13 ksi, or 6.5% of f_{pbt}, by the adjusted refined-*LRFD* provisions.
- Use of the *AASHTO LRFD* (2013) simplified or refined prestress-loss provisions with *design* material properties (f'_{ci} and others) led to very conservative predictions. Long-term design predictions under-predicted f_{pe} (from measured concrete-strain results) by up to 27 ksi (13% of f_{pbt}) and under-predicted equivalent f_{pe} predictions that incorporated measured properties by up to 19 ksi (10% of f_{pbt}).
- In light of these findings, the long-term time-dependent behavior of full-scale SCC girders was considered to be conservatively predictable and acceptably similar to that of the companion VC girders.

4.5.3 Recommendations

- Concerns about the time-dependent structural behavior of SCC in full-scale precast, prestressed girders should not restrict the implementation of the material in that type of construction. Measured full-scale time-dependent structural responses were essentially identical in companion SCC and VC girders and all behaviors were conservatively predictable based on measured material properties.
- The effects of the differences in CTE between girder mixtures and between the girder mixtures and deck mixture were minimal in this application (with simply supported spans).
- For prediction of long-term time-dependent losses, the approximate and refined *AASHTO LRFD* estimation methods (Sections 5.9.5.3 and 5.9.5.4 of the provisions, respectively) should provide acceptably conservative estimates of time-dependent behavior, at least when measured mechanical properties are incorporated.
- The adjustment factors used to account for Alabama materials and construction practices (A_{AL}) were found to improve the predictions of VC time-dependent behavior, and their use is recommended.
- The use of A_{AL} factors led to more distinct under-prediction of SCC time-dependent prestress maintenance; their inclusion had only a minor effect, though, and all existing and A_{AL}-adjusted predictions were slightly more conservative concerning SCC time-dependent behavior than concerning VC time-dependent behavior.

- Full-scale time-dependent performance of SCC girders was more conservatively predicted relative to small-scale tests than was VC-girder behavior. While the source of this discrepancy could not be isolated in this research, further research concerning the discrepancy between small-scale cylinder-tested properties and full-scale properties may be of value.
- The difference between predictions that incorporated measured properties and those based on design properties was distinctly larger than the difference between SCC and VC. Further research concerning the discrepancy between measured time-dependent behavior and the values that would be predicted during design should be investigated.

CHAPTER 5: ELASTIC-RESPONSE BEHAVIOR OF GIRDERS

5.1 INTRODUCTION

In the complementary report prepared by Keske et al. (2015), self-consolidating concrete was shown to exhibit slightly different mechanical properties and performance characteristics than equivalent-strength VC as a result of its different constituent materials and proportions. Differences in hardened mechanical properties (f_c, f_{ct}, and E_c) were shown to be expectable not only of the tested SCC and VC, but of any two concrete mixtures proportioned differently. Also, elastic responses to the transfer mechanism (camber and initial prestress losses) were found to be reasonably predictable using an iterative time-step program developed by Schrantz (2012). In this chapter, the full-scale elastic structural performance of the girders is evaluated further—both in an extended comparison of SCC and VC responses, as well as in relation to the non-iterative approach included in the *AASHTO LRFD* provisions.

The primary full-scale elastic structural performance characteristics evaluated in the Hillabee Creek Bridge girders were the elastic concrete strains, and associated prestress changes, due to construction and service loads. Deflections due to the construction of the deck and due to service-level live loads were also measured to corroborate these concrete-strain findings. Evaluation of these full-scale behaviors is critical because existing full-scale evaluations of SCC have been limited, and their implications for SCC girders of the scale used in this bridge and made using Alabama materials and methods are unclear. Furthermore, no previously documented live-load testing has been conducted on an in-service bridge constructed with SCC girders.

Predictions of full-scale elastic load-response behaviors are frequently based on properties measured in representative cylinders. For this project, these small-specimen tests were conducted on the exact batches of concrete placed in the girders, so the measured material properties were directly implemented in the predictions. In this way, the predictability of full-scale behavior of SCC girders was assessed while using the most accurate material definitions determinable in representative cylinders.

5.2 REVIEW OF EXISTING LITERATURE

Much of the literature pertinent to this research has been reviewed by Miller (2013) and Keske et al. (2014). Furthermore, the *AASHTO LRFD* Section 5.9.5.2 provisions employed to calculate responses to the prestress transfer mechanism and to superimposed loads were discussed in Section 4.3.6.1 because these calculations were necessary to develop estimates of time-

dependent prestress losses. In summary from that section, the initial, elastic loss of prestress (and increase in concrete strain) at transfer depends on the transformed section properties of the girder, the assumed stress in the steel immediately before transfer (f_{pbt}), and the counteracting self-weight of the girder. Instantaneous strain changes in response to loads applied later can be calculated using an elastic analysis as long as the stresses in the concrete and prestressing steel remain in the elastic range (a safe assumption during this research).

As noted by Miller (2013), very few static load tests of SCC girders have been reported to date and none have included results obtained from the live-load testing of an in-service bridge made with SCC girders. Most have involved experimental girders that were loaded to failure (Boehm et al. 2010; Khayat and Mitchell 2009; Naito et al. 2005; Ozyildirim 2008; Trejo et al. 2008). Meanwhile, Zia et al. (2005) tested several SCC girders to service-load levels prior to erection in a bridge. No girder cracking was observed and full deflection recovery occurred after the removal of the applied load, indicating an elastic service-load response in SCC girders. The researchers further determined that the equivalent-stiffness SCC and VC girders "exhibited virtually identical" load-deflection relationships throughout service-level loading (Zia et al. 2005).

All of the researchers cited above that tested experimental girders in a laboratory setting (Boehm et al. 2010; Khayat and Mitchell 2009; Naito et al. 2005; Ozyildirim 2008; Trejo et al. 2008) reported that SCC girders behaved predictably and acceptably similarly to comparable VC girders under a variety of service- or ultimate-load conditions. Among them, three reported minor but unexpected differences between SCC and VC girders:

- Boehm et al. (2010) documented that the poor top-surface roughening of the tested SCC girders occasionally led to the occurrence of horizontal slip at the deck-girder interface when approaching the ultimate flexural capacity. The service-load behavior was not affected, but special attention to this construction procedure was recommended.
- Trejo et al. (2008) found that both SCC and VC girders exhibited nominal flexural capacity as much as 12% larger than predicted even when incorporating measured material properties. The service-load behavior was not affected, but the SCC girders appeared to exhibit more and smaller cracks at failure, thus causing a larger ultimate-deflection response at the same strength.
- Naito et al. (2005) found that girder behavior contradicted the material results obtained from representative cylinders. They found that SCC girders exhibited increased elastic stiffness and the same ultimate strength versus VC girders while cylinder tests indicated the opposite. They suggested that the contradiction could have been the result of the difference in curing conditions between the girders and representative cylinders (cylinders were moist-cured prior to testing).

5.3 EXPERIMENTAL PROGRAM

5.3.1 Hardened Mechanical Property Evaluation

In addition to the mechanical property evaluation reported by Keske et al. (2015) regarding girder properties, measured results from the deck and barriers were needed for transformed-section analysis (elastic and time-dependent). Thus, samples of concrete were collected for f_c and E_c testing according to ASTM C39 and ASTM C469 during construction of each bridge deck span and during construction of the slip-formed barriers. The cylinders were capped and stored in a shaded area near the girders at the bridge site. They were demolded approximately five to seven days after casting to coincide with when contractors ceased applying curing to the deck. All cylinders were left adjacent to the bridge for another week after demolding (total of two weeks after casting). Afterwards, they were transported to the AUHRC laboratory (approximately 40 miles southeast of the bridge site) and stored in a sheltered outdoor location with approximately similar humidity and temperature conditions as at the bridge site. Cylinders prepared in this way were tested at various ages up to ninety-one days after production, at which time hardened mechanical property evolution was assumed to have sufficiently plateaued.

During each deck construction day, the representative cylinders were produced from a sample taken at approximately halfway through the day's construction. While the researchers attempted to sample deck concrete near where embedded gauges were installed at midspan (discussed in the next subsection), the placement location of the batches could not be precisely controlled by the researchers. Regardless, location would be of minimal value, as each span required at least eighteen 8 yd^3 batches of ready-mixed concrete.

In addition to 6 in. by 12 in. cylinders, drying-shrinkage prisms (11.25 in. by 3 in. by 3 in.) were produced similarly to those described for girder concrete evaluation. A set of three prisms was produced for each span to evaluate the variability between spans and to compare to the limited number of SCC and VC girder prisms. The deck-concrete prisms were stored in the same climate-controlled storage room, where the drying process ensued until July of 2013 (following completion of all field deformation measurements and live-load testing). At this time, deck-concrete prisms were approximately 675 days old.

5.3.2 Evaluation of Elastic Responses to Construction Loads

Elastic responses to construction loads (prestress transfer and deck addition) were measured through the use of the VWSGs described in Section 4.3.3.1 and the measurement of camber according to the procedures described in Section 4.3.5. Considerations of the measurement and prediction of these properties are presented in the following subsections.

5.3.2.1 Concrete Strain Responses to Construction Loads

The data acquisition system used in this research was capable of recording VWSG strain readings at user-specified intervals as short as approximately two minutes. While readings were, consequently, incapable of identifying the truly instantaneous responses to the transfer or deck-weight loading, neither of these loads is applied instantaneously. Transfer by flame-cutting was observed to require approximately 6–10 min., while several hours were required to place the cast-in-place concrete deck over each span.

The creep and shrinkage of the girders in response to the addition of the deck load were likely minimal during the few hours of construction because the girders were approximately 300 days old. Still, the analysis of the elastic strain response to the addition of the deck weight was inherently variable because it was impossible to precisely measure the volume of concrete placed over each girder. Efforts were made to accurately measure the total thickness of the deck and haunch (as described in Section 4.3.5), but the thickness of the deck was always assumed to equal the thickness specified on the plan drawings—7.0 inches.

In all cases, cylinder-measured E_c is an approximation of the elastic stiffness of concrete because it is tested in unreinforced concrete subjected to uniaxial compression. The loading of concrete during E_c testing according to ASTM C469 occurs over less than three minutes, so this measurement is the best available estimate of elastic concrete stiffness. Thus, the direct comparison of measured results to those calculated using the E_c measured in representative cylinders was deemed acceptable, and construction-load results are understood to include some inherent variability.

5.3.2.2 Camber Responses to Construction Loads

The camber response to the addition of the deck weight was measured using the instrumentation and methodology described in Section 4.3.5. As explained in that section, error could have been introduced in camber readings by the implementation of the underside surveying method, and the value of camber measurements in girders that are mechanically joined by diaphragms and a deck is unclear. Therefore, the main purposes of this camber evaluation were to determine the change in camber due to the addition of the deck and the approximate camber after that addition. Such an evaluation may illustrate the precast, prestressed bridge behavior typical of Alabama highway construction, and the comparison of the relative performance of SCC and VC girders should supported the other conclusions of this chapter.

5.3.3 Service-Level Live-Load Response Evaluation

The live-load response instrumentation and methodology utilized in this research was described by Miller (2013) and has been summarized in an article by Keske et al. (2014). In summary, two live-load responses were evaluated: bottom-surface concrete strains at midspan in each girder, and midspan deflection. These two measures were evaluated within and between two load tests conducted before and after one year of bridge service.

5.3.3.1 Live-Load Response Instrumentation

For simply supported bridge girders with a composite, cast-in-place concrete deck, bottom-flange strains near midspan are the most sensitive indicators of individual girder response to service-level live loads. Therefore, these strains were measured with surface-mounted 2.4 in.-long electrical-resistance strain gauges (ERSGs) mounted longitudinally along the girder centerline on the bottom of each girder. Additionally, the VWSGs that were embedded in each girder could be used to extrapolate internal strain results to the depth of the bottom surface (assuming plane sections remain plane) if the ERSG failed during testing. One of the ERSGs used in this research is shown in Figure 5.1.

Figure 5.1: Strain gauge applied to bottom surface of girder at midspan

Vertical deflections were measured at midspan in each girder during the first round of live-load testing and in each girder of Spans 1, 2, and 4 during the second round of testing after one year of service. At the time of the second load test, an elevated creek water level and the presence of traffic precluded the installation of deflection instrumentation in Span 3. All vertical deflections were measured using deflectometers that were calibrated to determine deflection to the nearest 0.01 in. and were attached to each girder via thin steel wire. All deflectometers, data cables, and wires were shaded from direct sunlight, thus avoiding changes in thermal effects during the short measurement intervals. One of the deflectometers used in this research is shown in Figure 5.2.

Figure 5.2: Deflectometer used to measure midspan live-load deflection

The relative displacement between the bottom of the girder and the ground was measured through the use of these deflectometers. Measured displacements include compressive deformations of the neoprene bearings and bridge foundations; however, the magnitude of these small bearing and substructure deformations is estimated to be insignificant relative to the precision of the measured displacements.

Backup VWSG measurements were only collected during the first load test, at which time construction was essentially completed but the bridge was not yet open for service. The extended amount of time required to receive signals from all VWSGs during testing precluded their use during the second load test because traffic could only be stopped for brief intervals. All deflection and ERSG measurements were collected using an Optim MEGADAC data acquisition system, and additional details concerning this instrumentation are discussed by Miller (2013).

5.3.3.2 Live-Load Test Procedure

The pre-service round of live-load tests was performed using a single load-testing truck owned by ALDOT. One year later, the second round of tests was performed using the same truck and an additional, identical ALDOT load-testing truck. These trucks were each configured to have a gross weight of 85.7 kips supported by three axles with the geometry shown in Figure 5.3. These trucks, one of which is shown in Figure 5.4, are further described by Miller (2013) and Keske et al. (2015).

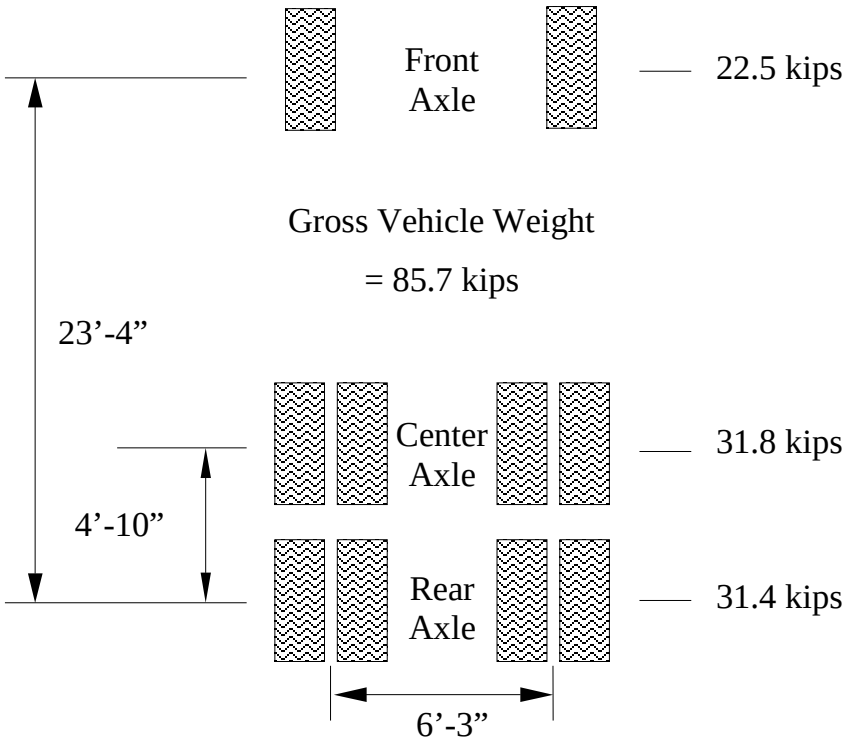

Figure 5.3: Configuration of ALDOT load test truck

Figure 5.4: ALDOT load test truck used for this research (Note: only rear two axles of the tri-axle rear end of the vehicle are in contact with the deck)

For all static load tests, each truck was positioned longitudinally such that the center of the center axle was directly over midspan. Transverse truck positions and combinations that are pertinent to the results discussed in this chapter are illustrated in Figure 5.5. During the pre-service load testing, the single load truck was placed at each load position (A, E, and H) a minimum of twice per span in order to confirm consistency of results. During the second load test, the single-truck testing regime from the first round was repeated entirely. In addition, Loads A&E and E&H were tested using two trucks (simultaneously) a minimum of two times. With this load testing scheme, superimposed single-truck results and actual two-truck responses were directly comparable. The final position shown in Figure 5.5 represents the superposition of Loads A, E, and H.

Additional truck positions that were used during the first test are described by Miller (2013). Results from that testing indicated that Load A+E+H provided the critical load combination for interior-girder (Girder 6) and exterior-girder (Girder 7) design, so a total of five static truck positions (A, E, H, A&E, and E&H) were utilized during the second load test. The nomenclature used during the first round of testing was maintained during the second round and in this report for the sake of continuity.

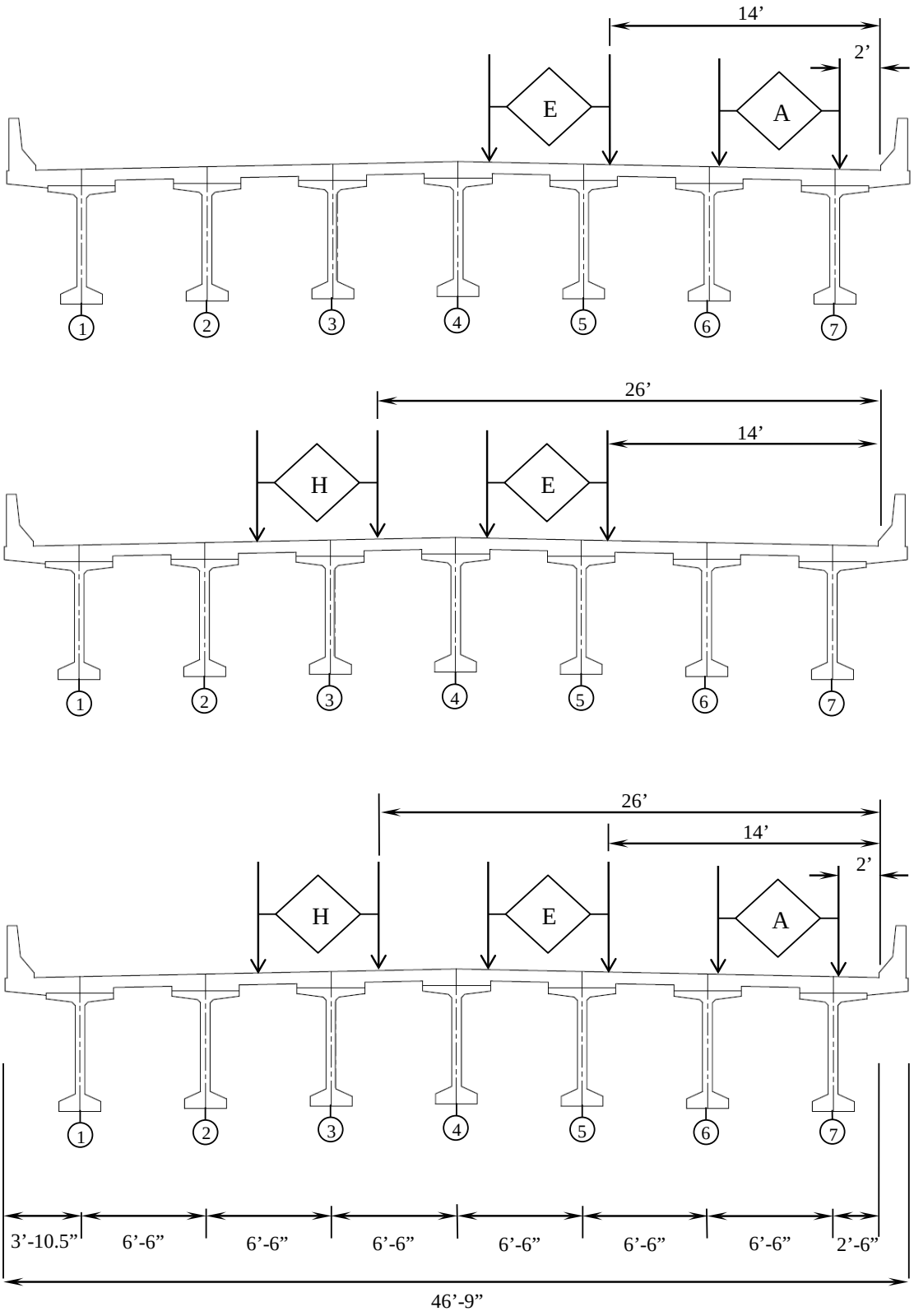

Figure 5.5: Transverse truck positions for Loads (*top*) A+E, (*middle*) E+H, and (*bottom*) A+E+H

5.3.4 Comparisons of Elastic Strain Responses

When assessing the load response of a bridge to construction and service loads, it is important to understand *how* results should be compared to meet the objectives of the test. Bridge members designed for the same load capacity but constructed of different materials deform differently under the same external load due to their different geometries and material properties. When evaluating a new material, it is important to establish whether its load-response performance is as reliable as that of a conventional material after accounting for reasonable differences in geometry and material properties.

The Hillabee Creek Bridge is configured so that the span pairs (1 versus 4 and 2 versus 3) are each geometrically equivalent (within normal construction tolerances). Thus, equitable comparisons between the deformation responses of an SCC girder and its companion VC girder were made after accounting for the different stiffnesses of the girder materials (quantified by E_c in this linear-elastic response range). When comparing responses to construction and service loads, the reference response was taken to be that of the SCC girders.

To equitably determine if the SCC girders responded as should be expected, the measured strain response of each VC girder was transformed to the value that would be expected if its measured value of E_c equaled that of its companion SCC girder. In summary of the previously published discussion of this topic (Keske et al. 2014, Miller 2013), transformed-section analysis was used to solve for the expected strain change in a VC girder in terms of the strain change measured in an identically loaded, companion SCC girder. This adjustment procedure, which is based on engineering beam theory, is shown in Equations 7-1 and 7-2:

$$\varepsilon_{gauge} = \frac{My_{tr}}{E_c I_{tr}} \tag{7-1}$$

And

$$\varepsilon_{gauge,SCC} = \varepsilon_{gauge,VC} \frac{\left[\frac{E_c I_{tr}}{My_{tr}}\right]_{VC}}{\left[\frac{E_c I_{tr}}{My_{tr}}\right]_{SCC}} \tag{7-2}$$

Where

ε_{gauge} is the calculated strain change at a given location due to an applied live load bending moment,

M is the bending moment present at a given cross section due to an applied load (such as the distributed permanent weight of the deck),

y_{tr} is the vertical distance from the transformed-section centroid to the gauge location,

$\varepsilon_{gauge,SCC}$ is the change in SCC strain due to the applied load, and

$\varepsilon_{gauge,VC}$ is the change in VC strain due to the same live load.

Use of Equation 7-2 allowed evaluation of whether the SCC girder responded elastically to applied loads as would a VC girder with the same material stiffness. In Equation 7-1, the equivalence of *M* is clear during live-load testing, so this term is cancelled during calculation of an adjustment factor according to Equation 7-2. Such equivalence is less clear during construction. The differences in deck loading due to variable haunch thickness could be significant in relation to the weight of the cast-in-place deck—a haunch-thickness difference of 0.5 in. would equate to a difference of 4% of the deck weight, so consideration of haunch thicknesses was important during the comparison of measured results and expected results.

Determination of a prestress transfer strain adjustment factor is slightly more complicated than determination of the previously described adjustment factors because the elastic change in strain both affects and is affected by the transfer mechanism. Conveniently, Equation 4-8 is a non-iterative approach to determining concrete *stress* at the *cgp*, and that may be directly converted into an expected strain through the use of a linear stress-strain relationship as shown in Equation 7-3.

$$\varepsilon_{cgp} = \frac{f_{cgp}}{E_{ci}} \tag{7-3}$$

Where

ε_{cgp} is the concrete strain at the *cgp* immediately after transfer and

f_{cgp} is the concrete stress at the *cgp* immediately after transfer, per Equation 4-8.

The use of Equation 7-3 to determine the elastic strain change in concrete at the *cgp* is convenient because a VWSG strain gauge was installed at this approximate location. Thus, the expected strain change in a VC girder due to prestress transfer—in terms of the strain change measured in an identically configured, companion SCC girder—was calculated according to Equation 7-4 as shown below.

$$\varepsilon_{gauge,SCC} = \varepsilon_{gauge,VC} \frac{\left[\frac{E_{ci}}{f_{cgp}}\right]_{VC}}{\left[\frac{E_{ci}}{f_{cgp}}\right]_{SCC}} \tag{7-4}$$

Where

$\varepsilon_{gauge,SCC}$ is the change in SCC strain at the *cgp* due to transfer of an assumed prestress force and

$\varepsilon_{gauge,VC}$ is the change in VC strain due to transfer of the same assumed prestress force.

Calculation of f_{cgp} only requires calculation of transformed properties and determination of the bending moment due to girder self-weight. Girder self-weight was based on a reinforced-concrete unit weight of 150 lb/ft^3; while the applied bending moment varied slightly due to the differences in the unit weight of SCC and VC (SCC unit weight was approximately 2.5–3 lbs/ft^3 less than VC w_c), use of a more precise unit weight was not warranted considering the precision of the measured properties. Under-prediction of the self-weight bending moment would lead to over-prediction of the expected concrete strain (a larger self-weight bending moment would reduce the concrete contraction experienced at transfer), which was considered when comparing measured responses to calculated responses.

The use of an adjustment factor to account for expectable differences in concrete strain was also discussed by Miller (2013), but there was an error in its application to this work: an incorrect y_{tr} was used in determining the adjustment factors for ERSG gauges which reduced the significance of the adjustments. The error only affected the comparison of SCC strain to VC strain during live-load testing, and all other conclusions from Miller (2013) were unaffected by it. The correct y_{tr} is shown in Figure 5.6 alongside that used to compare VWSG strains.

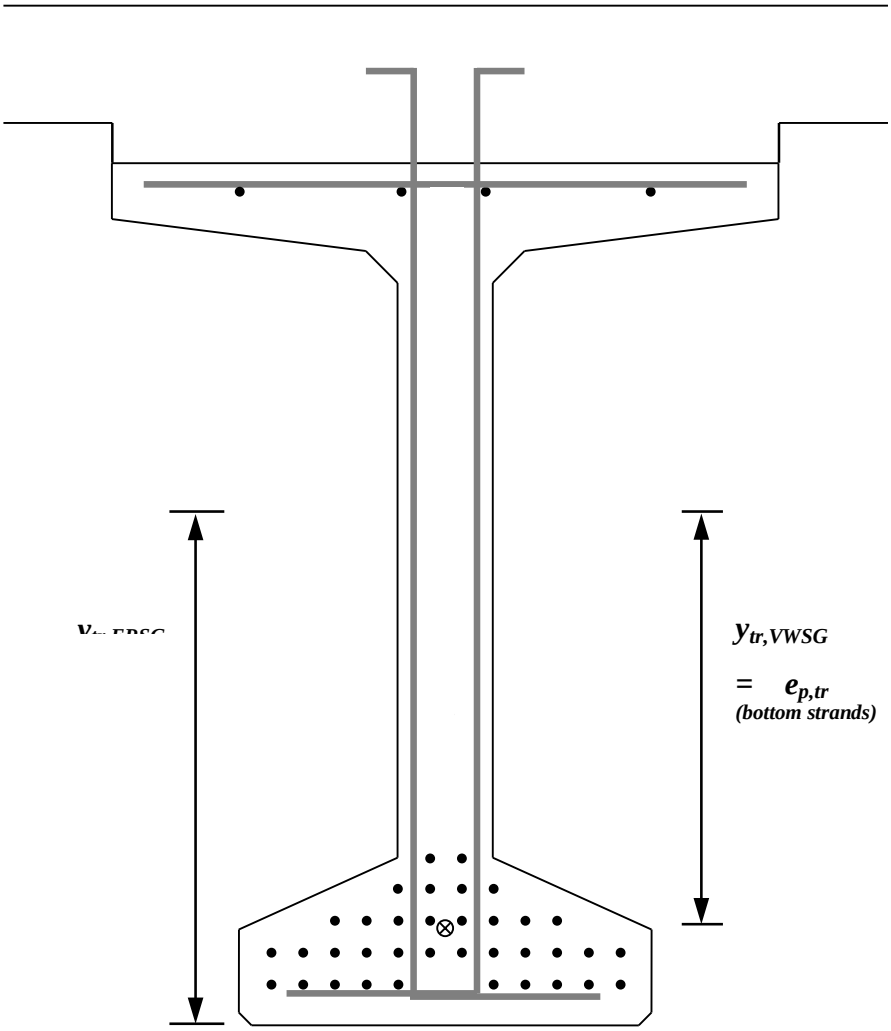

Figure 5.6: Determination of y_{tr} for strain comparisons

It would be difficult to accurately determine a transformation factor for use with measured changes in camber or live-load deflection. Therefore, only the actual deflection responses are considered. These results are instructive because they may illustrate the precast, prestressed bridge behavior typical of Alabama highway construction. It was also informative to observe whether these as-produced SCC girders deflected similarly to the companion VC girders and whether the difference in stiffnesses observed in representative cylinders corresponded to the full-scale responses.

5.3.5 Nomenclature and Additional Considerations

5.3.5.1 Nomenclature and Use of Data

Only the basic nomenclature shown in Figure 4.12 was necessary to identify the girders during this full-scale analysis. As with the assessments of the other chapters, the exact placement location of the batches sampled for laboratory testing could not be isolated within the girders. Samples taken at the midpoint of each girder-production day and deck-casting day were assumed to be representative of the majority of concrete placed during those days. Essentially only three mixtures (for SCC girders, VC girders, and all cast-in-place elements) were used throughout production, but every element could have been subjected to different curing and ambient exposure histories. This directly affected the expected elastic response to the transfer mechanism.

Since the use of production-group mechanical properties was necessary during evaluation of transfer-load responses, it was acceptable to continue using these group-specific properties after the girders achieved composite action. Between-batch variability of later-age E_c was minimal, so the distinction between production-group and span-average E_c was of little concern. Meanwhile, span-average haunch thicknesses were used to determine the expected responses to construction and service loads in consideration of the composite-bridge distribution of this weight. The precision of all comparisons should be considered in light of the inherent variability of concrete material testing and full-scale geometry and load measurement.

5.3.5.2 Additional Analysis Considerations

During the elastic-response analyses described in this chapter, only the internal strains determined using VWSGs were corrected for concrete thermal effects. VWSG concrete-strain measurements were collected every two minutes during prestress release and every ten minutes during deck placement, and the observed lengths of time required to apply these loads was previously noted to equal up to ten minutes and up to several hours, respectively. Consequently, the time elapsed between pre- and post-load strain measurements equaled up to approximately fourteen minutes during transfer (while the girders rapidly cooled) and four hours during deck construction.

Adjustments described in Section 4.3.4 and shown in Section 4.4.2 to accurately account for thermal effects were thus required for analysis of construction-load strain responses. Meanwhile, readings of live-load deflections and strains were obtained directly before, during, and after each truck movement, so thermal effects were directly negated by averaging the baseline readings from before and after each truck movement.

Elastic responses to construction loads were measured in different girders: strain due to transfer was measured in all girders, but the changes in camber and concrete strain due to the addition of the deck were only measured in a few robustly instrumented girders. In accordance with the previous discussion of this topic, the responses of a few robustly instrumented girders should indicate the behavior of all girders. Therefore, only the same girders assessed for time-dependent behavior in Chapter 4 are evaluated with respect to construction loads in this chapter: 54-4S, 5S, 6S, 4V, and 6V, and 72-4S, 6S, 2V, 3V, and 4V. Comparisons are reasonably well filled—five SCC girders and five VC girders, or five BT-54s and five BT-72s, and the results shown in Chapter 4 illustrate that variability between companion girders should be minimal.

Meanwhile, the responses to service-level live loads were assessed in all seven girders within each span. The loadings due to the transfer mechanism and the deck construction affect all girders (at least interior girders) equally, within construction tolerances, but the same cannot be said of truck loads. By placing the load trucks at the same transverse locations on matching spans, companion girders (54-6S and 54-6V, for example) were loaded congruently, but every girder *pair* (54-6 or 72-1, for example) was loaded differently. Furthermore, girders in lines 1 and 7 also included the additional flexural stiffness of the barriers. Thus, it was appropriate to compare the response of all girders within each span.

5.4 Presentation and Analysis of Results

Results and discussion relevant to the assessment of the elastic-response behavior of the full-scale girders are presented in this section. First, measured material and transformed-section properties are presented because they are necessary for the subsequent evaluations. Then, evaluations of construction-load and service-load responses are documented in separate sections. Each of these sections include direct comparisons of measured responses (applicable because these girders are companions in an in-service bridge) and comparisons of the measured SCC responses to adjusted VC responses expected had the girders exhibited the same measured E_c and geometry. Where readily calculable, design responses that would have been expected based on design engineering properties are also reported for context.

5.4.1 Material and Section Properties

5.4.1.1 Strength and Elasticity

Summary results of the strength and modulus of elasticity testing conducted on field-cured deck-concrete cylinders are presented in Table 5.1 below. The average results from the SCC and VC girders are presented for reference (see Keske et al. 2014 for further information). As previously

discussed in Section 5.3.1, only one batch was sampled per deck span; these samples, which were obtained near the middle of each casting day, were expected to be representative of the majority of concrete in the deck. Also, only one sample was collected during the full day of slip-form casting of the barriers; this information was only used to determine the transformed composite-section properties of girders in lines 1 and 7 that would be needed to adjust measured live-load responses.

Table 5.1: Strength and modulus of elasticity of field-cured concrete

Component	Compressive Strength (psi)		Modulus of Elasticity (ksi)	
	28-Day f_c	91-Day f_c	28-Day E_c	91-Day E_c
SCC Girder Avg.	*9,010*	-	*6,200*	-
VC Girder Avg.	*8,360*	-	*6,750*	-
Span 1 Deck	6,030	6,750	6,300	6,600
Span 2 Deck	6,510	7,410	6,400	6,900
Span 3 Deck	6,060	6,940	6,100	7,000
Span 4 Deck	5,910	6,430	6,400	6,500
Deck Average	*6,130*	*6,900*	*6,300*	*6,750*
Barriers	5,860	-	6,000	-

All four deck spans were cast using the same concrete mixture, but conditions varied between casting days. The measured results conveniently minimized the influence of the variability—matched spans (1 and 4 or 2 and 3) exhibited especially similar f_c and E_c. All four spans also exhibited fairly uniform strength and stiffness gains between three and ninety-one days, as expected given the 20% fly-ash replacement and moderate *w/cm* employed (see Table 4.1 for mixture details and Keske (2014) for f_c and E_c results from other ages).

Notably, the concrete used to cast the bridge deck exhibited practically the same E_c as that of the concrete in the girders. That it achieved this stiffness while at a distinctly lower f_c is peculiar—the predicted E_c equaled 5,050 ksi even when incorporating an improved assumuption of w_c = 150 lb/ft^3. Thus, the measured results yield a K_1 factor of 1.34. The source of this difference between girder- and deck-concrete specimens was impossible to isolate, but future research considering its effects may be beneficial.

5.4.1.2 Transformed Section Properties

Based on the stiffnesses presented in the previous subsection, transformed properties were determined to equitably compare elastic responses to applied loads in accordance with Equations 7-2 and 7-4. Transformed properties are shown below in Table 5.2. Non-composite girder properties at the time of deck addition are shown because only the non-composite section resisted the fresh weight of the deck concrete; composite-section properties determined at a deck age of ninety-one days are shown because the live-load testing was conducted well after the deck surpassed that age. Among these composite-section transformed properties, girders in lines 1 and 7 exhibit a larger magnitude I_{tr} and y_{tr} because the flexural stiffness of the cast-in-place barriers is attributed to them. Transformed-section release properties are shown in Appendix G of Keske (2014) because additional variables were required for determination of f_{cgp} according to Equation 4-8.

Table 5.2: Transformed section properties of girders

Girders	Avg. Haunch (in.)	Non-Composite, At Deck Addition		Composite, Deck Age > 91 Days	
		y_{tr} (in.)	I_{tr} (10^3 in.^{4})	y_{tr} (in.)	I_{tr} (10^3 in.^{4})
54-1S	1.72	21.94	278	48.50	894
54-2S, 5S, 6S		21.91	279	42.51	615
54-3S, 4S		21.89	278	42.23	607
54-7S		21.96	279	48.33	916
54-1V	1.14	22.00	278	47.74	860
54-V2, V5, V6		21.96	277	40.83	569
54-3V, 4V		28.07	278	41.33	582
54-7V		28.08	278	47.86	865
72-1S	1.50	28.08	570	60.31	1982
72-2S, 5S		28.02	570	54.44	1172
72-3S, 4S		28.18	570	54.44	1172
72-6S		28.22	572	54.96	1195
72-7S		28.27	570	60.31	1982
72-1V	1.48	28.16	567	60.38	1921
72-2V, 5V		21.94	566	53.28	1124
72-3V, 4V		21.91	565	52.86	1106
72-6V		21.89	568	53.86	1148
72-7V		21.96	567	60.38	1921

Based on these measured concrete properties and transformed-section properties shown in Appendix G of Keske (2014) and Table 5.2, respectively, adjustments to measured VC strains were made to reflect the strain that would be expected of a VC girder if it had exhibited the same stiffness as the companion SCC girder. These adjustments are summarized in Table 5.3, and supplemental information is presented in Keske (2014).

Table 5.3: Strain adjustments applied to VC girders

Girders	Quantity Normalized			VC Strain Adjustment Factor		
	$\left(\frac{E_{ci}}{f_{cgp}}\right)$ Transfer	$\left(\frac{E_c I_{tr}}{y_{tr}}\right)$ Deck	$\left(\frac{E_c I_{tr}}{y_{tr}}\right)$ Live	Prestress Transfer	Deck Weight	Live Load
	(ksi/ksi)	(10^6 kip-in.^{2})				
54-1S	2,326	84	121	-	-	-
54-2S, 5S, 6S	2,271	81	92	-	-	-
54-3S, 4S	2,326	78	95	-	-	-
54-7S	2,224	87	116	-	-	-
54-1V	2,427	93	123	1.08	1.14	1.01
54-V2, V5, V6	2,572	87	102			1.11
54-3V, 4V	2,427	128	96			1.02
54-7V	2,321	129	124			1.06
72-1S	1,956	129	207	-	-	-
72-2S, 5S	1,983	122	137	-	-	-
72-3S, 4S	1,983	141	137	-	-	-
72-6S	1,922	146	130	-	-	-
72-7S	1,956	153	207	-	-	-
72-1V	2,333	138	222	1.17	1.14	1.08
72-2V, 5V	2,350	84	154			1.13
72-3V, 4V	2,274	81	160			1.17
72-6V	2,198	78	146			1.12
72-7V	2,297	87	222			1.08

The factors shown in Table 5.3 were calculated for adjustment of strains only in *matching* girders. However, selection of "matching" girders was different during the comparison of live-load results than during the comparison of construction effects. By placing the load trucks at the same transverse locations on matching spans, companion girders were loaded congruently but every girder *pair* was loaded differently. Furthermore, girders in lines 1 and 7 included the additional flexural stiffness of the barriers. Thus, it was appropriate to adjust VC strains relative to their direct counterpart during the live-load response analysis. For example, the VC adjustment factor equaling 1.06 was applied to strain readings from 54-7V for comparison only to strains measured in 54-7S under the same live load.

Meanwhile, matching sizes of girders were identically configured and subject to the same transfer loads, and girders grouped by material and size were subject to approximately the same deck load (within construction tolerances). In other words, all fourteen BT-54s were subject to one transfer load while all fourteen BT-72s were subject to a different transfer load; meanwhile, SCC BT-54s may have been subject to a noticeably different deck weight if the seven girders were cast with a different average haunch thickness than their VC BT-54 counterparts.

Considering the variability of these construction loads and that only a few girders were consistently monitored through deck construction, it was appropriate to adjust the measured changes in strain using an *average* adjustment factor. The factors were not determined by the direct averaging of the normalized quantities shown in Table 5.3 but by weighting these values by the number of girders exhibiting them. For example, three of seven SCC BT-54 girders would resist the deck weight based on a normalized flexural constant of $81(10^6)$ kip-in.^{2}.

The adjustment factors shown closely relate to the observed reduction in SCC E_c. Based on the presented factors and discussion of Section 5.3.4, the SCC girders in this bridge were expected to exhibit *strain* changes approximately 10% greater than in the companion VC girders under identical applied loads. Recall that the adjustment factor is applied to measured VC strains, though, because the measured SCC readings were taken as the reference for comparison.

5.4.2 Full-Scale Responses to Construction Loads

Initial cambers at the time of prestress transfer have been previously discussed by Keske et al. (2015). Meanwhile, Miller (2013) evaluated measured live-load responses but incorrectly calculated the strain-adjustment factor used to compare responses on an equal-stiffness basis per Equation 7-2. Therefore, considerations in this section include comparisons of the

- *LRFD*-predicted, measured, and adjusted instantaneous changes in concrete strain at the midspan *cgp* due to the transfer of prestressing,
- Measured elastic loss in camber due to the addition of the deck,
- Predicted, measured, and adjusted elastic changes in concrete strain at the midspan *cgp* due to the addition of the deck,
- Measured deflections due to service-level live loads, and
- Predicted, measured, and adjusted bottom-fiber concrete strains due to service-level live loads.

In subsequent comparisons, “measured” responses are those directly measured in the girders; they do not account for observed differences in concrete properties (such as E_c) or geometry (such as haunch thickness). While comparisons of measured responses are limited for

this reason, they are instructive because the SCC and VC girders are direct companions in an in-service bridge. "Adjusted" responses are the measured VC responses that have been adjusted to account for differences in measured properties per Equations 7-2 or 7-4; they are evaluated similarly to "measured responses." Meanwhile, "predicted" responses are those calculated using Equations 7-1 and 7-3, respectively, with material properties measured in representative cylinders. Comparisons of predicted responses to measured responses are only made *within* each material to assess the predictability of measured responses.

In addition to these measured, adjusted, and predicted results, "design" responses are those calculated using Equations 7-1 or 7-3 with design properties (f'_{ci}, f'_c, etc.). Thus, SCC responses were compared to measured VC responses, adjusted VC responses, and predicted SCC responses in each section. Measured VC responses were compared to predicted VC responses, and all measured and predicted responses were compared to the design responses (which are equally applicable to SCC and VC responses).

5.4.2.1 Instantaneous Concrete Strain at Transfer

The change in measured concrete strain due to the release mechanism was previously discussed in relation to Equation 4-8 concerning f_{cgp}, Equation 7-3 concerning ε_{cgp}, and Equation 7-4 concerning the change in strain expected of a VC girder exhibiting the same E_{ci} as the assessed SCC. Using these equations and the adjustment factors shown in Table 5.3, the measured immediate change in concrete strain was compared to that inferred from the *AASHTO LRFD* (2013) calculations for f_{cgp} using measured properties. Results from this comparison are summarized below in Table 5.4; the individual adjusted VC responses are included in Appendix I of the dissertation prepared by Keske (2014).

Table 5.4: Comparison of changes in concrete strain at transfer

Girder	Initial Elastic Concrete Strain (με)			SCC/VC Response		
	Measured	Predicted (Eq. 7-1)	Measured/ Predicted	Measured	Predicted	Adjusted[1]
54-4S	-405	-430	0.94			
54-5S	-568	-440	1.29			
54-6S	-437	-440	0.99			
54-S Average	-470	-437	1.07	0.98	1.09	0.91
54-4V	-467	-412	1.26			
54-6V	-488	-389	1.13			
54-V Average	-477	-400	1.19			
72-4S	-473	-504	0.93			
72-6S	-503	-520	0.97			
72-S Average	-488	-512	0.95			
72-2V	-488	-426	1.14	1.04	1.18	0.89
72-3V	-465	-440	1.06			
72-4V	-459	-440	1.04			
72-V Average	-471	-435	1.08			
SCC Average	-	-	1.02	1.01	1.13	0.90
VC Average	-	-	1.12			

Note: [1] = adjusted VC responses are summarized in Table I.1 of Keske (2014)

In the above table, elastic concrete strains in response to the transfer mechanism were directly measured at the midspan *cgp* and those predicted using Equation 7-3 were based on the measured material properties. Almost all measured responses were greater than predicted (by an average of 7%), indicating that almost all girders exhibited greater concrete strain (and elastic prestress losses) than expected at transfer based on measured properties. However, SCC girders regularly exhibited less elastic strain relative to that predicted using measured E_{ci} than did VC girders relative to measured E_{ci}—measured SCC strains were 102% of predicted strains, on average, versus 112% in the VC girders.

SCC girders also strained noticeably less than expected of VC girders of the same measured stiffness (see “Adjusted” in the table). While SCC girders were predicted to strain 9–18% more than the companion VC girders based on measured properties (see “Predicted” in the table), they actually strained approximately as much as directly measured in the VC girders (see “Measured” in the table). The difference in measured responses, an average of 10 με, is

practically insignificant, representing a difference of less than 0.2% of f_{pbt}. From these observations, several conclusions are warranted:

- SCC-girder elastic strain due to prestress transfer (and associated prestress losses) is at least as accurately predicted as those properties in VC girders when using measured material properties, and
- Because SCC-girder elastic strain responses due to prestress transfer were consistently less than expected of VC girders of the same E_{ci}, SCC prestress-transfer behavior is acceptably similar to that of VC.

For context, the elastic concrete strain assumed during design was calculated according to Equation 4-8 in conjunction with the specified f'_{ci} and the E_{ci} estimated as $57{,}000\sqrt{f'_c}$. Design elastic concrete strains equaled -640 and -650 με for BT-54s and BT-72s, respectively. These responses are approximately 160 με greater in magnitude than the concrete strains *measured* in either material and 140–240 με greater in magnitude than the concrete strains *predicted* based on measured mechanical properties. The strain difference between either measured or predicted results and design results equates to approximately 5 ksi of effective prestress.

This confirms two conclusions drawn in Chapter 4: 1) the difference in the predictability of SCC behavior relative to that of VC behavior when using measured material properties is minor, and 2) design predictions can be conservative when calculated using design properties in place of expected material properties. The 5 ksi difference between measured-property and design initial elastic prestress loss calculations represents approximately 2.5% of f_{pbt}. However, the difference directly relates to the over-prediction of prestress losses discussed in Chapter 4 when using design properties, as time-dependent losses are calculated as a multiple of the elastic strain response (per the creep coefficient). The difference between time-dependent responses predicted using measured properties and using design properties equaled approximately 19 ksi or 10% of $f_{pbt,}$ illustrating the importance of accurate prediction of elastic and time-dependent losses.

5.4.2.2 Change in Camber Due to Addition of Deck

Changes in camber due to the addition of the permanent deck weight were measured within days after the placement using the apparatus described in Section 4.3.5. While some amount of time-dependent change occurred during that period, the majority of the measured camber change should be attributed to the elastic response of the non-composite girders. This applied load is larger (up to 500 kips over the full width of the bridge) than service-level live loads *and* it is resisted only by the non-composite sections.

Only interior-girder cambers are presented here because the exterior girders were differently restrained and were subjected to slightly different deck loads (due to the free outer

edge of the slab). Changes in camber due to the addition of the deck load and post-addition cambers are summarized in Table 5.5.

Table 5.5: Comparison of changes in camber due to deck addition

Girder	Camber at Time of Deck Addition (in.)		Change in Camber (in.)
	Immediately Prior	Immediately After	
54-4S	1.8	1.0	-0.8
54-6S	2.0	1.5	-0.5
54-2V	1.7	1.4	-0.3
54-4V	2.3	1.7	-0.6
72-4S	2.0	1.0	-1.0
72-6S	2.4	1.2	-1.2
72-2V	1.9	0.8	-1.1
72-4V	2.1	1.2	-1.2

The variability of both the method and the measurements of girder camber were previously discussed by Johnson (2012) and in Section 4.3.5, and it must be considered when evaluating these results. Post-addition changes in camber varied by up to approximately ¼ in. between adjacent girders, and the girder that experienced the least change (54-2V) was also the girder with the lowest *pre*-addition camber. Measured post-addition cambers were all small (ranging *L/2100* to *L/700*), but no measured cambers were negative. While further research may be useful to evaluate the implications of these small cambers, these measured SCC and VC results appear to be comparable. They should serve as confirmation of the more precisely measured change in concrete strain due to the same load, which is reviewed next.

5.4.2.3 Elastic Gain in Prestress Due to Additional of Deck

The change in measured concrete strain due to the addition of the deck was previously mentioned in relation to Equation 4-10 concerning the change in elastic stress due to an externally applied bending moment, Equation 7-1 concerning ε_{gauge}, and Equation 7-2 concerning the change in strain expected of a VC girder exhibiting the same E_c as its companion SCC girder. Using these equations and the adjustment factors shown in Table 5.3, the measured change in concrete strain was compared to those predicted and expected for the linear-elastic response to the deck weight. Results from this comparison are summarized below in Table 5.6.

Table 5.6: Comparison of changes in concrete strain due to deck addition

Girder	Elastic Concrete Strain Due to Deck Wt. (με)			SCC/VC Response		
	Measured	Predicted (Eq. 7-1)	Measured/ Predicted	Measured	Predicted	Adjusted[1]
54-4S	123	111	1.11	1.13	1.14	1.00
54-5S	112	115	0.98			
54-6S	117	115	1.02			
54-S Average	*118*	*113*	*1.04*			
54-4V	111	102	1.08			
54-6V	97	96	1.01			
54-V Average	*104*	*99*	*1.05*			
72-4S	129	140	0.92	1.04	1.20	0.91
72-6S	134	147	0.91			
72-S Average	*131*	*143*	*0.92*			
72-2V	142	123	1.16			
72-3V	116	118	0.99			
72-4V	121	118	1.02			
72-V Average	*126*	*119*	*1.06*			
SCC Average	-	-	*0.99*	*1.09*	*1.17*	*0.95*
VC Average	-	-	*1.06*			

Note: [1] = adjusted VC responses are summarized in Table I.2 of Keske (2014)

In the above table, measured elastic concrete strains in response to the addition of the deck weight were directly determined at the *cgp*, and those predicted using Equation 7-1 were based on the measured mechanical properties and average haunch thicknesses. The average haunch thicknesses measured in SCC and VC BT-54s were noticeably different (SCC-girder haunch was approximately 0.6 in. thicker). Consequently, the strain expected in a VC girder of the same stiffness as the companion SCC girder under the same load as applied to the SCC girder accounts for this difference (see "Adjusted" in the table). Meanwhile, SCC BT-54s were predicted to strain 14% more ("Predicted" in the table), and they actually strained 13% more ("Measured").

Similar to the earlier comparison of transfer prestress losses, many girders exhibited greater changes in strain due to deck weight than predicted according to Equation 7-1 when using measured material properties. Potential reasons for this include that the exact thickness of the deck could have varied (a minor difference in the 7.0 in. deck thickness would noticeably affect the applied bending moment) or the load could have been distributed differently than

expected because of the presence of intermediate diaphragms (less stiff girders would redistribute some of the load to the adjacent girders).

Measured changes were, on average, slightly more accurately predicted in SCC girders based on measured material properties than were VC-girder responses. The distinction was especially noticeable in the BT-72 girders, in which SCC girders were predicted to strain 20% more than the companion VC girders ("Predicted"). Instead, the SCC BT-72s strained noticeably less than would be expected of VC girders of the same measured stiffness (see "Adjusted" in the table). From all of the above observations, several conclusions are warranted:

- SCC-girder elastic strain due to deck weight can be at least as accurately predicted as in VC girders when using measured material properties, and
- Because SCC elastic strain responses to the deck weight were similar or less than would be expected of VC girders of the same E_c, SCC-girder deck-construction elastic response behavior is acceptably similar to that of VC girders.

For context, the elastic concrete strain assumable during design was calculated according to Equation 4-10 in conjunction with the specified f'_c and the E_c calculated as $57{,}000\sqrt{f'_c}$. Design elastic concrete strains equaled 155 and 170 με for BT-54s and BT-72s, respectively. These responses are approximately 40 με greater than the concrete strains *measured* in either material and 30–50 με greater than the concrete strains *predicted* based on measured mechanical properties. The strain difference between either measured or predicted results and design strain results equates to approximately 1 ksi of effective prestress. Thus, these elastic-response results indicate conservative prediction of SCC and VC performance through the testing of representative cylinders.

5.4.3 Responses to Service-Level Live Loads

Many of the results relating to the live-load testing of the Hillabee Creek Bridge have been published elsewhere by Miller (2013) and Keske et al. (2014). Prior to the evaluation of measured responses, several conclusions determined from that work are noted below:

- It was determined that the superimposed three-truck load "A+E+H" illustrated in Figure 5.5 induced the largest service load on an interior girder (girder 6 of each span) and exterior girder (girder 7 of each span), and
- The effective precision of measured deflections and bottom-flange strains should be considered to equal ±0.01 inches and ±1 με, respectively.

If the bridge response to service loads is linear, then the principle of superposition should be valid for the load test results. The use of two load trucks during the second round of testing

allowed evaluation of response linearity via comparison of measured two-truck response to superposition of measured responses to single-truck loads. A representative example of these comparisons is illustrated for strains and deflections in the BT-54 spans in **Figure**. Truck positions are indicated on the horizontal axis. These results are compared for individual gauges, not between girders; therefore, no adjustment for concrete stiffness is necessary. In the figure, the Girder 6 deflections have not been plotted because the deflectometer at both of these locations malfunctioned during the second load test.

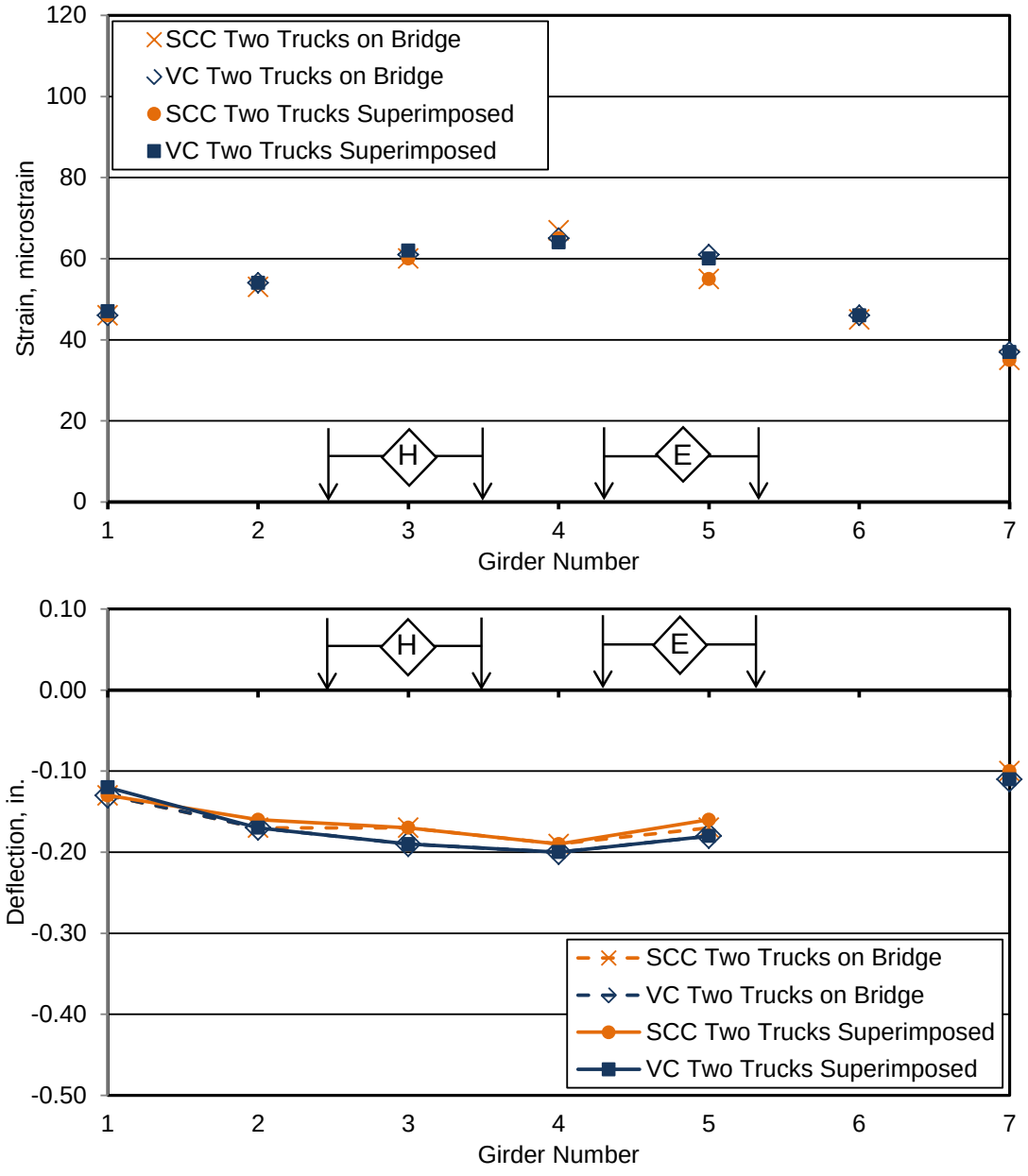

Figure 5.7: Comparison of measured two-truck and superimposed single-truck (*top*) bottom-fiber strain and (*bottom*) midspan deflection responses

In the figure, dashed with empty markers are barely distinguishable from solid lines with filled markers because the measured two-truck responses are essentially identical to the corresponding, summed single-truck responses. This is true for the SCC girders and the VC girders. Superimposed single- and actual two-truck responses never differed by more than 1 microstrain or 0.01 in. (0.3 mm), which roughly correspond to the precision of the measurement techniques. Therefore, the bridge is clearly responding to these service loads in a linear-elastic manner, and superposition may therefore be used to estimate the response of the bridge to three-truck load configurations.

7.1.1.1 Comparison of Deflection

Directly measured deflection responses of each girder to superimposed Load A+E+H are compared below in Figure 5.8. Instances in which deflectometer measurements are unavailable (due to malfunction or absence) are omitted.

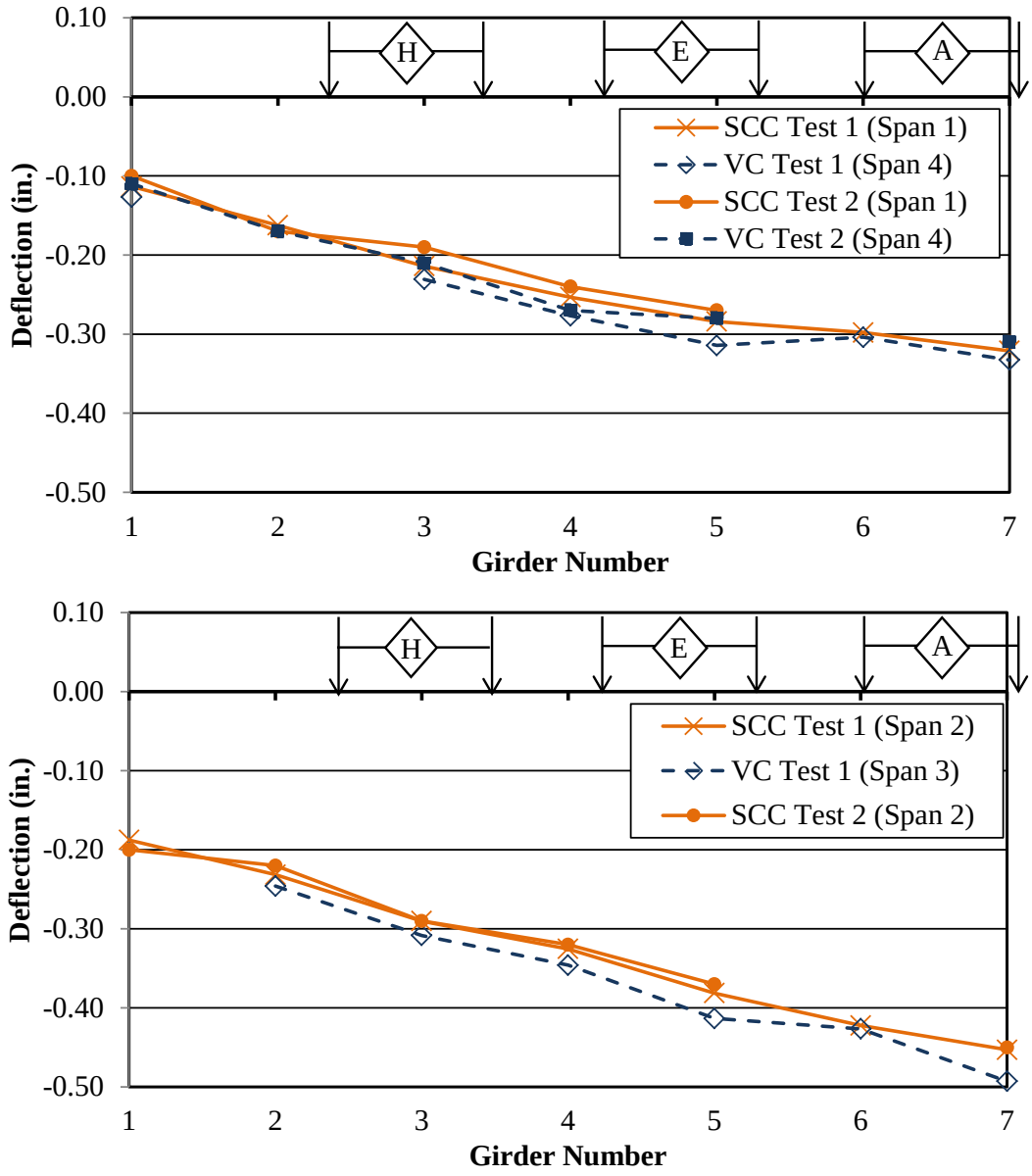

Figure 5.8: Measured service-load deflections in (*top*) BT-54s and (*bottom*) BT-72s

The deflections shown in the previous figure are not adjusted to account for the differences in measured E_c. Despite the differences in stiffness measured in representative cylinders, no SCC girder deflection exceeded that of its companion VC girder. Furthermore, in each load test, no SCC girder deflection differed from that of the companion VC girder by more than 0.02 in. among the BT-54s or more than 0.04 in. among the BT-72s. Considering the precision of the measured values, there is no indication that the SCC girders are performing any differently than the VC girders either in deflection magnitude or distribution.

It is unclear whether deflection responses should be sensitive to the observed differences in cylinder-tested properties; instead, these measured deflections should mainly be used to

confirm the more precisely measured bottom-flange strain results discussed next. These deflection results may also coarsely confirm that the girders have not experienced any deterioration in service-load response during the first year of service—the measured deflections were generally less in the second year than in the first. While the difference is probably trivial, it confirms that the bridge did not experience any abnormal deterioration of deflection response during the first year of service.

7.1.1.2 Comparisons of Bottom-Surface Strain

Bottom-flange strains of all girders in response to Load A+E+H are illustrated in Figure 5.9 and Figure 5.10, and the single-truck responses used to develop these superimposed responses are summarized in Appendix I of the dissertation prepared by Keske (2014). VC girder strains have been transformed using Equation 7-2 for the comparison illustrated in Figure 5.10 such that the VC strains presented in that figure are those that would be expected if the VC had exhibited the same measured properties as the tested SCC. Instances in which surface strain measurements were unavailable during the second test are omitted.

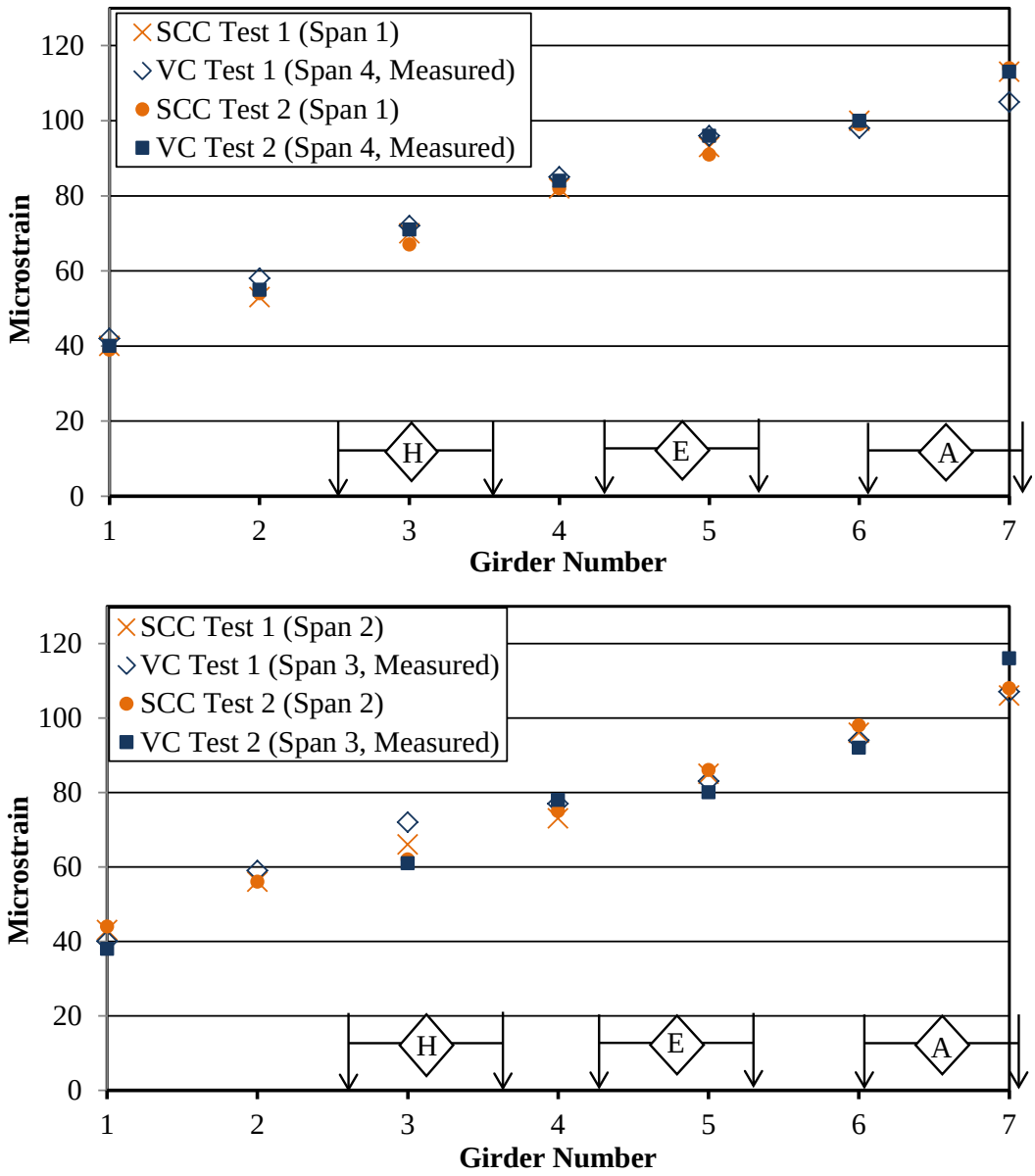

Figure 5.9: Measured service-load changes in bottom-flange concrete strain in (*top*) BT-54s and (*bottom*) BT-72s

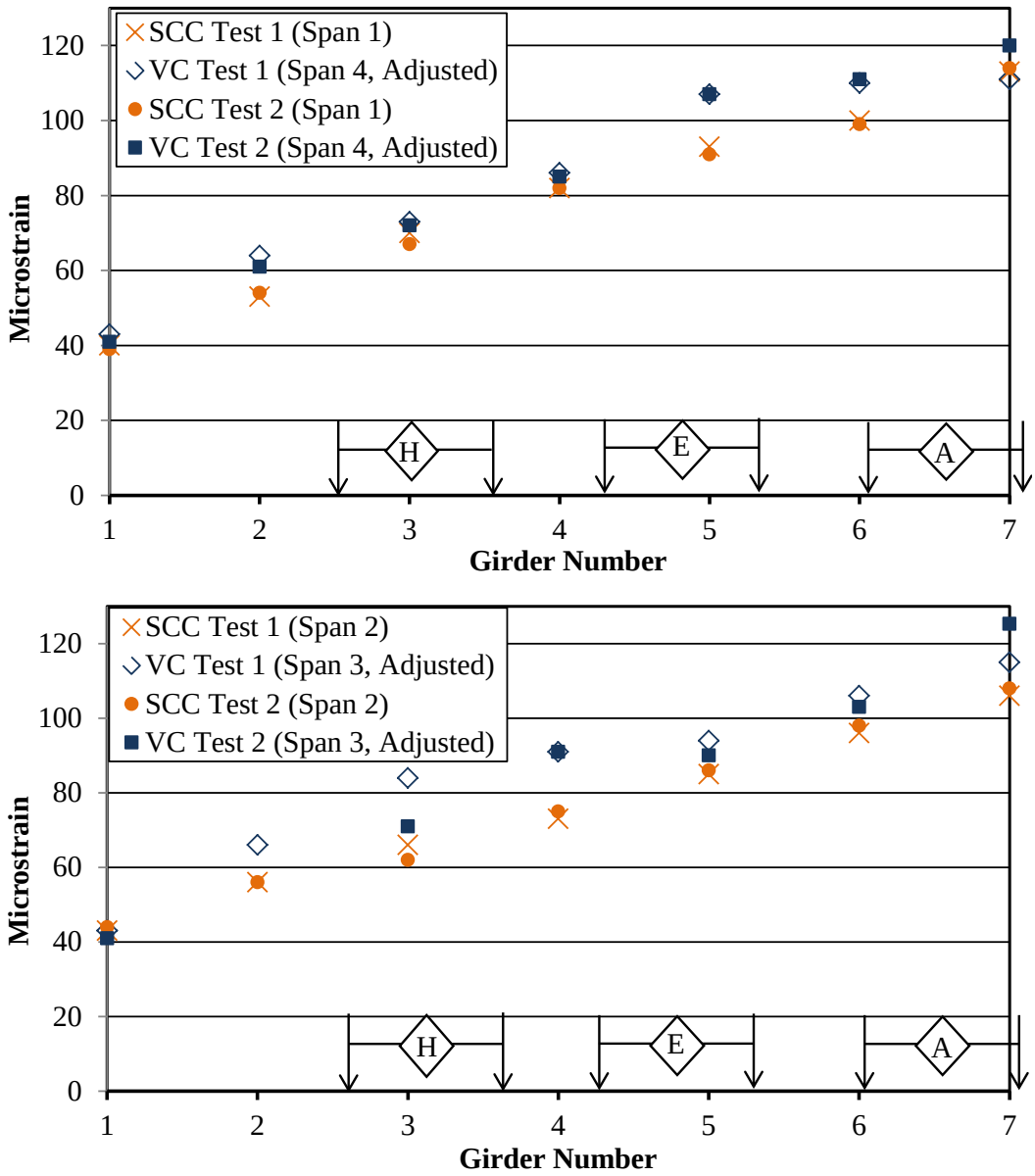

Figure 5.10: Adjusted service-load changes in bottom-flange concrete strain in (*top*) BT-54s and (*bottom*) BT-72s

Two conclusions are warranted based on these figures: SCC girder bottom-flange strains were practically no different than *measured* companion VC strains, and the SCC girders strained less in response to service loads than would be *expected* based on measured elastic properties. The SCC strains were an average of 8.0 με, or approximately 9%, less than the adjusted VC strains for the same loading but were an average of 0.6 με less than the comparable, directly measured VC strains.

Considering the precision of these field measurements, these measured values indicate that each SCC girder strain is essentially identical to its companion VC girder strain. The

similarity between the two test responses after one year of service apparent in the figure was also confirmed numerically. All year-over-year changes are acceptable considering the precision of the measured values, and no results indicate any abnormal degradation of strain response within the first year of normal service. This confirms that the ability of SCC girders to resist service loads over time is acceptably similar to that of VC girders.

5.5 SUMMARY AND CONCLUSIONS

5.5.1 Summary

The work documented in this chapter was conducted to evaluate the elastic-load responses of the full-scale SCC girders used to construct the bridge over Hillabee Creek, both in relation to the companion VC girders used in the bridge and in relation to currently employed predictions. The primary full-scale performance characteristics evaluated were the elastic concrete strain and deflection responses of the bridge to construction and service loads. By incorporating the measured mechanical properties in this evaluation and comparing responses to design-property estimated responses, the acceptability of the SCC-girder elastic behavior and any ways in which it may differ due to its unique characteristics was thoroughly evaluated. Not only are such full-scale evaluations of SCC limited or nonexistent, but their implications for SCC girders of the scale used in this bridge and made using Alabama materials and methods are unclear.

The work of this chapter was divided into three components: material and section properties determined through the testing of representative specimens, full-scale elastic responses to construction loads (prestress transfer and deck addition), and full-scale elastic responses to service-level live loads. The observations and conclusions made concerning these three topics are summarized in Section 5.5.2. The recommendations made based on this research are then given in Section 5.5.3.

5.5.2 Observations and Conclusions

5.5.2.1 Material and Section Properties

- The concrete used to construct the bridge deck exhibited a distinctly greater E_c relative to $\sqrt{f_c}$ than did the two girder mixtures—its 91-day E_c exceeded that measured in the SCC and equaled that measured in the VC-girder mixture while f_{cd} was approximately 80% of f_c of the girders.
- Using a novel system to measure camber during the bridge construction, it was determined that the haunches over the SCC BT-54s were noticeably thicker than those

over the companion VC BT-54s—haunch thickness was an average of approximately 0.6 in. greater over the SCC BT-54s. Because the haunch thickness would affect transformed-section analyses and imposed deck weight, it was necessary to account for this difference when comparing SCC and VC composite behavior.

- Using engineering principles of compatibility, load equivalence, and linear-elastic behavior, adjustment factors were calibrated that would indicate the amount of strain expectable in a VC girder of equivalent material stiffness as an equivalently loaded SCC girder. These factors ranged from 1.08–1.17 for different girders and loading conditions; measured VC elastic strain responses would need to be multiplied by such factors to indicate the amount of strain expected had the VC girders exhibited the same stiffness as the complimentary SCC girders.

5.5.2.2 Responses to Construction Loads

- Almost all girders exhibited greater elastic deformation than predicted in response to the transfer mechanism (by an average of 7%). SCC-girder elastic deformations were approximately 2% greater than predicted when considering the SCC E_{ci}, while VC deformations were approximately 12% greater than predicted.
- SCC-girder elastic strains due to prestress transfer were expected to be approximately 9–18% greater than in geometrically identical VC girders based on differences in measured material properties. Measured SCC elastic strains at transfer were approximately 10 με greater in magnitude than in the companion VC girders (out of a total elastic strain of approximately -470 με), which was well within the precision of this testing.
- Considering these results, SCC-girder elastic strain (and, by extension, prestress loss) due to prestress transfer was at least as accurately predicted as that of VC girders when using measured material properties.
- Average measured strain responses to prestress transfer (in both materials) were approximately 160 με less in magnitude than the non-iterative design estimate found in the *AASHTO LRFD* provision (equating to approximately 5 ksi of prestress). Considering this, SCC-girder prestress-transfer behavior is acceptably similar to that of VC girders and is at least as conservatively predictable.
- Measured changes in camber due to the addition of the deck varied between adjacent girders of the same material (up to ¼ in.), but SCC girders appeared to behave comparably without consideration for differences in material properties or haunch-thickness variation.

- Changes in elastic strain due to the addition of the deck were comparable in SCC and VC girders, despite the expectation that SCC could strain up to 20% more based on measured material properties.
- Because SCC-girder elastic-strain responses due to prestress transfer and deck addition were similar or less than would be expected of VC girders of the same E_c, and all measured responses were conservatively predictable relative to design estimates, SCC-girder construction-load behavior is acceptably similar and as predictable as that of VC girders.

5.5.2.3 Responses to Service Loads

- Superimposed single-truck load responses were essentially identical to those measured in response to two-truck loads, which confirms that the bridge is exhibiting linear-elastic behavior in response to service loads. Deflections were trivially less during the second load test conducted after the bridge had been in service for a year, which confirms that the bridge is behaving conservatively over time.
- No SCC girder deflected more than its companion VC girder in response to service-level live loads. Likewise, bottom-surface concrete strains measured in SCC girders were, on average, 0.6 με less than those measured in identically loaded companion VC girders.
- Bottom-surface concrete strains measured in SCC girders were, on average, 8.0 με (or 9% of the measured result) less than those expected in the companion VC girders after accounting for differences in measured properties.
- In light of these findings, the full-scale elastic-responses of SCC girders to service loads are considered to be acceptably similar and at least as conservatively predictable as those of the companion VC girders.

5.5.3 Recommendations

- Concerns about the elastic-response behavior of SCC in full-scale precast, prestressed girders should not restrict the implementation of the material in that type of construction. Measured full-scale structural responses were essentially identical in companion SCC and VC girders and all behaviors were conservatively predictable based on measured mechanical properties.
- Measured post-deck-addition cambers were small, ranging from *L/2100* to *L/700*; the implications of this tendency are unclear, and additional research may be useful to investigate its prevalence and effects.

- Full-scale elastic performance of SCC girders was slightly more conservatively predictable relative to measured mechanical properties and small-scale tests than was VC-girder performance. While the source of this discrepancy could not be isolated in this research, further research concerning the discrepancy between small-scale cylinder-tested properties and full-scale behaviors may be of value.
- The difference between predictions that incorporated measured properties and those based on design properties was larger than the difference between measured or expected SCC and VC responses. Further research concerning the discrepancy between measured elastic responses and the responses that would be predicted during design may be of value.

CHAPTER 6: RESEARCH CONCLUSIONS AND RECOMMENDATIONS

6.1 SUMMARY OF WORK

Because of its fluid nature, SCC can efficiently fill congested or irregularly shaped members more easily than vibrated concrete while also providing an improved uniformity and surface finish. Therefore, one of the most advantageous uses of SCC is in the production of precast, prestressed bridge girders, where reinforcement congestion and member shape make filling and consolidation of VC difficult. SCC achieves its unique fresh characteristics through the use of differences in mixture proportions. However, research concerning the effects of these mixture changes has been limited, both with regard to fresh behavior and hardened-material and structural behavior.

Understanding these effects is critical in the especially demanding implementation of the material in the production of precast, prestressed girders. Consequently, prior to statewide acceptance of SCC in precast, prestressed bridge member production, ALDOT sponsored an investigation of the material to be performed by the AUHRC. The work presented in this report completed this investigation and included a performance evaluation of precast, prestressed SCC girders produced for Alabama's first full-scale implementation of SCC in an in-service bridge.

The final phase of laboratory work for the AUHRC investigation focused on quantification of SCC stability, a unique property of the material that has been difficult to assess previously. In the investigation, five fresh concrete stability tests were conducted on twenty SCC mixtures each placed in walls of heights equaling 54, 72, and 94 inches. The same walls were also constructed with four VC mixtures, and the in-place hardened concrete uniformity of each of the twenty-four groups of walls was evaluated. Fresh SCC stability test results were then compared to the results of the hardened concrete uniformity testing. Based on those results, suitable fresh SCC test methods and acceptance criteria are recommended for ALDOT use during the implementation of SCC in the statewide production of precast, prestressed elements.

During the evaluation of full-scale SCC-girder behavior, fresh and hardened mechanical properties, prestress transfer bond length, and early-age time-dependent properties were assessed at the precast plant. Observations of hardened mechanical properties, full-scale time-dependent behavior, and elastic responses to construction and service loads continued until all girders were approximately 1,000 days old and had been in service for one year. Results related to the construction of the bridge and in-place behavior of the girders are summarized in this report, while fabrication and pre-erection behaviors and properties are summarized elsewhere (Keske et al. 2015).

While some concrete material properties and isolated structural behaviors appeared to be less conservative in the SCC, the differences were within expectations considering the differences between its mixture proportions and those of the companion VC. In other words, the observed differences were not unique to the use of SCC because any two concretes proportioned differently would exhibit such differences. All predictions were conservative based on measured material properties and more so based on design properties. The differences between the as-produced SCC and VC were frequently within the precision of the testing or were less significant than the observed variability that resulted from typical construction practices.

Analyses of several important full-scale structural behaviors (long-term time-dependent deformation and elastic responses to construction and service loads) suggest that the SCC girders are behaving essentially identically to the companion VC girders. This slightly disagrees with the findings of complimentary small-scale testing but indicates that SCC behavior can be at least as conservatively predicted when using measured material properties. Based on these results, some modifications to the current prediction models, design procedures, and construction practices are recommended for use with both materials. Acceptance of SCC as an alternative to vibrated concrete in the construction of precast, prestressed bridge girders is also recommended.

6.2 RESEARCH CONCLUSIONS AND RECOMMENDATIONS

The work documented in this report was conducted in two parts. The first involved the evaluation of fresh stability test methods during the production of twenty different SCC mixtures and the second involved the evaluation of a variety of fresh material, hardened material, and structural behaviors in a one-to-one comparison of an plant-produced SCC and VC. The conclusions and recommendations summarized in Section 6.2.1 are supported by the work of the first part, and the conclusions and recommendations summarized in Sections 6.2.2–6.2.4 are supported by the second part.

6.2.1 Concrete Stability, Hardened Uniformity, and Fresh Test Methods

Conclusions and recommendations are supported by the research presented in Chapter 2:

- Embedded-reinforcement pullout tests and ultrasonic pulse velocity (UPV) measurements indicate that acceptable hardened concrete uniformity is achievable in a variety of SCC mixtures relative to that of high-quality VC and to code-accepted behavior.
- The HVSI (AASHTO PP-58) correlated well with a quantifiable result of the coarse aggregate uniformity in the top-cast samples that were also tested according to the HVSI but not with any other assessed measures of fresh stability or hardened uniformity of

concrete. This indicates that the subjective HVSI can be quantified but that the significance of these results is unclear.

- Among five evaluated fresh SCC stability test methods, the VSI, sieve stability, and surface settlement tests were found to most strongly correlate to several measures of in-situ hardened concrete uniformity in full-scale specimens. Strong preference for these tests is therefore recommended during the assessment of fresh stability in SCC.
- The results obtained from the sieve stability test after an abbreviated 80 sec. rest period were strongly correlated to those obtained after the currently standardized 15 min. rest period. Use of the abbreviated 80 sec. rest period is therefore recommended to provide accelerated results which will be best to use for job-site quality assurance testing.
- The column segregation test (ASM C1610) and rapid penetration test (ASTM C1712) were found to poorly correlate to other measures of fresh stability and in-situ uniformity of concrete, so their use is of little value relative to use of the three fresh concrete stability tests recommended above.
- Fresh concrete stability tests were compared to each other when using all available SCC test results (twenty results) and when using results subdivided by coarse aggregate NMSA, total aggregate volume, or both. While the VSI exhibits the same range of results within all subdivisions, results from all other fresh concrete stability tests are affected by one or more of these mixture variables.
- The VSI correlated well with quantitative measures of concrete stability and in-situ uniformity, and it was the only assessed fresh concrete stability test whose results were not affected by coarse aggregate NMSA or aggregate volume fraction. It is, therefore, the most versatile fresh concrete stability test studied and can be valuable in determining SCC stability despite its subjective nature.
- The sieve stability test and surface settlement test were differently affected by the different evaluated mixture variables: the sieve stability test yielded larger sieved-fraction results when testing SCC of a larger NMSA, while the surface settlement test yielded larger settlement-rate results when testing mixtures with a reduced total aggregate volume. These results suggest subdivision by NMSA (greater or less than ½ in.) or total aggregate volume (greater or less than 65%) when using the two test methods.
- While fresh concrete stability test results may indicate reduced apparent stability in SCC of a reduced total aggregate volume or larger coarse aggregate NMSA, in-situ concrete uniformity of large-scale specimens made with these mixtures can be equal to that of SCC of a larger total aggregate volume or smaller coarse aggregate NMSA, as well as that of a variety of vibrated concretes.

Based on these results, a stability testing protocol is recommended for use during ALDOT implementation of SCC in precast, prestressed girder production. If initial testing according to the VSI indicates questionable stability (VSI result greater than 1.0), then the use of the sieve stability test (with an abbreviated rest period of 80 sec.) should provide a quickly assessable and quantitative means of determining final batch acceptance. Acceptance criteria for the sieve stability test are presented in Chapter 2.

6.2.2 Time-Dependent Deformation of Concrete Cylinders

Conclusions and recommendations are supported by the work presented in Chapter 3:

- Measured SCC compliance was approximately 15% greater than that of the companion VC through a concrete age of three years. On average, creep of the SCC was no more than 10% greater than that of the equivalent-strength VC.
- The increased *J* of the SCC was in line with its reduced E_{ci}, and any increased creep was minor and expectable considering its mixture proportions. These differences suggest that differences in *J* and creep are not uniquely associated with the use of SCC—the difference should occur in any two concretes whose proportions differ.
- Creep in cylinders that were underloaded was insignificantly different than that of standard specimens, while creep was expectably reduced in cylinders aged before loading—creep of the aged cylinders was approximately 50% of that measured in cylinders loaded to coincide with prestress release of the bridge girders. This suggests that creep behavior is predictable under varied load intensities (less than 40% of f_c) and loading ages (up to one year), in both materials.
- Measured SCC unrestrained shrinkage was approximately 30% greater than that of the equivalent-strength companion VC. The increased shrinkage of the SCC was expectable in response to the differences in its proportions but was more severe than the difference between SCC and VC *J* or creep.
- Shrinkage growth of SCC was comparable to that of VC; free shrinkage approximately doubled between seven days and fifty-six days but did not double again through three years, in both materials.
- In both materials, time-dependent creep was approximately equal to that predicted by several models while shrinkage was less than predicted, when using measured properties and testing times. Because the models that over-predicted shrinkage also under-predicted creep, all evaluated models were reasonably accurate at predicting total time-dependent deformation. Prediction of the separate components of time-dependent behavior should be improved through the use of mixture-specific adjustment factors.

- Adjustment factors to several current models were proposed to more accurately reflect the separate components of time-dependent deformation in concrete produced with local Alabama materials. Recommended adjustment factors, termed A_{AL} in this work, equaled 1.1–1.2 and 0.8–1.0 for SCC creep and shrinkage and 1.0–1.1 and 0.5–0.8 for VC creep and shrinkage, respectively.

After applying A_{AL} corrections, all code-referenced models were used to predict total strain to within 5% of measured results at multiple concrete ages, on average. Use of the A_{AL} corrections improved the correspondence of each predicted and measured strain component, which should allow for more accurate prediction of time-dependent behavior in specimens of other dimensions or exposure conditions. SCC time-dependent behavior appears to be no less predictable using the existing models, but prediction of time-dependent behavior in both materials should benefit from the use of A_{AL}.

6.2.3 Time-Dependent Behavior of Full-Scale Girders

Conclusions and recommendations are supported by the work presented in Chapter 4:

- Small-scale testing revealed that the studied SCC exhibited a CTE approximately 5% greater than that of the companion VC-girder mixture. The difference was explained by the difference in mixture proportions and is therefore not a unique concern of SCC—the difference should occur between any two concretes exhibiting differences in proportions or materials.
- All specimens made with the girder concrete exhibited CTEs approximately 20% greater than in the concrete utilized to construct the cast-in-place portions of the bridge superstructure. The difference between the mixtures appears to be due to a combination of SCM type, SCM replacement rate, *w/cm*, and within-aggregate-type mineralogy.
- In light of the difference between girder- and deck-mixture CTEs, SCC CTE is considered to be acceptably similar to that of VC that is proportioned with similar aggregates and cementitious materials. The significance of the difference between the girder and deck CTEs should be minimal in this type of application (simply supported girders not restrained against thermal deformation).
- Thermal effects distinctly affected the apparent internal-strain measurements obtained in the girders. These changes in apparent strain (up to 250 με at the *cgp* of the composite girders between seasons when accounting for gauge temperature but not concrete temperature) do not necessarily correspond to changes in f_{pe} because both steel and concrete deform in response to thermal effects. Therefore, thermal effects must be

accounted for to effectively study the time-dependent creep and shrinkage behavior of full-scale girders.

- Transient thermal effects were accurately isolated in this work using simplified representations of the measured thermal gradients and cross sections. By determining the axial deformation and curvature caused by nonlinear thermal effects, thermal-strain effects were isolated from the effects of long-term time-dependent material deformation. The implemented correction method should be applicable in other situations, and its use is recommended in this type of testing.
- After accounting for thermal effects, SCC girders exhibited practically the same prestress losses as the companion VC girders throughout the first 1,000 days after casting. Differences in total measured losses between the materials at 1,000 days equated to no greater than 1% of the pre-release strand stress, f_{pbt}. This indicates that the long-term prestress maintenance behavior of SCC girders can be acceptably similar to that of VC girders.
- Use of the simplified *AASHTO LRFD* Section 5.9.5.3 provisions for f_{pe} led to reasonably accurate predictions of long-term time-dependent prestress losses when calculated using measured material properties—predictions of time-dependent losses were conservative but within approximately 6 ksi, or 3% of f_{pbt}, of measured results.
- Use of the refined *AASHTO LRFD* (2013) Section 5.9.5.4 provisions for f_{pe} led to over-predictions of time-dependent prestress losses at all ages when calculated using measured material properties—predictions of time-dependent losses were conservative but within approximately 11 ksi, or 5% of f_{pbt}, of measured results.
- The accuracy of the *LRFD* (2013) Section 5.9.5.4 predictions was moderately improved in the VC girders when applying the recommended A_{AL} adjustments and was somewhat reduced in the SCC girders. Measured f_{pe} in SCC girders was under-predicted by approximately 6.5% of f_{pbt}, while measured VC-girder f_{pe} was under-predicted by less than 2.5% of f_{pbt}. Therefore, use of adjustment factors to account for material-specific creep and shrinkage behavior can lead to conservative predictions of time-dependent behavior in full-scale girders.
- Use of the *AASHTO LRFD* (2013) simplified or refined time-dependent prestress-loss provisions with *design* material properties (such as f'_{ci}) led to very conservative predictions. Long-term design predictions under-predicted measured f_{pe} by up to 27 ksi (13% of f_{pbt}) and under-predicted equivalent predictions of f_{pe} that incorporated measured properties by up to 19 ksi (10% of f_{pbt}).
- In light of these findings, the long-term time-dependent behavior of full-scale SCC girders is considered to be conservatively predictable and acceptably similar to that of the companion VC girders.

- Concrete strain was unchanged during the approximately 650 days after the casting of the deck. Based on both measured and predicted results, time-dependent changes in behavior (other than transient thermal effects) are expected to be minimal during the remainder of the service life of these girders.

6.2.4 Elastic-Response Behavior of Full-Scale Girders

Conclusions and recommendations are supported by the work presented in Chapter 5:

- The haunches over the SCC BT-54s were noticeably thicker than those over the companion VC BT-54s—haunch thickness was an average of 0.6 in. greater over the SCC BT-54s. Because the haunch thickness affects both transformed-section dimensions and deck weight, it is important to account for this difference when comparing composite-section behaviors of companion girders.
- SCC-girder elastic strains due to prestress transfer were predicted to be approximately 9–18% greater than in geometrically identical VC girders because of the difference in measured E_{ci}. Measured SCC-girder elastic strains were no more than 2% greater than measured VC-girder elastic strains, which would correspond to 0.1% of f_{pbt} in the strands. Thus, the elastic response of SCC girders to the transfer mechanism is acceptably similar to that of VC girders.
- Almost all girders exhibited greater elastic deformation than predicted in response to the transfer of prestress (by an average of 7%) when using measured properties; SCC-girder elastic deformations were approximately 2% greater than predicted based on measured E_{ci}, while VC-girder deformations were approximately 12% greater than predicted. This indicates that the elastic response of SCC girders to the prestress transfer mechanism is conservatively predictable.
- Changes in elastic strain due to the addition of the deck were comparable in SCC and VC girders, despite the expectation that SCC girders could strain up to 20% more based on measured material properties. While the strain responses predicted using measured properties and using design properties were insignificantly different relative to the accuracy of this assessment, they indicate that the measured responses are conservatively predictable.
- SCC-girder elastic-strain responses due to prestress transfer and deck addition were similar or less than would be expected of VC girders of the same E_c, and all measured responses were conservative relative to design predictions. Therefore, SCC-girder construction-load behavior can be acceptably similar and as conservatively predicted as that of VC girders.

- During two rounds of live-load testing conducted one year apart, measured SCC deflection and bottom-flange strain responses were practically identical to those of the VC girders and were unchanged from the first test to the second. This indicates that the bridge did not experience any abnormal service-load degradation during the first year of service and that SCC-girder live-load behavior can be acceptably similar to that of VC girders.
- Bottom-surface concrete strains measured in SCC girders were, on average, 8.0 με (or 9% of the measured result) less than those expected in the companion VC girders based on differences in measured properties. This indicates that SCC-girder service-load behavior can be at least as conservatively predicted as that of VC girders when using measured mechanical properties.
- All measured SCC-girder responses to construction and service loads were as conservatively predictable as those of VC girders, and predictions that incorporated design properties were more conservative. Therefore, the full-scale elastic-response behavior of SCC girders is acceptably similar and as predictable as that of VC girders.

6.3 RECOMMENDATIONS FOR FUTURE RESEARCH

Based on the research presented in this report, the following recommendations are given for potential areas of future research:

1. It was clear during the fresh concrete stability testing of different SCC mixtures that total aggregate volume and the maximum coarse aggregate size affect the results of fresh concrete stability testing, but it was not possible to determine whether these dependencies are continuous (over various gradations or aggregate volumes) or discrete. This should be investigated further.
2. Predictions of time-dependent prestress losses and elastic gains and losses based on measured material properties were compared to those predicted using design properties. Design predictions of elastic gains and losses were up to 5 ksi different than equivalent *AASHTO LRFD* predictions that incorporated measured properties. Design predictions of long-term time-dependent losses compounded the error and over-predicted equivalent predictions of losses that incorporated measured properties by up to 19 ksi (10% of f_{pbt}). Since measured-property predictions were still conservative, the use of expected material properties, instead of design material properties, during the prediction of prestress losses may be significant. This should be investigated further.

REFERENCES

AASHTO. 2010. *AASHTO Bridge Construction Specifications.* 3rd ed. Washington, DC: American Association of State Highway and Transportation Officials.

AASHTO. 2013. *AASHTO LRFD Bridge Design Specifications: Customary U.S. Units.* 6th ed. Washington, DC: American Association of State Highway and Transportation Officials.

AASHTO. 2012. *Standard Specification for Transportation Materials and Methods of Sampling and Testing*. 28th ed. Washington, DC: American Association of State Highway and Transportation Officials.

Abo-Qudais, S.A. 2005. Effect of Concrete Mixing Parameters on Propagation of Ultrasonic Waves. *Construction and Building Materials* 19 (4): 257–263.

ACI 209. 1992. Prediction of Creep, Shrinkage, and Temperature Effects in Concrete Structures (ACI 209R-92). (Reapproved 1997). Farmington Hills, MI: American Concrete Institute.

ACI 209. 2008. Guide for Modeling and Calculating Shrinkage and Creep in Hardened Concrete (ACI 209.2R-08). Farmington Hills, MI: American Concrete Institute.

ACI 214. 2002. Evaluation of Strength Test Results of Concrete (ACI 214R-02). Farmington Hills, MI: American Concrete Institute.

ACI 237. 2007. Self-Consolidating Concrete (ACI 237R-07). Farmington Hills, MI: American Concrete Institute.

ACI 318. 2011. Building Code Requirements for Structural Concrete (ACI 318-11) and Commentary. Farmington Hills, MI: American Concrete Institute.

Alabama Department of Transportation. 2012. Bridge Standard Drawing I-131. *ALDOT Standard and Special Drawings for Highway Construction*. Montgomery, AL: Alabama Department of Transportation.

Alabama Department of Transportation. 2014. Alabama Traffic Database, Counter ID AL-62-572. *ALDOT Transportation Planning Bureau*. Accessed May 19, 2014. http://aldotgis.dot.state.al.us/atd/default.aspx.

Alavi-Fard, M., and H. Marzouk. 2004. Bond of High-Strength Concrete Under Monotonic Pull-Out Loading. *Magazine of Concrete Research* 56 (9): 545–557.

Almeida Filho, F.M., B.E. Barragan, J.R. Casas, and A.L.H.C. El Debs. 2010. Hardened Properties of Self-Compacting Concrete – A Statistical Approach. *Construction and Building Materials* 24 (9): 1608–1615.

Almeida Filho, F.M., M.K. El Debs, and A.L.H.C. El Debs. 2008. Bond-Slip Behavior of Fresh Self-Compacting Concrete and Vibrated Concrete Using Pull-Out and Beam Tests. *Materials and Structures* 41 (6): 1073–1089.

Al-Omaishi, N. 2001. Prestress Losses in High Strength Pretensioned Concrete Bridge Girders. Report, University of Nebraska-Lincoln.

Al-Omaishi, N., M.K. Tadros, and S.J. Seguirant. 2009. Elasticity Modulus, Shrinkage, and Creep of High-Strength Concrete as Adopted by AASHTO. *PCI Journal* 54 (4): 44–63.

Al-Ostaz, A. 2007. *Effect of Moisture Content on the Coefficient of Thermal Expansion of Concrete*. Report FHWA/MS-DOT-RD-07-187. Oxford, MS: University of Mississippi.

Assaad, J., K.H. Khayat, and J.A. Daczko. 2004. Evaluation of Static Stability of Self-Consolidating Concrete. *ACI Materials Journal* 101 (3): 207–215.

ASTM C39. 2010. Standard Test Method for Compressive Strength of Cylindrical Concrete Specimens. *ASTM International*. West Conshohocken, PA.

ASTM C94. 2011. Standard Specification for Ready-Mixed Concrete. *ASTM International*. West Conshohocken, PA.

ASTM C157. 2008. Standard Test Method for Length Change of Hardened Hydraulic-Cement Mortar and Concrete. *ASTM International*. West Conshohocken, PA.

ASTM C469. 2010. Standard Test Method for Static Modulus of Elasticity and Poisson's Ratio of Concrete in Compression. *ASTM International*. West Conshohocken, PA.

ASTM C496. 2011. Standard Test Method for Splitting Tensile Strength of Cylindrical Concrete Specimens. *ASTM International*. West Conshohocken, PA.

ASTM C512. 2002. Standard Test Method for Creep of Concrete in Compression. *ASTM International*. West Conshohocken, PA.

ASTM C597. 2002. Standard Test Method for Pulse Velocity Through Concrete. *ASTM International*. West Conshohocken, PA.

ASTM C1610. 2006. Standard Test Method for Static Segregation of Self-Consolidating Concrete Using Column Technique. *ASTM International*. West Conshohocken, PA.

ASTM C1611. 2005. Standard Test Method for Slump Flow of Self-Consolidating Concrete. *ASTM International*. West Conshohocken, PA.

ASTM C1712. 2009. Standard Test Method for Rapid Assessment of Static Segregation Resistance of Self-Consolidating Concrete Using Penetration Test. *ASTM International*. West Conshohocken, PA.

Barr, P.J., B.M. Kukay, and M.W. Halling. 2008. Comparison of Prestress Losses for a Prestress Concrete Bridge Made with High-Performance Concrete. *Journal of Bridge Engineering*, ASCE. (September/October): 468–475.

Bartos, P.J.M. 2005. Assessment of Key Characteristics of Fresh Self-Compacting Concrete: A European Approach to Standardisation of Tests. In *Second North American Conference On The Design And Use Of Self-Consolidating Concrete And The Fourth International RILEM Symposium On Self-Compacting Concrete*. Edited by S.P. Shah. pp. 807–829. Addison, IL: Hanley-Wood.

Bazant, Z.P. and L. Panula. 1978. Practical Prediction of Time Dependent Deformations of Concrete, Parts I–IV. *Materials and Structures* 11: 307–378, 425–343, and 12: 169–183.

Boehm, K.M., R.W. Barnes, and A.K. Schindler. 2010. *Performance of Self-Consolidating Concrete in Prestressed Girders.* Auburn, AL: Auburn University Highway Research Center.

Bonen, D., and S.P. Shah. 2004. The Effects of Formulation on the Properties of Self-Consolidating Concrete. In *Concrete Science And Engineering: A Tribute To Arnon Bentur.* Edited by K. Kovler, J. Marchand, S. Mindess, and J. Weiss. pp. 43–56. Cachan Cedex, France: RILEM Publications s.a.r.l.

Bonen, D., and S.P. Shah. 2005. Fresh and Hardened Properties of Self-Consolidating Concrete. *Progress in Structural Engineering and Materials* 7 (1): 14–26.

Bui, V.K., E.K. Attiogbe, D. Vojtko, S. Schaef, and H.T. See. 2007. A Rapid Test for Segregation Resistance of Self-Consolidating Concrete. In *2007 Concrete Technology Forum: Focus On High Performance Concrete*. Dallas: National Ready Mixed Concrete Association.

Buettner, D.R. and R.L. Hollrah. 1968. Creep Recovery of Plain Concrete. *ACI Materials Journal* 65 (6): 452–461.

Castel, A., T. Vidal, K. Viriyametanont, and R. Francois. 2006. Effect of Reinforcing Bar Orientation and Location on Bond with Self-Consolidating Concrete. *ACI Structural Journal* 103 (4): 559–567.

Cattaneo, S., G. Muciaccia, and G. Rosati. 2008. Bond Strength in Limestone Self-Compacting Concrete. In *3rd North American Conference On The Design And Use Of Self-Consolidating Concrete: Challenges And Barriers To Application*. Evanston, Illinois: Center for Advanced Cement Based Materials (ACBM). CD-ROM.

Chan, Y., Y. Chen, and Y. Liu. 2003. Development of Bond Strength of Reinforcement Steel in Self-Consolidating Concrete. *ACI Structural Journal* 100 (4): 490–498.

Cussigh, F. 1999. Self-Compacting Concrete Stability Control. In *First International RILEM Symposium On Self-Compacting Concrete*. Edited by A. Skarendahl and O. Petersson. pp. 153–167. Cachan Cedex, France: RILEM Publications s.a.r.l.

Daczko, J.A. 2003. Stability of Self-Consolidating Concrete, Assumed or Ensured?. In *First North American Conference On The Design And Use Of Self-Consolidating Concrete*. Edited by S. Shah, J. Daczko, and J. Lingscheit. pp. 245–251. Addison, IL: Hanley-Wood.

El-Chabib, H., and M. Nehdi. 2006. Effect of Mixture Design Parameters on Segregation of Self-Consolidating Concrete. *ACI Materials Journal* 103 (5): 374–383.

Ellis, M.A. 2012. Time-Dependent Deformations of Concrete for Precast/Prestressed Bridge Components. M.S. Thesis, Auburn University.

Emanuel, J.H. and J.L. Hulsey. 1977. Prediction of the Thermal Coefficient of Expansion of Concrete. *ACI Journal* 74 (4): 149–155.

EPG (Self-Compacting Concrete European Project Group). 2005. *The European guidelines for self-compacting concrete*. Farnham, UK: EFNARC.

Erkmen, B., C.K. Shield, and C.E. French. 2008. *Self-Compacting Concrete (SCC) for Prestressed Bridge Girders*. MnDOT Report 2008-51. Minneapolis, MN: University of Minnesota.

Esfahani, M.R., M. Lachemi, and M.R. Kianoush. 2008. Top-Bar Effect of Steel Bars in Self-Consolidating Concrete (SCC). *Cement and Concrete Composites* 30 (1): 52–60.

Fang, W., C. Jianxiong, and Y. Changhui. 1999. Studies on Self-Compacting High Performance Concrete with High Volume Mineral Additives. In *First International RILEM Symposium On Self-Compacting Concrete*. Edited by A. Skarendahl and O. Petersson. pp. 569–578. Cachan Cedex, France: RILEM Publications s.a.r.l.

Fang, C.F. and S. Labi. 2006. Evaluating the Static Segregation Resistance of Hardened Self-Consolidating Concrete Using Image Processing Technology. In *Proceedings of the 86th Annual Meeting of the Transportation Research Board*. Washington, DC: Transportation Research Board.

fib. 2010. Creep and Shrinkage. In *fib Model Code for Concrete Structures 2010*. Lausanne, Switzerland: International Federation for Structural Concrete (*fib*).

FHWA. 2011. Coefficient of Thermal Expansion in Concrete Pavement Design. *ACPT TechBrief* FHWA-HIF-09-015.Springfield, VA: ACPT.

Gardner, N.J. and M.J. Lockman. 2001. Design Provisions for Drying Shrinkage and Creep of Normal-Strength Concrete. *ACI Materials Journal* 98 (2): 159–167.

Gardner, N.J. and H. Tsuruta. 2004. Is Superposition of Creep Strains Valid for Concrete Subjected to Drying Creep? *ACI Materials Journal* 101 (5): 409–415.

Gaydecki, P.A., F.M. Burdekin, W. Damaj, D.G. John, and P.A. Payne. 1992. The Propagation and Attenuation of Medium-Frequency Ultrasonic Waves in Concrete: A Signal Analytical Approach. *Measurement Science And Technology* 3 (1): 126–134.

Geokon. 2010. Model 4200/4204/4210 Vibrating Wire Strain Gauge Instruction Manual. Rev. N, 8/10.

Girgis, A.F.M., and C.Y. Tuan. 2005. Bond Strength and Transfer Length of Pretensioned Bridge Girders Cast with Self-Consolidating Concrete. *PCI Journal* 50 (6): 72–87.

Hamilton, H.R., T. Labonte, and M.H. Ansley. 2005. *Self-Consolidating Concrete (SCC) Structural Evaluation*. University of Florida Report BD545, RPWO#21. Gainesville, FL: University of Florida.

Hassan, A.A.A., K.M.A. Hossain, and M. Lachemi. 2010. Bond Strength of Deformed Bars in Large Reinforced Concrete Members Cast with Industrial Self-Consolidating Concrete Mixture. 2010. *Construction and Building Materials* 24, (4): 520–530.

Horta, A. 2005. Evaluation of Self-Consolidating Concrete for Bridge Structure Applications. M.S. thesis, Georgia Institute of Technology.

Hossain, K.M.A., and M. Lachemi. 2008. Bond Behavior of Self-Consolidating Concrete with Mineral and Chemical Admixtures. *Journal of Materials in Civil Engineering* 20 (9): 608–616.

Hwang, S., K.H. Khayat, and O. Bonneau. 2006. Performance-Based Specifications of Self-Consolidating Concrete Used in Structural Applications. *ACI Materials Journal* 103 (2): 121–129.

Jeanty, P.R., D. Mitchel, and M.S. Mirza. 1988. Investigation of "Top-Bar" Effects in Beams. *ACI Structural Journal* 85 (3): 251–257.

Johnson, B.R. 2012. Time-Dependent Deformations in Precast, Prestressed Bridge Girders. M.S. Thesis, Auburn University.

Johnson, D., G. Johnson, and I.N. Robertson. 2010. *Qualifying Segregation in Self-Consolidating Concrete through Image Analysis*. Research report UHM/CEE/10-04. Manoa, HI: Department of Civil and Environmental Engineering.

Kamgang, J. 2013. Compliance of Self-Consolidating Concrete for Prestressed Applications. M.C.E. report, Auburn University.

Kavanaugh, B. 2008. Creep Behavior of Self-Consolidating Concrete. M.S. thesis, Auburn University.

Keske, S.D. 2014. Use of Self-Consolidating Concrete in Precast, Prestressed Girders. Ph.D. dissertation, Auburn University.

Keske, S.D., R.W. Barnes, A.K. Schindler, E.L. Dunham, B.R. Johnson, and M.A. Ellis. 2015. *Self-Consolidating Concrete for Prestressed Applications—Phase I: Girder Fabrication and Pre-Erection Performance.* Auburn, AL: Auburn University Highway Research Center.

Keske, S.D., R.W. Barnes, A.K. Schindler, E.L. Dunham, M.A. Ellis, B.R. Johnson, and W.O. Bullock. 2013a. SCC Precast, Prestressed Girders in the Hillabee Creek Bridge. In *Proceedings of the 5th North American Conference on the Design and Use of Self-Consolidating Concrete*. Chicago, May 12–15, 2013. Center for Advanced Cement-Based Materials, Chicago.

Keske, S.D., D.E. Miller, R.W. Barnes, and A.K. Schindler. 2014. Live-Load Response of In-Service Bridge Constructed with Precast, Prestressed, Self-Consolidating Concrete Girders. *PCI Journal* 59 (4).

Keske, S.D., A.K. Schindler, and R.W. Barnes. 2013b. Assessment of Stability Test Methods for Self-Consolidating Concrete. *ACI Materials Journal* 110 (4): 385–393.

Khan, L.F. and K.E. Kurtis. 2010. Self-Consolidating Concrete in Congested Sections: Mixture Characteristics and Assessment of Performance. *PCI Journal* 55 (5): 79–96.

Khayat, K.H., 1998. Use of Viscosity-Modifying Admixtures to Reduce Top-Bar Effect of Anchored Bars Cast with Fluid Concrete. *ACI Materials Journal* 95 (2): 158–167.

Khayat, K.H. 1999. Workability, Testing, and Performance of Self-Consolidating Concrete. *ACI Materials Journal* 96 (3): 346–353.

Khayat, K.H., and J. Assaad. 2002. Air-Void Stability in Self-Consolidating Concrete. *ACI Materials Journal* 99 (4): 408–416.

Khayat, K.H., E.K. Attiogbe, and H.T. See. 2007. Effect of Admixture Combination on Top-Bar Effect of Highly Flowable And Self-Consolidating Concrete Mixtures. In *Special Publication SP-247: Self-Consolidating Concrete for Precast Prestressed Applications*, ed. A.K. Schindler, D. Trejo, and R.W. Barnes. Farmington Hills, MI: American Concrete Institute. CD-ROM.

Khayat, K.H., A. Ghezal, and M.S. Hadriche. 2000. Utility of Statistical Models in Proportioning Self-Consolidating Concrete. *Materials and Structures* 33 (5): 338–344.

Khayat, K.H., S.D. Hwang, and K. Belaid. 2010. Performance of Cast-In-Place Self-Consolidating Concrete Made With Various Types of Viscosity-Enhancing Admixtures. *ACI Materials Journal* 107 (4): 403–412.

Khayat, K.H., K. Manai, and A. Trudel. 1997. In Situ Mechanical Properties of Wall Elements Cast Using Self-Consolidating Concrete. *ACI Materials Journal* 94 (6): 491–500.

Khayat, K.H., and D. Mitchell. 2009. *National Cooperative Highway Research Program (NCHRP) Report 628: Self-Consolidating Concrete for Precast, Prestressed Concrete Bridge Elements*. Washington, DC: Transportation Research Board.

Khayat, K.H., N. Petrov, E.K. Attiogbe, and H.T. See. 2003. Conventional Flowable and Self-Consolidating Concrete Mixtures. In *Third International Symposium on Self-Compacting Concrete*. Edited by O. Wallevik and I. Nielsson. pp. 703–712. Bagneux, France: RILEM Publications S.A.R.L.

Kim, Y.H., D. Trejo, H.N. Atahan, and M.B.D. Hueste. 2012. Mechanical Property Prediction for High Early Strength Self-Consolidating Concrete. *Journal of Materials in Civil Engineering* 24 (12): 1501–1512.

Koehler, E.P., and D.W. Fowler. 2008. Static and Dynamic Yield Stress Measurements of SCC. *Third North American Conference on the Design and Use of Self-Consolidating Concrete*, Chicago, IL. CD-ROM.

Koehler, E.P., and D.W. Fowler. 2010. Comparison of Workability Test Methods for Self-Consolidating Concrete. *Journal of ASTM International* 7 (2).

Koehler, E.P., D.W. Fowler, E.H. Foley, G.J. Rogers, S. Watanachet, and M.J. Jung. 2007. *Self-Consolidating Concrete for Precast Structural Applications: Mixture Proportions, Workability, and Early-Age Hardened Properties*. CTR Technical Report 0-5134-1. Austin, TX: Center for Transportation Research, The University of Texas at Austin.

Komlos, K., S. Popovics, T. Nurnbergerova, B. Babal, and J.S. Popovics. 1996. Ultrasonic Pulse Velocity Test of Concrete Properties as Specified in Various Standards. *Cement and Concrete Composites* 18 (5): 357–364.

Kwan, A.K.H., and I.Y.T. Ng. 2009. Optimum Superplasticizer Dosage and Aggregate Proportions for SCC. *Magazine of Concrete Research* 61 (4): 281–292.

Lange, D.A., L.J. Struble, M.D. D'Ambrosia, L. Shen, F.Tejeda-Dominguez, B.F. Birch, and A.J. Brinks. 2008. *Performance and Acceptance of Self-Consolidating Concrete: Final Report*. Illinois Center for Transportation Report FHWA-ICT-08-120. Urbana, IL: Illinois Center for Transportation.

Lemieux, G., S.D. Hwang, and K.H. Khayat. 2010. Effect of Material Constituents and Mix Design on Performance of SCC for Precast, Prestressed Girders. In *Design, Production, and Placement of Self-Consolidating Concrete*. Edited by K.H. Khayat and D. Feys. pp. 25–35. New York, NY: Springer.

Levy, K.R. 2007. Bond Behavior of Prestressed Reinforcement in Beams Constructed with Self-Consolidating Concrete. M.S. Thesis, Auburn University.

Levy, K.R., R.W. Barnes, and A.K. Schindler. 2010. Time-Dependent Deformations of Pretensioned, Self-Consolidating Concrete. In *Think Globally, Build Locally: Proceedings of the Third International fib Congress and Exhibition in Washington, D.C*. 29 May-2 June 2010, Chicago: Precast/Prestressed Concrete Institute.

Lin, Y., S. Kuo, C. Hsiao, and C. Lai. 2007. Investigation of Pulse Velocity-Strength Relationship of Hardened Concrete. *ACI Materials Journal* 104 (4): 344–350.

Lin, Y., C. Lai, and T. Yen. 2003. Prediction of Ultrasonic Pulse Velocity (UPV) in Concrete. *ACI Structural Journal* 100 (1): 21–28.

Malhotra, V.M. and V. Sivasundaram. 2004. Resonant Frequency Methods. In *Handbook on Nondestructive Testing of Concrete,* 2nd ed. Edited by V.M. Malhotra and N.J. Carino. Boca Raton, FL: CRC Press LLC.

Mehta, P.K., and P.J.M. Monteiro. 2006. *Concrete: Microstructure, Properties, and Materials*. 3rd ed. New York, NY: The McGraw Hill Companies.

Mindess, S., J.F. Young, and D. Darwin. 2003. *Concrete*. 2nd ed. Upper Saddle River, NJ: Pearson Education.

Mitchell, D., W.D. Cook, A.A. Kahn, and T. Tham. 1993. Influence of High-Strength Concrete on Transfer and Development Length of Pretensioning Strand. *PCI Journal* 38 (3): 52–66.

Mouret, M., G. Escadeillas, and A. Bascoul. 2008. Metrological Significance of the Column Test in Assessment of the Static Segregation of Self-Compacting Concrete in the Fresh State. *Materials and Structures* 41 (4): 663–679.

Naito, C., G. Brunn, G. Parent, and T. Tate. 2005. *Comparative Performance of High Early Strength and Self-Consolidating Concrete for Use in Precast Bridge Beam Construction: Final Report*. ATLSS Report 05-03. Lehigh, PA: Advanced Technology for Large Structural Systems.

Naik, T.R., V.M. Malhotra, and J.S. Popovics. 2004. The Ultrasonic Pulse Velocity Method. In *Handbook on Nondestructive Testing of Concrete,* 2nd ed. Edited by V.M. Malhotra and N.J. Carino. Boca Raton, FL: CRC Press LLC.

Neal, T.L. 2015. Long-Term Deformations and Prestress Losses in Precast, Prestressed Bridge Girders. M.S. Thesis, Auburn University.

Neville, A.M. 1996. *Properties of Concrete,* Fourth Edition. New York: John Wiley & Sons, Inc.

Nilson, A.H. 1987. *Design of Prestressed Concrete*, Second Edition. New York: John Wiley & Sons, Inc.

Ng, I.Y.T., H.H.C. Wong, and A.K.H. Kwan. 2006. Passing Ability and Segregation Stability of Self-Consolidating Concrete with Different Aggregate Proportions. *Magazine of Concrete Research* 58 (7): 447–457.

Ozyildirim, C. 2008. *Bulb-T Beams with Self-Consolidating Concrete on the Route 33 Bridge Over the Pamunkey River in Virginia.* FHWA/VTRC Report 09-R5. Charlottesville, VA: VTRC.

Ozyildirim, C., and D.S. Lane. 2003. *Virginia Transportation Research Council (VTRC) Report: Evaluation of Self-Consolidating Concrete.* Charlottesville, VA: VTRC.

Panesar, D.K. and B. Shindman. 2011. Elastic Properties of Self-Consolidating Concrete. *Construction and Building Materials* 25 (8): 3334–3344.

Parra, C., M. Valcuende, and F. Gomez. 2011. Splitting Tensile Strength and Modulus of Elasticity of Self-Compacting Concrete. *Construction and Building Materials* 25 (1): 201–207.

PCI (Precast/Prestressed Concrete Institute). 2004. *Interim Guidelines for the Use of Self-Consolidating Concrete in Precast/Prestressed Concrete Institute Member Plants*, 1st ed. Chicago: Precast/Prestressed Concrete Institute.

Peterman, R.J. 2007. The Effects of As-Cast Depth and Concrete Fluidity on Strand Bond. *PCI Journal* 52 (3): 72–101.

Peterson, K., L. Sutter, and T. VanDam. 2002. Air Void Analysis of Hardened Concrete with a High-Resolution Flatbed Scanner. In *Proceedings of the 24th International Conference on Cement Microscopy*. pp. 611–617. San Diego, CA: International Cement Microscopy Association.

Pierard, J., V. Dieryck, and J. Desmyter. 2005. Autogeneous Shrinkage of Self-Compacting Concrete. In *Second North American Conference on the Design and Use of Self-Consolidating Concrete and the Fourth International RILEM Symposium on Self-Compacting Concrete*. pp. 1013–1022. Addison, Illinois: Hanley-Wood.

Pozolo, A.M. and B. Andrawes. 2011. Transfer Length in Prestressed Self-Consolidating Concrete Box and I-Girders. *ACI Structural Journal* 108 (3): 341–349.

Raghavan, K.P., Sarma, B.S., Chattopadhyay, D. 2003. Creep, Shrinkage and Chloride Permeability Properties of Self-Consolidating Concrete. In *First North American Conference on the Design and Use of Self-Consolidating Concrete.* Edited by S. Shah, J. Daczko, and J. Lingsheit. pp. 307–317. Evanston, Illinois: Hanley-Wood.

Ramge, P., T. Proske, and H.C. Kuhn. 2010. Segregation of Coarse Aggregates in Self-Compacting Concrete. In *Design, Production, And Placement Of Self-Consolidating Concrete*. Edited by K.H. Khayat and D. Feys. pp. 113–126. New York, NY: Springer.

Saak, A.W., H.M. Jennings, and S.P. Shah. 2001. New Methodology for Designing Self-Compacting Concrete. *ACI Materials Journal* 98 (6): 429–439.

Sahmaran, M., O. Yaman, and M. Tokyay. 2007. Development of High-Volume Low-Lime and High-Lime Fly-Ash-Incorporated Self-Consolidating Concrete. *Magazine of Concrete Research* 59 (2): 97–106.

Sakyi-Bekoe, K.O. 2008. Assessment of the Coefficient of Thermal Expansion of Alabama Concrete. M.S. Thesis, Auburn University.

Schindler, A.K., R.W. Barnes, J.B. Roberts, and S. Rodriguez. 2007. Properties of Self-Consolidating Concrete for Prestressed Members. *ACI Materials Journal* 104 (1): 53–61.

Schrantz, C.E. 2012. Development of a User-Guided Program for Predicting Time-Dependent Deformations in Prestressed Bridge Girders. M.S. Thesis, Auburn University.

Schwartzentruber, L.D., and G.V.M. Broutin. 2005. Quantifying the Segregation Risk of Self-Compacting Concrete by Gammadensitometry. In *Second North American Conference on The Design and Use of Self-Consolidating Concrete and the Fourth International RILEM Symposium on Self-Compacting Concrete*. Edited by S.P. Shah. pp. 713–720. Addison, IL: Hanley-Wood.

Shen, L. 2007. Role of Aggregate Packing in Segregation Resistance and Flow Behavior of Self-Consolidating Concrete. Report, University of Illinois.

Shen, L., L. Struble, and D. Lange. 2007. New Method for Measuring Static Segregation of Self-Compacting Concrete. *Journal of Testing and Evaluation* 35 (3).

Solis-Carcano, R., and E.I. Moreno. 2008. Evaluation of Concrete Made with Crushed Limestone Aggregate Based on Ultrasonic Pulse Velocity. *Construction and Building Materials* 22 (6): 1225–1231.

Sonebi, M., and P.J.M. Bartos. 1999. Hardened SCC and Its Bond with Reinforcement. In *First International RILEM Symposium on Self-Compacting Concrete*. Edited by A. Skarendahl and O. Petersson. pp. 275–284. Cachan Cedex, France: RILEM Publications s.a.r.l.

Sonebi, M., and P.J.M. Bartos. 2002. Filling Ability and Plastic Settlement of Self-Compacting Concrete. *Materials and Structures* 35 (8): 462–469.

Soshiroda, T., K. Voraputhaporn, and Y. Nozaki. 2006. Early-Age Inspection of Concrete Quality in Structures by Combined Nondestructive Method. *Materials and Structures* 39 (2): 149–160.

Soylev, T.A., and R. Francois. 2003. Quality of Steel-Concrete Interface and Corrosion of Reinforcing Steel. *Cement and Concrete Research* 33 (9): 1407–1415.

Stallings, J.M., R.W. Barnes, and S. Eskildsen. 2003. Camber and Prestress Losses in Alabama HPC Bridge Girders. *PCI Journal* 48 (5): 90–104.

Staton, B.W., N.H. Do, E.D. Ruiz, and W.M. Hale. 2009. Transfer Lengths of Prestressed Beams Cast with Self-Consolidating Concrete. *PCI Journal* 54 (2): 64–83.

Stocker, M.F., and M.A. Sozen. 1970. *Engineering Experiment Station Bulletin 503: Investigation of Prestressed Reinforced Concrete For Highway Bridges, Part Five: Bond Characteristics of Prestressing Strand*. Edited by V. Griffin. Urbana, IL: University of Illinois

Storm, T.K., S.H. Rizkalla, and P.Z. Zia. 2013. Effects of Production Practices on Camber of Prestressed Concrete Bridge Girders. *PCI Journal* 58 (2): 96–111.

Su, J. K., S.W. Cho, C.C. Yang, and R. Huang. 2002. Effect of Sand Ratio on the Elastic Modulus of Self-Compacting Concrete. *Journal of Marine Science and Technology* 10 (1): 8–13.

Swords, J.S. 2005. Transfer Length in Prestressed Self-Consolidating Concrete. M.S. thesis, Auburn University.

Tadros, M.K., N. Al-Omaishi, S.J. Seguirant, and J.T. Gallt. 2003. *NCHRP Report 496: Prestress Losses in Pretensioned High-Strength Concrete Bridge Girders*., National Cooperative Highway Research Program (NCHRP). Washington, DC: Transportation Research Board.

Tregger, N., L. Ferrara, and S.P. Shah. 2010. Predicting Dynamic Segregation of Self-Consolidating Concrete from the Slump-Flow Test. *Journal of ASTM International* 7 (1).

Trejo, D., M.B. Hueste, Y.H. Kim, and H. Atahan. 2008.*Characterization of Self-Consolidating Concrete for Design of Precast, Prestressed Bridge Girders*. College Station, Texas: Texas Transportation Institute.

Trent, J.D. 2007. Transfer Length, Development Length, Flexural Strength, and Prestress Loss Evaluation in Pretensioned Self-Consolidating Concrete Members. M.S. thesis, Virginia Polytechnic Institute and State University.

Ye, Y., D. Bonen, and S.P. Shah. 2005. Fresh Properties and Segregation Resistance of Self-Compacting Concrete. In *Second North American Conference on the Design and Use of Self-Consolidating Concrete and the Fourth International RILEM Symposium on Self-Compacting Concrete*. Edited by S.P. Shah. pp. 621–627. Addison, IL: Hanley Wood.

Yue, L.L. and L. Taerwe. 1993. Two-Function Method for the Prediction of Concrete Creep Under Decreasing Stress. *Materials and Structures* 26 (159): 268–273.

Zhu, W., J.C. Gibbs, and P.J.M. Bartos. 2001. Uniformity of In Situ Properties of Self-Compacting Concrete in Full-Scale Structural Elements. *Cement and Concrete Composites* 23 (1): 57–64.

Zia, P., R.A. Nunez, and L.A. Mata. 2005. *Implementation of Self-Consolidating Concrete for Prestressed Concrete Girders*. Raleigh, NC: North Carolina Department of Transportation.

Ziehl, P.H., D.C. Rizos, J.M. Caicedo, F. Barrios, R.B. Howard, and A.S. Colmorgan. 2009. *Investigation of the Performance and Benefits of Lightweight SCC Prestressed Concrete Bridge Girders and SCC Materials*. Report No. FHWA-SC-09-02. Columbia, South Carolina: University of South Carolina.